

UNIVERZA NA PRIMORSKEM
FAKULTETA ZA MATEMATIKO, NARAVOSLOVJE IN
INFORMACIJSKE TEHNOLOGIJE

DOKTORSKA DISERTACIJA
(DOCTORAL DISSERTATION)

NAPREDNE UPORABE LEPIL ZA KONSTRUKCIJSKE ELEMENTE
IZ LESA

(ADVANCED ADHESIVE APPLICATIONS FOR TIMBER
CONSTRUCTION ELEMENTS)

JAKA GAŠPER PEČNIK

KOPER, 2023

UNIVERZA NA PRIMORSKEM
FAKULTETA ZA MATEMATIKO, NARAVOSLOVJE IN
INFORMACIJSKE TEHNOLOGIJE

DOKTORSKA DISERTACIJA
(DOCTORAL DISSERTATION)

NAPREDNE UPORABE LEPIL ZA KONSTRUKCIJSKE ELEMENTE
IZ LESA

(ADVANCED ADHESIVE APPLICATIONS FOR TIMBER
CONSTRUCTION ELEMENTS)

JAKA GAŠPER PEČNIK

KOPER, 2023

MENTOR: IZR. PROF. DR. MATTHEW SCHWARZKOPF
SOMENTOR: DR. VÁCLAV SEBERA

Acknowledgement

I would like to express my sincere gratitude to my mentor, Assoc. Prof. Matthew Schwarzkopf, for supporting and guiding me, during my early academic years. I also thank my co-mentor, Dr Václav Sebera, for motivating and challenging me to solve and deal with many scientific problems. This thesis would not be possible without Dr Andreja Kutnar, who encouraged me to start my PhD, and my other early-career research colleagues, Dr Michael David Burnard and Dr David Devallance. The PhD thesis was conducted with the financial support of the European Commission for the InnoRenew project [Grant Agreement #739574] under the Horizon2020 Widespread-2-Teaming program and Republic of Slovenia (Investment funding of the Republic of Slovenia and the European Union of the European Regional Development Fund), Slovenian Research Agency (infrastructure program IO-0035). I would also like to thank all my co-authors in my scientific papers. Finally, I would like to express my gratitude to my closest family members for supporting me during my entire educational path.

Abstract

Advanced adhesive applications for timber construction elements

*Findings of this doctoral thesis contribute to a better understanding of diverse adhesive applications in the field of wood material science. It combines four studies that assessed adhesive interactions with timber elements from various methodological perspectives. The first study evaluated the fracture properties of adhesive bondline in European beech (*Fagus sylvatica* L). Fracture energy and energy release rate were evaluated under mode I by adopting single edge notched-three-point bending test regime. Bondline fracture characteristics of two adhesives exposed to room temperature and to two elevated temperatures were examined with respect to two wood grain orientations. Fracture properties were found to be significantly different among adhesive systems; in addition, elevated temperatures resulted in reduced fracture properties. Regardless of sufficient bondline properties of the studied adhesives, adhesive type and conditions of bonded products exposed to cleavage should be carefully selected. The second study assessed the fracture properties in shear level of selected adhesives for bonded beech wood in mode II. Experimental results obtained from three-point bend end-notched flexure test and compliance-based beam theory were implemented for bilinear cohesive models used for finite element modelling, through which the effect of friction and wood grain orientation were analysed. The model was a good fit with the experimental values and demonstrated feasibility of the experimental setup for estimating fracture properties of adhesive bondline for numerical models. The third study exploited the use of flexible thick adhesive bondline as an energy dissipating member for timber connection. Monotonic and reverse cyclic double lap-shear testing was performed on two target thicknesses and three adhesives with different mechanical characteristics. Shear strength, elastic stiffness, and strength degradation capacity were found to be higher compared to the selected standard mechanical fasteners used in timber construction. Overall the study showed that with greater bondline thickness and desired adhesive type such joints can be utilised in the seismic design of timber buildings. The last study focused on the impacts of phenol formaldehyde resin impregnated wood on the dynamic mechanical properties of timber elements. Beside higher bending strength and bending modulus of elasticity for modified Scots pine (*Pinus sylvestris* L.) and European beech, impact bending strength and fatigue strength were greatly reduced while cyclic modulus of elasticity remained constant with constant creep level at stationary phase. Such findings show the importance of*

applications when modified wood is exposed to dynamic loadings, as its lifespan is reduced.

Key words: adhesive bondline, fracture properties, flexible adhesives, fatigue strength, adherents mechanical properties

Povzetek

Napredne uporabe lepil za konstrukcijske elemente iz lesa

*Spoznanja te doktorske disertacije prispevajo k boljšem razumevanju različnih načinov uporabe lepil na področju znanosti o biomaterialih. Doktorsko disertacijo sestavljajo štiri eksperimentalno usmerjene študije, ki proučujejo interakcije lesa in lepila z metodološko različnimi pristopi. V prvi študiji smo ocenili lomne lastnosti lepilnih spojev na lepljeni evropski bukovini (*Fagus sylvatica* L). Energijo loma in hitrost sproščanja energije smo z uporabo metode enojne zareze in tritočkovnim upogibom proučevali v načinu I. Lomne lastnosti na lepilnih spojih treh lepil, ki smo jih izpostavili sobni in dvema povišanima temperaturama, smo analizirali tudi v odvisnosti od usmeritve lesnih vlaken, v dveh različnih smereh. Ugotovili smo, da se lomne lastnosti med različnimi lepilnimi sistemi bistveno razlikujejo, povišana temperatura pa je lomne lastnosti drastično poslabšala. Standardizirani strižni testi lepilnih spojev so pokazali, da so vsa testirana lepila ustrezala zahtevam za njihovo kvalifikacijo. Ker pa pri takšnih testih pogosto prihaja do porušitev v lesu, kar je tudi zaželeno, nam takšni testi velikokrat zakrijejo podrobnejše prepoznavanje razlik med lepilnimi sistemi. Ravno to raznolikost pa smo lahko potrdili s karakterizacijo lomnih lastnosti lepilnih spojev, kjer z gotovostjo lahko prikažemo, kako se lepilni sistemi medsebojno razlikujejo. V drugi študiji smo ocenili lomne lastnosti izbranih lepil v strižni ravnini v načinu II, prav tako na lepljeni evropski bukovini. S pomočjo eksperimentalnih rezultatov, pridobljenih s tritočkovnim upogibnim testom nosilca s končno-čelno zarezo in teorijo nosilcev, smo ovrednotili lomne karakteristike in izdelali bilinearni kohezijski model, ki smo ga uporabili za numerično modeliranje. S pomočjo slednjega smo opravili analizo vpliva trenja in vpliva usmeritev lesnih vlaken na rezultate. Rezultati modela so se ujemali z eksperimentalnimi in potrdili primernost eksperimentalne študije za ovrednotenje lomnih lastnosti lepilnih spojev in izdelavo numeričnih modelov. V tretji študiji smo proučevali uporabo fleksibilnega debelega lepilnega spoja kot disipativnega veznega sredstva pri lesenih spojih. S tremi izbranimi lepili z različnimi mehanskimi lastnostmi, vsakega smo nanesti v dveh različnih debelinah, smo izvedli monotone in povratno ciklične strižne preizkuse na vzorcih z dvojnimi strižnimi spojem s prelopom. Ugotovili smo, da so strižna trdnost, elastična togost in zmogljivost ohranjanja trdnosti pri cikličnem obremenjevanju, večje v primerjavi z izbranimi standardnimi mehanskimi vijačnimi elementi, ki se uporabljajo pri leseni gradnji. S študijo smo pokazali, da se lepilni spoji z večjo debelino in ustrezno vrsto lepila lahko uporabijo pri sezmičnem projektiranju lesenih stavb. Poudarek zadnje študije je bil na proučevanju vpliva fenol formaldehidne smole z majhno molekulsko maso, s katero smo impregnirali celične stene lesa, na spremembe dinamičnih mehanskih lastnosti lesa.*

*Kljub večji statičnih trdnosti pri modificiranem rdečem boru (*Pinus sylvestris* L.) in evropski bukvi sta bili udarna upogibna trdnost in odpornost na utrujanje močno zmanjšani, medtem ko sta ciklični elastični modul, kot tudi stopnja lezenja v stacionarni fazi, ostala nespremenjena. Tovrstne ugotovitve kažejo na pomembnost zavedanja načina uporabe modificiranega lesa, saj izpostavljenost dinamičnim obremenitvam zmanjšano njegovo življenjsko dobo.*

Ključne besede: : lepilni spoj, lomne karakteristike, fleksibilna lepila, odpornost na utrujanje, mehanske lastnosti lepljencev

Contents

Acknowledgement	III
Abstract.....	V
Povzetek.....	VII
Contents	IX
1 Introduction	1
1.1 Problem and Purpose.....	3
1.1.1 Fracture properties of adhesives	3
1.1.2 Flexible adhesive as an energy dissipator.....	5
1.1.3 Dynamic mechanical properties of resin-modified timber	7
1.2 Research Aims and Goals	10
1.3 Hypotheses	10
1.4 Authors contributions	11
1.5 Materials and Methods	11
1.5.1 Article 1	12
1.5.2 Article 2	12
1.5.3 Article 3	13
1.5.4 Article 4	14
2 Published Articles	15
2.1 Article 1.....	15
2.2 Article 2.....	27
2.3 Article 3.....	41
2.4 Article 4.....	54
3 Summary of Studies	66
3.1 Article 1.....	66
3.2 Article 2.....	67
3.3 Article 3.....	68
3.4 Article 4.....	69
4 Conclusions	70
4.1 Summary	70
4.2 Contribution to Science and Considerations for Future Research	72
Bibliography	75

5	Povzetek v slovenskem jeziku	85
5.1	Uvod	85
5.2	Raziskovalni nameni, cilji in hipoteze.....	87
5.3	Materiali in metode.....	88
5.3.1	Članek 1.....	88
5.3.2	Članek 2.....	89
5.3.3	Članek 3.....	90
5.3.4	Članek 4.....	90
5.4	Rezultati in diskusija	91
5.4.1	Članek 1.....	91
5.4.2	Članek 2.....	92
5.4.3	Članek 3.....	93
5.4.4	Članek 4.....	94
5.5	Zaključek	95
6	Appendix.....	97

Chapter 1

Introduction

The structure of wood enables the tree to live long, and grow taller and larger in mass than any other organism on earth. This very same material is responsible for the new engineering trends in modern society and is used in constructing multistorey and tall rise timber buildings. Wood as a construction material has many beneficial characteristics; among the most important are good strength to weight ratio, high thermal resistivity, and insulation, while its relatively low weight is desired in seismic actions. Besides the sustainable, environmental, and carbon-negative footprint of wood, in combination with improved processing technologies and building methods, there are favorable reasons for making timber an alternative to concrete and steel when used as construction material [1]. Initially the drive to use timber elements more efficiently led to applications of natural casein glue for glulam production and soy glue for the production of interior plywood in the early 19th century. After 1930 natural adhesives were quickly replaced with synthetic ones because of their resistance to water, ease of use, and economic advantages. A strong petroleum infrastructure and advances in polymer science made it possible for the widespread use of synthetic adhesives [2]. Replacing solid wood with engineered timber products (ETP) resulted in a growing interest in bonding various wooden elements, driving the demand for better performance and expanding the range of applications. Among these are products like glue laminated timber – glulam (GLT), laminated veneer lumber (LVL), cross laminated timber (CLT), and others. ETP show higher mechanical performance, can be manufactured in various dimensions from smaller tree diameters of lower timber quality, and have fewer variations in properties than solid timber [1,3,4].

According to Hunt et al. [5], more than 65 % of wooden products are bonded, which is a strong indicator of how essential it is to understand the adhesive properties in relationship to wood and wood-based products in timber structures under different conditions, and to comprehensively address its demands. Adhesive bonding is a technique for material joining where an adhesive bond forms between two surfaces – adherends [6]. The adhesive that forms an adhesive joint must transfer loads between bonded members and correspond to the level of stress concentration a bond can withstand [7]. A well-known adhesive bondline model introduced by Marra [8] emphasises the importance of how the weakest link is responsible for bondline failure. A better understanding of adhesive failure leads to progressive improvements in developing better performing adhesives [5]. For a long-term timber adherent joining, the relationship between adhesives and timber is indispensable. Adhesive bondline properties are affected by

several factors deriving from adhesive and wood properties as well as bonding processes [9,10]. Kamke and Lee [7] described bondline as forming a conglomeration of resin (adhesive) and wood by creating an interphase region. In general, adhesives often have to meet certain requirements, show structural integrity at different levels and conditions, and follow European Standards such as EN 301, EN 15425 [11] or other. Hunt et al. [5] stated that in an ideal bondline that exceeds quality standards the failure initiates in the wood far from the bondline, which means that the adhesive strength is greater than the strength of the wood. Lap-shear tests for structural adhesives following EN 302-1 are the methods most used to assess adhesive bondline strength. When bondline strength exceeds wood shear stress, this often leads to wood failure, and fewer properties and distinction between adhesives can be determined. Veigel et al. [12] emphasised how fracture energy testing offers a more diverse degree of information than standardised lap-shear testing when comparing two different adhesive systems. Fracture energy, specifically strain energy release rate (G), can be studied in three fundamental modes: mode I (tension), mode II (in-plane shear), and mode III (out-of-plane shear) as well as mixed modes [13]. Delamination phenomena can be described from the perspective of fracture propagation of adhesive bondline, where the fracture initiates under exceeding stress, and results in crack growth and formation of newly developed surfaces. In case of bondline, such a reaction takes place near material discontinuity, i.e. lumens, cell wall layers, air bubbles, agglomerates of adhesives, poor wetting of surface, and different material properties of wood-adhesives [14]. Similar actions take place under the delamination processes at any timber elements. Studies on adhesive bondline fracture are important for describing fracture material phenomena, especially by determining how different factors, from conditions to adhesive types and other, affect bonding properties [15].

Joints or connections in timber structures represent important building components, which by joining together structural elements provide stiffness, strength, ductility, and energy dissipation to the timber structure [16]. The purpose of bonding is to join elements, which also makes adhesive bonds a connection. Adhesive connections are desired and beneficial since they distribute stress more uniformly along the connection/bonded surface and reduce localised high stresses [17]. This is an advantage over typical mechanical fasteners that may cause undesired damage in the wood fibrous structure, introduce local stress concentrations, and change the structure such that water can enter the wood structure [4]. On the beneficial side, adhesive joints prevent crack propagation and can result in a longer fatigue life [18]. Recently, flexible connections have become a field of study in retrofitting heritage timber joints, strengthening timber-glass beams, and timber-glass walls [19–21]. Applications of flexible adhesive have shown comparable flexural stiffness between wooden laminated beams connected by elastomeric adhesives and standard, mechanical inclined screw connections [22] while better ductility of elastomeric adhesives for higher ultimate tensile loads were obtained compared with non-flexible brittle epoxy adhesives [23]. Using flexible polyurethane (PUR) adhesive layers in the design of glulam beams was shown to be beneficial with improved bending performance [24]. More recent innovations demonstrated alternative timber building

concept “Timber structures 3.0”, with a novel application of structural timber bonding without the use of mechanical fasteners [25]. Enhancing energy dissipation under seismic events, using a flexible bondline as a dissipating connecting element, has great potential for improvement of timber structures.

In the case of timber bonding applications, the bondline is essential for stress distribution but adhesive resins can be used in other fields. For example, they have been intensively studied as chemicals for wood modification. Thermal, chemical, or mechanical treatments to modify wood can improve its service life, dimensional stability, and mechanical properties [26,27]. A well-established wood modification process is chemical modification with thermosetting resins by using low molecular weight monomers and oligomers for wood impregnation. After the wood has been impregnated, it is cured, and a cross-linked polymer matrix is formed within the cell walls, which reduces penetration of water. Typical representatives for the in-situ polymerised adhesives are formulated based on formaldehyde co-monomers. They tend to be more reactive and usually are components with lower molecular weight that can penetrate the wood structure. Penetration of adhesive impacts bonding properties [7], but when adhesives are used as a reactant for wood modification, penetration is often a measure of a successful process. This is typically expressed in weight percentage gain as a result of residual adhesive resin in the wooden structure [28]. However, Furuno et al. [29] discussed how alkaline components in phenolic resins might result in changes in the cell wall components, leading to decreased elastic properties. Formaldehyde-based resins are highly brittle in nature [15] and, therefore, special attention must be given when PF modified wood is used for structural elements. Due to the rheological change between modified and natural timber, dynamic mechanical properties should not be neglected. High cyclic fatigue resembles millions of low-stress loading cycles, and it estimates the relationship between the stress and number of cycles to failure. The type of stress and duration cause initiation of micro-cracks that grow to macro-cracks, which further cause wood failure [13].

This thesis will address several innovative adhesive applications and experimental methods in the field of adhesive use in structural timber elements. The following section will identify knowledge gaps needing to be addressed to support the use of adhesives in these applications.

1.1 Problem and Purpose

1.1.1 Fracture properties of adhesives

Bonding properties of wood evaluated under shear tests are the most frequent loading mode in the service life of adhesives [30]. Sterley et al. [31] emphasised that using shear tests, which are a standardised test method for analysing adhesive bonds, identify the percentage of wood to adhesive failure, and only indicates if either the wood or the adhesive bondline is more likely to fail, but does not provide any information about the fracture. Adhesive joints are commonly loaded in different loading modes, i.e mode I -

tension, mode II – shear, and mode III – torsion, including their combination; among these mode I is of primary importance due to its lowest fracture energy to the onset of cracks [14]. Among many simulation models applicable to adhesives, cohesive zone modelling is a numerical technique for describing crack initiation and propagation with traction-separation law which can be represented by triangular, linear-parabolic, polynomial, exponential, trapezoidal, or the most widely used bilinear law, constructed by initial joint stiffness, ultimate load, and critical energy release rate [32]. Ease of implementation into various finite element platforms, simulating adhesively bonded joints in debonding and crack growth in complex geometries, has made cohesive zone modelling a commonly used approach. In mode I and II, the technique requires input parameters from experimental tests such as critical energy release rate, peak traction, and ultimate displacement [32]. Fracture properties of adhesive bondline can be studied through beam theories where double cantilever beam (DCB) test for mode I and end-notched flexure (ENF) test for mode II are the methods used most often [33,34]. Different testing methods and experimental setups for obtaining cohesive zone models were presented for *Picea abies* L. under mode I test using single-edge notched three-point bending method [35], *Pinus pinaster* under mode II with end-notched flexure method [36] as well as for timber bonded joints [37–40]. There are fewer studies that describe fracture phenomena on European beech, which is an important wood species since it is currently the most widely spread hardwood in Central Europe [41]. Beech wood also shows great potential to be used for structural elements, i.e. GLT due to its high mechanical performance, beneficial bonding, and availability [42]. For the European beech wood, Rhône et al. [43,44] studied mode I and mode II including cohesive law model for welded beech wood joints under impact of moisture content. Sebera et al. [45] confirmed good agreement on the cohesive zone models developed for natural and thermally modified beech wood under mode II while cohesive zone models under mode I testing regime were developed for natural beech wood by Gómez-Royuela et al. [46]. Fewer studies have so far dealt with models with adhesives for bonded beech wood while on the other hand, fracture properties such as fracture toughness (K) or energy release rate (G) were more often studied on beech wood and bonded beech wood composites. With compact tension test, authors studied the fracture properties of thermally modified wood [47], and use of fractal dimension of cracks for describing fracture failure modes [48]. A study by Watson et al. [49] evaluated fracture properties of glued beech wood with one-component polyurethane (1C-PUR), polyvinyl acetate (PVAc), and melamine-urea formaldehyde (MUF) adhesives using compact tension test under mode I, and various climate conditions. A reduction in fracture toughness and wood failure was observed in samples with higher moisture content. Fracture toughness was also affected by adhesive type. Instead of end-notched flexure test or double cantilever beam test, mode I and II for bonded beech were also evaluated under the Arcan test using phenol resorcinol formaldehyde (PRF) and PUR adhesives [50]. In the study the authors reported no differences in energy release rate values between PRF and wood; however, a significant difference was found between PUR adhesive bond and wood. Clerc et al. [51] studied the effect of adhesive elastic properties on energy release rates under static and cyclic fatigue

testing under mode II and observed different G values for both adhesives and test regimes. According to River [14], loading in mode I is of high importance due to the tendency of wood joints to cleave and requires less energy for crack initiation [52]. There are many different test regimes and geometries for the application of mode I test, such as double cantilever beam, compact test, single edge-notched tension, asymmetric four-point bending regime, and single edge-notched three-point bending (SEN-TPB) [53]. The latter is favoured over double cantilever beam due to the crack plane direction, complex post processing adopting beam theories and influence of size and dimensions [35,53].

Literature indicates how some adhesive systems respond differently towards fracture, for bonded beech wood. However, these studies are often limited to either fewer number of adhesive systems and utilise diverse testing methods, which do not deliver a consistent comparison among the adhesive types. For that reason, a more comprehensive interpretation of the adhesive fracture would greatly benefit both perspectives (materials and methods) and contribute to a wider spectrum of results.

In the study an alternative testing method will be evaluated for analyses of adhesive bondline fracture characteristics. In the first part of the study we will determine fracture properties of adhesive bondline under tensile stress (mode I) by adopting single edge-notched three-point bending test for selected adhesives on bonded beech with bondline in both radial and tangential wood orientation. Additionally the impact of two elevated temperatures will be analysed. In the second part we will determine fracture properties under shear stress (mode II) of adhesive bondline for various structural adhesives used in bonded beech wood. Also a cohesive-law model for selected adhesives will be developed, which will be applied in the finite-element modelling for analyses of friction and grain angle effect.

1.1.2 Flexible adhesive as an energy dissipator

Connections in timber buildings are one of the factors that represent the ductile and energy dissipating elements. Behavior of CLT buildings under seismic events is dependent on connection performance along the structural elements [54]. Due to the lightweight timber structure larger deformations can occur in case of earthquake accelerations and a too stiff connection may result in higher accelerations in the upper floors [55] which results in poor serviceability for the occupants and property damage etc. To reduce such events, mechanical dissipative elements with desired mechanical behavior (stiffness – ductility) are placed in the structures where the largest deformations may be present. Besides commonly used nails, screws, dowels with combination of metal connectors (hold-downs, angle brackets, nail plates), few novel solutions using mechanical steel type connections have been further studied [56–60].

By addressing the benefits of adhesive connections against mechanical type connections such as uniform stress distributions, reduced high localised stress, preventing damage to the wood structure, less water ingress points, and lower cost [4,17] adhesive connections

may be beneficially utilised. Additionally, mechanical fasteners increases the weight, which for lightweight timber structures is not relevant, but the potential for the formation of a crack tip around the joints at numerous locations due to the occurrence of stress concentrations is more crucial [18]. Rigid thin bondlines are typical in bonding wood for load-bearing structural applications where creep needs to be prevented, and desired rigidity and strength need to be obtained. Flexible adhesives, on the other hand, show lower elastic modulus but higher extension at failure. Simultaneously transferring high loads and high deformations, highly deformable polyurethane-based flexible adhesive joints gain attention for alternative bonding and reinforcement of various materials [61]. Such adhesive systems were used to repair and increase the ductility of new connections for masonry composites and concrete [62,63]. Flexible adhesives have also been successfully applied for the repair and seismic strengthening of cracked masonry infills [61,64–66]. Their higher deformation capacity and energy dissipating properties are potentially useful in various applications in CLT structures [67] by increasing their seismic performance. Large overlapping areas in step joints and dissipative capabilities make connections designed with flexible adhesive a good candidate for improved timber joints for certain applications. Flexible adhesives have higher deformability and can even exhibit ductile behavior in comparison with traditional adhesives for joining timber elements, which are stiff, brittle [4], and have higher load-bearing capacity than wood, i.e. bonded material.

Greater bondline thickness in structural adhesives often result in internal bondline imperfections which leads to poor performance. On the other hand for more ductile-like adhesives, increasing overlap length results in increasing strength [68]. Studies investigated the effect of thickness and overlap length on ductile thick PUR joints and reported that with greater thickness joints are more flexible but with increasing overlap length, there is higher rigidity in the joints. Banea et al. [69] studied the effect of the thickness of flexible PUR adhesives and found a decrease in lap-shear strength with increasing bondline thickness, as opposed to an increase in fracture toughness. The latter can be explained by the fact that the more flexible – ductile adhesives undergo more plastic deformation which forms more plastic zones ahead of the crack tip and limit the damage zone, so it can dissipate more energy.

Thick flexible adhesive bonds can exhibit higher deformations and absorb more energy within dynamic events than rigid thin bondlines. Additionally, their damping capacity is beneficial since it reduces the transfer of noise and undesirable vibrations between timber elements. Among these benefits, more uniform distribution of shear stresses in the thick adhesive bondlines can improve fatigue resistance [70], resistance to seismic action [61,71], and damping properties [72]. Large strain capacity and peel force distribution make flexible adhesives good components in forming structural joints [68]. Bondline thickness and overlap length play an important role in the mechanical properties of the connection in the case of flexible adhesives but has not been intensively studied in combination with timber elements. Applications of flexible adhesive bondline along

timber connections could potentially be utilised in vertical step joints between adjacent CLT wall panels which may result in reduced stiffness but with higher displacement capacity when exposed to cyclic loads [73,74]. Literature shows the advantages of flexible adhesives, which so far have been identified through limited studies and indicate great opportunities for utilising such adhesive systems bondline as an energy dissipating member in timber connections. The great potential in the area of flexible adhesives used with structural timber offers new innovative research topics with promising applications, in particular, topics related to connections with enhanced damping capacity, load transfer, or improve energy absorbance.

In the study related to evaluation of mechanical properties of thick flexible adhesives we will assess adhesive bondline and its properties under reverse cyclic shear loading as an energy dissipating connection for timber structures and analytically compare these with common timber mechanical screw-type fasteners.

1.1.3 Dynamic mechanical properties of resin-modified timber

Wood modification alters properties of the raw material to improve resistance to biotic and abiotic factors, changes visual appearance, and physical or mechanical properties. Modification of wood adds value to less valuable, underutilised wood species and can successfully increase the use of wooden products [27]. A well-established wood modification process is chemical modification with thermosetting resins by impregnating wood with monomers and oligomers of low molecular weight. The general mechanism behind impregnation of wood with chemicals is that these molecules enter the wood structure (cell wall) and polymerise inside the structure. This results in cell wall bulking and changes in the hygroscopic properties of the cell wall [26]. One such resin is phenol formaldehyde (PF). PF has a long service record (> 50 years) in the wood industry as an adhesive used for manufacturing engineered wood products such as GLT. Impreg and Compreg were among the first commercially available products where wooden veneer sheets were impregnated with PF resins, then dried and oven-cured when the cell wall structure is swollen (Impreg), or additionally cured under pressure for increased density (Compreg). Such material resulted in improved dimensional and anti-swelling properties [75].

Besides the various studies that investigated the effects of PF modification on dimensional or color stability, durability, acoustic properties, and resistance to biotic factors [28,76–82], there are studies that looked at the impact on mechanical properties. Deka and Saikia [83] impregnated *Anthocephalus cadamba* Miq. with PF resin and found an increase in strength properties with the material showing a 12 % increase in modulus of elasticity (MOE) and a 21 % increase in modulus of rupture (MOR) with respect to the untreated one. Huang et al. [84] treated Chinese fir (*Cunninghamia lanceolata*) using low molecular weight PF resin and obtained a 31 % increase in longitudinal tensile modulus of elasticity. Impregnation of beech veneers for LVL and plywood composites as well showed improved bending properties [85,86].

On the other hand, literature often reports that embrittlement of impregnated modified wood results in decreased ultimate tensile strength and dynamic strength like impact bending strength (IBS) among others. Evans et al. [87] showed reduced tensile strength of PF modified veneers with positive correlation between increasing PF concentration level and tensile strength loss. Bicke et al. [85] modified beech (*Fagus sylvatica* L.) veneers with PF resins for plywood production and reported 34 % lower IBS values in a parallel orientated direction. Bollmus et al. [88] modified Scots pine using melamine formaldehyde resin of low and high molecular weight PF resin and dimethylol dihydroxyethyleneurea (DMDHEU) using various solution concentration loadings. Overall, the study reported significantly decreased IBS values with already very small concentration solution levels (0.5 %). Authors reported that embrittlement could be more related to molecular weight and its ability to penetrate the cell wall rather than the degree of modification. According to Kielmann et al. [89], ash (*Fraxinus excelsior* L.), beech (*Fagus sylvatica* L.), and maple (*Acer platanoides* L.) wood modified with methylated N-methylol melamine showed decreased impact bending strength (IBS) for treated samples compared to controls. IBS decreased between 35 % and 48 % for ash and beech, and between 55 % and 67 % for maple while also Epmeier et al. [90] reported a more than 50 % reduction in IBS for pine wood (*Pinus sylvestris* L.) treated with methylated melamine formaldehyde. Increased brittle behavior of chemically modified timber has often been discussed [82,88,91]. Bollmus et al. [88] who also studied impregnation using small molecular weight PF resin, pointed out that penetration into cell wall, pH-value, cross-linking, and formaldehyde content are as main factors influencing elastic mechanical properties like brittleness. The authors discussed how low-molecular PF resin successfully penetrate through nano-pores and are distributed in the cell wall. Furuno et al. [29], reported about alkaline components in phenolic resins that might cause changes in cell wall components, and lead to decreased elastic properties of such material. Moreover, entry of PF molecules into the wood cell wall and cell lumen, with a combination of acidic catalysts polymers, establishes a new cross-linking cell wall network and leads to a rigid, non-pliable cell wall structure [92]. The effect of long-term repeated loading stresses on the material can lead to its sudden failure. An increasing number of cracks, their growth, and material fatigue can lead to weakening of the material and its sudden unpredicted failure [13]. Besides IBS, fatigue limit is also associated with dynamic mechanical properties. To assess fatigue strength or fatigue life, materials typically undergo fatigue test until failure or a series of a high number of cyclic loadings (10^6). Results are presented with the Wöhler S-N curve as a relationship between the number of loading cycles and stress level (fatigue strength). Fatigue limit is the largest stress amplitude that does not lead to continuous crack growth until failure [93].

Stress level at which the specimen is being tested and the ratio between minimum and maximum stress level (R ratio) must be precisely selected as they have a strong impact on test performance. With the $R = -1$ loading is in fully reverse cycle going from extreme negative to extreme positive position (largest amplitude) with specimen being under constant load. The intensity of these regimes was reported in [94]. The authors tested

fatigue life in flexure and reported an increase in damage with decreasing R values from 0.5 to -1. This is just one parameter that influences fatigue performance of wood. For loading frequency, studies reported fewer number of cycles with lower loading frequencies [95,96]. After each loading cycle, damage is accumulated in the wood and the amount of work per cycle is also dependent on loading waveform due to stress rate and peak stress [13]. Literature also reports that a square wave loading form, compared to sinusoidal or triangular, results in the most damage for solid wood and some wood-based composites [95–98]. Another loading variable that impacts fatigue behavior is also accumulation of loading sequence and how accumulated deformation increases with low-to-high or high-to-low loading sequence [13]. These are parameters related to test setup, while there are additional variabilities derived from wood's natural heterogeneity and anisotropy. Scots pine and beech wood (*Fagus orientalis* L.) were tested under three-point bending test at different stress levels in terms of the ultimate strength of the material. A total of 10^6 number of cycles were reached at 40 % and 50 % stress level for pine and beech, respectively [99]. This indicates how wood with higher density experience less fatigue reduction regardless of the material ultimate load. Similar conclusions were reached by other researchers [94,100]. However, a limited number of studies have evaluated the effects of wood modification on fatigue properties. Ratnasingam and Mutthiah [101] studied fatigue strength of oil palm (*Elaeis guineensis*) wood with test specimens taken from different stem positions. With increasing density, improved fatigue life was observed in the middle and center parts of the tree treated with PF. Yet another study by Sharapov et al. [102] investigated the impact of thermally modified pine (*Pinus sylvestris* L.) on residual strength at different moisture content levels. Authors have reported that the initial moisture content before the fatigue test and highest level of thermal treatment were identified as the most important parameters regarding the residual strength. Nevertheless, it can be concluded that stress level derives from estimated ultimate strength of the specimens which is also density dependent. Since both parameters are positively related with wood modification, the ultimate threshold level is consequently higher. On the other hand, highly brittle PF modified timber results in decreased dynamic properties; therefore, fatigue strength must be extensively evaluated, especially when modification is used to achieve improved strength properties for loadbearing elements.

The dynamic mechanical properties of PF resin-modified wood of soft and hardwood species will be investigated by performing three-point bending cyclic fatigue tests and impact bending tests.

1.2 Research Aims and Goals

The overall research aim of this thesis is to describe wood-adhesive interactions which are considered important for applications in structural engineering. The following research questions have been identified:

Research Question 1

How do fracture properties differ based on the type of adhesive used?

Research Question 2

Can flexible adhesives be used as alternatives to mechanical fasteners in structural timber joints?

Research Question 3

How does resin-modification of wood affect the dynamic strength properties?

Based on these research questions, the thesis is divided into three sections which are addressed by four studies exploring the interactions between wood and adhesives which are considered important for applications in structural engineering.

Articles 1 and 2 describe fracture properties of selected structural adhesives on bonded beech wood. Specifically, in Article 1 the main goals were to: (i) verify the test method, (ii) assess impact of the adhesive system on fracture characteristics, (iii) examine the effect of elevated temperature, and (iv) examine the effect of wood grain orientation. Article 2 further deals with fracture properties and the goals were to: (i) develop cohesive law models for selected structural adhesives based on the experimental inputs and data analyses, (ii) report adhesive fracture properties, (iii) model and examine the impact of friction, and (iv) analyse impact of wood grain orientation on stiffness using developed numerical model. Article 3 describes applications of thick flexible adhesive to describe mechanical characteristics of adhesive timber joints. The main goals of the study were to: (i) evaluate impact of adhesive properties under cyclic testing, (ii) show the effect of bondline thickness on joint mechanical characteristics, and (iii) compare adhesive connections with mechanical-type connections. The last experimental study (Article 4) deals with the dynamic strength of resin modified timber elements and it focused on the following goals: (i) modify wood with low molecular weight polymers, (ii) examine the impact of modification on static bending strength and IBS, (iii) examine cyclic fatigue strength on modified wood, and (iv) show the impact of modification on a cyclic creep.

1.3 Hypotheses

The following hypotheses will address selected aspects of the research questions in section 1.2. The article in which individual hypotheses are tested is identified in parentheses.

H1: Fracture energy (G_f) and critical strain energy release rate (G_c) will perform significantly different along the adhesive type (Article 1 and 2).

H1.1 Different G_f and G_c will be obtained as a result of wood bondline plane orientation (Article 1).

H2: Adhesives with a lower modulus of elasticity and with a greater bondline thickness will satisfy required mechanical characteristics of joints for seismic design (Article 3).

H3: Wood impregnation with PF resin will have a negative impact on the fatigue strength of modified wood (Article 4).

1.4 Authors contributions

Article 1

The candidate, Jaka Gašper Pečnik, was responsible for the design of the study, conducting the preliminary design of testing, preparation of sample tests and testing groups, conducting the experimental analyses for compression, lap-shear and fracture three point bending tests and participated in the analysis of fracture properties, statistical analyses, and for being the principle writer of the manuscript.

Article 2

The candidate was responsible for conducting the experiment, including bending test for fracture properties in combination with digital image correlation (DIC). The candidate contributed to evaluation of the DIC data which were combined and necessary for development of cohesive law models. The candidate contributed in the parts of fracture analyses results. Candidate contributed in the writing the manuscript section of introduction and materials and methods.

Article 3

The candidate was responsible for developing an analytical approach which adopted a selected standard for cyclic testing of the specimens. Candidate prepared the samples, conducted both monotonic and cyclic testing, prepared the loading protocols and analysed the results. Candidate participated in the evaluation of the entire set of the results and with that contributed to producing main outcomes of the experimental test. Candidate was and the principle writer of the manuscript.

Article 4

The candidate was responsible for the static bending testing, dynamic impact bending testing and had a major role in fatigue testing. Candidate conducted modification of wood specimens for additional study following the procedure in manuscript. The candidate

conducted and participated in the analyses of the results. Candidate was and the principle writer of the manuscript

1.5 Materials and Methods

1.5.1 Article 1

Polyurethane (PUR) and melamine urea formaldehyde (MUF) were used as structural adhesives and emulsion polymer isocyanate (EPI), was used as a non-structural adhesive. Lap-shear specimens were prepared according to EN 302-1 [103] to evaluate bondline shear strength under lap-shear testing based on the selected manufacturing conditions and mixed wood grain orientation. For the fracture tests, beech lamellae were planed, cut, and conditioned at standard climate conditions (20 °C, RH = 65 %) prior to bonding. Composite lamellae were cut into small blocks to follow geometry from NT BUILD 422 [104] standard for mode I testing by controlling area of the crack vs adhesive bondline. To study the impact of wood grain orientation bonded lamellae were manufactured with two wood plane orientations by having RT and TR orientation: the first index indicates normal plane to crack, and the second index is the direction of crack propagation. The testing method followed single edge notched-three-point bending tests (SEN-TPB) [35] which were performed at the universal testing machine. To assess the impact of temperature, soaking and tempering of specimens was performed at two selected elevated temperatures (70 °C and 140 °C) prior to testing. The detailed plan of material groups and testing procedure is described in Article 1. Procedure from Dourado et al. [105] was followed to calculate the strain energy release rate (G_I), and the critical fracture energy (G_c). According to the size of small specimens, factor k from the proposed study was adjusted. Total fracture energy (G_f) was calculated as area under the F/δ curve. For estimating the impact of temperature on the modulus of elasticity of beech wood in the longitudinal direction, compression tests of tempered specimens were also performed, from which values were used in the calculation of the G_I . Linear models were fitted to log-transformed G_c and G_f as independent variables. Each model had the following dependent variables: adhesives, orientation, and treatment. Analytical results were presented as medians with 95 % confidence intervals, and comparisons were ratios between the medians of the levels of each presented factor. Tukey's HSD test was used to test for differences in the results of the lap-shear and compression tests.

1.5.2 Article 2

Article 2 focused on the experimental evaluation of three structural adhesives: PUR, MUF, PRF, and one non-structural adhesive (EPI) loaded by three-point end-notched flexure test (3ENF). Using the compliance-based beam method, cohesive laws were constructed for different adhesive systems tested on bonded beech wood loaded under mode II. Beech lamellae were glued together to follow the geometry according to Yoshihara [106] and an artificial crack with 182 mm was introduced. All specimens were conditioned at standard climate conditions prior to testing. The artificial crack was

introduced by the inserted Teflon paper which served as a barrier for adhesive spread over the wooden surface. The surface of specimens was covered with black and white stochastic pattern to better utilise digital image correlation computation afterwards. Three-point bending tests were conducted with a universal testing machine, while digital image correlation was used to optically monitor displacement slips and to compute strains over the specimens' surface. Force-displacement diagrams were obtained from the universal testing machine, which was synchronised with optical measurements for accurate recording of the specimens. Displacements slips (w) around the crack tip from recorded data were used to analyse displacement at the crack tip with crack propagating during the shear slip. Energy release rate (G_{IIc}) was obtained according to [36,107], which precisely describes the procedure for data reduction and G_{II-w} curves (fracture crack propagation). Experimental results were coupled by finite element analyses adopting boundary conditions from the experimental tests. Cohesive law was modeled using bilinear function. Three different material models were considered for analysing properties of beech. With the proposed finite element model, two sensitivity analyses were made to assess effect of friction coefficient between wooden lamellae and effect of fiber angle in the longitudinal orientation. Details on the parameters selected for modelling is presented in Article 2.

1.5.3 Article 3

Article 3 follows EN 12512 and ISO 16670 standard testing procedure [108,109] for testing mechanical fasteners for timber structures using the reverse cyclic shear testing method to evaluate flexible adhesive joints. Three adhesives with different mechanical properties were tested using double lap-shear test specimens, made with two thick target thicknesses of 10 and 15 mm. Norway spruce (*Picea abies* L.) was selected for this study as it is the most commonly used wood species in the production of CLT elements. Based on the static shear tests, for each adhesive group and thickness, a cyclic loading protocol was prepared. Experimental test was obtained on the universal testing machine to obtain force-displacement diagrams while linear position transducer was used for cyclic testing to locally monitor displacements of the joints. Force-displacement diagrams from static loading and hysteresis loops from cyclic loading were analysed according to proposed standard methods for elastic and plastic stiffness, shear modulus, force and displacement at the yielding point, maximum load, displacement at maximum force, maximum shear strength, ultimate load, ultimate displacement, ultimate shear strain, and ductility. Analytical comparison between experimentally observed results and commonly used mechanical screw-type connections typical for CLT obtained from [54] were made for adhesive joints, a single screw, and a series of equally spaced screws. In addition, double lap-shear experiments were modelled using finite elements to numerically describe behavior of double-lap shear specimens and perform a sensitivity study on the influence of adhesive bondline thickness by “what-if” scenarios that were not tested experimentally.

1.5.4 Article 4

Article 4 evaluated the impact of wood impregnation with low molecular weight phenol formaldehyde resin on the behavior of dynamic mechanical properties. Softwood (Scots pine) and hardwood (European beech) species were selected for the test. The treated group was impregnated with low molecular weight phenol formaldehyde resin and the untreated group represented the control group. After conditioning all the specimens, a dedicated number of specimens was submerged in aqueous phenol formaldehyde solution and placed in the vacuum chamber. After 30 min the specimens were exposed to a slow drying regime followed by oven drying and curing to complete the treatment procedure. After that the specimens remained at standard climate conditions until testing. For the treated group, weight percentage gain and wood bulking due to impregnation methods were obtained. Modification of the wooden specimens was demonstrated on cross sections of selected specimens using the scanning electron microscope. Specimens were first tested under static three-point bending following DIN 52186 [110] standard testing method. Based on the static bending test ratio between plastic and elastic, strain was calculated, and correlation between modulus of elasticity and modulus of rupture was established to propose different stress levels under which cyclic three-point bending tests were held. Cyclic loading tests were performed with pulsative sinusoidal waveform with constant mean stress calculated for each material type and stress level. Cyclic tests were performed at a frequency of 10 Hz until failure or until the threshold value of 10^6 loading cycles was reached. This threshold was selected as the fatigue strength limit for the proposed study. Based on the cyclic loading diagrams, change in the cyclic modulus of elasticity and cyclic creep were evaluated over the recorded number of loading cycles. Additionally, Charpy impact bending tests following DIN 52189 [111] were performed to determine the effect of modification on impact bending strength.

Chapter 2

Published Articles

2.1 Article 1

Title: Mode I fracture of beech-adhesive bondline at three different temperatures

Authors: Jaka Gašper Pečnik, Andreja Pondelak, Michael David Burnard, Václav Sebera

Year: 2022

Journal: Wood Material Science and Engineering (ISSN: 1748-0280)

DOI: <https://doi.org/10.1080/17480272.2022.2135135>

Link: <https://www.tandfonline.com/doi/full/10.1080/17480272.2022.2135135>

Mode I fracture of beech-adhesive bondline at three different temperatures

Jaka Gašper Pečnik ^{a,b}, Andreja Pondelak ^c, Michael David Burnard ^{a,b} and Václav Sebera ^d

^aInnoRenew CoE, Izola, Slovenia; ^bAndrej Marušič Institute, University of Primorska, Koper, Slovenia; ^cSlovenian National Building and Civil Engineering Institute, Ljubljana, Slovenia; ^dDepartment of Wood Science and Technology, Faculty of Forestry and Wood Technology, Mendel University in Brno, Brno, Czech

ABSTRACT

Single edge-notched three-point bending tests (SEN-TPB) for mode I were utilized to experimentally evaluate fracture properties of adhesive bondlines in European beech (*Fagus sylvatica* L.). The bondline was examined at two anatomical planes with TR and RT orientation and at control and two elevated temperatures (70°C and 140°C). Among epoxy (EPI), melamine-urea formaldehyde (MUF), and polyurethane (PUR) adhesives, the highest average critical energy G_c with 0.80 N/mm and fracture energy G_f with 1079.4 N/mm were obtained for EPI in the TR plane and under standard climate conditions (20°C/65% relative humidity), followed by MUF ($G_c = 0.50$ N/mm and $G_f = 620$ N/mm) and PUR ($G_c = 0.25$ N/mm and $G_f = 290.9$ N/mm), respectively. PUR was least effected by elevated temperature, and no significant differences for G_c and G_f between TR and RT bondline orientations were found for MUF and PUR treated at 20°C/65% relative humidity while comparisons between other factors varied significantly. Treatment of specimens at elevated temperatures resulted in reduced fracture performance regardless of wood grain orientation or the adhesive system.

ARTICLE HISTORY

Received 15 July 2022
Revised 3 October 2022
Accepted 9 October 2022

KEYWORDS

crack; fracture; grain orientation; temperature; European beech

Introduction

European beech (*Fagus sylvatica* L.) is currently the most widely spread hardwood species in Central Europe (Ehrhart 2019). Although a recent model shows a decline in stock and negative long-term yields in decades to come, due to severe climate change (Ehrhart 2019, Martinez del Castillo *et al.* 2022), beech could become a prospective hardwood species for structural/timber members, such as glue-laminated timber (GLT), due to its high mechanical performance, good bonding characteristics, and wide availability (Glavnič Uzelac *et al.* 2020). Adhesive joints are commonly loaded in all three modes (mode I – tension, mode II – shear, and mode III – torsion), and their combination is of concern. Mode I is regarded to be of primary importance due to its lowest fracture energy to onset cracks (River 2003). Since the fracture toughness of wood tends to be smaller in mode I than for mode II or III, the crack onset in mode I requires less energy for its initiation (Yoshihara and Kawamura 2006). To characterize fracture in mode I, one can use several tests and specimen geometries such as double cantilever beams (DCB), compact tensile tests (CT), single edge-notched three-point bending tests (SEN-TPB), or single edge-notched-tension and asymmetric four-point bending (Yoshihara 2010). The linear elastic fracture mechanics (LEFM) approach of strain energy release rate (G) and stress-intensity factor (K) are known as global energy balance and local stress distribution around the crack tip, respectively, with G standing for available energy for crack

growth and K as fracture toughness (Smith *et al.* 2003). The author favors G , as it is directly measured from the energy input needed for developing a new surface, while K is more of an integration constant with high accuracy on crack tip geometry and indirect physical meaning.

Some studies conducted on beech wood followed CT test for analyzing adhesive bondlines (Watson *et al.* 2013), impacts of thermal treatment (Majano-Majano *et al.* 2012), fracture properties in relation to fractal dimensions (Hu *et al.* 2021), and methods comparison for calculation of K value (Merhar and Bučar, 2013). According to Yoshihara and Usuki (2011) K_{IC} often measured by CT test delivers material's localized parameters as a material property and provides less information than G . With a smaller effect of crack length on outputs, the DCB test was favored and recognized as the most appropriate testing approach (Yoshihara and Kawamura 2007). DCB tests were used to investigate G for two structural adhesives with the impact of different climate conditions (Ammann and Niemz 2015b), to develop a cohesive law for beech wood in TL plane (Gomez-Royuela *et al.* 2022), and to study the impact of wood thermal modification on fracture phenomena in mode II (Sebera *et al.* 2019). Bondline fracture of various structural adhesives in mode II was also studied by Sebera *et al.* (2020) who confirmed the application of DCB three-point bending test for characterizing adhesive bondlines on bonded beech. While Clerc *et al.* (2019) studied crack propagation in mode II under a cyclic loading regime coupled with acoustic emission. On the other hand, according

CONTACT Jaka Gašper Pečnik  jaka.pecnik@innorenew.eu  Andrej Marušič Institute, University of Primorska, Muzejski trg 2, 6000 Koper, Slovenia

 Supplemental data for this article can be accessed online at <https://doi.org/10.1080/17480272.2022.2135135>.

© 2022 The Author(s). Published by Informa UK Limited, trading as Taylor & Francis Group
This is an Open Access article distributed under the terms of the Creative Commons Attribution License (<http://creativecommons.org/licenses/by/4.0/>), which permits unrestricted use, distribution, and reproduction in any medium, provided the original work is properly cited.

to the published studies adopting the SEN-TPB test, authors favor this method over DCB because (i) the crack plane direction due to orthotropic wood structure, where among six principal systems, RL and TL are adequate for DCB only (de Moura *et al.* 2010), (ii) complexity of adopting beam theory for calculating fracture toughness (Yoshihara 2010), and (iii) influence of size and dimensions for reduced material variability (de Moura *et al.* 2010, Dourado *et al.* 2015). Dourado *et al.* (2008) described that the fracture process zone (FPZ) in the SEN-TPB test is determined by specimen geometry and material characteristics, which led to more developed data reduction schemes to overcome the issues with various test setups. A data reduction scheme using compliance-based beam theory, equivalent crack length approach, and triangular-shaped stress relief region (SRR) allowed the formation of crack-resistance curve without using crack tip displacement monitoring, only by means of load-displacement diagrams and not being material sensitive (De Moura *et al.* 2010). Since the triangular shape of SRR was not fully applicable for specimens with any beam dimension and with difficulties using alternative procedures such as the bisection method, Dourado *et al.* (2011) proposed modification of the method towards the use of rectangular SRR, which enabled a direct calculation of equivalent crack length (a_{eq}) and G_I .

The effect of elevated temperature on adhesive-bondline performance has been investigated in several studies that show a general pattern – an increase in temperature typically results in decreased mechanical performance. Richter *et al.* (2006) reported the importance of the chemical composition of PUR adhesives and bondline thickness on the mechanical performance of adhesives under elevated temperatures. The impact of the chemical composition of PUR adhesives on the shear strength obtained by a lap-shear tensile test was also confirmed by Clauß *et al.* (2011) who examined various adhesives against resistance to temperatures from 20 to 220°C. For most adhesives, the study showed decent thermal stability up to 150°C, while higher temperatures resulted in greater decreases and changes in failure behavior. Study by Sedláčik and Šmidriaková (2012) found decreasing shear strength for bonded beech and spruce wood on several adhesives with increasing temperature up to 110°C as well as for spruce finger joints under bending test. Finger joints glued with four 1C-PUR adhesives and melamine-urea formaldehyde (MUF) tested at elevated temperatures were also studied by Klippel *et al.* (2011), who reported PUR systems were more affected by increasing temperature than MUF. A comprehensive study on the fracture toughness of wood and wood-based composites exposed to elevated temperatures was done by Sinha *et al.* (2012). With elevated temperature, fracture properties (steady-state strain energy release rate – G_{SS}) were also reduced, and for the laminated composites with higher resin content, an even more severe decrease was observed.

Previous findings clearly demonstrate the importance of studying and reporting the effect of elevated temperature when performing adhesive bond testing and fracture properties should be included in these studies. Accordingly, the objectives of this study were: (i) to employ SEN-TPB to

characterize beech-adhesive bondline made with three different structural adhesives, (ii) to obtain strain energy release rate and fracture energy of adhesive bondline with selected adhesives, (iii) to evaluate the influence of bondline plane orientation (RT and TR) on fracture properties, and (iv) to evaluate the adhesive-bondline fracture performance under three different temperature regimes; 20°C, 70°C, and 140°C.

Materials and methods

For the process of bonding, the following structural adhesives were selected for the study: (i) a one-component polyurethane (1C-PUR) adhesive (PURBOND HB S309 type I), an adhesive for a non-brittle bond with chemical reaction during hardening and with fire resistance properties: (ii) a two-component D4 emulsion-polymer isocyanate (EPI) adhesive (Rakollit 280 and RAKOLLIT-Härter WS 1 hardener), which is an aqueous synthetic-based resin using an isocyanate compound for crosslinking; and (iii) a two-component liquid melamine-urea-formaldehyde (MUF) adhesive (Prefere 4535 with 5046 hardener, a type I) adhesive for load-bearing applications. The adhesive spread rate, pressing time, and pressure used for bonding were adopted from the manufacturers' guidelines and are presented in Table 1.

Specimen preparation and conditions

Knot and crack-free boards with growth ring orientation in tangential and radial directions were cut from European beech and conditioned in a climate chamber using standard conditions (20°C/65% relative humidity (RH)) to reach 12% equilibrium moisture content. Three pairs of lamellae were selected for each group of adhesives and each wood grain orientation to manufacture glued samples for each variable. Lamellae were planed and cut to final dimensions (length × width × thickness/400 × 40 × 10 mm) prior bonding. Density was determined for all lamellae, and grouped in pairs with similar densities. A thin layer of adhesive tape of 20 mm width was applied on the longer flat-side of one lamella to introduce an area without the bondline and ensure the initial crack tip. The flat-side bonded surface of the lamellae is differentiated in two wood plane orientations by having RT and TR orientations where the first index is normal plane to crack, and the second index is the direction of crack propagation. Beams were then inserted into the press following the selected pressing regime for each adhesive (Table 1). All the samples were pressed at approx. 20°C. After bonding, samples were conditioned at 20°C/65% RH. Wooden blocks

Table 1. Adhesive selection and processing conditions.

Adhesive	Spread rate (g/m ²)	Pressing time (h)	Pressure (MPa)	Mixing ratio	Viscosity (mPa s)
PUR	180	2	1	/	24,000 at (20°C)
EPI	150	2	1	100:14	10,000 at (20°C)
MUF	375	5	1	100:60	3000–3500 (25°C)

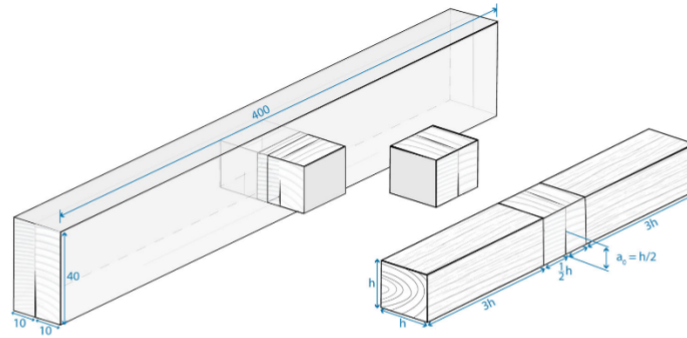


Figure 1. Manufacturing of beams (dimensions in mm) and schematic presentation of wooden block cut outs with geometry proportions (h = height) for SEN-TPB test specimens.

with dimensions of 20×20 mm (height \times width) were cut from the beams with a targeted 10 mm bondline area and 10 mm of an unglued area over the block height. These blocks were further extended with lateral beech arms with dimensions of $60 \times 20 \times 20$ mm (length \times width \times thickness) using PUR adhesive to manufacture the final specimen geometry. The proposed geometry followed the NT BUILD 422 standard (NT Build, 1993). In Figure 1, a schematic view of specimen with RT crack orientation is presented.

For each adhesive system and both wood plane orientations, 10 specimens were manufactured from each beam for a total of 30 specimens. Groups with specimens and orientations are presented in Table 2.

In addition to fracture specimens, standard lap-shear specimens were manufactured according to the EN 302-1 standard (CEN 2013) geometry to evaluate the adhesive strength and confirm the relevance of selected bonding parameters. Clean, knot-free beech lamellae were conditioned at $20^\circ\text{C}/65\%$ RH prior to planning and bonding. For each adhesive system, three pairs of lamellae were prepared with mixed grain orientation with a total of 18 specimens. Specimens were further conditioned until testing. The fracture specimens were randomly distributed into three groups for conditioning regimes with an even number of specimens per treatment. Specimens in the control (reference) group were conditioned at $20^\circ\text{C}/65\%$ RH until the testing. To assess the impact of elevated temperature on fracture properties, thermal treatments at 70°C and 140°C were held in the oven for the remaining two groups. One adhesive group at a time (20 specimens) was inserted into the

preheated oven. To estimate the time to reach the target temperature, a wired thermocouple temperature was inserted into a single extra specimen to monitor its temperature. After the target temperature was reached ($\pm 3^\circ\text{C}$), the specimens stayed in the chamber for one more hour. On average, the heating phase took 30 and 60 min prior to soaking at 70°C and 140°C , respectively. Additionally, the specimen was treated to obtain the MC of the group after the heating phase.

Lap shear, compression tests, and SEM

Lap-shear tests were performed on a Zwick Roell Z50 universal testing machine, using a 50 kN load cell and hydraulic grips. A testing speed of 5 mm/min was used. After specimen failure, its bonded area was measured with a caliper, and a visual estimation between wood and adhesive failure was carried out. To obtain the influence of temperature treatment on the modulus of elasticity in the longitudinal direction (E_L), compression tests parallel to the fiber (CT_{II}) were carried out using a Zwick Roell Z50 at a feeding rate of 2 mm/min. Information from CT_{II} was used as a material property of glued arms needed in the computation of equivalent crack length (a_{eq}) and flexural modulus (E_{IT}) using the beam compliance approach for mode I. For the CT_{II} tests, two groups of nine specimens with dimensions $60 \times 20 \times 20$ mm (height \times width \times thickness) were prepared. The first group of specimens provided E_L for the control group and group at 70°C since it is assumed that a temperature of 70°C does not have an impact on E_L as this temperature does not decompose the main structural polymerous constituents of the wood. Compression strain was determined as a relative change in distance between two points on the body surface recorded with an Aramis (Carl Zeiss GOM Metrology GmbH, Braunschweig, Germany) digital image correlation (DIC) system with 2 Hz data acquisition rate and camera resolution of 5 MPx. Volume and mass were determined prior to testing. After testing, the remaining specimens were dried at 103°C to determine the wood moisture content (MC) at testing. After the fracture testing, six specimens were cut into small fragments to obtain fractured images using a JEOL

Table 2. Crack plane orientations, adhesive system, average lamellae densities with standard deviation (SD), and number of specimens (n).

Crack plane	Adhesive	Average lamellae density (kg/m ³)	SD (l)	n. of specimens
RT	PUR	701	14.3	30
	EPI	716	25.1	30
	MUF	680	37.9	30
TR	PUR	761	45.3	30
	EPI	731	18.6	30
	MUF	691	6.5	30

JSM-IT500 scanning electron microscope (Oxford Instruments, Tokyo, Japan) operating at a low vacuum (70–80 Pa), at a working distance of 10 mm at an accelerated voltage of 15 kV.

Fracture measurements and analyses

Fracture testing was done using a Zwick Roell Z100 universal testing machine equipped with a 1 kN load cell to obtain the force–displacement response of specimens in three-point bending. The span between supports was 120 mm, and the loading speed was 3 mm/min. Tests were interrupted after reaching about zero force level. Treated specimens were tested one by one immediately after leaving the oven. After failure, the fractured area was visually estimated and the initial crack length (a_0) was measured with the caliper. SEN-TPB test was used to assess the fracture properties and develop crack–resistance curves. The selection of this geometry was guided with the aim of reducing wood anatomy impacts to obtain clearer grain orientation in the fracture area. LEFM, based on a data reduction scheme with the rectangular SRR proposed by Dourado *et al.* (2011), was used in this study. Calculation consisted of three steps. First, the flexural modulus (E_{TF}) was calculated:

$$E_{TF} = \left(\frac{L_2^3 - L_1^3}{bH^3} + \frac{L^3 - L_2^3}{b(H - ka_0)^3} \right) \cdot \left(\frac{C_0}{2} - \frac{L_1^3}{E_L bH^3} \right)^{-1} \quad (1)$$

where L is the half span, L_1 is the arm length from bondline to support, L_2 is the arm length shortened by SRR ($L_2 = L - ka$), b is the width of the specimen, H is the specimen height, E_L is the normal elastic modulus of arms parallel to fiber, a_0 is the initial crack length, C_0 is the initial compliance, and k is the non-dimensional parameter equal to 0.9. For smaller cross-sections, where higher compressive stresses occur due to bending, the k factor needs to be higher and closer to 1, which would define square SRR. Once the E_{TF} is obtained and used instead of E_T , equivalent crack length (a_{eq}) can be computed:

$$a_{eq} = \frac{1}{k} \left\{ H - \left[\left(\frac{C}{2} - \frac{L_1^3}{ELbH^3} - \frac{L_2^3 - L_1^3}{E_{TF}bH^3} \right)^{-1} \cdot \frac{L^3 - L_2^3}{E_{TF}b} \right]^{\frac{1}{3}} \right\} \quad (2)$$

where C is the current compliance. Utilizing Irwin–Kies solution, direct computation of strain energy release rate (G_i) was obtained by:

$$G_i = \frac{3P^2}{b^2} \frac{(L^3 - L_2^3)k}{E_{TF}(H - ka_{eq})^4} \quad (3)$$

where P is the force. Subsequently, from the G_i , the critical value of G_{ci} was obtained at maximal force P_{max} . Total fracture energy (G_f) was calculated as the area under the curve P vs. deflection. All fracture calculations were made using Matlab

R2021b (Mathworks Inc). Average Force–displacement curves were made as an arithmetic mean of the group till the end of the shortest group data set and using the linear interpolation function `interp1` available in Matlab package.

Statistical analysis

Fracture energy (G_f) and critical fracture energy (G_c) were analyzed to determine if and how wood grain orientation at bonded surfaces, adhesive or treatment temperature affected them. Linear models (LM) were fitted to log-transformed G_c and G_f as dependent variables (Suppl. Table 1, Suppl. Table 2). In each model, the independent variables were adhesives, orientation, and treatment. Individual factor effects and all two-way interactions were included in both models. Once transformed, the data met the assumptions of ordinary least squares regression. Due to the transformed dependent variables, analytical results are presented as medians on the untransformed scale with 95% confidence intervals (CI), and comparisons (contrasts) between levels of the variables are ratios between the medians of those levels when other variables are held constant. For example, comparing G_c between control specimens bonded in the TR plane, using two adhesive systems – e.g. EPI and MUF – would be reported as the ratio between the median G_c of the sample group with EPI and the sample group with MUF with a 95% CI of the ratio. P -values are omitted, but CI of comparisons that do not include one (1) are considered statistically significant. CI were adjusted using Tukey's method for comparing a family of three estimates. Only results of interest are presented in the paper; full results are available in supplemental tables. Tukey's HSD test was used to test for differences in the results of the lap-shear and compression tests. Effect sizes from these tests are reported as differences between estimated mean values with 95% CIs. Data analysis was conducted in R (version 4.2) using RStudio (version 2022.02.03). Comparisons between factors were calculated as marginal means using the `emmeans` package (Lenth 2022). The data and analytical code that support the findings of this study are available on Zenodo at <https://doi.org/10.5281/zenodo.7143370>.

Results and discussion

Lap-shear and compression tests

Results of the lap-shear test are presented in Table 3. The highest lap-shear strength was obtained for MUF adhesive with the lowest number of adhesive failures. In contrast, PUR adhesive group showed a 12.4% lower strength and also had the highest number of adhesive failures. Tukey's HSD test showed a significant difference in strength only

Table 3. Results of lap-shear tests for different adhesives, with number of tested specimens (n), average lamellae densities with standard deviation (SD), average strength, overall percentage of adhesive area failure, and number (n) of failed specimens in adhesive bondline.

Adhesive	n	Density (kg/m ³)	SD (°)	Strength (MPa)	SD (°)	Adhesive failure area (%)	Adhesive failure (n)
PUR	18	700	41.01	14.8	1.9	50–100	18
EPI	18	730	32.2	16.2	3.1	10–50	7
MUF	17	732	47.3	16.9	1.9	40	1

between MUF and PUR adhesive groups (MUF-PUR: 2.02 MPa, 95% CI: 0.09–3.96 MPa, $p = 0.038$). Nevertheless, bonding strengths of all adhesives surpassed a threshold strength of 10 MPa according to EN 302-1, A1 class for standardized climate conditions.

Clauß *et al.* (2011) reported slightly lower values for glued beech; 12.7 and 12.3 MPa for EPI and MUF, respectively, and between 12.1 MPa to 13.4 MPa for different PUR adhesive systems. Bachtiar *et al.* (2017) reported values of 13.4 and 12.9 MPa for PUR and MUF, respectively. The reported studies followed the wood grain angle between 30° and 90° but in the present study, the entire orientation range with radial and tangential (0°–90°) was tested. According to Hass *et al.* (2009), grain orientation in terms of bondline shear strength showed to be an important factor. Finally, all above-mentioned studies observed a lower percentage of wood failure for PUR adhesives compared to other adhesives. Nevertheless, in this study, lap-shear experiments were conducted only to confirm the quality of the selected bonding process.

Control specimens for compression tests were tested with an average MC of 10%, while treated specimens at 140°C reached MC below 1%. For the control group, the average density was 706 kg/m³, and the average E_L was 14.6 GPa (SD = 3.7); for the specimens treated at the elevated temperature (140°C), the average density and E_L were found 655 kg/m³ and 13.6 GPa (SD = 2.8), respectively. Tukey's HSD test suggested no significant difference between the two groups ($p = 0.53$); therefore, testing of specimens with elevated temperature treated at 70°C was skipped. Results for the control group are comparable with the existing reported literature below and it was expected that stiffness would increase for thermally treated specimens due to MC reduction (Kollmann and Côté 1968, Ozyhar *et al.* 2013, Straže *et al.* 2016). Hering *et al.* (2012) reported 13.9 GPa for E_L in CT_{II} measured by crosshead for beech wood with a density of 691 kg/m³ and 12% MC. Measurements of local deformation on the surface of the specimens using DIC provide more precise and reliable strain data than a global measuring

system based on reading displacement from the test machine. Gomez-Royuela *et al.* (2021) employed DIC for strain measurement in CT_{II} test and obtained E_L of 13.8 GPa for beech with a density of 677 kg/m³ and 12% MC. Further, Ozyhar *et al.* (2013) obtained E_L of 11 and 12.9 GPa for beech wood of 0% and 11% MC, respectively. However, none of the mentioned studies were conducted on the heated specimens. Visco-elasticity becomes more pronounced with a combination of heat and moisture which plasticize and soften the wood (Sandberg *et al.* 2021). Values of E_L obtained in the study were used for further calculations of fracture characteristics.

Fracture test and analyses

The fracture tests consisted of a series of SEN-TPB tests that resulted in force-displacement (F/δ) data sets for each adhesive and temperature (Figure 2). As is demonstrated in Figure 2, the maximal force (F_{max}) reached differs from adhesive to adhesive; however, all adhesives reveal the same pattern with respect to the effect of the temperature. As the temperature increases, F_{max} decreases significantly. The smallest decrease of F_{max} due to raised temperature is for the PUR adhesive. For the control and 70°C treatment groups, the highest rate of wood fracture was found for MUF in TR orientation, where most of the specimens fractured in the wood-adhesive interface (from 70 to 100% of fractured area). Fiber bridging in wood-adhesive interface failures resulted in a slower and longer decline in force after F_{max} was reached. Typically, the crack was initiated at the tip of the adhesive line and then propagated along the interface parallel to the bondline. In RT orientation, the majority of cracks propagated in the adhesive with specimens ranging between 30 and 50% wood fracture area. Similar observations were obtained for EPI in TR orientation but with a lower percentage of fractured area in wood (ranging from 40 to 90%). For the few cases within this group, crack propagated away from the bondline direction, i.e. in the direction of the wooden rays which ended up in slightly higher F_{max}

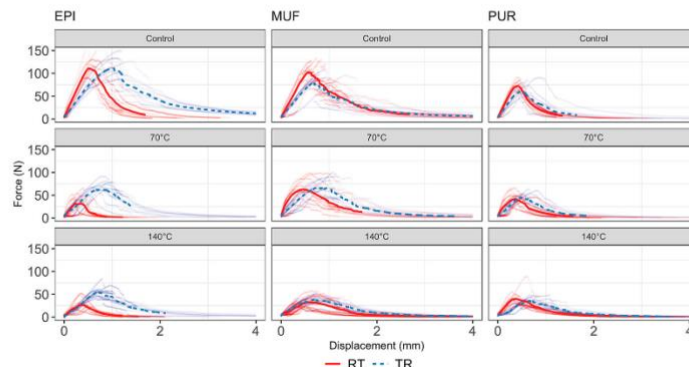


Figure 2. Force–displacement diagrams for each group of adhesives with different treatments. Average curves are presented with bold and dashed lines for RT and TR planes.

6  J. G. PEČNIK ET AL.

compared to those fractured in the bondline. Such cases are likely due to the variability of wood properties, which results in highly complex crack paths in the wood and around the bondline. On the other hand, EPI in RT orientation and PUR in both orientations resulted in pure adhesive (bondline) fracture with little or no fiber bridging in the wood-adhesive interface. For the 140°C group, MUF and EPI with TR orientation also exhibited an overall wood fracture area ranging from 50 to 100% failure. In RT orientation, all the adhesive groups fractured purely within the adhesive; only a few MUF specimens fractured in the wood-adhesive interface.

In Figure 2, bold lines represent the average curves of F/δ diagrams. In most cases, except for the MUF group at 140°C, the RT orientation resulted in higher initial stiffness. Conversely, it could be observed that after F_{max} was reached, the curves in groups with the RT bonding dropped more abruptly and in a more brittle manner. These findings can be attributed to the (i) impact of bonding direction and its influence on the adhesive penetration; (ii) adhesive system; (iii) difference in expected surface topography for the TR and RT planes, and (iv) MC of tested specimens. Not just orientation but also temperature treatment impacts the general curve shape. Regardless of the plane orientation for the control groups, a rather sharp decline in force was notable after reaching F_{max} . While on the other hand, temperature-treated groups reduced the brittle-like failures with a more steady force reduction. Such behavior can be argued with reduced fracture properties of wood material in the case of wood-adhesive fracturing, impact of moisture, and impact of temperature on the material properties, i.e. softening. MC for tested specimens was on average 7% and below 1% for 70°C and 140°C temperature treatment, respectively.

Reiterer (2001) observed the largest decrease in specific G_I when testing beech in the RL fracture plane from 60°C to 80°C. Changes in fracture parameters due to elevated temperature on solid wood were also reported for birch and spruce by Tukiainen and Hughes (2016) and Dourado and Moura (2019). On the other hand, Ammann and Niemz (2015b) reported higher G_I for PRF bondlines on beech wood when specimens showed 12% and 15% MC rather than 21%, but

no such influence was found for PUR bondline. It was also noted that composites with higher resin loading showed a larger decrease in G_{55} as temperature may deteriorate resins' capacity (Sinha *et al.* 2012).

Using Equations (1–3) resulted in relationships between strain energy release rate (G_I) and equivalent crack length (a_{eq}), as shown in Figure 3. For better clarity, Figure 3 shows only data slightly after reaching the critical value of G at F_{max} (G_c), so the effect of fiber bridging is visible only on F/δ diagrams.

In general, Figure 3 shows that all of the groups have a certain plateau for stable crack growth after reaching G_c , even though the data reveal high variability and noise at low values of G due to computational reasons at low forces and displacements. The variability of G progression might be lowered using even smaller loading speed than in our case (3 mm/min). It should be noted that G_c decreases as the temperature of treatment rises.

SEM studies of fractured surfaces for selected control specimens with the inserted images of the fractured specimens are presented in Figure 4. As it can be seen from these images, MUF and EPI with TR orientation are showing typical wood failure (Figure 4(c,e)) while PUR resulted in adhesive failure (Figure 4(a)). In the RT orientation, wood failure occurred only in the case of MUF adhesives, while adhesive failure occurred in the case of EPI and PUR adhesives (white arrows in Figure 4). There are several factors affecting bond properties like, i.e. gluing process, adhesive system, and wood (Gavrilović-Grmuša *et al.* 2012, Sterley 2012). It is well known that adhesives with high viscosity have low penetration ability into the wood; a thick interface results in a large portion of wood failure compared to a thin interface (Gavrilović-Grmuša *et al.* 2012). Low viscosity and a high amount of adhesive can explain the higher proportion of wood failure in MUF compared to the other two adhesives. It was reported that the penetration depth for European beech in the tangential direction is greater than in the radial direction (Sernek *et al.* 1999) while others indicate no major differences in penetration depth between radial and tangential directions (Gavrilović-Grmuša *et al.* 2012). Similar mechanisms of fractured

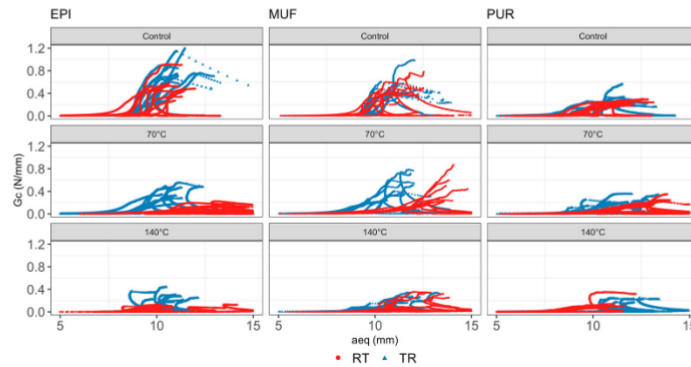


Figure 3. Strain–energy release rate vs. equivalent crack length at examined temperature for all adhesives.

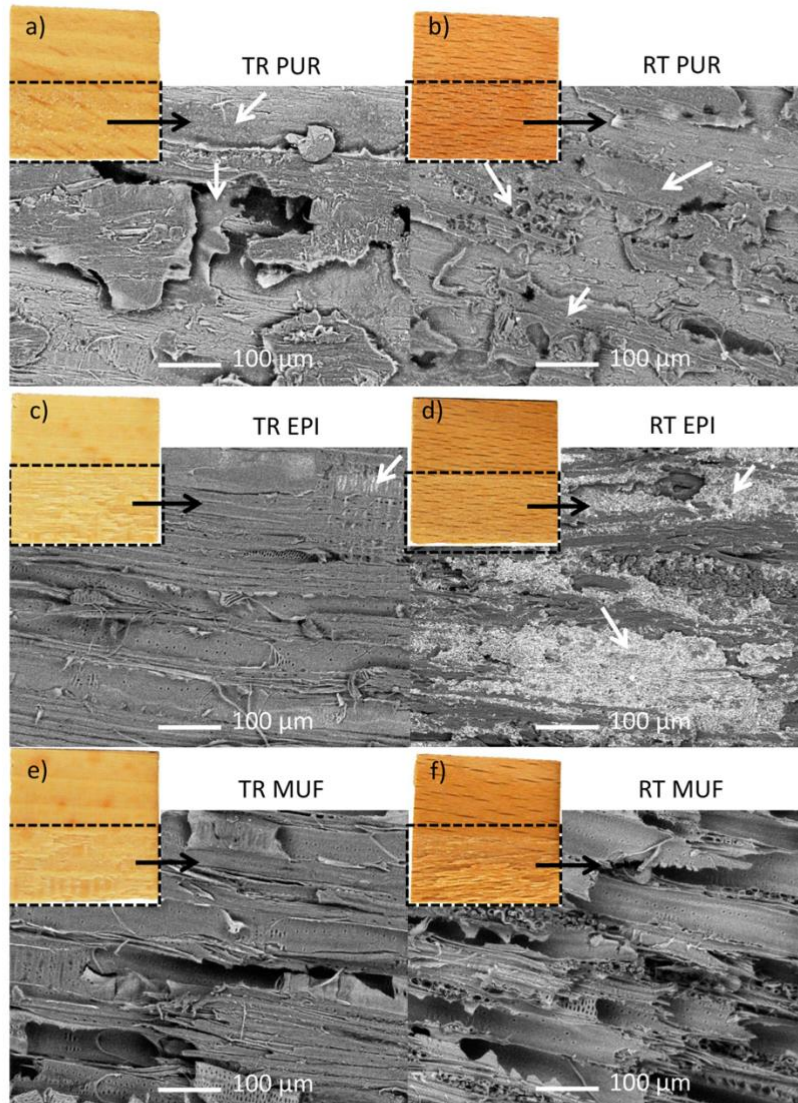


Figure 4. SEM images of the fractured surfaces for selected control specimens for TR and RT plane orientation for (a,b) PUR, (c,d) EPI, and (e,f) MUF. Wooden inlays are fractured bondline images for each representative specimen after the fracture test (the marked dotted area is the observed, glued area). White arrows indicate the adhesive residues.

adhesive joint failures for PUR and MUF were reported also by Watson *et al.* (2013) and for PUR by Ammann *et al.* (2015a, 2015b). In addition, cured PUR adhesive on the surface was identical to that reported by Richter *et al.* (2006), who also reported an excess of bubbles for the CO₂ release during the

curing which is closely related to a high failure rate in case of a thick bondline.

Experimentally observed results for G_c , G_f with average, standard deviation, and median values are presented in Table 4.

Table 4. Number of analyzed specimens, observed average values with standard deviation (SD), and median results (med) of G_c and G_f for adhesive groups, TR and RT orientation and temperature level of the temperature treatment.

	TR			RT		
	PUR	EPI	MUF	PUR	EPI	MUF
Control						
Count	10	10	10	10	10	10
G_c (N/mm)	0.25	0.80	0.50	0.19	0.45	0.47
SD	0.11	0.20	0.16	0.04	0.17	0.16
G_c – med (N/mm)	0.24	0.71	0.45	0.19	0.45	0.43
G_f (N/mm)	290.9	1079.4	620.0	246.9	485.2	617.2
SD	122.1	197.2	195.9	34.6	200.8	145.6
G_f – med (N/mm)	266.6	1090.5	652.3	245.4	438.3	578.7
70°C						
Count	9	10	10	10	10	10
G_c (N/mm)	0.21	0.34	0.44	0.16	0.13	0.31
SD	0.08	0.12	0.12	0.08	0.05	0.22
G_c – med (N/mm)	0.19	0.36	0.43	0.15	0.12	0.24
G_f (N/mm)	218.3	407.2	509.9	171.2	83.4	401.7
SD	61.3	107.1	151.8	58.6	27.0	219.6
G_f – med (N/mm)	211.0	395.4	448.3	174.1	73.1	335.3
140°C						
Count	8	10	10	8	7	10
G_c (N/mm)	0.18	0.27	0.19	0.18	0.08	0.18
SD	0.07	0.08	0.10	0.09	0.04	0.12
G_c – med (N/mm)	0.19	0.27	0.20	0.09	0.08	0.18
G_f (N/mm)	224.7	367.3	290.9	192.8	90.3	204.9
SD	65.6	99.7	80.5	64.6	42.8	109.4
G_f – med (N/mm)	194.6	357.7	309.4	183.6	88.9	199.7

For the control group (20°C/ 65% RH), the lowest G_c and G_f values were found for RT bondline, and the temperature increase intensified this trend. In the control group, PUR adhesive showed the lowest average for G_c and G_f in TR (0.25 and 290.9 N/mm) and RT plane (0.19 and 246.9 N/mm), respectively.

For MUF and EPI, this relation is less clear. The highest G_c and G_f were found for EPI control in TR plane (0.80 and 1079.4 N/mm), but closer more similar results between MUF and EPI were observed in RT plane. Treatment at 70°C had a lower impact on fracture properties for the MUF adhesive with 0.44 and 509.9 N/mm in TR plane and 0.31 N/mm and 401.7 in RT plane for G_c and G_f , respectively. Finally, EPI was found to maintain the highest G_c and G_f values at a temperature treatment of 140°C in TR plane. Similarly, this was observed for MUF in RT plane. Estimating the average area under the curve in Figure 2, fracture propagation in the PUR group was more rapid and of higher intensity compared to the other two adhesives, resulting in lower G_f values for the latter. The effect of thermal treatment was observed to have an impact on G_c and G_f values, resulting in lower values with increasing temperature treatment. G_c and G_f for EPI obtained the highest measures at 140°C treatment in a TR plane. For MUF, the crack orientation did not seem to have a strong impact even at elevated temperatures. Further, PUR remain with poor performance in both TR and RT bondline orientation, regardless of the temperature treatment. Treatment at 140°C was severe for few specimens; therefore, experiments were not able to analyze.

Analytical results

The LM of G_c and G_f revealed the complex relationship between bondline grain orientation, treatment temperature,

and adhesive system. Performance is presented as the median estimated value for G_c or G_f with a 95% confidence interval for that estimate. When comparisons are made between groups, the estimated difference is the ratio between the medians of the compared groups, with a 95% confidence interval of the ratio. The estimated performance of each group (in terms of G_c and G_f , with greater values indicating better performance) varied based on the specific combinations of the investigated factors. That is, no treatment, adhesive, or orientation performed best in all cases. It was clear that increasing treatment temperature had a negative impact on G_c and G_f , but that effect was not consistent between adhesives. Likewise, the effect of grain orientation on G_c and G_f was more pronounced with EPI, but in the TR plane median, G_f was between 2 and 3 times greater than the RT plane. For MUF and PUR, the effect was smaller, and only at 70°C and 140°C treatment; the control group of MUF and PUR performed approximately the same in TR and RT planes. Figure 5 shows predicted medians values for G_c (Figure 5(a)) and G_f (Figure 5(b)) with 95% CI. Treatment combinations are presented in ascending order from the smallest to largest median (see Suppl. Table 3). The most apparent observations from Figure 5 are that for both G_c and G_f , TR plane under control conditions using EPI performed better than all other combinations and the least performant combinations all had RT plane. Multiple R^2 for the LMs were 0.62 and 0.79 for G_c and G_f , respectively.

Treatment temperature had a significant but inconsistent effect on performance in most cases, as shown in the following analysis for each temperature group.

Control group

Under control conditions, bondline grain orientation had no discernible impact on the control group for either PUR or MUF adhesives. In contrast, the median G_c of specimens with EPI was 2.09 times greater in the TR plane than in the RT plane (95% CI: 1.52–2.89; See Suppl. Table 4). In the TR plane, control specimens with EPI adhesive also had the highest estimated G_c , 0.84 N/mm (95% CI: 0.64–1.09; Figure 5(a)). This pattern was similar for G_f , with EPI in the TR plane outperforming EPI in the RT plane by a factor of 2.82 (95% CI: 2.24–3.54) while having the greatest predicted median G_f (1165 N/mm, 95% CI: 963.2–1409; Figure 5(b), Suppl. Table 3). Analyses revealed that for G_c under control conditions, only EPI and MUF in RT plane orientation performed similarly while others varied significantly (See Suppl. Table 4). The median G_c of EPI was 1.78 times greater (95% CI: 1.18–2.71) than MUF in the RT plane orientation, with the highest estimated G_c in this treatment (0.84 N/mm with 95% CI: 0.64–1.09; Suppl. Table 3). On the other hand, in RT plane, MUF produced the highest estimated G_c (0.46 N/mm with 95% CI: 0.35–0.60; Suppl. Table 3). For G_f , all adhesives resulted in significantly different values with a similar trend.

Treatment at 70°C

When specimens were treated at 70°C, EPI no longer performed substantially better than other adhesives but was most significantly affected by bondline grain orientation (Suppl. Table 4). Under this treatment condition, the

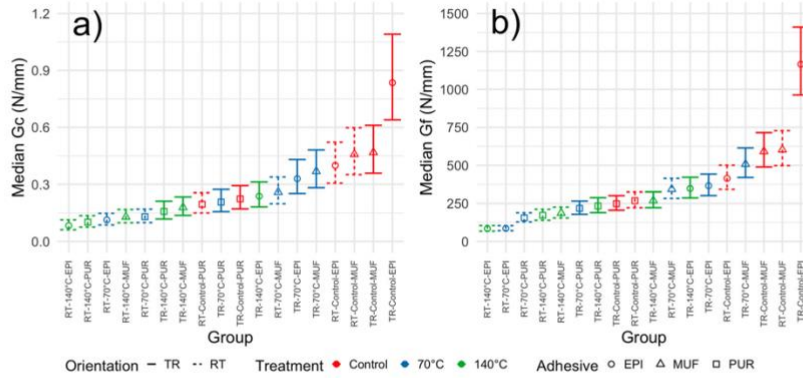


Figure 5. Estimated median (points) G_c (a) and G_f (b) of each group in ascending order with estimated 95% CI (error bars).

highest G_c and G_f were found for MUF in both bondline orientations. At a 70°C treatment temperature, orientation impacted the performance of G_c for all adhesive systems. The effect was most pronounced for EPI, where G_c in the TR plane orientation was 2.91 times (95% CI: 2.11–4.01) greater than in the RT plane orientation. Although the effect of orientation was lower for MUF, when oriented in the TR plane, MUF had the greatest estimated median G_c (0.37 N/mm, and 95% CI: 0.28–0.48; Suppl. Table 3) within the group treated at 70°C. The effect on G_f for EPI was found to be even larger than its G_c counterpart, being 4.25 times (CI: 3.38–5.35) greater in TR than RT plane, with estimated median values of 366 N/mm (95% CI: 302–442) and 86 N/mm (95% CI: 71–104), respectively (Figure 5(b); Suppl. Table 3). When treated at 70°C, group with EPI adhesive performed better than those with PUR in TR plane for both G_c and G_f . However, while there was no discernible difference between EPI and MUF in TR

plane for G_c , there was a small reduction in performance for G_f (0.72 times reduction, 95% CI: 0.53–0.97). In RT plane, EPI performed worse than MUF and worse than MUF in G_c , with no evidence of a difference in G_c between EPI and PUR. MUF performed approximately two times better than PUR in both TR and RT plane orientation for both G_c and G_f (Suppl. Table 4).

Treatment at 140°C

Treatment at 140°C was found to have the most severe impact overall. No significant differences in G_c were found among adhesives in this treatment. Median G_c and G_f were found to be significantly different for all adhesive system at 140°C between TR and RT plane (See Suppl. Table 4). EPI experienced the largest change between bondline grain orientations for G_c , with TR plane predicted to be 2.85 times greater (95% CI: 2.03–4.00) than RT plane. The effect was even more pronounced for G_f , with TR plane predicted to

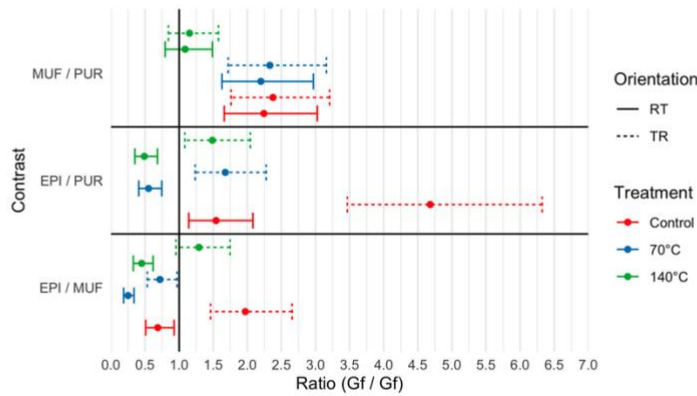


Figure 6. Ratios between the median G_f (points) of each group with estimated 95% CI (error bars), with solid or dashed lines representing the radial or tangential plane, respectively. Error bars that include ratio = 1 are not considered significantly different.

10  J. G. PEČNIK ET AL.

be 4.13 (95% CI: 3.24–5.26) times greater than in the RT plane. EPI in TR plane at 140°C treatment temperature was predicted to have the highest G_f (347.4 N/mm, 95% CI: 286.5–421.2; Suppl. Table 3) while the same combination with RT plane in the 140°C temperature group was the predicted to be the lowest (84.1 N/mm, 95% CI: 67.6–104.6). Surprisingly, these values are nearly identical to the predicted values for the same factor combinations at a treatment temperature of 70°C (Suppl. Table 3), indicating that while heat treatment does have an impact on EPI performance, it does not seem to change based on the treatment temperatures tested in this study. The dominant effect for EPI is clearly bondline grain orientation.

Comparison between treatments

Figure 6 shows an overview of the comparison for G_f between adhesives, for each temperature and orientation. More interesting is that EPI and PUR resulted in no significant differences in G_c between the two treatments for both orientations, while MUF experienced a more severe impact at this treatment level with 2.06 (95% CI: 1.35–3.13) and 2.01 (95% CI: 1.32–3.07) greater reductions from 70°C treatment in TR and RT plane orientation, respectively. G_f values were least impacted by PUR adhesive. Comparing G_c between the control and 140°C treatment groups, the most severe decreases were observed for EPI in RT plane with 4.77 (95% CI: 3.06–7.45) and 3.50 (95% CI: 2.29–5.36) greater reductions with RT and TR plane orientations, respectively.

Conclusion

In this paper, the adhesive-bondline fracture behavior of three structural adhesives on European beech wood was analyzed at three different temperature treatments and with two wood grain orientations with respect to the crack plane (TR and RT). Fracture energy and critical strain energy release rate were obtained from the SEN-TPB test in mode I. Regarding the fracture performance of the adhesive bondlines PUR, in general, performed the worst among all adhesives in terms of G_c and G_f , although it was the least impacted by elevated temperature treatment. Conversely, EPI reached the highest observed G_c and G_f values when tested at standard conditions but experienced the most severe decrease in fracture properties when tested after treatment at an elevated temperature. EPI in all treatment groups showed the most significant change in properties related to crack plane orientation, which was less pronounced for the other two adhesives (MUF and PUR). In general, the study showed that SEN-TPB test employing data reduction scheme may be advantageous for fracture analysis of adhesive bonds and that the impact of temperature on adhesive-bondline performance is significant when EPI, MUF, and PUR are used. As the examined treatment temperatures were lower than the decomposition temperature of wood's main components, it is clear that adhesive-bondline characteristics (grain orientation, adhesive) should be selected carefully in applications where the elevated temperature might occur.

Disclosure statement

No potential conflict of interest was reported by the author(s).

Funding

This work has been conducted with the financial support of the European Commission for the InnoRenew project [Grant Agreement #739574] under the Horizon2020 Widespread-2-Teaming program, Republic of Slovenia (Investment funding of the Republic of Slovenia and the European Union of the European Regional Development Fund), Slovenian Research Agency (infrastructure program IO-0035) and Slovenian Research Agency (basic research funding No. P4-0430). The authors also acknowledge the grant provided by Czech Science Foundation: "Experimental and numerical assessment of the bearing capacity of notches in timber beams at arbitrary locations using LEFM" (#21-293895).

ORCID

Jaka Gašper Pečnik  <http://orcid.org/0000-0002-8775-8230>
 Andreja Pandelak  <http://orcid.org/0000-0003-1078-389X>
 Michael David Burnard  <http://orcid.org/0000-0001-9357-0819>
 Václav Sebera  <http://orcid.org/0000-0002-2658-1179>

References

- Ammann, S. and Niemz, P. (2015a) Mixed-mode fracture toughness of bond lines of PRF and PUR adhesives in European beech wood. *Holzforschung*, 69(4), 415–420.
- Ammann, S. and Niemz, P. (2015b) Specific fracture energy at glue joints in European beech wood. *International Journal of Adhesion and Adhesives*, 60, 47–53.
- Bachtar, E. V., Clerc, G., Brunner, A. J., Kaliske, M. and Niemz, P. (2017) Static and dynamic tensile shear test of glued lap wooden joint with four different types of adhesives. *Holzforschung*, 71(5), 391–396.
- CEN (2013) *BS EN 302-1. Adhesives for Load-Bearing Timber Structures – Test Methods* (Brussels, Belgium).
- Clauß, S., Joscak, M. and Niemz, P. (2011) Thermal stability of glued wood joints measured by shear tests. *European Journal of Wood and Wood Products*, 69(1), 101–111.
- Clerc, G., Brunner, A. J., Josset, S., Niemz, P., Pichelin, F. and Van de Kuilen, J. W. G. (2019) Adhesive wood joints under quasi-static and cyclic fatigue fracture mode II loads. *International Journal of Fatigue*, 123 (February), 40–52.
- de Moura, M. F. S. F., Dourado, N. and Morais, J. (2010) Crack equivalent based method applied to wood fracture characterization using the single edge notched-three point bending test. *Engineering Fracture Mechanics*, 77(3), 510–520.
- Dourado, N. and de Moura, M. F. S. F. (2019) Effect of temperature on the fracture toughness of wood under mode I quasi-static loading. *Construction and Building Materials*, 223, 863–869.
- Dourado, N., De Moura, M. F. S. F. and Morais, J. (2011) A numerical study on the SEN-TPB test applied to mode I wood fracture characterization. *International Journal of Solids and Structures*, 48(2), 234–242.
- Dourado, N., de Moura, M. F. S. F., Morel, S. and Morais, J. (2015) Wood fracture characterization under mode I loading using the three-point-bending test. Experimental investigation of *Picea abies* L. *International Journal of Fracture*, 194(1), 1–9.
- Dourado, N., Morel, S., de Moura, M. F. S. F., Valentin, G. and Morais, J. (2008) Comparison of fracture properties of two wood species through cohesive crack simulations. *Composites Part A: Applied Science and Manufacturing*, 39(2), 415–427.
- Ehrhart, T. (2019) European beech glued laminated timber. Thesis (PhD). ETH Zürich.
- Gavrilović-Grmuša, I., Dunky, M., Miljković, J. and Djiporović-Momčilović, M. (2012) Influence of the degree of condensation of urea-formaldehyde adhesives on the tangential penetration into beech and fir and on the shear strength of the adhesive joints. *European Journal of Wood and Wood Products*, 70(5), 655–665.

- Glavnić Uzelac, I., Boko, I., Torić, N. and Vranković Lovrić, J. (2020) Application of hardwood for glued laminated timber in Europe subject. *Gradjevinar*, 72(7), 607–616.
- Gómez-Royuela, J. L., Majano-Majano, A., José Lara-Bocanegra, A. and Reynolds, T. P. S. (2021) Determination of the elastic constants of thermally modified beech by ultrasound and static tests coupled with 3D digital image correlation. *Construction and Building Materials*, 302, 124270.
- Gómez-Royuela, J. L., Majano-Majano, A., Lara-Bocanegra, A. J., Xavier, J. and de Moura, M. F. S. F. (2022) Evaluation of R-curves and cohesive law in mode I of European beech. *Theoretical and Applied Fracture Mechanics*, 118, 1–9.
- Hass, P., Müller, C., Clauss, S. and Niemz, P. (2009) Influence of growth ring angle, adhesive system and viscosity on the shear strength of adhesive bonds. *Wood Material Science and Engineering*, 4(3–4), 140–146.
- Hering, S., Keunecke, D. and Niemz, P. (2012) Moisture-dependent orthotropic elasticity of beech wood. *Wood Science and Technology*, 46(5), 927–938.
- Hu, W., Liu, Y. and Li, S. (2021) Characterizing mode I fracture behaviors of wood using compact tension in selected system crack propagation. *Forests*, 12(10), 1–13.
- Klippel, M., Frangi, A. and Fontana, M. (2011) Influence of the adhesive on the load-carrying capacity of glued laminated timber members in fire. *Fire Safety Science*, 10, 1219–1232.
- Kollmann, F. F. P. and Côté, W. A. (1968) *Principles of Wood Science and Technology I Solid Wood* (Berlin: Springer).
- Lenth, V. R. (2022) emmeans: Estimated Marginal Means, aka Least-Squares Means.
- Majano-Majano, A., Hughes, M. and Fernandez-Cabo, J. L. (2012) The fracture toughness and properties of thermally modified beech and ash at different moisture contents. *Wood Science and Technology*, 46(1–3), 5–21.
- Martinez del Castillo, E., Zang, C. S., Buras, A., Hacket-Pain, A., Esper, J., Serrano-Notivol, R., Hartl, C., Weigel, R., Klesse, S., Resco de Dios, V., Schamweber, T., Dorado-Liñán, I., van der Maaten-Theunissen, M., van der Maaten, E., Jump, A., Mikac, S., Banzragch, B. E., Beck, W., Cavin, L., Claessens, H., Čada, V., Cufar, K., Dulamsuren, C., Gričar, J., Gil-Pelegrin, E., Janda, P., Kazimirović, M., Kreyling, J., Latte, N., Leuschner, C., Longares, L. A., Menzel, A., Merela, M., Motta, R., Muffler, L., Nola, P., Petritan, A. M., Petritan, I. C., Prisan, P., Rubio-Cuadrado, A., Rydval, M., Stajić, B., Svoboda, M., Toroman, E., Trotsiuk, V., Wilking, M., Zlatanov, T. and de Luis, M. (2022) Climate-change-driven growth decline of European beech forests. *Communications Biology*, 5(1), 1–9.
- Merhar, M., Bučar, D. G. and Bučar, B. (2013) Faktor kritičnog intenziteta naprezanja (I. mod) bukovine (*Fagus sylvatica*) u TL presjeku: Usporedba različitih metoda. *Drvna Industrija*, 64(3), 221–229.
- NT BUILD 422 (1993) Wood: Fracture energy in tension perpendicular to the grain. Nordtest Method, 11. Tekniikantie, Finland.
- Ozyhar, T., Hering, S. and Niemz, P. (2013) Moisture-dependent orthotropic tension-compression asymmetry of wood. *Holzforschung*, 67(4), 395–404.
- Reiterer, A. (2001) The influence of temperature on the mode I fracture behavior of wood. *Journal of Materials Science Letters*, 20(20), 1905–1907.
- Richter, K., Pizzi, A. and Despres, A. (2006) Thermal stability of structural one-component polyurethane adhesives for wood-structure-property relationship. *Journal of Applied Polymer Science*, 102(6), 5698–5707.
- River, B. (2003) Fracture of adhesive-bonded wood joints. In A. Pizzi and K. L. Mittal (eds.), *Handbook of Adhesive Technology, Revised and Expanded* (2nd ed.). (New York: Marcel Dekker, Inc., 325–350).
- Sandberg, D., Kutnar, A., Karlsson, O. and Jones, D. (2021) *Wood Modification Technologies: Principles, Sustainability, and the Need for Innovation* (1st ed.) (London: CRC Press).
- Sebera, V., Pečnik, J. G., Azinović, B. and Huć, S. (2020) Wood-adhesive bond loaded in mode II: experimental and numerical analysis using elasto-plastic and fracture mechanics models, 5957, 1–13.
- Sebera, V., Redón-Santafé, M., Brabc, M., Děcký, D., Čermák, P., Tippner, J. and Milch, J. (2019) Thermally modified (TM) beech wood: Compression properties, fracture toughness and cohesive law in mode II obtained from the three-point end-notched flexure (3ENF) test. *Holzforschung*, 73(7), 663–672.
- Sedláčik, J. and Šmidriaková, M. (2012) Heat resistance of adhesive joints for wood constructions. *Acta Facultatis Xylogiae Zvolen*, 54 (2), 79–94.
- Sernek, M., Resnik, J. and Kamke, F. A. (1999) Penetration of liquid urea-formaldehyde adhesive into beech wood. *Wood and Fiber Science*, 31(1), 41–48.
- Sinha, A., Naim, J. A. and Gupta, R. (2012) The effect of elevated temperature exposure on the fracture toughness of solid wood and structural wood composites. *Wood Science and Technology*, 46(6), 1127–1149.
- Smith, I., Landis, E. and Gong, M. (2003) *Fracture and Fatigue in Wood* (New York: John Wiley & Sons, Inc.).
- Sterley, M. (2012) Characterisation of green-glued wood adhesive bonds. Thesis (PhD). Linnaeus University.
- Straže, A., Fajdiga, G., Pervan, S. and Gorišek, Ž. (2016) Hygro-mechanical behavior of thermally treated beech subjected to compression loads. *Construction and Building Materials*, 113, 28–33.
- Tukiainen, P. and Hughes, M. (2016) The effect of temperature and moisture content on the fracture behaviour of spruce and birch. *Holzforschung*, 70(4), 369–376.
- Watson, P., Clauss, S., Ammann, S. and Niemz, P. (2013) Fracture properties of adhesive joints under mechanical stresses. *Wood Research*, 58 (1), 43–56.
- Yoshihara, H. (2010) Examination of the mode I critical stress intensity factor of wood obtained by single-edge-notched bending test. *Holzforschung*, 64(4), 501–509.
- Yoshihara, H. and Kawamura, T. (2006) Mode I fracture toughness estimation of wood by DCB test. *Composites Part A: Applied Science and Manufacturing*, 37(11), 2105–2113.
- Yoshihara, H. and Kawamura, T. (2007) Influence of the measurement methods on the mode I fracture toughness of wood. *Zaiyo/Journal of the Society of Materials Science, Japan*, 56(4), 311–315.
- Yoshihara, H. and Usuki, A. (2011) Mode I critical stress intensity factor of wood and medium-density fiberboard measured by compact tension test. *Holzforschung*, 65(5), 729–735.

2.2 Article 2

Title: Wood-adhesive bond loaded in mode II: experimental and numerical analysis using elasto-plastic and fracture mechanics models

Authors: Václav Sebera, Jaka Gašper Pečnik, Boris Azinović, Jaromír Milch, Sabina Huč

Year: 2020

Journal: Holzforschung (ISSN: 1437-434X)

DOI: <https://doi.org/10.1515/hf-2020-0141>

Link: www.degruyter.com/document/doi/10.1515/hf-2020-0141/html



Original article

Václav Sebera*, Jaka Gašper Pečnik, Boris Azinovič, Jaromír Milch and Sabina Huč

Wood-adhesive bond loaded in mode II: experimental and numerical analysis using elasto-plastic and fracture mechanics models

<https://doi.org/10.1515/hf-2020-0141>

Received May 21, 2020; accepted November 4, 2020; published online December 17, 2020

Abstract: The goal of the study was to analyze fracture properties of adhesive bond using a three-point end-notched flexure test and the compliance-based beam method. Critical strain energy release rates (G_{IIc}) and cohesive laws were obtained for adhesive bonds made of European beech (*Fagus sylvatica* L.) and adhesives such as EPI, MUF, PRF and PUR. The experiments were assisted with FE analyses employing three different material models of wood: elastic (Elas), symmetric elasto-plastic (EP) and elasto-plastic with different compressive and tensile yield stresses parallel to fiber (EP+). The highest mean G_{IIc} was achieved for PUR (5.40 Nmm^{-1}) and then decreased as follows: 2.33, 1.80, 1.59 Nmm^{-1} for MUF, EPI, and PRF, respectively. The failure of bondline was brittle and occurred at bondline for EPI, MUF and PRF, and ductile and commonly occurring in wood for PUR adhesive. The FE simulations employing cohesive models agreed well with the experimental findings for all adhesives. FE model with Elas material was found accurate enough for EPI, MUF and PRF adhesives. For PUR adhesive, the model EP+ was found to be the most accurate in prediction of maximal force. The impact of friction between lamellas may be up to 4.2% when varying friction coefficient from 0 to 1. The impact of the grain angle distortion (α) with respect to longitudinal

specimen axis showed its high influence on resulting stiffness and maximal force. It was found that three-point end-notched test is suitable for EPI, MUF, and PRF, while it is less appropriate for a bond with PUR adhesive due to notable plastic behavior.

Keywords: adhesive bond; beech wood; cohesive law; elasto-plastic material; mode II; strain energy release rate.

1 Introduction

Adhesive bonding of wood in any shape and size is necessary for production of modern wood products. For the production of high-performance wood composites, a fundamental understanding of adhesive bond behavior and properties, including involved materials, is essential (Stoeckel et al. 2013). Mechanical tests of adhesive materials are primarily made on a macroscopic scale (e.g., following EN 302-1 2013), but microscopic investigations also bring important findings about adhesive bond, especially when coupled with X-ray μ CT (McKinley et al. 2018). Adhesive-wood complex is a very complicated mechanical system where many local events such as non-uniform cracking in adherend/adhesive, fiber bridging, etc. occur and, therefore, use of full-field technique such as digital image correlation (DIC) is advantageous when analyzing strains and crack openings around the bond area (Brault et al. 2013; Kamke et al. 2014; McKinley et al. 2019). An adhesive bond between adherents is strongly affected by the quality of manufacturing, which, consequently, significantly affects the physical properties of the bond and its service life in a material or construction. To investigate mechanical performance of adhesive bonds, lap shear test is often employed to reveal the basic properties such as shear strength of wood-adhesive complex. Adhesive bond can have similar and higher bearing capacity and stiffness to bonds using dowels connecting lamellas in laminated beams (Jelušič and Kravanja 2018). Another important property of adhesive bond is the fracture energy that needs

*Corresponding author: Václav Sebera, InnoRenew CoE, Livade 6, 6310 Izola, Slovenia; and Mendel University in Brno, Zemědělská 3, 61300, Brno, Czech Republic, E-mail: seberav@gmail.com <https://orcid.org/0000-0002-2658-1179>

Jaka Gašper Pečnik, InnoRenew CoE, Livade 6, 6310 Izola, Slovenia; and Andrej Marušič Institute, University of Primorska, Koper, Slovenia. <https://orcid.org/0000-0002-8775-8230>

Boris Azinovič and Sabina Huč, Slovenian National Building and Civil Engineering Institute, Dimičeva ulica 12, Ljubljana, Slovenia. <https://orcid.org/0000-0002-1810-5957> (B. Azinovič). <https://orcid.org/0000-0001-7658-4194> (S. Huč)

Jaromír Milch, Mendel University in Brno, Zemědělská 3, 61300, Brno, Czech Republic. <https://orcid.org/0000-0002-6970-0895>

to be spent on adhesive bond to initiate and propagate the crack in wood-adhesive complex. Fracture energy, specifically strain energy release rate (G), can be studied in three fundamental modes: mode I (tension), mode II (in-plane shear) and mode III (out-of-plane shear) as well as in mixed modes (Anderson 1995).

In the last two decades, the measurement of G in mode II (G_{II}) has undergone a big development from simple analytical models, over superposition, to models considering crack tip openings and compliance-based methods (Arrese et al. 2010; Wang and Qiao 2004; Yoshihara 2005). Models including crack propagation phenomena are most accurate because of their direct relation to strain energy release. This approach was successfully proved for both synthetic and wood-based composites (Matsumoto and Nairn 2009; Wang et al. 2009) and modified wood (Kutnar et al. 2008). Mode II fracture is often tested in bending by employing end-notched flexural tests (ENF), either in three-point (3ENF) or four-point (4ENF) schemes, or so-called end loaded split (ELS) tests (Silva et al. 2007). All reveal comparable and reliable data if certain qualitative measurement conditions and sample dimensions, such as span-to-height ratio, are met (Schuecker and Davidson 2000; Yoshihara 2001). Yoshihara and Ohta (2000) found that fracture properties of wood are dependent on a ratio of initial crack length and half span, which has to be considered in experimental designs. De Moura et al. (2006) employed a so-called equivalent crack length approach (ECLA) and incorporated it into the compliance-based beam method (CBBM). This combination was shown to be advantageous because it did not require tracking of crack propagation, which can be conveniently derived directly from the current compliance. Also, using Iosipescu specimen geometry and Arcan test was successfully demonstrated to reveal fracture properties of orthotropic materials (Khansaria et al. 2019; Murata et al. 2017).

Use of ECLA on pine wood was shown by Silva et al. (2006), who also developed the finite element (FE) model of crack propagation for wood in mode II that was successfully verified by ECLA. For medium density fiberboard, ECLA shows that fracture toughness in mode II continuously increased during crack propagation (Yoshihara 2010). Because of its relative ease, ENF in combination with ECLA is well suited for analysis of wood-adhesive bonds, too (Xavier et al. 2011), and for determination of cohesive zone models of a material (Silva et al. 2014; Xavier et al. 2014) or for adhesive bonds of composite materials (Fernandes et al. 2013). Cohesive laws are especially important as input data in numerical modeling of composite materials and structures. Using DIC and FEM may conveniently provide data enabling separation of mode I and mode II without considering local elastic mechanical properties as shown in

Meite et al. (2013). More recently, Clerc et al. (2019) showed a simplified four-point ENF test to examine G_{II} for the adhesive bond of wood and PRF and one-component PUR adhesives without the need for DIC. They showed that performance of all adhesive bonds has similar behavior under quasi-static loading in mode II.

In the last two decades, environmental aspects and considerations have pushed forestry to plant more broadleaved species that, consequently, initiated innovations in development of wood-based composites (WBCs) for glued timber structures (Vallée et al. 2017). Therefore, WBCs, such as Glued-Laminated Timber (GLT), cross-laminated timber (CLT) and laminated veneer lumber (LVL), made from various hardwoods were developed, including hybrid softwood-hardwood compositions (Fortuna et al. 2019; Franke 2016; Pollmeier 2019; Tapia and Aicher 2018). Due to their advantageous properties, they can replace steel elements (e.g., trusses). Therefore, knowledge about mechanical performance of adhesive bond with hardwoods, including fracture properties, is necessary to utilize its potential in timber structures as well as to increase the use of local raw materials that will be crucial for next generations.

The general goal of the study was to provide more insight into fracture properties of adhesive bond for beech wood glued by various adhesives loaded in mode II. The specific objectives are: (i) to carry out 3ENF tests of adhesive bonds with Emulsion Polymer Isocyanate (EPI), Melamine-Urea Formaldehyde (MUF), Phenol-Resorcinol Formaldehyde (PRF) and Polyurethane (PUR) adhesives; (ii) to compute strain energy release rate of adhesive bond using ECLA and DIC data; (iii) to assess whether 3ENF tests are suitable for all the tested adhesives; (iv) to develop and validate finite element model of the test including contact and cohesive zone model; (v) to assess whether elastoplastic material models of wood bring higher accuracy into FE modeling of crack growth for given adhesives, and (vi) to perform FE sensitivity analyses to examine an influence of friction and fiber angle on the outputs of 3ENF test.

2 Materials and methods

European beech wood (*Fagus sylvatica* L.) was used to prepare all the samples for testing. The samples were conditioned and submitted to 3ENF test. All tests were accompanied with a stereoscopic system to obtain optical data about the displacement slip around the crack tip (w) that was calculated by DIC later on.

2.1 Test specimens

Test specimens were cut from a defect-free board of European beech by cutting with standard band and circular saws. For the 3ENF test, the

specimens were prepared with dimensions of $17 \times 20 \times 500 \text{ mm}^3$ in radial (R), tangential (T) and longitudinal (L) directions, respectively, according to Yoshihara (2001) as orthotropic blocks and with the necessary span-to-height ratio to induce stable crack propagation and insignificant plastic deformation due to contact with supports and loading head (Figure 1). An artificial crack of length $\approx 182 \text{ mm}$ was introduced in L direction at the end of the specimen across the whole width of the specimen. All the specimens were weighed and dimensionally measured prior to the mechanical testing and without crack introduced. Test groups were defined as follows: (i) bond with EPI adhesive (Advantage EP-915 FS); (ii) bond with MUF adhesive (Prefere 4535); (iii) bond with PRF adhesive (Cascosinol 1711 with hardener 2520); and (iv) bond with PUR adhesive (PURBOND PR 3105). Lamellas were bonded using the recommended amount, pressure, time and temperature (20°C) for particular adhesive as follows: EPI – 400 g/m^2 , 1.4 MPa , 120 min ; MUF – 460 g/m^2 , 1.4 MPa , 270 min ; PRF – 535 g/m^2 , 1.0 MPa , 240 min ; PUR – 790 g/m^2 , 1.2 MPa , 120 min .

2.2 Physical testing

3ENF tests were performed on a universal testing machine (UTM) Zwick/Roell Z050 equipped with a 50 kN load cell; the load rate was set to 3 mmmin^{-1} (Figure 1b). A deflection of the specimen was measured using cross-head of the UTM. The 3ENF provided force-deflection data that were further processed using CBBM and ECLA to obtain fracture properties. Before testing, Teflon paper was inserted into the crack to reduce friction between lamellas. At the side of the samples, a stochastic black-and-white speckle pattern was applied before testing to create the area of interest (AoI) for later computation of displacement slip using DIC (Figure 1a). All 3ENF tests were recorded at a 2 Hz acquisition rate by means of an optical stereo-vision system consisting of two 9MPx CCD cameras focusing on one side of the AoI. The optical system was synchronized with the UTM. The images were further processed in 3D-DIC software Aramis 2016 (GOM Inc.) to obtain the full-field displacements and compute the strains over the AoI. The

analysis used a subset size of $27 \times 27 \text{ px}^2$ and a step size of 3 px . Postprocessing of the DIC results provided the displacement slip (w) that was obtained from two points at the introduced crack tip, one above and one below the assumed neutral axis (Figure 1a). The displacement slip is calculated from $w_{II} = |u^+ - u^-|$, where u^+ is for the upper component, u^- is for the lower component and both are in horizontal directions. After removing invalid measurements, such as for weakly bonded specimens, the total count was 17, 19, 16 and 20 specimens for EPI, MUF, PRF and PUR adhesive, respectively.

2.3 Calculation of strain energy release rate

The theoretical derivation of the strain energy release rate (G_{II}) by 3ENF and equivalent crack length (a_{eqv}) has been described by Yoshihara (2010), and Fernandes et al. (2013), so it is omitted here only for principal steps. The ECLA procedure does not require crack length monitoring during the test and leads to direct derivation of G_{II} respecting Irwin–Kies equation, which is for strain energy release rate as follows:

$$G_{II} = \frac{9P^2 a_{eqv}^2}{16b^2 h^3 E_f} \quad (1)$$

where P is force (N), a_{eqv} is equivalent crack length (m), b and h are specimen width and height (m) respectively, E_f is flexural elastic modulus. The main advantage of such a data reduction scheme is that the R -curve, i.e., $G_{II} = f(a_{eqv})$, can be obtained solely from the force-deflection (P/δ) curve. To obtain the G_{II} - w_{II} curve, the procedure shown in Xavier et al. (2014) was followed. To derive the cohesive law, the G_{II} - w_{II} curve was truncated at the beginning of the steady-state crack propagation (i.e., at maximal force). The truncated G_{II} - w_{II} curve was then differentiated to obtain the cohesive law in mode II. For this purpose, a continuous logistic function $Q(t)$ (Eq. (2)) was used to approximate the data points in the reconstruction of the fracture cohesive law. The logistic fit (Q) searched for parameters t , R and α with lowest residuals according to:

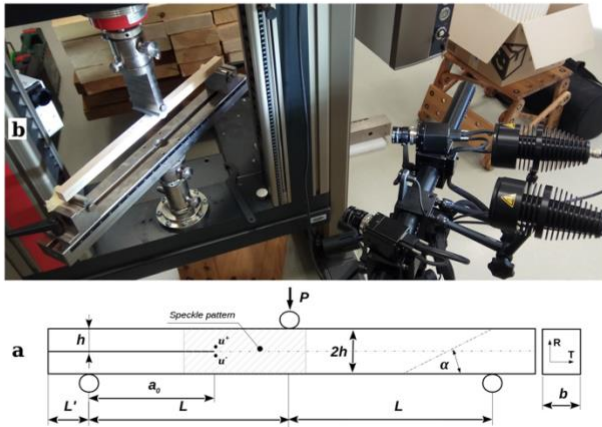


Figure 1: (a) Scheme of sample geometry for 3ENF test with marked AoI for DIC analysis and two points (u^+ , u^-) for obtaining displacement slip; $L = 230 \text{ mm}$, $L' = 20 \text{ mm}$, $a_0 = 182 \text{ mm}$, $b = 17 \text{ mm}$, $h = 10 \text{ mm}$, α is fiber angle, R and T denote radial and tangential directions, respectively. The solid line represents crack, the dashed line represents adhesive bond. (b) Experimental setup at universal testing machine including stereovision set accompanied with lights.

$$Q = \frac{Q_{inf}}{1 + e^{-\alpha(t-R)}} \quad (2)$$

where Q is the logistic function, Q_{inf} is curve maximum, t is quasi-time, R is symmetric inflection point, α is time decay constant. Once the continuous function of $G_{II}(w_{II})$ was obtained, the G_{II} was differentiated to obtain cohesive law as follows:

$$\sigma_{II} \frac{\partial G_{II}}{\partial w_{II}} \quad (3)$$

where σ_{II} is stress (Pa) and w_{II} is displacement slip (m). Above mentioned calculations were made on an averaged force-deflection (P/δ) curve. The average P/δ curve was obtained by calculating arithmetic mean P/δ curve from all specimens in the group. Average curve was subsequently fitted by polynomial of 6th degree, which resulted in representative P/δ curve for each group. These curves were further processed to calculate G_{II} and critical strain-energy release rate (G_{IIc}). To examine the differences between studied group mean values, single and multiple one-way analysis of variance test (one-way ANOVA) was used, assuming significance level of 0.05. The multiple tway ANOVA was made using 'multcompare' function. This test provided answers whether adhesive groups differ in terms of P_{max} and δ . Postprocessing, statistical analyses and other calculations were performed in Matlab 2014b (Mathworks Inc.).

2.4 Numerical modeling

The physical test carried out at UTM was modeled using finite element method (FEM) implemented in software Ansys 19.1 R1 (ANSYS Inc., USA). The 3D sample and boundary conditions reflected the physical test at UTM, so the geometry included the sample, steel supports and loading head (Figure 2). The wood material was modeled using quadratic finite element SOLID95, and the adhesive bond was modeled using cohesive zone model (CZM) and finite element INTER204. The traction-separation behavior in CZM was modeled using bilinear function, and the G_{II} for this function was taken as a mean value from the measurement for given adhesive. Lamellas below and above the introduced crack were covered by quadratic contact elements (CONTA170 and TARGE174) to simulate their interaction during the bending test. This contact pair was modeled as flexible-to-flexible. The contact of wood with steel supports and loading head was modeled as rigid-to-flexible, so deformation of steel parts was neglected. The element size was set to 3 mm in longitudinal direction, but around supports and load head, the FEmesh was refined. Element size of 2 mm was set thickness-wise, so each lamella consisted of five elements in thickness. The total number of elements/nodes, including contact and cohesive ones, was 18000/55366. After validation of the FE model based on the comparison with experimentally obtained data, FE sensitivity analyses were performed to analyze an influence

of: (i) friction coefficient between wooden lamellas (μ_{ww}) by varying it from 0 to 1; (ii) fiber angle with respect to the longitudinal axis of the specimen (α) from 0° to 18° ; (iii) fiber angle with respect to the cross-section axes from 0° to 90° . The sensitivity analysis was performed to examine the impact of these three parameters on resulting P/δ curves, namely stiffness and P_{max} .

Within the FE analyses, three material models of beech wood (Table 1) were employed: (i) orthotropic elastic model (Elas); (ii) orthotropic elasto-plastic model with the same compression and tension yield stresses (EP) and (iii) orthotropic elasto-plastic model with different compression and tension yield values (EP+). The first two models were taken from Milčič et al. (2016). The third one was developed based on the second model using a procedure that aimed to extend the difference between compression and tension yield values while preserving Hill plasticity conditions (Hill 1983). The coefficient of friction between steel supports, loading head and wood was set constant to $\mu_{sw} = 0.33$, and the same value was used for wood-wood interaction between wooden lamellas (μ_{ww}), except for analysis of impact of μ_{ww} on resulting P/δ response.

3 Results and discussion

3.1 End-notched flexural tests

The analytical calculation of strain energy release rate (G_{II}) follows the equivalent crack length approach (ECLA) for determination of the resistance curve (R -curve) that is explicitly determined from the experimental force-displacement (P/δ) curves (Figure 3). Figure 3 shows that slopes of the elastic zone for all samples is more or less within the same range no matter what adhesive was used; the scatter in stiffnesses may be explained by natural variability of wood properties rather than the type of adhesive. Mean values and standard deviations (in brackets) for flexural stiffnesses (E_f), as calculated according to Eq. (3) in Silva et al. (2014), are 16.1 GPa (251 MPa), 15.6 GPa (563 MPa), 19.0 GPa (434 MPa) and 16.9 GPa (327 MPa) for EPI, MUF, PRF, and PUR adhesive, respectively. Multiple one-way ANOVA test for E_f revealed that all groups do not have significantly different means (at $\alpha = 0.05$). The moisture content (MC) level of all groups was also proved as statistically equal using an ANOVA test and was in a range of 10.5–11.0%; the same holds true for the density having mean values between 705 and 728 kg/m³. These

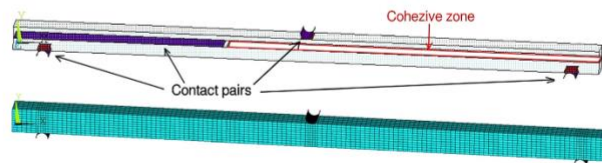


Figure 2: Geometrical and finite element model of the 3ENF test.

Table 1: Material models of beech wood used in FE simulations (moisture content 12%).

Elas	$E_L = 13439, E_R = 1880, E_T = 1031, G_{LR} = 1608, G_{RT} = 460, G_{LT} = 1059$ [MPa] $\nu_{LR} = 0.073, \nu_{RT} = 0.360, \nu_{LT} = 0.043$ [-]. Taken from Milch et al. (2016).
EP (MPa)	Elas , $\sigma_{L,Tc} = \sigma_{L,Cc} = 47.5, \sigma_{R,Tc} = \sigma_{R,Cc} = 9.49, \sigma_{T,Tc} = \sigma_{T,Cc} = 8.11, E_{L,Tc,Tan} = E_{L,Cc,Tan} = 10.39, E_{R,Tc,Tan} = E_{R,Cc,Tan} = 22.36, E_{T,Tc,Tan} = E_{T,Cc,Tan} = 14.38, E_{LR,Tan} = 16.08, E_{RT,Tan} = 7.61, E_{LT,Tan} = 10.59, \sigma_{LR} = 12.6, \sigma_{RT} = 14.2, \sigma_{LT} = 12.6$. Taken from Milch et al. (2016).
EP+ (MPa)	Elas , $\sigma_{L,Tc} = 114, \sigma_{L,Cc} = 47.5, \sigma_{R,Tc} = 8.03, \sigma_{R,Cc} = 9.49, \sigma_{T,Tc} = 8.59, \sigma_{T,Cc} = 8.11, E_{L,Tc,Tan} = 0.001, E_{L,Cc,Tan} = 10.39, E_{R,Tc,Tan} = 0.001, E_{R,Cc,Tan} = 22.36, E_{T,Tc,Tan} = 0.001, E_{T,Cc,Tan} = 14.38, E_{LR,Tan} = 16.08, E_{RT,Tan} = 7.61, E_{LT,Tan} = 10.59, \sigma_{LR} = 12.6, \sigma_{RT} = 14.2, \sigma_{LT} = 12.6$.

E_i is normal elastic modulus, G_{ij} is shear elastic modulus, ν_{ij} is Poisson's ratio, $\sigma_{i,Tc}$ is yield stress in tension, $\sigma_{i,Cc}$ is yield stress in compression, σ_{ij} is shear yield stress, $E_{i,Tc,Tan}$ is normal tangent modulus in tension, $E_{i,Cc,Tan}$ is normal tangent el. modulus in compression, $E_{ij,Tan}$ is shear tangent el. modulus. Indices i and j characterize anatomical directions L, R , and T . El. is orthotropic elastic model, EP orthotropic elasto-plastic with same tension and compression behavior, and EP+ is orthotropic elasto-plastic with different behavior in compression and tension parallel to fiber.

results imply that adhesive type did not influence mean E_f for the groups. Further, the highest maximal force (P_{max}) and maximal deflection at P_{max} (δ_{max}) was achieved for PUR adhesive that also possesses significant plastic region between yield point and P_{max} . This fact implies that PUR group has the highest apparent fracture toughness (i.e., area under the P/δ curve), which can be attributed to adhesive properties having a larger range of elastic and plastic deformation compared to other studied adhesives. On the other hand, EPI and PRF adhesives showed the most brittle-like behavior because deflection at P_{max} is lowest, so they would likely have the lowest apparent fracture toughness among studied adhesives.

Variability of P_{max} and δ_{max} for all adhesive groups is shown in the box plots in Figure 4. As seen in the EPI, MUF and PRF are more alike, contrary to PUR that has a significantly higher median value (red line in box plot). A one-way ANOVA test for adhesive groups revealed the same findings for both P_{max} and δ_{max} . For both physical quantities, significant differences between mean values were found only between PUR and all other adhesives ($\alpha = 0.05$). This phenomenon can be attributed to both higher elastic and plastic capacity of adhesive and plastic deformation that occurred in wood due to bending. PUR adhesive belongs with the elastomeric adhesives that show rigidity comparable to other used adhesives, but it also shows higher flexibility due to the aliphatic portions of the polymer, which could contribute to this behavior (Troughton 2009). Martins et al. (2019) examined the same groups of adhesives as in the presented study, but they did so only in terms of shear strength according to EN 14080. Their results showed very similar shear strengths and force vs. deflection diagrams in terms of both elastic and plastic ranges of strain for all adhesives, which is slightly different from findings of this study where PUR group had the highest P_{max} . However, PUR group results may be partially attributed to significant plastic strains developed in wood

due to bending. It is also necessary to mention Martins et al. (2019) used a different test, with higher strain rate (failure till 20 s) and different wood species (Maritime pine), so the comparison with this case is only partially valid. The effect of the bonding pressure on P_{max} was not studied in this work, but Santos et al. (2019) found no differences in shear strength of Maritime pine elements glued with PUR adhesive in this respect. Despite the pressure applied to the analyzed adhesives being slightly different, due to their specific technical recommendations, it is assumed it did not influence the test to a great extent, so it will not be discussed further. Mean relative difference between deflections at P_{max} obtained by cross-head and DIC was 2.57%.

3.2 DIC analysis

Optical image series were processed with 3D-DIC software (Aramis), which provided displacements in three directions with respect to fiber direction (L, R, T), normal strains in two directions ($\epsilon_{LL}, \epsilon_{RR}$) and shear strain (ϵ_{LR}). Since mode II is shear mode, ϵ_{LR} is the best to show strain concentration at the bondline (Figure 5a). Figure 5a clearly shows the shear opening and deformation at the adhesive bondline and, further, two points below and above the crack tip (green dots) that enabled obtaining displacement slip (w_{II}). The typical experimental horizontal displacements (u^+ and u^-) for these two points are plotted in Figure 5b. It shows that the horizontal displacement below and above the sample's ideal neutral axis (NA) follows different paths which, consequently, creates the w_{II} ; it may also identify linear zones and a moment of P_{max} where the specimen failed. The position of these points is crucial for further correct calculations of G_{II} . These points should be located as close as possible to a crack tip that is ideally located at the NA. However, to achieve this for bonded

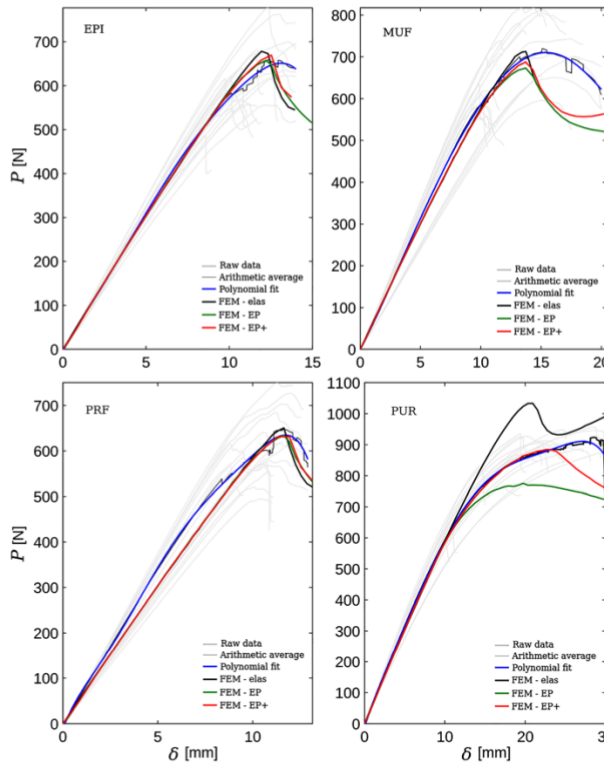


Figure 3: Experimental and numerical P/δ curves for tested adhesives.

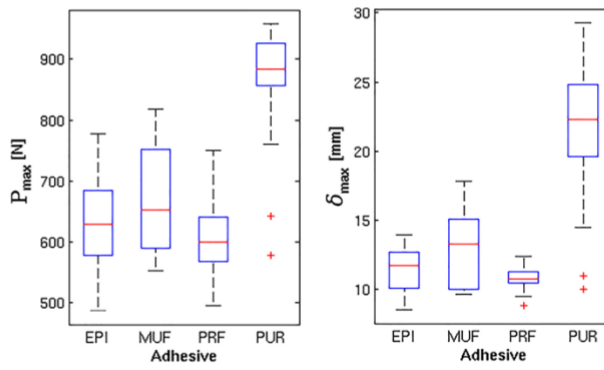


Figure 4: Box plots showing variability for tested adhesives in terms of P_{max} (left) and δ_{max} (right). The red line denotes median value, plus denotes outliers.

wood lamellas is very difficult due to variability of wood properties, their geometry and possible different elastic moduli in tension and compression as found for various species, for instance for beech at MC below 13% (Ozyhar et al. 2013) or for cherry and walnut (Bachtiar et al. 2017). In addition to the unknown position of the NA, these uncertainties contribute to the fact that it is very difficult to obtain true fracture toughness in mode II for wood-bonded specimens. Figure 5c shows three pairs of points above and below NA and their horizontal displacements vs. relative time (pseudo-time of analysis) obtained from FE model that has symmetry of both material properties and geometry with respect to the NA. Curves are paired from outer to inner, and they demonstrate that the closer the pair of points is to the NA, the greater the displacement slip (w_{II}) is, in this case, w_{II} is 2, 4 and 6 mm. The w_{II} is important for deriving a track-separation model, as seen below.

The w versus deflection for all specimens, including the averages for all adhesive groups, is presented in Figure 6. For the EPI, MUF and PRF adhesives, it shows mild increase with loading, and at the point of reaching elastic limit, the curves start progressing steeply. PUR group does not have such rapid change of steepness at the elastic limit. As visible, scatter of the w is very high, especially after reaching the elastic limit. The scatter is

caused by progression of the crack at the bondline that often has a tooth-like effect on a curve. Progression of the crack was not studied for individual specimens, so it is not possible to say whether it happened in the wood or adhesive for a given tooth-like step. Looking at the PUR, it may also be noticed that the polynomial curve experiences an inflection point at a deflection of about 25 mm. This is caused by w data and could be removed by limiting to a certain maximal deflection. However, because the P_{max} was achieved for several specimens after deflection of 25 mm, it would not be consistent to do this within the group and, therefore, it was left as it is. The question that arises from results of PUR (Figures 3 and 6) is whether the methodology used is convenient for testing wood-adhesive bonds made with PUR or PUR-like adhesives, i.e., adhesives with large elastic and plastic strain capacity. Furthermore, using 3D-DIC cannot fully assist in exploration of microcracking at adhesive bond loaded in mode II at such a level of observation. Wood-adhesive bond is a very different situation compared to the adhesive bonds in man-made composites (e.g., carbon-adhesive) where identification of differences for adhesives of various toughness is possible, including the pattern of microcracking because the crack predominantly propagates through adhesive (Bradley 1991). Therefore, displaying

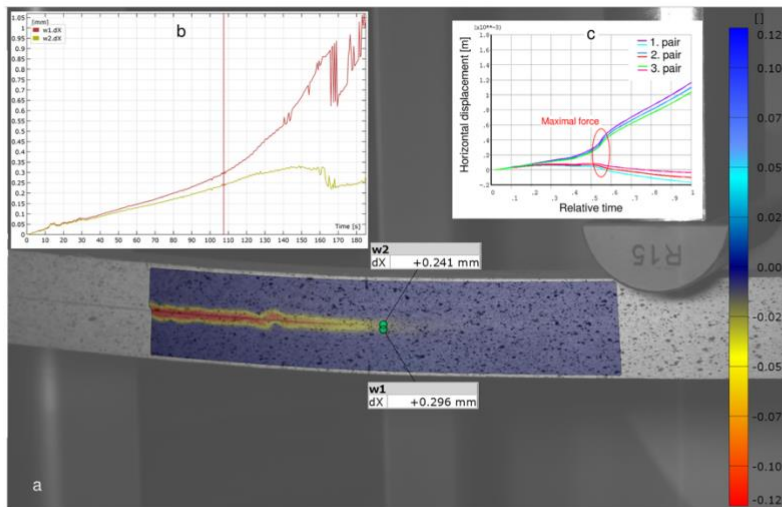


Figure 5: (a) Shear strain (ϵ_{xy}) computed using DIC with the two points used for calculation of displacement slip highlighted (w). (b) Graph showing displacements in horizontal direction vs. time for the two green points at crack tip; (c) horizontal displacements from FE simulation for 3 pairs of points with various vertical distance from the crack tip.

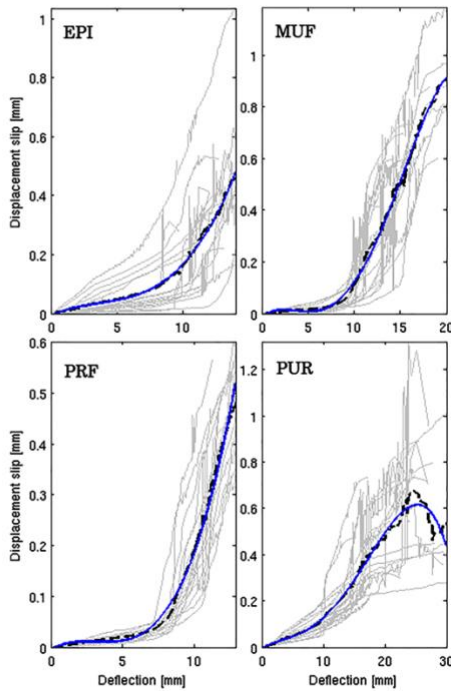


Figure 6: Displacement slip (w) vs. deflection for tested adhesives. Raw data are plotted as grey. The black dashed line represents arithmetic average of curves, and the blue solid line is polynomial fit of 6th degree.

raw data is important and useful for wood-adhesive bondline because it may reveal common phenomena within individual specimen's behavior.

3.3 Strain energy release rate and cohesive model

The procedure of ECLA and Eq. (1) for average P/δ curves and average w enabled to obtain a relationship between G_{II} and equivalent crack length (a_{eq}). The result of this procedure is shown in Figure 7a as four average curves for particular adhesive groups. The curves include mean critical strain energy release rate G_{IIc} (denoted as red asterisk), which attributes for P_{max} . The mean G_{IIc} is 1.80, 2.33, 1.59 and 5.40 Nmm^{-1} for EPI, MUF, PRF and PUR, respectively. PUR has the highest G_{IIc} because the P_{max} was achieved

much later after reaching the elastic limit for other groups of adhesives. All obtained mean values of G_{IIc} are higher than the value for clear beech wood ($1.41 Nmm^{-1}$) at similar MC presented by Sebera et al. (2019). However, with respect to wood variability, it can be claimed that only EPI, MUF and PUR have likely significantly higher G_{IIc} than mentioned value of clear wood due to a presence of adhesive bond. The increase of shear stiffness and shear strength due to a presence of adhesive bondline may happen; for instance, it was reported for balsa wood tested in pure shear using Iosipescu specimens (Osei-Antwi et al. 2013). Such increase is attributed to higher rigidity and shear strength of adhesive compared to wood at loaded plane. From a practical perspective, it is important to know that adhesive bond enhances stiffness and strength

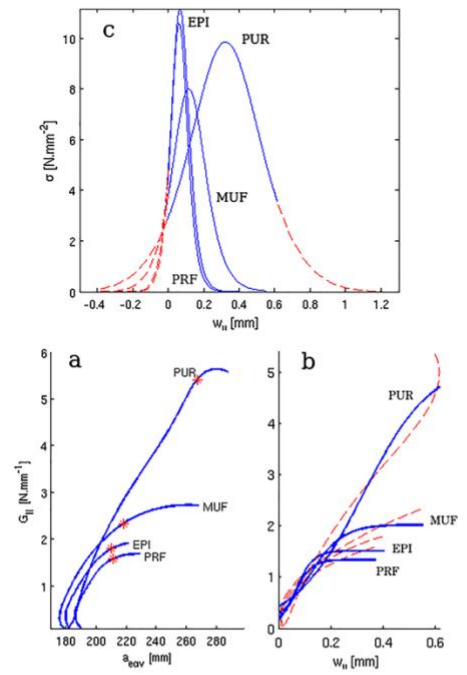


Figure 7: (a) Average strain energy release rate (G_{II}) vs. average equivalent crack length (a_{eq}). Red asterisk denotes average critical strain energy release rate at P_{max} (G_{IIc}). (b) Average G_{II} vs. average displacement slip (w_n). Red lines represent data up to G_{IIc} and blue lines represent logistic function fitted to the averaged curves. (c) Cohesive model computed by differentiating logistic functions (blue part of the curves) shown in Figure 7b and extrapolated cohesive model using Gaussian fit from Table 1 (red dashed parts of curves).

of beam elements which might be used to an advantage when designing timber construction elements.

Using Eq. (2) enabled to find parameters to fit the relationships of G_{II} vs. w_{II} with a logistic function. This functional fit, together with average curves ending at G_{IIc} , is plotted in Figure 7b. The use of logistic function decreased the value of G_{IIc} , which is the value logistic function asymptotically converges to on a given range.

It may also be noticed that those fits do not start at zero of the y -axis, which is due to the fact that the best logistic fit to the G_{II} vs. w_{II} data was used. Differentiation of the logistic curves following Eq. (3) led to a cohesive model for studied adhesives (Figure 7c). The fact that logistic curves do not have a zero tangent at position of $x = 0$ resulted in cohesive models that do not start at zero y -axis (stress) positions (see blue sections of the curves in Figure 7c). Such cohesive models are not complete; i.e., the area under the curves is not equal to the G_{IIc} , so they need to be extrapolated up to $y = 0$. For this, the Gaussian model of 2nd order (GM2) was used, and the result of the fit is listed in Table 1 and plotted as red dashes on the cohesive model in Figure 7c. The GM2 has a form of $a_1 \times e^{-((x - b_1)/c_1)^2} + a_2 \times e^{-((x - b_2)/c_2)^2}$, where x is variable and e is Euler's number. It is also necessary to mention a certain error affecting the derivation of G_{II} stemming from the fact that residual stresses in specimens were neglected. This also implies that obtained toughness is apparent and not true. However, assessing this issue is out of the scope of this study; a method to address this problem was published for double cantilever beams loaded in mode I (Nairn 2000).

3.4 FE model

Cohesive models for all adhesives in the form of 2nd order Gaussian function in Table 2 can be easily transformed into the bilinear cohesive model (BCM) because the Gaussian fit is an evenly symmetric function. The BCM presented in Table 2 was used in FE simulations of the physical test for all adhesives. The results of the simulations are shown in Figure 3 as three solid lines (black for Elas, green for EP and red for EP+). FE prediction of force-displacement response

in the elastic part of the test is sufficient compared to polynomial fit (blue line); only the PRF group shows a certain bump in the middle of the elastic part due to using arithmetic average as the base for polynomial fit. An agreement of FE model with the experiments regarding stiffness is determined by an orthotropic material model taken from the literature (Milch et al. 2016). This implies that wood used in this work had very similar properties as one in the Milch et al. (2016), despite the fact that both woods came from different growing positions within the region of Central Europe.

The prediction of FE models in terms of relative difference (RD) regarding the maximal force (P_{max}) is shown in Table 3. It shows that using the elastic model with cohesive zone predicts P_{max} very accurately for EPI, MUF and PRF groups (RD <5%), but for the PUR adhesive it reaches RD about 13.5%. The EP material model predicts P_{max} within the same accuracy as the elastic one (RD <5.2%), except for the PUR, which has RD of about 15%. This is due to the fact that wood in PUR group started to plasticize parallel to the fiber before reaching stress needed to open the crack. The crack in PUR group opened later at higher load levels and propagated less than for other adhesive groups. This is clearly visible from the green line in Figure 3 that shows the scenario of beech wood with the same tensile and compressive yield stresses. The FE model with EP+ material predicts P_{max} with the lowest RD's (<3.4%); although for EPI, MUF and PRF adhesive, it sometimes exceeds RD compared to Elas and EP material models. The biggest improvement in using EP+ was achieved for PUR adhesive, whose RD decreased to -3.35%. This means the material model with different tensile and compressive yield stresses is the most suitable for modeling PUR-like adhesives for this test. Illustration of this phenomenon when using EP+ material model for the 3ENF test is depicted in Figure 8. It shows that when using elastic material only (Figure 8a), the maximal deflection, and also maximal compressive strain (3rd principal strain ≈ 0.013), occur in the middle of the specimen; meanwhile, when using EP+ material (Figure 8b), the maximal deflection and compressive strain (3rd principal strain ≈ 0.037) occur away from the specimen center

Table 2: Coefficients for 2nd order Gaussian fits ($R > 0.99$ for all) and data for bilinear cohesive model.

Group	a_1	a_2	b_1	b_2	c_1	c_2	G_{IIc} (Nmm ⁻²)	σ_{max} (MPa)	w_{max} (mm)
EPI	5.062	6.096	0.06555	0.06649	0.09984	0.05697	1.51	11.2	0.25
MUF	4.433	3.56	0.1166	0.1153	0.1068	0.187	2.02	7.99	0.43
PRF	5.783	4.816	0.06234	0.06144	0.05283	0.09262	1.33	10.6	0.24
PUR	3.693	6.161	0.3222	0.324	0.204	0.3507	4.69	9.85	0.80

σ_{max} is the peak of the bilinear model and w_{max} is displacement slip at the σ_{max} .

near the introduced crack tip due to reaching yield stress in compression parallel to fiber in the upper part of lamellas. This phenomenon was also observed within the experiments with the PUR group that showed the highest deflection and failure at the crack tip (Figure 8c).

To evaluate the most precise material model of wood for all adhesive bonds altogether, the summation of absolute values of RD's for a given material model can be used (see ΣRD in Table 3). Then, the EP+ performs the best, followed by Elas and EP. However, for a quick, simple, valid and sound prediction of P_{max} , the orthotropic elastic material model is a high-quality choice for EPI, MUF and PRF adhesive bonds. To model adhesive bonds made with PUR, this work suggests using orthotropic elasto-plastic material models of wood with different tensile and compressive yield stresses. This holds true especially for Mode II-dominating problems or problems of bending where induced stresses might get higher yield than stress parallel to fiber of wood. This work implies that used geometrical configuration needs to be modified for testing PUR adhesive bond to achieve deformations only at adhesive bond, i.e., without having plastic strains at surface fibers of specimen. It has been shown that using orthotropic elasto-plastic material models to analyze phenomena occurring when wooden elements are mechanically loaded has become a valid approach leading to more precise predictions. This was demonstrated for clear pine wood (Pěňčík 2015), spruce and beech wood (Milch et al.

2017), and glulam beams made from softwoods with various connection surfaces (Uzel et al. 2018).

3.5 Friction

In the experiment, Teflon paper to reduce the friction between non-glued lamellas was used since it affects the measurement of force and displacement and, consequently, the obtained G_{II} values. The FE model enabled analysis of the impact of friction coefficient between lamellas (μ_{WW}) on stiffness and P_{max} of the specimen. The friction between specimen and steel grips was kept at constant value of $\mu_{SW} = 0.33$. Varying μ_{WW} from 0 to 1 resulted in an increase in P_{max} of ~4.3% and increase of stiffness (P/δ) of ~2.5%. The impact μ_{WW} on both is depicted in Figure 9a; only a scenario with EPI adhesive was computed to illustrate this effect. This means that it is physically justified to insert Teflon paper into the crack to obtain more precise results. The Teflon paper should be located right above the support where the highest contact pressure occurs (Figure 9b). Visual comparison of the two most typical failures that occurred is shown in Figure 9c. It shows that the failure of adhesive bond with PUR adhesive occurred primarily in wood (Figure 9c left); meanwhile, for EPI adhesive (Figure 9c right), it showed brittle-like failure at adhesive-wood interface, which was found to be a typical failure of PRF and MUF groups, too.

Table 3: Relative differences of FE models (%) for various material models of beech wood (constant friction coefficient and no fiber angle distortion), ΣRD is summation of absolute values of all groups for given material model.

Material model	EPI	MUF	PRF	PUR	ΣRD
Elas	4.15	0.28	2.52	13.5	20.45
EP	0.92	-5.14	-0.16	-14.8	21.04
EP+	2.74	-3.27	-0.47	-3.35	9.83

3.6 Fiber angle

The specimens for 3ENF test are relatively long (0.5 m) and, therefore, there is higher probability that fiber direction will not be precisely aligned with specimen main axis. Therefore, the impact of fiber angle distortion on P_{max} and stiffness response with respect to longitudinal axis was analyzed using Elas and EP+ material models because

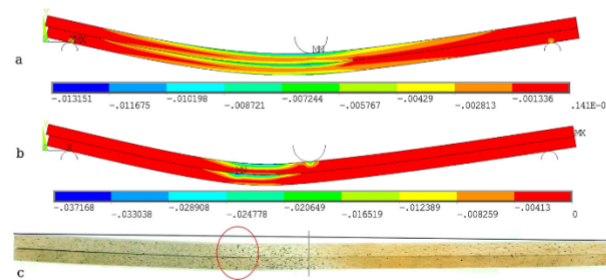


Figure 8: (a) Computed 3rd principal strain at max. deflection for PUR adhesive with Elas material. (b) Computed 3rd principal plastic strain for PUR at δ_{max} with EP+ material. (c) Typical specimen from PUR group with denoted specimen center (grey line) and the δ_{max} at crack tip (red ellipse), photographed after the test.

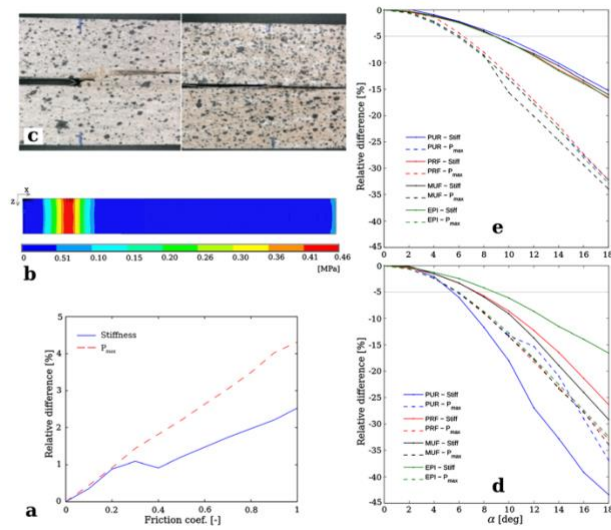


Figure 9: (a) FE analysis of impact of μ_{WW} on stiffness and P_{max} . (b) FE computed friction stress (Pa) at introduced crack (red zone is located right above the support, top view). (c) Typical failure for PUR (left) and EPI & PRF (right). (d) FE analysis of impact of α on stiffness and P_{max} using EP+ material. (e) FE analysis of impact of α on stiffness and P_{max} using Elas material.

these two were shown to be the best to simulate the 3ENF test for given adhesives. Results of these 80 simulations are displayed in Figure 9d and 9e. Figure 9e shows scenarios with Elas material, and it reveals the P_{max} is more impacted by angle distortion than stiffness on average, e.g., at 6° angle distortion, P_{max} is reduced by 5%; meanwhile, stiffness is reduced the same at an angle of 9°. It is clear that by using Elas material, all the adhesive groups behave very alike. On the contrary, using EP+ material shows that the more brittle the adhesive bond is, the less impact the fiber angle has on P_{max} . For instance, for PUR, the 5% or RD is reached at 6°, but for EPI, this RD is achieved at 9°. The impact of grain angle on stiffness using EP+ is similar when Elas material is used. This concludes in a finding that adhesive bonds made by various adhesives react differently to grain angle distortion. If angle distortion below 4° is kept, the impact will be maximally 2.5% in RD for all the adhesives in terms of P_{max} and even lower in terms of stiffness. FE analysis of the effect of fiber angle distortion at specimen cross section (RT plane) on stiffness and P_{max} is not shown since it does not influence the behavior as much; changing the angle at RT plane from 0 to 90° impacted resulting P_{max} until 2% and stiffness below 1%.

4 Conclusions

The presented work deals with an experimental and numerical assessment of fracture behavior for adhesive bond

loaded in mode II using 3-point end-notched flexure tests when various adhesives are used. The work showed results for materials commonly used in wood composites and timber structures, and it also demonstrated applicability of the test to determine fracture properties of wood composites that are suitable for numerical modeling. The work resulted in several important findings that can be concluded as follows:

- Adhesive bond with EPI, PRF and MUF showed rather brittle behavior as the failure and crack occurred primarily at the interface of adhesive and wood. These three adhesives can be conveniently investigated by 3-point end-notched flexure test to obtain apparent fracture toughness and strain energy release rate (G_{IIc}).
- Adhesive bond with PUR showed substantial nonlinear response due to plastic strains occurring in specimens' outermost fibers and PUR elastomeric nature. This phenomenon was also confirmed by numerical analysis and, altogether, results suggest modifying the test configuration to reveal more accurate values of G_{IIc} for bondline made with PUR. Failure and crack propagation in specimens with PUR bondline occurred mostly in wood.
- For EPI, MUF and PRF, elastic material model with cohesive zone offers accurate prediction of maximal force (relative difference below 5%) and character of failure.
- For PUR adhesive, elastic and elasto-plastic model with same tension and compression yields parallel to grain do not offer such high accuracy (relative

difference ~13.5%) compared to model with distinguished yield stresses in tension and compression parallel to fiber (rel. diff. ~3.4%).

- Friction between wooden lamellas in 3-point end-notched flexure test has negligible effect on stiffness (max. ~2%) and minor effect on P_{\max} (max. ~4%). However, to get a more accurate G_{IIc} , introducing any material to reduce friction in between lamellas is recommended.
- Grain angle distortion with respect to longitudinal specimen axis impacts the flexural stiffness and P_{\max} variously depending on adhesive type. In general, having fiber angle below 4° results in a maximal relative difference of 2.5%.

Author contributions: All the authors have accepted responsibility for the entire content of this submitted manuscript and approved submission.

Research funding: The authors gratefully acknowledge the financial support from the European Commission for funding the InnoRenew project (grant agreement #739574) under the Horizon 2020 Widespread-Teaming program and the Republic of Slovenia (investment funding from the Republic of Slovenia and the European Union's European Regional Development Fund), Slovenian Research Agency (Research Core Funding no. P2-0273), Slovenian Research Agency infrastructural program (IO-0035) and company KLP d.o.o. for providing the adhesives for testing.

Conflict of interest statement: The authors declare that they have no conflicts of interest.

References

- Anderson, T. (1995). *Fracture mechanics: fundamentals and applications*, 2nd ed. B. Raton: CRC.
- Arrese, A., Carbajal, N., Vargas, G., and Mujika, F. (2010). A new method of determining mode II R-curve by the End-Notched Flexure test. *Eng. Fract. Mech.* 77: 51–70.
- Bachtliar, E.V., Rüggeberg, M., and Niemi, P. (2017). Mechanical behavior of walnut (*Juglans regia* L.) and cherry (*Prunus avium* L.) wood in tension and compression in all anatomical directions. Revisiting the tensile/compressive stiffness ratios of wood. *Holzforschung* 72: 71–80.
- Bradley, W.L. (1991). Understanding the translation of neat resin toughness into delamination toughness in composites. *Key Eng. Mater.* 37: 161–198.
- Brault, R., Germaneau, A., Dupre, J.C., Doumalin, P., Mistou, S., and Fazzini, M. (2013). In-situ analysis of laminated composite materials by X-ray micro-computed tomography and digital volume correlation. *Exp. Mech.* 53: 1143–1151.
- Clerc, G., Brunner, A., Josset, S., Niemi, P., Pichelin, F., and Van de Kuilen, J.W.G. (2019). Adhesive wood joints under quasi-static and cyclic fatigue fracture Mode II loads. *Int. J. Fatig.* 123: 40–52.
- de Moura, M.F.S.F., Silva, M.A.L., de Morais, A.B., and Morais, J.J.L. (2006). Equivalent crack based mode II fracture characterization of wood. *Eng. Fract. Mech.* 73: 978–993.
- EN 302-1 (2013). *Adhesives for load-bearing timber structures – Test methods – Part 1: determination of bond strength in longitudinal tensile shear*. European Committee for Standardization, Brussels, Belgium.
- Fernandes, R.M.R.P., Chousal, J.A.G., de Moura, M.F.S.F., and Xavier, J. (2013). Determination of cohesive laws of composite bonded joints under mode II loading. *Compos. Part B* 52: 269–274.
- Fortuna, B., Azinović, B., Plos, M., Šuligoj, T., and Turk, G. (2019). Tension strength capacity of finger joined beech lamellas. In: *International scientific conference on hardwood processing*. ISCHP, Delft, Netherlands, pp. 244–251.
- Franke, S. (2016). *Mechanical properties of beech CLT*. World Conference for Timber Engineering (WCTE), Vienna, Austria.
- Hill, R. (1983). *The mathematical theory of plasticity*. Oxford University Press, New York.
- Jelušič, P. and Kravanja, S. (2018). Flexural analysis of laminated solid wood beams with different shear connections. *Construct. Build. Mater.* 174: 456–465.
- Kamke, F.A., Nairn, J.A., Muszynski, L., Paris, J.L., Schwarzkopf, M., and Xiao, X. (2014). Methodology for micromechanical analysis of wood adhesive bonds using X-ray computed tomography and numerical modeling. *Wood Fiber Sci.* 46: 15–28.
- Khansaria, N.M., Farrokhi, A., and Mosavid, A. (2019). Orthotropic mode II shear test fixture: iospesque modification. *Eng. Solid Mech.* 7: 93–108.
- Kutnar, A., Kamke, F., Nairn, J., and Sernek, M. (2008). Mode II fracture behavior of bonded viscoelastic thermal compressed wood. *Wood Fiber Sci.* 40: 362–373.
- Martins, C., Dias, A.M.P.G., and Cruz, H. (2019). Bonding performance of Portuguese Maritime pine glued laminated timber. *Construct. Build. Mater.* 223: 520–529.
- Matsumoto, N. and Nairn, J.A. (2009). The fracture toughness of medium density fiberboard (MDF) including the effects of fiber bridging and crack-plane interference. *Eng. Fract. Mech.* 76: 2748–2757.
- McKinley, P., Kamke, F.A., Sinha, A., De Andrade, V., and Jakes, J.E. (2018). Analysis of adhesive penetration into wood using nano-X-ray computed tomography. *Wood Fiber Sci.* 50: 66–76.
- McKinley, P., Sinha, A., and Kamke, F.A. (2019). Understanding the effect of weathering on adhesive bonds for wood composites using digital image correlation (DIC). *Holzforschung* 73: 155–164.
- Méité, M., Dubois, F., Pop, O., and Absi, J. (2013). Mixed mode fracture properties characterization for wood by digital images correlation and finite element method coupling. *Eng. Fract. Mech.* 105: 86–100.
- Milch, J., Tippner, J., Sebera, V., and Brabec, M. (2016). Determination of the elasto-plastic material characteristics of Norway spruce and European beech wood by experimental and numerical analyses. *Holzforschung* 70: 1081–1092.
- Milch, J., Brabec, M., Sebera, V., and Tippner, J. (2017). Verification of the elastic material characteristics of Norway spruce and European beech in the field of shear behaviour by means of digital image correlation (DIC) for finite element analysis (FEA). *Holzforschung* 71: 405–414.
- Murata, K., Bachtliar, E.V., and Niemi, P. (2017). Determination of mode I and mode II fracture toughness of walnut and cherry in TR

DE GRUYTER

V. Sebera et al.: Wood-adhesive bond loaded in mode II — 13

- and RT crack propagation system by the Arcan test. *Holzforschung* 71: 985–990.
- Nairn, J.A. (2000). Energy release rate analysis for adhesive and laminate double cantilever beam specimens emphasizing the effect of residual stresses. *Int. J. Adhesion Adhes.* 20: 59–70.
- Osei-Antwi, M., de Castro, J., Vassilopoulos, A.P., and Keller, T. (2013). Shear mechanical characterization of balsa wood as core material of composite sandwich panels. *Construct. Build. Mater.* 41: 231–238.
- Ozyhar, T., Hering, S., and Niemz, P. (2013). Moisture-dependent orthotropic tension-compression asymmetry of wood. *Holzforschung* 67: 395–404.
- Pěnčík, J. (2015). Modelling of experimental tests of wooden specimens from Scots pine (*Pinus sylvestris*) with the help of anisotropic plasticity material model. *Drv. Ind.* 66: 27–33.
- Pollmeier. (2019). Comparison of BauBuche and other building materials. Pollmeier Massivholz GmbH & Co.KG, Available at: <http://www.abc.net.au/science/articles/2009/03/31/2530686.htm?site=science&topic=latest>.
- Santos, P., Correia, J.R., Godinho, L., Dias, A.M.P.G., and Dias, A. (2019). Bonding quality assessment of cross-layered Maritime pine elements glued with one-component polyurethane adhesive. *Construct. Build. Mater.* 211: 571–582.
- Schuecker, C. and Davidson, B.D. (2000). Evaluation of the accuracy of the four-point bend end-notched flexure test for mode II delamination toughness determination. *Compos. Sci. Technol.* 60: 2137–2146.
- Sebera, V., Redón-Santafé, M., Brabec, M., Děcký, D., Čermák, P., Tippner, J., and Milch, J. (2019). Thermally modified (TM) beech wood: compression properties, fracture toughness and cohesive law in mode II obtained from the three-point end-notched flexure (3ENF) test. *Holzforschung* 73: 663–672.
- Silva, F.G.A., Morais, J.J.L., Dourado, N., Xavier, J., Pereira, F.A.M., and De Moura, M.F.S.F. (2014). Determination of cohesive laws in wood bonded joints under mode II loading using the ENF test. *Int. J. Adhesion Adhes.* 51: 54–61.
- Silva, M.A.L., de Moura, M.F.S.F., and Morais, J.J.L. (2006). Numerical analysis of the ENF test for mode II wood fracture. *Compos. Part A-Appl. S 37*: 1334–1344.
- Silva, M.A.L., Morais, J.J.L., de Moura, M.F.S.F., and Lousada, J.L. (2007). Mode II wood fracture characterization using the ELS test. *Eng. Fract. Mech.* 74: 2133–2147.
- Stoeckel, F., Konnerth, J., and Gindl-Altmutter, W. (2013). Mechanical properties of adhesives for bonding wood—a review. *Int. J. Adhesion Adhes.* 45: 32–41.
- Tapia, C. and Aicher, S. (2018). *A stochastic finite element model for glulam beams of hardwoods*. World Conference for Timber Engineering (WCTE), Seoul, South Korea.
- Troughton, M.J. (Ed.) (2009). *Chapter 17 - adhesive bonding in handbook of plastics joining, a practical guide*, 2nd ed. William Andrew Publishing, pp. 145–173. Cambridge, UK, ISBN 9780815515814.
- Uzel, M., Togay, A., Anil, Ö., and Söğütü, C. (2018). Experimental investigation of flexural behavior of glulam beams reinforced with different bonding surface materials. *Construct. Build. Mater.* 158: 149–163.
- Vallée, T., Tannert, T., and Fecht, S. (2017). Adhesively bonded connections in the context of timber engineering – a review. *J. Adhes.* 93: 257–287.
- Wang, J. and Qiao, P. (2004). Novel beam analysis of end notched flexure specimen for mode-II fracture. *Eng. Fract. Mech.* 71: 219–231.
- Wang, W.X., Nakata, M., Takao, Y., and Matsubara, T. (2009). Experimental investigation on test methods for mode II interlaminar fracture testing of carbon fiber reinforced composites. *Compos. Part A-Appl 40*: 1447–1455.
- Xavier, J., Morais, J., Dourado, N., and De Moura, M.F.S.F. (2011). Measurement of mode I and mode II fracture properties of wood-bonded joints. *J. Adhes. Sci. Technol.* 25: 2881–2895.
- Xavier, J., Oliveira, M., Morais, J.J.L., and De Moura, M.F.S.F. (2014). Determining mode II cohesive law of *Pinus pinaster* by combining the end-notched flexure test with digital image correlation. *Construct. Build. Mater.* 71: 109–115.
- Yoshihara, H. (2001). Influence of span/depth ratio on the measurement of mode II fracture toughness of wood by end-notched flexure test. *J. Wood Sci.* 47: 8–12.
- Yoshihara, H. (2005). Mode II initiation fracture toughness analysis for wood obtained by 3-ENF test. *Compos. Sci. Technol.* 65: 2198–2207.
- Yoshihara, H. (2010). Mode I and mode II initiation fracture toughness and resistance curve of medium density fiberboard measured by double cantilever beam and three-point bend end-notched flexure tests. *Eng. Fract. Mech.* 77: 2537–2549.
- Yoshihara, H. and Ohta, M. (2000). Measurement of mode II fracture toughness of wood by the end-notched flexure test. *J. Wood Sci.* 46: 273–278.

2.3 Article 3

Title: Mechanical performance of timber connections made of thick flexible polyurethane adhesives

Authors: Jaka Gašper Pečnik Igor Gavrić, Václav Sebera, Meta Kržan, Arkadiusz Kwiecien, Bogusław Zając, Boris Azinović

Year: 2021

Journal: Engineering Structures (ISSN: 1873-7323)

DOI: <https://doi.org/10.1016/j.engstruct.2021.113125>

Link: www.sciencedirect.com/science/article/pii/S0141029621012608?via%3Dihub



Mechanical performance of timber connections made of thick flexible polyurethane adhesives

Jaka Gašper Pečnik^{a,b}, Igor Gavrić^{a,b}, Václav Sebera^a, Meta Kržan^c, Arkadiusz Kwiecień^d, Bogusław Zając^d, Boris Azinović^{c,*}

^a InnoRenew Coe, Ljvade 6, 6310 Izola, Slovenia

^b University of Primorska, Tilov trg 4, 6000 Koper, Slovenia

^c Slovenian National Building and Civil Engineering Institute, Dimičeva ulica 12, 1000 Ljubljana, Slovenia

^d Cracow University of Technology, Warszawska 24, 31 155 Kraków, Poland

ARTICLE INFO

Keywords:

Flexible adhesive
Timber connection
Polyurethane
Double lap shear
Cyclic loading
Energy dissipation

ABSTRACT

This study investigates timber connections with flexible polyurethane adhesives, which prove to have the potential for timber-adhesive composite structures without mechanical connections for seismic regions. Results of conducted cyclic double lap-shear adhesive timber joints tests were compared with available experimental results on timber connections with standard mechanical dowel-type fasteners and with results of numerical finite element analysis. The study found that the shear strength, elastic stiffness and strength degradation capacity of the flexible adhesive connections were significantly higher compared to mechanical fasteners commonly used in seismic-resistant timber connections. The latter, however, manifested larger ultimate displacements but also yielded at lower displacements.

1. Introduction

Mass timber, especially cross-laminated timber (CLT), is becoming an increasingly popular building material in Europe and across the world. The versatility of CLT has encouraged engineers to build from low to tall rise buildings. CLT panels perform in high stiffness, resistance to shear, tension and compression in-plane, and act in low ductility and dissipation of energy [1]. The connections between the CLT elements play a key role in ductility and energy dissipation of timber structures in addition to providing sufficient stiffness and strength between the structural elements and, thus, require special attention [2]. Therefore, the behaviour of CLT buildings during earthquakes depends mainly on the performance of connections between adjacent panels and other structural elements [3]. Several full-scale CLT building tests showed that damage and eventual failures during earthquakes are primarily localized in connections. When connections are too rigid, large accelerations can occur in the upper stories due to the lightweight nature of timber structures [4]. This may result in injuries to occupants and damage to property, which is not acceptable in terms of serviceability. Therefore, the structural system should be adapted by incorporating elements with

sufficient strength and desired stiffness, which possibly reduces the structural damage through different energy dissipation mechanisms. This is typically achieved by applying mechanical dissipative connections that are installed in various parts of the structure, where deformations and, consequently, energy dissipation are desired. Furthermore, these elements are usually designed to have sufficient ductility to sustain extreme loads to prevent brittle failure of structural elements in case of extreme seismic events. They are usually not cost-effective or even feasible to design in order to sustain such high strength and displacement demands without significant damage. In addition to standard fastening solutions such as dowel-type fasteners (nails, screws, dowels) and metal connectors (hold-downs, angle brackets, nail plates), which cause plasticizing of timber under cyclic loads [5,6], several solutions for dissipative connections have already been suggested to improve the ductile response of CLT buildings [7–13]. These solutions have been mainly focused on mechanical connections with concentrated plasticity. In such systems, the dissipation is concentrated in a small area that must be very carefully designed to prevent damage to other parts of the structure. Moreover, plasticized connectors must be exchanged for new ones to continue the protection

* Corresponding author.

E-mail addresses: jaka.pecnik@innorenew.eu (J.G. Pečnik), igor.gavric@innorenew.eu (I. Gavrić), vaclav.sebera@innorenew.eu (V. Sebera), meta.krzan@zag.si (M. Kržan), akwiciec@pk.edu.pl (A. Kwiecień), bozajac@pk.edu.pl (B. Zając), boris.azinovic@zag.si (B. Azinović).

<https://doi.org/10.1016/j.engstruct.2021.113125>

Received 31 January 2021; Received in revised form 29 July 2021; Accepted 31 August 2021

Available online 24 September 2021

0141-0296/© 2021 The Authors. Published by Elsevier Ltd. This is an open access article under the CC BY license (<http://creativecommons.org/licenses/by/4.0/>).

of a structure.

On the other hand, recent studies of adhesive bonding show several advantages. Adhesive connections can exhibit uniform stress distribution along the connection and, therefore, can reduce localized high stresses [14,15]. Mechanical fasteners may, on the other hand, cause undesired damage in the wood fibrous structure, introducing local stress concentrations [5,6], and cause bridging water into the wood structure [16]. In addition, they contribute to weight, cost, presence of corrosive elements and require additional machining operations [17]. Furthermore, damages caused by mechanical fasteners during ductile behavior of connections result in irreversible deformations of the structure, which may result in demanding and expensive repair after the earthquake. Elastic joining of structural elements and use of highly deformable adhesives have been successfully used for flexible joints or fibre grids for seismic strengthening of reinforced concrete frames with brick masonry infills [18]. Such polyurethane-based flexible adhesives have been studied for increasing the ductility of existing structures by repairing composite-to-brick bond or concrete elements [19–21].

Studies related to timber have been looking at the use of flexible adhesives for improving bending resistance of beams [22,23], comparison of rigid and flexible adhesives to connections with screws [24] and tensile loading performance of bonded timber elements with brittle and ductile adhesives [25] as well as studying the behaviour of joints for prefabricated timber structures [26] and repair of historical timber structures [27]. Recent innovation showed applications of polyurethane butt-joint bonding for structural timber bonding [28]. Shear characteristics are usually decisive in the design of durable timber adhesive bonds [29,30]. For thin bondlines, the methods for shear testing are well-established and standardized [31], while on the contrary, flexible adhesives are not commonly addressed from a mechanical perspective. Thick flexible adhesive bonds exhibit higher deformations, have better load transfer, and absorb more energy over impact events than rigid thin bondlines. Additionally, their damping capacity is beneficial since it reduces the transfer of noise and undesirable vibrations between timber elements, while the more uniform distribution of shear stresses in the thick adhesive bondlines can also result in better fatigue resistance [32], resistance to seismic action [18] and improved damping properties [33]. Bondline thickness and overlap length are important characteristics for the mechanical performance of joints with flexible adhesives. As reported by Banea and Silva [34], increasing bondline thickness results in decreasing joint strength, while increasing overlap length improves rigidity of the joint. Scale effect was proven in the case of NSM (near surface mounted) composite strengthening application with PS adhesive loaded in shear, where small-scale specimen tests on flexible adhesives [35] manifested lower effectiveness than the same system applied in large-scale specimens [36].

Characteristics of flexible adhesives indicate opportunities for applications in timber constructions for either mechanical or physical improvements. Therefore, the objective of this paper is to identify the potential of thick flexible adhesive bondlines as a dissipative connection in timber structures in seismic-prone areas as a possible addition or alternative to common traditional timber connections. Possibilities of innovative timber connections with thick flexible polyurethane adhesives will be examined for application in seismic areas. These types of connections could serve as dissipative connections or high strength and high stiffness elastically deformable non-dissipative connections. One of the possible applications for such adhesives in CLT connections could be in vertical step joints between adjacent CLT wall panels, which behave with reduced stiffness but exhibit higher displacement capacity under cyclic loading compared to single layout monolithic CLT wall panels [37,38]. Large overlapping areas in step joints and dissipative capabilities make this type of connection a good candidate for improvements with flexible adhesives. Increasing the number of coupled panels into smaller segments would allow more panel rocking movement during seismic events. Additionally, the application of timber connections with thick flexible polyurethane adhesives could serve for flexible glued-in

rod connections in timber structures and other types of structural connections such as steel-to-timber flexible connections and potentially even in structural glass-to-timber connections, where additional elastic flexibility with sufficient strength capacity would be desired. Further, secondary and non-load bearing elements in buildings that are sensitive to brittle failures during seismic events (such as large windows) could be additional field of application of these type of innovative connections in buildings. To verify such application, this paper fully describes the mechanical behaviour of thick flexible adhesive bondline exposed to monotonic and reversed cyclic loading.

The study highlights the following goals: (i) evaluation of mechanical characteristics of timber connections using three different flexible adhesives and two different bondline thicknesses obtained under monotonic and reverse cyclic loading; (ii) theoretical/analytical comparison of results to mechanical properties of standard dowel-type fasteners used in current CLT building applications; (iii) finite element model design for further investigation of bondline characteristics and its effect on the mechanical performance of flexible adhesive joints.

2. Materials and methods

2.1. Specimens and adhesives

Double lap-shear wood samples were made from Norway spruce (*Picea abies* L.). First, the wood was cut into elements with dimensions $30 \times 35 \times 200$ mm (width \times thickness \times length) for middle parts and $20 \times 35 \times 200$ mm for side parts of the specimen. Surfaces of adherends were coated with SIKAZP Primer as recommended by the producer [39]. After 24 h of drying, the primer, double lap-shear forms with targeted thickness gaps between the adherends and 100 mm overlap length were assembled. Gaps and open spaces in the specimen geometry were closed using blocks of extruded polystyrene to prevent the adhesive from leaking. The middle timber part of the double lap-shear specimen was increased in width by adding two smaller timber blocks to each side to provide a greater clamping area for testing grips.

Three different types of two-component polyurethane-based adhesives, originated from SIKAPoland, were used in this study. To evaluate the mechanical characteristics of the adhesives, 6 specimens of each were tested in tension with a 5 mm/min loading rate (Fig. 1). To derive the material model for the finite element (FE) model of lap shear, arithmetic mean curves (thick lines in Fig. 1) were transferred into 7–12 stress-strain points. Adhesive PS has the highest modulus of elasticity but the lowest strength and elongation at break; PTS has a larger elongation at break than PS but the lowest modulus of elasticity; PST adhesive has the highest tensile strength and modulus of elasticity and elongation at break between PS and PTS (Fig. 1).

For the construction of specimens for double-lap shear testing of timber connections with the flexible adhesives, all adhesives' components were precisely weighed according to the producer's instructions on the component ratios and stirred together using a hand pistol and a mixing tool. The adhesive was poured into the double lap-shear timber-molds and dried for 24 h. No additional pressure was applied on the adherend. After the adhesive had hardened, the specimens were again planed to the final thickness of 30 mm and the excess adhesive on the top was removed to assure a plain surface. The specimens were stored in a climate chamber at $(20 \pm 2)^\circ\text{C}$ and $(65 \pm 5)\%$ relative humidity for at least one week before the first test started.

For each of the three selected adhesives (PS, PST, PTS), two different thicknesses (10 and 15 mm) were used, resulting in a total of 6 sample groups. A number of at least 4 repetitions for monotonic tests and cyclic tests for each type of adhesive and each bond-line thickness was chosen prior to the experimental campaign. For this, a limited number of specimens was produced in advance, and the tests were performed on all available specimens. In some cases, the specimen production was not successful due to out-of-factory conditions (non-uniform adhesive consistency, trapped air bubbles in specimens, etc.), and therefore, the

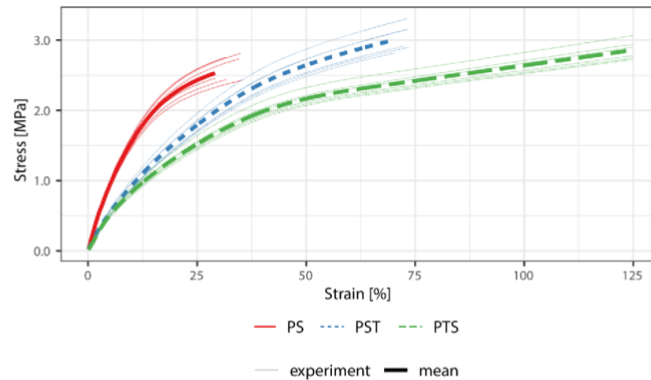


Fig. 1. Stress–strain relationship of the tested PS, PST and PTS adhesives (mean values in bold).

specimens were not suitable for tests. To provide additional valuable information, such as the influence of the number of specimens on the variance of the mechanical properties, all suitable specimens were tested, and all the obtained results are presented in the paper. Therefore, 4 monotonic tests and 4–8 cyclic tests were performed within each of the groups for a total of 55 double lap-shear tests (Table 1).

The specimen labelling is uniform throughout the paper, indicating each group by type of adhesive, thickness (10 or 15 mm) and type of tests (“M” for monotonic, “C” for cyclic).

2.2. Experimental test design

Both cyclic and monotonic tests were performed on a universal testing machine (UTM) Zwick Roell Z050. The specimens were clamped with hydraulic grips on the top part (central element) and the bottom part (two side elements), applying 7.5 MPa side pressure, to prevent specimens from slipping. The top part of the specimen was fixed, while displacement-controlled loading was induced to the lower part with a loading rate of 5 mm/min.

First, monotonic tests were conducted to further design cyclic protocol according to ISO 16670 standard [40], a reverse cyclic testing method for mechanically joint fasteners. Ultimate displacements from force-displacement ($F-u$) curves obtained from monotonic tests were used to determine cyclic steps. Ultimate displacement (u_b) of the specimens, i.e., failure, was defined as the point where the force decreases to 80 % of the maximum force (F_{max}). For each specimen group, average u_b displacements from monotonic tests were used to determine group loading protocols. The test started when the specimen was in the neutral unloaded position, following the positive (downward) and negative (upward) direction. Loading protocol was strain-controlled over external linear position transducer (LPT) Novotechnik connected to a digital amplifier that was connected to UTM. Specimen setup during the testing phase is shown in Fig. 3.

To fully characterize mechanical properties from cyclic test results, a

Table 1
Double lap-shear test schedule (M – monotonic, C – cyclic).

Name	Adhesive thickness [mm]	No. of tests(M/C)
PS-10-M	PS-10-C	10
PST-10-M	PST-10-C	4/4
PTS-10-M	PTS-10-C	4/5
PS-15-M	PS-15-C	4/8
PST-15-M	PS-15-C	4/4
PST-15-M	PST-15-C	4/6
PTS-15-M	PTS-15-C	4/4

procedure from EN 12512 standard [41] was combined with ISO 16670 [40]. Elastic and plastic stiffness values, forces and corresponding displacements at yield point, maximum strength point and failure point, and ductility values were for results of both monotonic and cyclic tests assessed following the EN 12512 procedure. For cyclic tests, equivalent viscous damping ratio and strength degradation were also calculated for each loading cycle (see Section 3). Additionally, average values of ultimate shear strain at the failure point (γ_u) were derived as a ratio between ultimate displacement (u_u) and adhesive thickness (t), maximum shear strength (f_{max}) as a ratio between maximum force and the total bond area (A), and shear modulus (G) as a ratio between shear stress at the yield point ($\bar{f}_y = F_y / A$) and shear strain at the yield point ($\gamma_y = u_y / t$).

2.3. Numerical model

The physical tests – double lap-shear – carried out on the UTM was modelled using finite elements (FE) implemented in software Ansys 19.1 R1 (Ansys® Academic Research, Release 19.1) [42]. The specimen geometry, material composition and boundary conditions reflected the physical test on UTM, although the geometry was modelled as plane-stress with a defined thickness (Fig. 2).

Both wood material and adhesive were modelled using solid quadratic finite element PLANE183. Wood was modelled as linear elastic orthotropic material, adhesives were modelled as hyper-elastic material using two-parameter Yeoh model (YM2), see Table 2. Parameters of YM2 were obtained by curve-fitting the spline curves that interpolated data given from the experiments (Table 2), parameters d_1 and d_2 of YM2 were equal to zero for all adhesives. The curve fitting to YM2 was carried out in Ansys 19.1 [42].

The contact of wood with steel grips from the UTM was neglected as the boundary conditions were applied directly to the nodes of the wooden component. The connection between the adhesive and wood was defined as fully fixed, so no debonding was considered. The element size was set to 5 mm for wooden parts, but the adhesive element size reflected the thickness of the adhesive layer. The total number of elements/nodes was approximately 1100/3500 for a scenario with 10 mm thick adhesive. The geometrical model does contain right angles with infinitely small radii because stress and strain at corners was not analysed in our work. The FE model enabled us to perform a sensitivity study on the influence of adhesive thickness on resulting $F-u$ response and stress distribution along horizontal and vertical paths cutting the specimen (see Fig. 2).

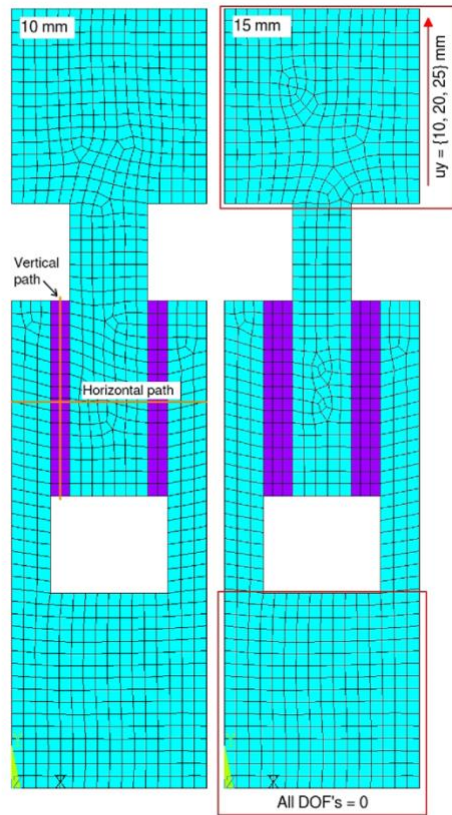


Fig. 2. Finite element mesh for adhesive bonds of 10 mm and 15 mm thickness, including defined paths and boundary conditions of nodes in red rectangles. Colours represent different material (wood vs. adhesive).

3. Results and discussion

3.1. Failure mechanisms

Initial deformations were, as expected, a result of elastic shear deformations of the adhesive due to considerably higher flexibility of the adhesive in comparison with wood. In general, four different failure scenarios were observed, as presented in Fig. 3. In most cases, failure occurred in the area between adherend and adhesive as a consequence of debonding at the interface between wood and adhesive.

In both testing regimes, the adhesive peeled from the adherend either on the edge of the inner or the edge of the outer side of the adhesive bond. It was also often observed that the peeling started on the top of adherend in either the inner or outer side and propagated to a certain length and then further propagated on the opposite side until significant stress reduction occurred (Fig. 3a, 3b). Particularly under the cyclic test, the peeling was also present on the bottom side of the adherend under compression loading of the specimen (positive direction). Under cyclic loading, the peeling in the middle adherend propagated with every cycle and with every increase in displacement step. Thicker (15 mm) PTS and PST bondlines often also exhibited failure in the adhesive (Fig. 3c). Rarely, brittle failure occurred in wood in the central or side component due to exceeded strengths combined by tension perpendicular to grain and shear parallel to the grain. This was especially caused by eccentricity in loading in the latter phase of the test, where unequally peeled adhesive on either side of the sample caused slight rotation of the timber elements (Fig. 3d). In such cases, specimens were eliminated from further analyses.

Table 2
Material properties used in FE analyses.

Material	Orthotropic elastic	Yeoh model parameters	
Spruce*	$E_L = 14850 \text{ MPa}$, $E_R = 352 \text{ MPa}$, $E_T = 289 \text{ MPa}$, $G_{LR} = 573 \text{ MPa}$, $G_{RT} = 53 \text{ MPa}$, $G_{LT} = 474 \text{ MPa}$, $\nu_{LR} = 0.023$, $\nu_{RT} = 0.557$, $\nu_{LT} = 0.014$ [-] Isotropic hyperelastic	C10	C20
	Strain/Stress [-/MPa]	[MPa]	[MPa]
PS	0/0.022, 0.05/0.938, 0.1/1.555, 0.15/1.984, 0.2/2.257, 0.25/2.4316, 0.3/2.531	-2.977	-2.812
PST	0/0.0173, 0.1/0.933, 0.2/1.541, 0.3/2.025, 0.4/2.392, 0.5/2.645, 0.6/2.838, 0.7/3.001	1.578	-0.241
PTS	0/0.0173, 0.1/0.840, 0.2/1.321, 0.3/1.701, 0.4/1.983, 0.5/2.168, 0.6/2.286, 0.7/2.377, 0.8/2.466, 0.9/2.554, 1/2.641, 1.1/2.727, 1.2/2.816, 1.26/2.869	1.167	-0.092

E , G , and ν denote normal and shear moduli and Poisson's ratio, respectively; Indices L, R, T stand for anatomical directions of wood – longitudinal, radial and tangential, respectively. * Data taken from [43].

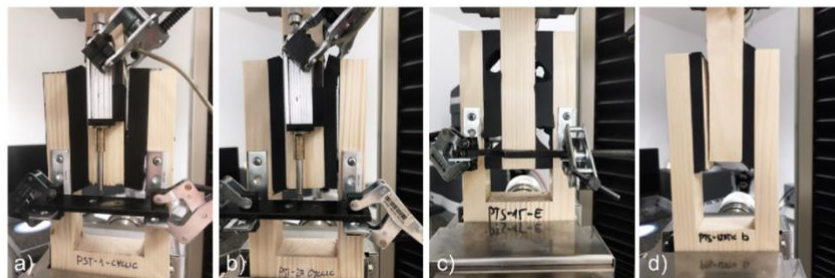


Fig. 3. Four typical types of failure: peeling on the side of the middle adherend (a), peeling on the side of a side adherend (b), dissipative adhesive failure (c), brittle failure in the adherend (d).

3.2. Monotonic tests

Force-displacement (F - u) diagrams for three types of adhesive and both thicknesses are depicted in Fig. 4 with some notable differences visible for both thicknesses and adhesives. For all adhesives, a higher maximum force (F_{max}) was reached for thinner bondlines. Displacement at F_{max} (D_{max}) grows in order of adhesives PS, PST, and PTS, respectively and also implies their hyper-elastic behaviour. Dashed lines in Fig. 4 indicate results of FE analyses based on material data (Fig. 1). The relative difference (RD) of stiffness (K_d) between FE models and experiments (Table 3) is given by $RD = (X_{FEM}/X_{EXP} - 1) * 100$. The RD for PS, PST and PTS adhesives for both thicknesses (10 and 15 mm) is following: 54 and 39 %; 24 and 7.3 %, 14 and 38 %. It is clear that all FE models are overestimating K_d compared to experiments, which is due to a fact the experiments always contain certain imperfections in material and boundary conditions contrary to flawless FE models. Numerical prediction of bondline strength using F_{max} and D_{max} is complicated since FE models do not have adhesion strength between wood and adhesive defined, which showed to be a key factor reducing bond strength in the experiments. Besides that, FE models do not fail at higher thicknesses either due to tremendous strain at failure of the adhesives, so their comparison with experiments is very limited and omitted here. However, the simulated F - u curves exhibit clearly that predicted F_{max} are or would be higher than experimental ones. To overcome the limitation of strength predictions of such FE models, one has to combine fracture mechanics models defined on an interface of wood and adhesive, together with presented hyperelastic material models. Nonetheless, even though this work showed importance in definition of fracture models to predict strength of such bonds, it was not aim of this work and, therefore, it is kept as a task for further research.

In Table 3, average values of evaluated mechanical properties from monotonic tests for each specimen group are presented, together with standard deviation values and coefficient of variance.

The highest elastic stiffness and shear modulus were achieved in PS adhesives, followed by PST adhesives, while the lowest stiffness was for PTS adhesive. With increased bondline thickness, the elastic and plastic stiffness were reduced by 25 %, on average, for all three adhesives. Among 15 mm thick bondlines, PS showed the highest stiffness. PTS-15 showed the lowest stiffness, with an average of 45 % lower values compared to the PS-15 group, while PST-15 resulted in a 30 % lower elastic stiffness value compared to PS-15. Average strength capacities were found to be higher for 10 mm thick adhesives descending from PST-10, PTS-10 and PS-10 with 1.74 MPa, 1.71 MPa and 1.48 MPa, respectively. The difference in average strength capacity between PS, PST and PTS adhesives with 15 mm in thickness compared to 10 mm

showed values decreased by 19 %, 32 % and 19 %, respectively. The achieved strength capacity values were significantly lower in all cases compared to the measured tensile strength values (Fig. 1). This can be attributed to the fact that the full-strength capacity of the adhesive could not be achieved due to the weaker strength capacity of the bond between the adherent and adhesive, as previously reported in Section 3.1 and shown in Fig. 3. To achieve higher strength capacities of such lap-shear connections, the bond strength capacity between wood and adhesive should be enhanced by roughening the wood surface or optimizing the primer to achieve higher adhesion capacity between wood and adhesive. In terms of deformability, PTS-15 adhesive exhibited significantly better performance, namely 1.8 times and 2.3 times higher displacement capacity and ultimate shear strain compared to PST-15 and PS-15 adhesives, respectively. The effect of adhesive thickness was not as pronounced, namely the differences between average values of 10 mm and 15 mm thick adhesives varied between 8 and 14 %, while achieved ultimate shear strain values were significantly higher in 10 mm thick adhesives compared to 15 mm (31–71% difference). Further, PTS adhesive showed the highest ductility (ratio between ultimate displacement and yield displacement) among all adhesives and both thicknesses. PTS-15 exhibited 21 % and 7 % higher ductility than PST-15 and PS-15, respectively. In the case of thinner bondlines, the PTS-10 group showed only 8 % and 2 % higher ductility compared to PST and PS adhesive, respectively. Similarly, as in the case of displacement capacity, ductility values were not affected by increased bondline thickness, namely the ductility values increase or decrease was 10 % or less in all three adhesives.

3.3. Cyclic tests

Overall behaviour, in terms of strength and deformation capacity, and failure mechanisms in cyclic tests correlated with the prior observations from monotonic tests. Typical hysteresis loops for each group in Fig. 5 display the effects of thickness and type of adhesive by different shape of the hysteresis loops, number of achieved steps and loading cycles. The shapes of the hysteresis loops are not like typical mechanical timber connection or timber wall elements using mechanical fasteners [3,37,38], namely flexible adhesive hysteresis loops display a considerably higher proportion of elastic deformability; while on the other hand, they usually display lower plastic deformation capacity. In addition, recovery stiffness in 2nd and 3rd cycles at the same amplitude displacement is more linear than in the case of mechanical connections, as there is no effect of metal fasteners embedment into the wood. Moreover, the level of the stiffness reduction after the 1st cycle is generally lower in the case of flexible adhesive connections as there is no

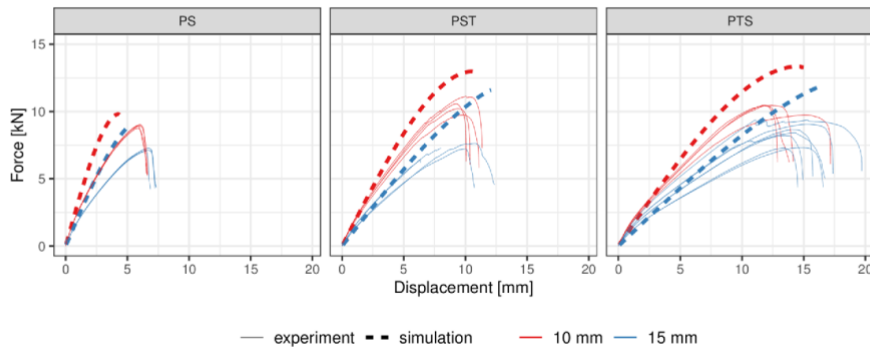


Fig. 4. Force-displacement diagrams of monotonic tests for different adhesives and thicknesses (10 mm thickness in red, 15 mm thickness in blue).

Table 3

Average values of mechanical properties from monotonic test results: elastic and plastic stiffness (k_{el} , k_{pl}), shear modulus (G), force and displacement at the yielding point, (F_y , u_y), maximum load (F_{max}), displacement at maximum force (u_{Fmax}), maximum shear strength (f_{max}), ultimate load ($F_{u,80\%}$), ultimate displacement (u_u), ultimate shear strain (γ_u), and ductility (D).

Adhesive	k_{el} [kN/mm]	G [MPa]	k_{pl} [kN/mm]	F_y [kN]	u_y [mm]	F_{max} [kN]	u_{Fmax} [mm]	f_{max} [MPa]	$F_{u,80\%}$ [kN]	u_u [mm]	ϵ_u	D [-]	D [-]
PS-10-M	avg	2.13	3.68	0.35	8.13	3.68	8.90	5.93	1.48	7.12	6.45	0.65	1.75
	stdev	0.03	-	0.00	0.11	0.07	0.11	0.11	0.02	0.09	0.06	-	0.03
	cov [%]	1.23	-	1.23	1.33	1.96	1.26	1.87	1.26	1.26	0.98	-	1.59
PS-15-M	avg	1.55	4.01	0.26	6.53	4.07	7.18	6.64	1.20	5.74	7.03	0.47	1.73
	stdev	0.01	-	0.00	0.09	0.04	0.10	0.10	0.02	0.08	0.20	-	0.04
	cov [%]	0.58	-	0.58	1.39	0.94	1.43	1.55	1.43	1.43	2.90	-	2.51
PST-10-M	avg	1.44	2.49	0.24	9.68	6.49	10.41	9.63	1.74	8.33	10.64	1.06	1.64
	stdev	0.05	-	0.01	0.57	0.20	0.59	0.36	0.10	0.47	0.57	-	0.10
	cov [%]	3.51	-	3.51	5.90	3.04	5.64	3.78	5.64	5.64	5.36	-	6.23
PST-15-M	avg	1.09	2.75	0.18	6.69	6.08	7.15	8.77	1.19	6.33	9.16	0.61	1.49
	stdev	0.13	-	0.02	0.41	1.03	0.50	2.00	0.08	0.63	2.45	-	0.16
	cov [%]	12.15	-	12.15	6.06	16.89	7.04	22.76	7.04	9.95	26.79	-	11.09
PTS-10-M	avg	1.13	1.98	0.19	9.47	7.98	10.27	12.66	1.71	8.22	14.26	1.43	1.79
	stdev	0.04	-	0.01	0.57	0.36	0.36	1.66	0.06	0.29	1.99	-	0.32
	cov [%]	3.32	-	3.32	6.03	4.45	3.51	13.09	3.51	3.51	13.93	-	17.91
PTS-15-M	avg	0.85	2.19	0.14	7.66	8.75	8.34	13.76	1.39	6.67	16.31	1.09	1.88
	stdev	0.13	-	0.02	0.75	0.75	0.81	1.34	0.13	0.64	1.69	-	0.32
	cov [%]	15.66	-	15.66	9.85	8.54	9.67	9.76	9.67	9.67	10.37	-	17.02

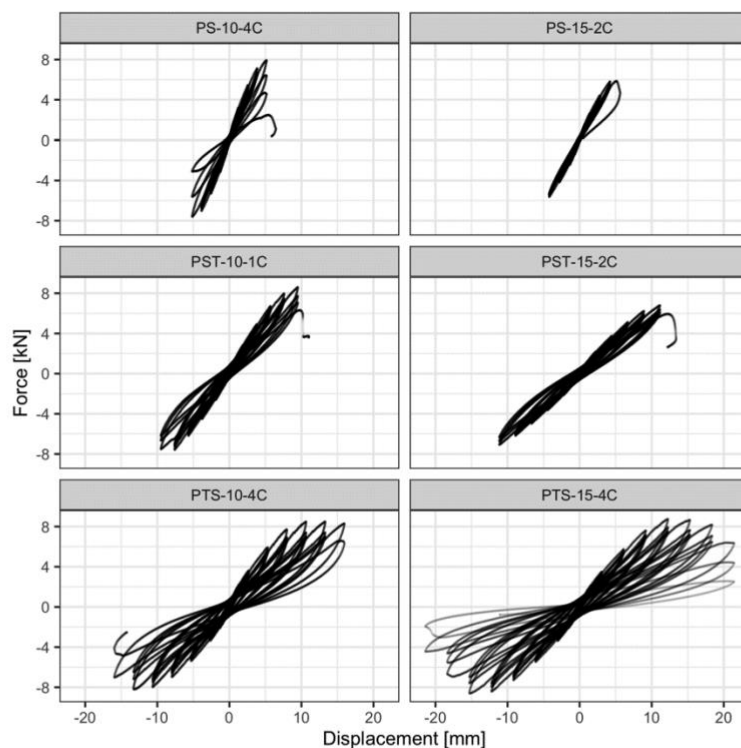


Fig. 5. Examples of typical hysteresis curves for each test group from cyclic testing.

formed gap between the fastener and wood, as is the case in mechanical connections. In the case of flexible adhesive connection, the connection between the wood and adhesives remains intact in the linear part of the response; while in the non-linear part, the stiffness reduction is due to partial peeling of the adhesive, which causes gradual progressive stiffness reduction. In addition, the hysteresis shapes differ in the unloading part of the cycles, where the force drop in mechanical connections is usually rapid, and the force drop in the case of adhesive connections is more gradual. Consequently, this results in a smaller hysteresis loop area, which indicates lower energy dissipation capacity. Further comparison among flexible adhesive connections' cyclic behaviour properties from this study is directly compared with corresponding mechanical connection's properties in Section 3.4. The least flexible PS adhesive shows better performance with a thinner adhesive layer, while in the case of two other types of adhesives, the thicker bondline outperforms the thinner one. Fewer loading steps were also reached for PS than PST or PTS in the case of the thicker bondline.

Fig. 6 displays backbone curves for all cyclic tests performed for six different test groups. A comparison was done for different types of adhesives and different thicknesses among the same type of adhesive. Bold lines present 10 mm adhesive thickness, while dashed lines present 15 mm adhesive thickness. Typically, slightly higher ultimate displacements are met for thicker bondline in PS and PST cases, while in the case of PTS, more loading steps and, consequently, significantly larger ultimate displacements are reached. Inclination of the curve identifies decreasing stiffness among adhesives from less to more flexible.

In Table 4, strength and deformability properties evaluated from backbone envelope curves (Fig. 6) are presented by considering average values from the positive and negative part of loading in absolute values following the same assessment procedure as presented in Section 3.2.

Higher elastic and plastic stiffness were observed in tests with thinner bondlines among the tests with the same type of adhesive. For instance, the average k_{el} for PS, PST and PTS was 27 %, 29 % and 16 % lower in tests with 15 mm thick bondline. Percentwise, a similar reduction was observed for PS and PTS in the monotonic test, while a lower reduction was obtained in the case of the cyclic PTS group. Similar to in the monotonic test, again PS adhesive showed the highest elastic stiffness and PTS adhesive the lowest. In this case, the PTS-15 group showed, on average, 41 % lower stiffness in comparison to the PS-15 group. This result is close to the result of the monotonic test (45 % reduction), while greater stiffness reduction was also noticed for the PST-15 group with a 41 % reduction. On the other hand, comparison between monotonic and cyclic tests has shown that in the case of cyclic test, values for elastic stiffness were higher for all cases except for the PST-15 group that showed comparable value.

While PS adhesive displayed higher initial stiffness, its deformation capacity was much more limited compared to PST and PTS adhesives, while it also displayed slightly lower strength capacity compared to the other two adhesives. PTS adhesive performed with the highest deformation capacity, while also being the most flexible (the lowest elastic stiffness values). The strength capacity of PTS adhesive was comparable with PST adhesive.

In terms of ductility, the highest values were observed for PTS adhesive. The highest average value, of 2.37 for PTS-10, showed 44 % and 31 % higher ductility (D) against PST-10 and PS-10, respectively. PTS-15 group showed 4 % lower D against PTS-10, which overall resulted, on average, to 49 % and 47 % higher D against PST-15 and PS-15 group, respectively. Similar to stiffness, the ductility was lower for thicker bondline with a 4 %, 7 % and 14 % decrease in the group for PTS, PST and PS, respectively. The most significant increase between monotonic and cyclic test was found for PTS adhesive with almost 1.2 and 1.3 higher D for 15 and 10 mm thick bondline.

Average strength degradation between the 1st and the 3rd loading cycle (ΔF_{1-3}) for each group separated by adhesive thickness is presented in Fig. 7. Strength degradation values are a measure of percentage difference in force drop at a certain displacement step between the 1st and the 3rd loading cycle. This mechanical property indicates the connection's behaviour under low cycle fatigue events such as earthquakes. Average strength degradation was derived from the total number of specimens per cyclic group test. Overall, five amplitude displacement steps were considered to show adequate information, except in the case of PS adhesive where only three steps were used due to early failure of the specimen. Comparing 10 mm and 15 mm thick bondline, lower strength degradation was obtained for thicker 15 mm adhesives bondline specimen in all three types of adhesives. The final displacement step shows the highest increase in strength degradation due to reaching the failure of the specimens. The average strength degradation at the failure point in the case of PS adhesives was less than 10 % in both cases (10 mm and 15 mm); while in cases of PST and PTS adhesives, these values were less than 20 % in all cases. According to the current version of Eurocode 8 [44], the dissipative connections shall be able to deform plastically for at least three fully reversed cycles without having more than a 20 % reduction of their resistance. This means that the analysed flexible adhesive connections satisfied this condition in all cases, yet none of the cases reaches a sufficient static ductility ratio of 4 to comply with ductility class DCM (medium capacity to dissipate energy). Therefore, in this current state, these connections are appropriate for use only in the DCL class (low capacity to dissipate energy) according to Eurocode 8 [44].

The equivalent viscous damping ratio (ν_{eq}) was calculated for the 1st

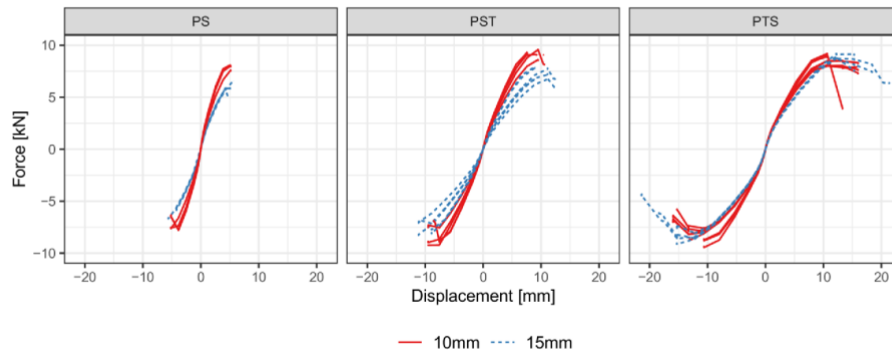


Fig. 6. Backbone curves obtained from cyclic testing of specimens with all three adhesives and both thicknesses.

Table 4
Average values of mechanical properties from cyclic test results: elastic and plastic stiffness (k_{el} , k_{pl}), shear modulus (G), force and displacement at the yielding point, (F_y , u_y), maximum load (F_{max}), displacement at maximum force (u_{pmax}), maximum shear strength (f_{max}), ultimate load ($F_{u-90\%}$), ultimate displacement (u_u), ultimate shear strain (γ_u), and ductility (D).

Adhesive	k_{el} [kN/mm]	G [MPa]	k_{pl} [kN/mm]	F_y [kN]	u_y [mm]	F_{max} [kN]	u_{pmax} [mm]	f_{max} [MPa]	$F_{u-90\%}$ [kN]	u_u [mm]	γ_u	D
PS-10-C	avg	2.37	4.07	0.40	7.01	2.87	7.78	4.97	1.30	7.35	5.16	0.52
	stdev	0.22	-	0.04	0.16	0.23	0.13	0.35	0.02	0.35	0.02	-
	cov [%]	9.34	-	9.34	2.23	8.04	1.70	7.07	1.70	4.82	0.44	-
PS-15-C	avg	1.74	4.46	0.29	5.60	3.14	6.01	4.67	1.00	5.86	4.87	0.32
	stdev	0.07	-	0.01	0.32	0.31	0.41	0.65	0.07	0.50	0.51	-
	cov [%]	3.94	-	3.94	5.76	9.77	6.89	14.01	6.89	8.49	10.41	-
PST-10-C	avg	1.47	2.51	0.24	8.36	5.55	9.04	8.53	1.51	8.51	9.18	0.92
	stdev	0.15	-	0.03	0.56	0.47	0.60	0.94	0.10	0.54	1.02	-
	cov [%]	10.38	-	10.38	6.70	8.53	6.62	11.03	6.62	6.31	11.07	-
PST-15-C	avg	1.03	2.61	0.17	6.85	6.55	7.37	9.63	1.23	7.13	10.04	0.67
	stdev	0.14	-	0.02	0.64	0.85	0.70	1.37	0.12	0.70	1.74	-
	cov [%]	13.28	-	13.28	9.34	13.01	9.55	14.19	9.55	9.77	17.25	-
PTS-10-C	avg	1.22	2.13	0.20	7.47	5.85	8.50	11.59	1.42	7.86	13.76	1.38
	stdev	0.07	-	0.01	0.50	0.19	0.48	1.18	0.08	0.80	2.51	-
	cov [%]	5.69	-	5.69	6.68	3.19	5.70	10.19	5.70	10.18	18.27	-
PTS-15-C	avg	1.02	2.66	0.17	7.84	7.36	8.75	12.98	1.46	7.65	16.75	1.12
	stdev	0.01	-	0.00	0.24	0.31	0.29	0.90	0.05	0.96	1.75	-
	cov [%]	1.39	-	1.39	3.06	4.15	3.32	6.92	3.32	12.58	10.44	-

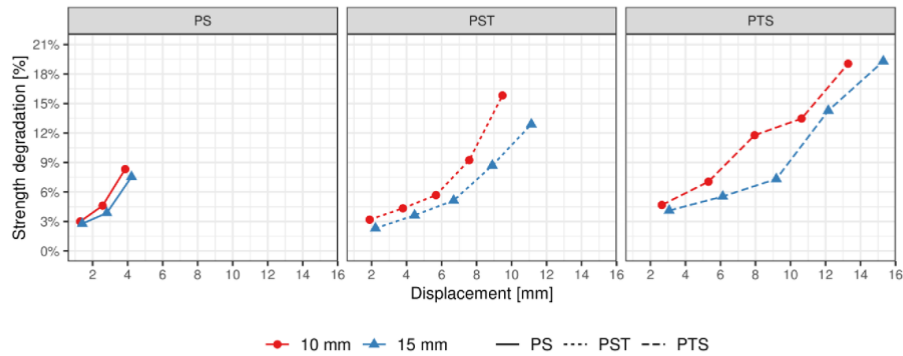


Fig. 7. Average strength degradation for 3rd cycles of loading compared to 1st cycles in % for each amplitude displacement step for each group.

and 3rd cycles for all displacement steps, and it is summarized in Fig. 8a for the 1st cycles and Fig. 8b for the 3rd loading cycles. It is a non-dimensional parameter to represent the hysteresis energy dissipation capacity of a connection, expressed as a ratio between the dissipated energy in one-half cycle (the area of hysteresis) and approximation of exhibited potential energy multiplied by 2π [41]. The 3rd cycles v_{eq} ratio represents the connection's behaviour in subsequent low cycle loads caused during a seismic event, while the 1st cycles represent the connection's response in the peak loads caused by a seismic event. Among the three different tested adhesives, PTS adhesive performed with the highest energy dissipation capacity, resulting in 3rd cycle v_{eq} equal to 5.5–7.1 %, while these ranges were 3.9–5.5 % for PST adhesive and 2.0–2.9 % for PS adhesive. This finding is in correlation with connections' deformation capacity in the plastic region (expressed through ductility in Table 4), in which most of the hysteretic energy is dissipated.

3.4. Comparison with mechanical connections

A comparison between the most commonly used mechanical types of connection between parallel wall panels in CLT structures (so-called half-lap or step joint) and flexible polyurethane adhesive shear connections, investigated in this study, is presented in this section. The

mechanical properties are compared with the values reported in a study by Gavric et al. [45] on cyclic behaviour of typical screwed connections for cross-laminated timber structures. The type of CLT connection chosen for the comparison is the so-called half-lap connection with self-tapping screws HBS $\Phi 8 \times 80$ mm between parallel wall panels, which is considered as a dissipative connection between CLT wall panels, where in addition to strength and stiffness capacity to transfer seismic loads, also sufficient deformation capacity shall be provided due to rocking kinematic mechanism of CLT wall panels during seismic events [38]. Average experimental values of mechanical properties of half-lap connection in Gavric et al. [45] are evaluated according to EN12512 procedure, the same as in the study on flexible adhesive connections presented in this paper.

A direct comparison of mechanical properties is performed on a hypothetical $L = 100$ cm long connection with $B = 5$ cm overlap between two CLT wall elements, which is a generally used width for half-lap joints in CLT structures. Force related mechanical properties from the cyclic tests on double lap-shear adhesive connections presented in this study (see Table 5) are increased proportionally to the hypothetical connection's adhesive surface, while displacements remain at the same levels. Mechanical properties of half-lap screwed connection [45] are presented for a single screw and for a series of equally spaced screws

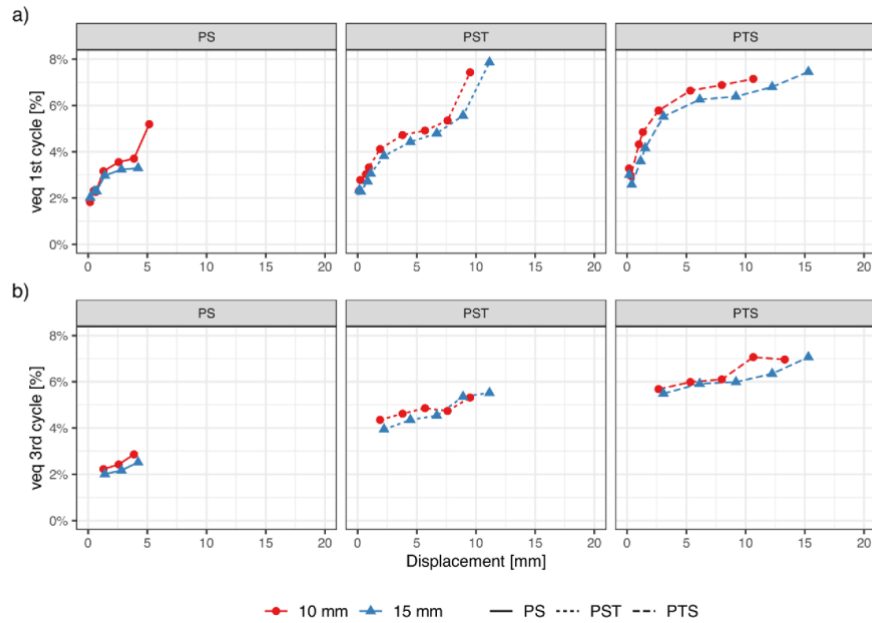


Fig. 8. Equivalent viscous damping ratio for a) 1st and b) 3rd loading cycles by type of adhesive and bondline thickness.

Table 5

Comparison of cyclic behaviour for mechanical properties of flexible adhesive connections and screwed half-lap CLT mechanical connections [45]: elastic and plastic stiffness (k_{el} , k_{pl}), force and displacement at the yielding point, (F_y , u_y), maximum load (F_{max}), displacement at maximum force (u_{Fmax}), ultimate load ($F_{0.80\%}$), ultimate displacement (u_u), and ductility (D).

Connection type	k_{el} [kN/mm]	k_{pl} [kN/mm]	F_y [kN]	u_y [mm]	F_{max} [kN]	u_{Fmax} [mm]	$F_{0.80\%}$ [kN]	u_u [mm]	D [-]
PS-10-C*	19.79	3.30	58.43	2.87	64.86	4.97	61.23	5.16	1.81
PS-15-C*	14.53	2.43	46.63	3.14	50.11	4.67	48.80	4.87	1.55
PST-10-C*	12.24	2.04	69.69	5.55	75.31	8.53	70.94	9.18	1.65
PST-15-C*	8.57	1.43	57.05	6.55	61.40	9.63	59.40	10.04	1.53
PTS-10-C*	10.17	1.69	62.23	5.85	70.85	11.59	65.52	13.76	2.37
PTS-15-C*	8.49	1.42	65.31	7.36	72.89	12.98	63.73	16.75	2.28
HBS 48 × 80 (1 screw)**	1.24	0.11	3.23	2.55	5.25	23.50	4.20	31.55	12.81
HBS 48 × 80 (e = 10 cm)	12.40	1.10	32.30	2.55	52.50	23.50	42.00	31.55	12.81
HBS 48 × 80 (e = 20 cm)	6.20	0.55	16.15	2.55	26.25	23.50	21.00	31.55	12.81
HBS 48 × 80 (e = 30 cm)	4.13	0.37	10.77	2.55	17.50	23.50	14.00	31.55	12.81

* calculated values for the connection length L = 100 cm and connection width B = 5 cm.

** average experimental test values reported in [45].

(spacing $e = 10\text{--}30$ cm) along the length of the connection, which is the most commonly used screw spacing range in CLT-to-CLT panel connections, where 30 cm spacing represents the most common structural spacing [46,47], while smaller spacings represent cases with higher structural demands.

In terms of elastic stiffness properties, all types of flexible adhesive connections exhibit significantly higher values compared to 30 cm spaced screwed connection. For example, PS adhesive connection results in 4.8 times and 3.5 times higher k_{el} for 10 mm and 15 mm adhesive thickness, respectively; while in the case of PST and PTS adhesives, these values range between 2.0 and 3.0 times the mechanical connection's k_{el} . To achieve the same k_{el} value as the most flexible adhesive connection PST-15, the screws would need to be spaced at 14.6 cm.

Comparison of strength properties shows that the selected adhesive

connections have significantly higher strength capacity than all three screw spacing scenarios. Strengths of adhesive connections are 2.9–4.3 times higher than the strength of half-lap screwed connection with screw spacing of 30 cm. Therefore, to achieve the same level of strength capacity, the screw spacing would need to be in the range of 7.0–10.5 cm.

On the other hand, a screwed connection performs significantly better in terms of deformation capacity and ductility. Namely, the ultimate displacement capacity of the screwed connection is 6.1–6.5 times higher than in the case of PS adhesive connections, 3.1–3.4 times higher than in the case of PST and 1.9–2.3 times higher than the PTS. In all cases, the mechanical connection enters the plastic range (reaches the yielding point) at lower displacements than the adhesive connections. Consequently, the ductility values of the mechanical connection are 5.4–8.4 times higher than the ductility of analysed adhesive

connections.

Strength degradation as a result of low cycle fatigue is more pronounced in mechanical connection, reaching almost 30 % at the maximum strength point, while these levels in adhesive connections are less than 10 % for PS and less than 20 % for PST and PTS adhesives, as reported in Section 3.3.

Equivalent viscous damping ratio in the case of a screwed connection is averaging around 14.5 % in 1st cycles and 9.1 % in 3rd cycles at the maximum strength level [45], while these values are less than 10 % in 1st cycles and 2.9 %, 5.5 % and 7.1 % in 3rd cycles for PS, PST and PTS, respectively (see Fig. 8). Total dissipated energy in mechanical connection is additionally higher because it can withstand significantly higher ultimate displacements (Table 4 and Table 5).

3.5. Numerical sensitivity study

Numerical analysis aimed to investigate the influence of adhesive thickness on force–displacement (F - u) elastic response and stress in the adhesive. The F - u responses were used to calculate the relative change of elastic stiffness (k_d) with respect to the scenario with adhesive thickness of 1 mm (as shown for PS adhesive in Fig. 9c). It shows that stiffness decreases parabolically for all adhesives in a similar manner, but for PST and PTS adhesives it is more abrupt. Thicker bonds provide higher compliance and allow greater displacement before reaching strength level, which was confirmed also by the experiments (Fig. 4). This character may be used to an advantage in applications that need a relatively strong, but more flexible, adhesive bond. On average, k_d decreased by about 92–94 % when adhesive thickness changed from 1

mm to 20 mm. The relative change of F_{max} was not analyzed because F_{max} was not reached for thicker bondlines within the range of experimental displacements, which comes from the hyperelastic character of adhesives (Fig. 1). As discussed before, experiments showed that for all adhesives the failure of the specimen occurred at the interface with wood and not in the adhesive itself. Therefore, the limitation of FE models that generally provided higher values of F - u response has to be acknowledged when compared to experiments and that it did not cover debonding phenomena. This also means that the practical limitation of thick bonds lies in debonding, i.e., in the capabilities of primer to assure adhesion. To precisely predict the F_{max} with help of the FE model, it would be necessary to include fracture phenomenon at the interface. However, to describe the fracture behaviour of such bonds was not the aim of this research but may be a meaningful research aim for the future.

The distribution of stress on the specimen surface for 10 mm and 15 mm thick samples is shown in Fig. 9a. It can be seen that shear stresses are distributed symmetrically in the specimens, and that the highest strain occurs in adhesive bond (not shown). The stress was then analysed on two paths (black dashed lines in Fig. 9a): path cutting specimen in the middle of specimen height (horizontal line – H, Fig. 9d) and path going in the middle of adhesive vertically along the bondline (vertical line – V, Fig. 9b). The shear stress at the XY plane mapped onto these paths was created within the elastic deformation for all thicknesses at a displacement of 0.25 mm just for mutual comparison. Both paths show that increasing thickness of the adhesive substantially reduces maximal shear stress in adhesive, from ~ 3.5 MPa at 1 mm to ~ 0.13 MPa at 20 mm, which is ~ 29-fold reduction. Further, the horizontal path shows the highest shear stress occurs in the middle of the adhesive layer; the

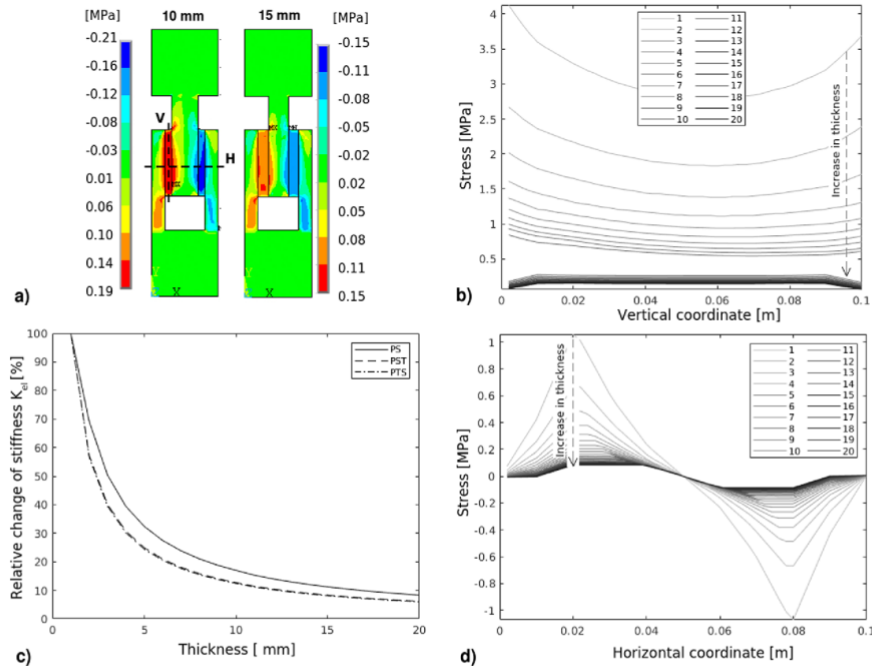


Fig. 9. a) shear stress in XY plane for 10 mm and 15 mm thick adhesive bondline, b) shear stress at vertical path (V) for all simulated thicknesses, c) relative change of k_d of the connection with PS adhesive with respect to 1 mm thick bondline, d) shear stress at horizontal path (H) for all simulated thicknesses.

vertical path shows that shear stress is almost constant along the adhesive bond length.

4. Conclusion and future work

An experimental testing program on thick flexible polyurethane adhesive double lap-shear connections was performed with the aim to better understand their performance and explore potential in-use for high performance timber-adhesive composite structures in seismic regions. Mechanical properties used in the design of timber connections, such as stiffness, strength, deformation capacity, ductility, strength degradation, and equivalent damping ratios were derived according to the EN 12512 procedure for three different adhesives and two different bondline thicknesses.

Thicker adhesive bonds provided both higher elasticity and plasticity, which was confirmed by the experiments and by further numerical investigations. This quality may be used to an advantage in timber connection applications that need a relatively strong, but more flexible, adhesive bond. Further, the numerical investigation showed that increasing the thickness of the adhesive substantially reduces maximal shear stress in the adhesive. All three types of tested adhesive connections showed symmetrical cyclic shear behaviour, which is favourable for seismic-resistant shear connections with utilized capacity design approach.

Compared to mechanical dowel-type screwed half-lap connection with a typically used arrangement of fasteners, all tested adhesives displayed significantly higher values in terms of elastic stiffness and strength. Further, adhesive connections also performed better in terms of low cycle fatigue strength degradation compared to mechanical connections. On the other hand, screwed connections performed significantly better in terms of deformation capacity, ductility, and energy dissipation; yet again, adhesive connections were able to elastically deform to substantially higher deformations than screwed connections, meaning they would be able to sustain higher seismic loads with less/no damage. Nevertheless, the tested flexible adhesives can withstand numerous cycles without damage and residual deformation, as it was also shown in [18].

PTS adhesive proved to be the best candidate for further investigation for potential applications due to its relatively good ratio between elastic stiffness and strength capacity compared to other tested adhesives while showing relatively good performance in deformation capacity. With improvements of wood-adhesive bond and increase of the bond length, the connection's deformation capacity and ductility could be further improved. Possible applicability of thick flexible polyurethane adhesive in timber structures might be limited low-to-medium ductile connections or high strength and high stiffness elastically deformable non-dissipative connections in glued-in rod connections, half-lap or step joint connections, secondary elements that are sensitive to brittle failures during seismic events (such as large windows), steel-to-timber flexible connections and potentially even in structural glass-to-timber connections.

Further research on improving bonding capacity by modifying the roughness of wood surface or enhancing the wood-adhesive bonding capacity with different types of primers would be the first next step. In addition, large-scale tests would presumably show the positive influence of increased bonding length and, consequently, also bonding surface, therefore, excluding the negative effect of stress concentration at edges and debonding. Currently, there are no available standard methods for large-scale tests of thick flexible adhesive in timber connections; therefore, further studies are also needed in this aspect. In terms of further numerical investigations, the logical next step would be including fracture phenomenon at the interface between wood and adhesive, as it was investigated for concrete, bonded with thick polyurethane flexible adhesives [21].

Declaration of Competing Interest

The authors declare that they have no known competing financial interests or personal relationships that could have appeared to influence the work reported in this paper.

Acknowledgements

The work has been conducted with the financial support of the European Commission for the InnoRenew project (Grant Agreement #739574) under the Horizon2020 Widespread-2-Teaming program as well as that of the Slovenian Research Agency (Research Core Funding No. [P2-0273] and infrastructural program No. [IO-0035]). Company SIKA is also gratefully acknowledged for providing the material for testing.

References

- [1] Ringhofer A, Brandner R, Blau HJ. Cross laminated timber (CLT): Design approaches for dowel-type fasteners and connections. *Eng. Struct.* 2018;171: 849–61. <https://doi.org/10.1016/j.engstruct.2018.05.032>.
- [2] Izzit M, Casagrande D, Bezi S, Pasa D, Follera M, Tomasi R. Seismic behaviour of Cross Laminated Timber structures: A state-of-the-art review. *Eng. Struct.* 2018; 170:42–52. <https://doi.org/10.1016/j.engstruct.2018.05.060>.
- [3] Gavric I. Seismic behaviour of cross-laminated timber buildings. Italy: University of Trieste; 2013.
- [4] Cecotti A, Sandhaas C, Okabe M, Yasunura M, Minowa G, Kawai N. SOFIE project – 3D shaking table test on a seven-storey full-scale cross-laminated timber building. *Earthq. Eng. Struct. Dyn. Earthq.* 2013;42(13):2003–21. <https://doi.org/10.1002/eqe.v42.1310.1002/eqe.2309>.
- [5] M. Valluzzi, E. Garbin, C. Modena, W. Bozza, D. Francescato, Modelling of timber floors strengthened with seismic improvement techniques, *Wind. Conserv. – J. Herit. Conserv.* 46 (2016) 69–79. 10.17425/WK46TIMBER.
- [6] Larsson G. Proposal of the Shear plate dowel joint. Sweden: Lund University; 2017.
- [7] Scotta R, Marchi L, Trutalli D, Pozza L. A dissipative connector for CLT buildings: Concept, design and testing. *Materials (Basel)*. 2016;9:1–17. <https://doi.org/10.3390/ma9030139>.
- [8] Latour M, Rizzano G. Cyclic behavior and modeling of a dissipative connector for cross-laminated timber panel buildings. *J. Earthq. Eng.* 2015;19(1):137–71. <https://doi.org/10.1080/13632469.2014.948645>.
- [9] Loo WY, Kan G, Querneville P, Chauw H, Nawawi, Experimental testing of a rocking timber shear wall with slip-friction connectors. *Earthq. Eng. Struct. Dyn.* 2014;43(11):1621–39. <https://doi.org/10.1002/eqe.v43.1110.1002/eqe.2413>.
- [10] Hashemi A, Zarnani P, Masoudnia R, Querneville P. Seismic resistant rocking coupled walls with innovative Resilient Slip Friction (RSF) joints. *J. Constr. Steel Res.* 2017;129:215–26. <https://doi.org/10.1016/j.jcsr.2016.11.016>.
- [11] Iqbal A, Pampanin S, Palermo A, Buchanan AH. Performance and design of LVL walls coupled with UFP dissipaters. *J. Earthq. Eng.* 2015;19(3):383–409. <https://doi.org/10.1080/13632469.2014.987406>.
- [12] A. Baird, T. Smith, A. Palermo, S. Pampanin, Experimental and numerical Study of U-shape Flexural Plate (UFP) dissipaters, in: NZSEE Conf., Aucld and, New Zealand, 2014; pp. 1–9. http://db.nzsee.org.nz/2014/poster/2_Baird.pdf.
- [13] H.J. Blass, M. Schmidt, H. Litze, B. Wagner, Nail plate reinforced joints with dowel-type fasteners, in: 6th World Conference on Timber Engineering, Whistler, 2000.
- [14] Barile C, Casavola C, Pappalètera G, Vimalathithan PK. Damage propagation analysis in the single lap shear and single lap shear-riveted CFRP joints by acoustic emission and pattern recognition approach. *Materials (Basel)*. 2020;13. <https://doi.org/10.3390/ma13183963>.
- [15] Kwicielec A. Shear bond of composites-to-brick applied with highly deformable, in relation to resin epoxy, interface materials. *Mater. Struct. Constr.* 2014;47(12): 2005–20. <https://doi.org/10.1617/s11527-014-0363-y>.
- [16] Vallée T, Tannert T, Fecht S. Adhesively bonded connections in the context of timber engineering—A Review. *J. Adhes.* 2017;93(4):257–87. <https://doi.org/10.1080/00218464.2015.1071255>.
- [17] Jeevi G, Nayak SK, Abdul Kader M. Review on adhesive joints and their application in hybrid composite structures. *J. Adhes. Sci. Technol.* 2019;33(14):1497–520. <https://doi.org/10.1080/01694243.2018.1543528>.
- [18] Rousakis T, Ilki A, Kwicielec A, Viskovic A, Gams M, Triller P, et al. Deformable Polyurethane Joints and Fibre Grids for Resilient Seismic Performance of Reinforced Concrete Frames with Orthoblock Brick Infills. *Polymers (Basel)*. 2020; 12:2869. <https://doi.org/10.3390/polym12122869>.
- [19] Sánchez M, Faria P, Ferrara L, Horszezaruk E, Jonkers HM, Kwicielec A, et al. External treatments for the preventive repair of existing constructions: A review. *Constr. Build. Mater.* 2018;193:435–52. <https://doi.org/10.1016/j.conbuildmat.2018.10.173>.
- [20] Kwicielec A, de Felice G, Oliveira DV, Zajac B, Bellini A, De Santis S, et al. Repair of composite-to-masonry bond using flexible matrix. *Mater. Struct. Constr.* 2016;49 (7):2563–80. <https://doi.org/10.1617/s11527-015-0668-5>.

J.G. Pečnik et al.

Engineering Structures 247 (2021) 113125

- [21] Zdanowicz E, Seroga S, Tekieli M, Kwieceń A. Polymer flexible joint as a repair method of concrete elements: Hexural testing and numerical analysis. *Materials (Basel)*. 2020;13:1–14. <https://doi.org/10.3390/ma13245732>.
- [22] Brunner M, Lehmann M, Kraň S, Fankhauser U, Richter K, Konzett J. A flexible adhesive layer to strengthen glued lam beams. *J. Adhes. Sci. Technol.* 2010;24(8-10): 1665–701. <https://doi.org/10.1163/016942410X507759>.
- [23] K. Rodacki, Z. Bogusław, A. Kwieceń, M. Tekieli, K. Furtak, The Strength of Wooden (Timber)-Glass Beams Combined with the Polyurethane Adhesive - DIC and Finite Element Analysis, in: *Struct. Anal. Hist. Constr., RILEM Book*, 2019; pp. 323–331. 10.1007/978-3-319-99441-3.
- [24] Jelušić P, Kravanja S. Hexural analysis of laminated solid wood beams with different shear connections. *Constr. Build. Mater.* 2018;174:456–65. <https://doi.org/10.1016/j.conbuildmat.2018.04.102>.
- [25] Angelidi M, Vassilopoulos AP, Keller T. Ductile adhesively-bonded timber joints – Part 1: Experimental investigation. *Constr. Build. Mater.* 2018;179:692–703. <https://doi.org/10.1016/j.conbuildmat.2018.05.214>.
- [26] K. Śliwa-Wieczorek, B. Zając, T. Kozik, Tests of polymeric adhesive joints in aspect of their application in prefabricated timber structures, *Arch. Civ. Eng.* 66 (2020) 113–125. 10.24425/ace.2020.131778.
- [27] Arkadiusz K, Konrad R, Bogusław Z, Kozik T. In: *Mechanical Behavior of Polyurethane Adhesives Applied to Timber Joints in Repair of Historical Timber Structures*. Springer, Cham: RILEM Book; 2019. p. 1603–12. <https://doi.org/10.1007/978-3-319-99441-3>.
- [28] S. Zöllig, A. Franzi, S. Franke, M. Muster, Timber structures 3.0 - New technology for multi-axial, slim, high performance timber structures, in: *WCTE 2016 - World Conf. Timber Eng., Vienna, Austria*, 2016.
- [29] Pizzo B, Lavisei P, Misani C, Triboulot P, Macchioni N. Measuring the shear strength ratio of glued joints within the same specimen. *Holz Als Roh - Und Werkst.* 2003;61(4):273–80. <https://doi.org/10.1007/s00107-003-0386-5>.
- [30] Szeptyński P. Comparison and experimental verification of simplified one-dimensional linear elastic models of multilayer sandwich beams. *Compos. Struct.* 2020;241:112088. <https://doi.org/10.1016/j.compstruct.2020.112088>.
- [31] SIST EN 302-1:2013 - Adhesives for load-bearing timber structures-Test methods, 2013.
- [32] Hasegawa K, Cocombo AD, Coppack F, Jewd D, Maher S. Characterising bonded joints with a thick and flexible adhesive layer-Part 1: Fracture testing and behaviour. *Int. J. Adhes. Adhes.* 2015;63:124–31. <https://doi.org/10.1016/j.jadhadh.2015.09.003>.
- [33] Lasowicz N, Kwieceń A, Jankowski R. Experimental study on the effectiveness of polyurethane flexible adhesive in reduction of structural vibrations. *Polymers (Basel)*. 2020;12:1–21. <https://doi.org/10.3390/polym12102364>.
- [34] M.D. Banea, L.F.M. da Silva, Mechanical Characterization of Flexible Adhesives, *J. Adhes.* 85 (2009) 261–285. 10.1080/0021846902881808.
- [35] Cruz JR, Sena-Cruz J, Rezaee M, Seroga S, Pereira E, Kwieceń A, et al. Bond behaviour of NSM CFRP laminate strip systems in concrete using stiff and flexible adhesives. *Compos. Struct.* 2020;245:112369. <https://doi.org/10.1016/j.compstruct.2020.112369>.
- [36] Cruz JR, Seroga S, Sena-Cruz J, Pereira E, Kwieceń A, Zając B. Hexural behaviour of NSM CFRP laminate strip systems in concrete using stiff and flexible adhesives. *Compos. Part B Eng.* 2020;195. <https://doi.org/10.1016/j.compositesb.2020.108042>.
- [37] M. Popovski, E. Karacabeyli, Seismic behaviour of cross-laminated timber structures, in: *15th World Conf. Timber Eng. WCTE, Lisbona*, 2012.
- [38] Gavric I, Fragiaco M, Popovski M, Ceccotti A. Behaviour of Cross-Laminated Timber Panels under Cyclic Loads. In: *Aicher S, Reinhardt H-W, Garrecht H, editors. Mater. Springer, Netherlands, Dordrecht: Joints Timber Struct; 2014. p. 689–702.*
- [39] Primer Sila ZP. Polyurethane primer for mineral substrate and steel. *Data Sheet: Prod.* 2014.
- [40] ISO 16670 Timber structures — Joints made with mechanical fasteners — Quasi-static reversed-cyclic test method, (2003) 1–9.
- [41] EN 12512:2001 Timber structures - Test methods - Cyclic testing of joints made with mechanical fasteners, 2001, 1–18.
- [42] Ansys®Academic Research, Release 19.1 (Ansys, Inc., USA), 2019.
- [43] Milčič J, Brabec M, Sebera V, Tippner J. Verification of the elastic material characteristics of Norway spruce and European beech in the field of shear behaviour by means of digital image correlation (DIC) for finite element analysis (FEA). *Holzforchung* 2017;71:405–14. <https://doi.org/10.1515/hf-2016-0170>.
- [44] EN 1998-1 (2004) Eurocode 8: Design of structures for earthquake resistance, Part 1: General rules, seismic actions and rules for buildings, (2004).
- [45] Gavric Igot, Fragiaco Massimo, Ceccotti Ario. Cyclic behavior of typical screwed connections for cross-laminated (CLT) structures. *Eur. J. Wood Wood Prod.* 2015; 73(2):179–91. <https://doi.org/10.1007/s00107-014-0677-6>.
- [46] Ceccotti Ario. New Technologies for Construction of Medium-Rise Buildings in Seismic Regions: The XLAM Case. *Struct. Eng. Int.* 2008;18(2):156–65. <https://doi.org/10.2749/101686608784218680>.
- [47] Popovski M, Gavric I. Performance of a 2-Story CLT House Subjected to Lateral Loads. *J. Struct. Eng.* 2016;142:1–12. [https://doi.org/10.1061/\(asce\)st.1943-541x.0001315](https://doi.org/10.1061/(asce)st.1943-541x.0001315).

2.4 Article 4

Title: Fatigue behavior of beech and pine wood modified with low molecular weight phenol-formaldehyde resin

Authors: Jaka Gašper Pečnik, Andreja Kutnar, Holger Militz, Matthew Schwarzkopf, Hannes Schwager

Year: 2022

Journal: Holzforschung (ISSN: 1437-434X)

DOI: <https://doi.org/10.1515/hf-2020-0015>

Link: <https://www.degruyter.com/document/doi/10.1515/hf-2020-0015/html>



Original article

Jaka Gašper Pečnik*, Andreja Kutnar, Holger Miltitz, Matthew Schwarzkopf and Hannes Schwager

Fatigue behavior of beech and pine wood modified with low molecular weight phenol-formaldehyde resin

<https://doi.org/10.1515/hf-2020-0015>

Received January 15, 2020; accepted April 14, 2020

Abstract: Modification of wood improves certain properties of natural wood and presents competitive alternatives to synthetic materials that may have larger environmental impacts. One aspect of modified wood that is currently not fully understood is the dynamic performance and how it is affected by the modification process. In this study, low-molecular weight phenol formaldehyde (PF) resin was applied to Scots pine (*Pinus sylvestris* L.) and European beech (*Fagus sylvatica* L.) wood. The effect of this modification was evaluated using a three-point bending test undergoing cyclic loading. Compared to reference samples, modified wood showed higher static performance but revealed a reduction in cyclic fatigue strength (9% for pine and 14% for beech). Cyclic fatigue strength of unmodified wood was found to be 67% of the static modulus of rupture for both species. With PF resin modification, the fatigue strength dropped to 58% for pine and 53% for beech. While fatigue strength decreased, there was no reduction in cyclic modulus or change in the creep rate within the stationary creep phase. It is important to consider the reduction in fatigue strength when using PF modified wood for any construction purposes with expected cyclic loading conditions.

Keywords: beech; creep rate; fatigue strength; phenol formaldehyde; pine; stress level; wood modification.

*Corresponding author: Jaka Gašper Pečnik, Innorenew CoE, Izola, Slovenia, Livade 6, Izola, 6310, Slovenia; and Andrej Marušič Institute, University of Primorska, Koper, Slovenia, E-mail: jaka.pecnik@innorenew.eu

Andreja Kutnar and Matthew Schwarzkopf: Innorenew CoE, Izola, Slovenia, Livade 6, Izola, 6310, Slovenia; Andrej Marušič Institute, University of Primorska, Koper, Slovenia

Holger Miltitz and Hannes Schwager: Wood Biology and Wood Products, University of Göttingen, Goettingen, Germany

Open Access. © 2020 Jaka G. Pečnik et al., published by De Gruyter. This work is licensed under the Creative Commons Attribution 4.0 Public License.

1 Introduction

Energy and resource efficiency have become two major topics for future development of engineering products. This has led to an enormous interest in lightweight design with advanced materials, such as high-performance alloys or fiber-reinforced composites, that might enhance mechanical performance during service life (Klein 2009). Recently, focus has returned to wood as a construction material. Wood is appealing not only for its low ecological impact but also for its beneficial physical properties in relation to its low density. Being a renewable resource, wood provides inherent advantages such as climate neutrality and environmental sustainability. It is also a domestically produced material with short transport links to processing facilities and provides good machinability (Ramage et al. 2017).

From an engineering point of view, wood exhibits specific mechanical properties comparable to most metals and many fiber composites (Ashby 2010). But technical use requires taking wood's particular characteristics, originating from its former function as a living organism, into account. One major restriction for technical application of wood arises from its moisture behavior. The capillary porous structure and strong hygroscopicity of wood cell walls, which results from their chemical composition, lead to fast water uptake that affects several other physical and biological properties such as dimensional stability, mechanical properties or durability. Modification of wood species by thermal, chemical, or mechanical treatment can improve service life, dimensional stability and, in many cases, mechanical properties (Hill 2006; Sandberg et al. 2013). A well-established wood modification process is chemical modification with thermosetting resins by impregnating wood with monomers and oligomers of low molecular weight. While curing, a cross-linked polymer matrix is formed from these monomers within the wood cell walls, which helps to prevent water penetration at a later time. One such resin is phenol formaldehyde (PF). PF has a long service record

(>50 years) in the wood industry as an adhesive used for manufacturing engineered wood products such as plywood or glue laminated timber. More recently, studies have focused on the use of PF to enhance wood and wood-composite properties related to dimensional stability, color stability, exterior exposure, acoustics and resistance against fungi, termites, and other pests (Ahmed and Adamopoulos 2018; Franke et al. 2017; Gabrielli and Kamke 2010; Gascon et al. 2015; Kielmann et al. 2018; Klüppel, 2017; Klüppel et al. 2015; Stamm et al. 1947; Xie et al. 2013). PF resin has also been used to improve mechanical properties of wood. Deka and Saikia (2000) reported increases in modulus of elasticity (MOE) by 12% and modulus of rupture (MOR) by 21% for wood impregnated with PF resin. Huang et al. (2013) treated Chinese fir (*Cunninghamia lanceolata*) with a low molecular weight PF resin and reported a 31% increase in MOE. Wan and Kim (2006) found slight improvements in MOE values for strand board treated with low molecular weight PF resin. Previous studies explained that cell wall bulking caused by thermosetting resins like PF reduced the flexibility of cell wall compounds (Hosseinpourpia et al. 2016). In addition, alkaline components in phenolic resins might also cause changes in cell wall components, which can lead to decreased elastic properties (Furuno et al. 2004). The brittle behavior of wood treated with PF resin can be attributed to PF molecules occupying the cell wall and cell lumina as well as by catalysts of acidic polymers establishing new cross-linking of the cell wall network, leading to a rigid, non-pliable cell wall (Mai and Elder 2016). Dynamical mechanical behavior of modified wood with thermosetting resins is greatly affected by this increased rigidity. Kielmann et al. (2013) modified ash (*Fraxinus excelsior* L.), beech (*Fagus sylvatica* L.), and maple (*Acer platanoides* L.) wood with methylated N-methylol melamine (NMM) and reported decreased impact bending strength (IBS) for treated samples against controls, with decreased IBS between 35 and 48% for ash and beech and an even higher decrease between 55 and 67% for maple. One large study on modifying wood's mechanical and physical properties with different chemicals was carried out by Epmeier et al. (2004). IBS of pine wood (*Pinus sylvestris* L.) treated with methylated melamine formaldehyde (MMF) was found to be reduced by more than 50%. Bicke et al. (2012) modified beech (*F. sylvatica* L.) veneers with PF resins for plywood and reported 34% lower IBS values in a parallel orientated direction. One method used to assess and characterize dynamic properties of a material is fatigue testing. There is currently a lack of knowledge concerning the cyclic fatigue life of modified wood due to demanding testing, high natural variability and anisotropy. Fatigue performance in wood is driven by many parameters.

One of the most important is the stress level under which a specimen is tested. The ratio of maximum and minimum stress applied to the test specimen (R ratio) must be considered. For example, R ratio with -1 would mean fully reverse loading. In other words, this would mean that the specimen is under constant load where maximum and minimum positions are extremes of the amplitude. In bending, this would mean that the specimen bends down and upwards. When R is 0 , (unidirectional) specimen is loaded and unloaded between maximum positive load and initial unloaded starting position. Tsai and Ansell (1990) tested fatigue life in flexure and reported increasing damage with decreasing R values from 0.5 to -1 . The waveform under which the specimen is tested also plays an important role in fatigue life. It has been reported that a square wave loading form, compared to sinusoidal or triangular, causes the most damage for solid wood and some other wood composite materials (Gong and Smith 2003; Sasaki et al. 2014; Sugimoto and Sasaki 2007; Sugimoto et al. 2006). Another important parameter is loading frequency. A shorter number of cycles is given by lower loading frequencies (Gong and Smith 2003; Sugimoto et al. 2007). Regarding modified wood, there are even fewer studies that have investigated fatigue performance. Ratnasingam and Mutthiah (2017) investigated fatigue strength of oil palm (*Elaeis guineensis*) wood from different positions in the stem. As density increased, improved fatigue life was observed in the middle and center parts of the tree treated with PF. Sharapov et al. (2016) investigated how cyclic bending influenced residual strength in thermally modified wood and effects of different moisture content levels for pine (*P. sylvestris* L.), reporting that initial moisture content before the fatigue test and highest thermal treatment play the most important roles in residual strength.

To better understand behavior of modified wood under cyclic loading, it is important to know if modification has a positive or negative effect on wood properties. Based on progress from initial studies on modified wood, there is now a need to assess the dynamic performance of other wood species that are commonly used in structural applications. Scots pine (*P. sylvestris* L.) and European beech (*F. sylvatica* L.) represent economically important softwood and hardwood species, respectively, as both are widely used in the European wood industry. Most structural timber and wood-based composites used in buildings are softwood species; however, more and more hardwood species are gaining attention for use in building applications. The objective of this study has been, to investigate static and dynamic mechanical properties such as impact bending, cyclic fatigue behavior and cyclic creep of PF modified pine and beech wood.

2 Materials and methods

2.1 Specimen preparation: modification procedure

Specimens of Scots pine sapwood (*P. sylvestris* L.) and heartwood-free European beech (*F. sylvatica* L.), with length of 180 mm in longitudinal, height of 10 mm in tangential and width of 10 mm in radial wood direction, were prepared. Before further processing, specimens from each species were distributed into two samples of 150 specimens, described in Table 1. One sample was modified (Mod) with phenol formaldehyde (PF) resin, while the other served as a reference (Ref).

Initially, all specimens were conditioned in a controlled environment at a temperature of 20 °C and relative humidity (RH) of 65% for two weeks. Following this initial step, the specimens designated for modification were stacked in containers and submerged in aqueous PF solution with 30% PF mass content and an average PF molecule weight of 440 g/mol. In order to ensure a maximum solution uptake, specimens were degassed in a vacuum chamber at a low pressure of 100 mbar for 30 min and subsequently infiltrated with PF resin by reverting to atmospheric pressure. Afterwards, specimens were desiccated in a slow drying regime. First, specimens were air dried overnight and then put into the oven to 60 °C. After 24 h, temperature was increased to 103 °C for another 24 h. This drying regime ensured smooth water removal from the specimens and prevented the formation of drying cracks. Final curing phase took place at 140 °C for 2 h. Before further investigation steps, specimens were conditioned again at 20 °C and 65% RH.

2.2 Evaluation of modification

Dimensions of all specimens along the three anatomical wood directions, longitudinal length (l_{long}), tangential height (h_{tang}), and radial width (w_{rad}), were measured with a sliding caliper after initial conditioning before infiltration and after final conditioning after curing. Specimen mass (m) was measured by two decimal number precision balance. With these values, bulk density (ρ) of the specimens was calculated.

Permanent relative change in dimension, the so-called bulking of wood, in all three anatomical stem directions (Bul_{dir}) after modification referred to the unmodified state is given by Eq. (1):

$$Bul_{dir} = \frac{(x_{dir,1} - x_{dir,0})}{x_{dir,0}} \times 100[\%] \quad (1)$$

where x_{dir} represents the dimensional values for longitudinal length l_{long} , tangential height h_{tang} or radial width w_{rad} and the index t where numbers are designating the modification state after initial conditioning (0) and after modification (1).

Weight percentage gain (WPG) after modification referred to the unmodified state was calculated according to Eq. (2):

$$WPG = \frac{(m1 - m0)}{m0} \times 100[\%] \quad (2)$$

with initial (m_0) and final (m_1) mass of the specimens.

Moisture content (MC) of a specimen was calculated from absolute dry state mass after exposure to 103 °C for 48 h in a ventilated oven and mass after reconditioning at 20 °C and 65% RH for three weeks.

2.3 Microscopic analyses

For both reference and modified samples, images of cross-sections were made with a scanning electron microscope (SEM), Supra-35 (Carl Zeiss AG, Germany), to demonstrate the distribution of PF molecules in the material. Specimens were dried overnight in a ventilated oven at 103 °C. A clear, smooth cut was created with a microtome, and specimens were coated by carbon sputtering. Analyses were conducted at 5 kV.

2.4 Mechanical test program

The mechanical test program used in this study combined static and dynamic tests with a three-point flexural test set-up and a central force application in tangential wood direction. All specimens were tested in static bending tests, following the recommendations of DIN 52186 (1978), to determine the modulus of elasticity (MOE). From each sample, selected specimens were tested until failure to determine the modulus of rupture (MOR). Charpy impact bending tests referred to DIN 52189 (1981) to determine the effect of modification on impact bending strength (IBS). Cyclic fatigue strength (CFS) was determined in a Wöhler test series under three-point bending test regime.

2.4.1 Static bending tests: Static bending tests were performed on a universal testing machine (Zwick/Roell Z010, supported by TestXpert software) with a span (l_s) between the support rollers of 150 mm. During the test, applied force (F) and corresponding deflection (d) were recorded. Test speed was set to 5 mm/min to ensure a test duration of 90 ± 30 s until failure in tests for determining MOR (DIN 52186 1978). MOE was calculated by using linear regression in the range of 50–200 N. Limit of proportionality (LOP) equals the stress level where the stress-strain curve deviates from the calculated regression line; ergo, the material behavior changes from strictly linear-elastic to plastic was as well. Determined total strain (ϵ_{max}) at maximum force (F_{max}) is given by Eq. (3):

$$\epsilon_{max} = \frac{6 \times d_{max} \times h_{long}}{l_s^2} [-] \quad (3)$$

from which elastic (E_e) is calculated as follows in Eq. (4):

Table 1: Description of samples and number of specimens designated for testing: modulus of elasticity, (MOE), modulus of rupture (MOR), impact bending strength (IBS), cyclic fatigue strength (CFS) and moisture content (MC).

Treatment type	Label	Resin average molecular weight	Total no. of specimens	Distribution no. of specimens included in the test program				
				MOE	MOR	IBS	CFS	MC
Reference	Ref	–	150	150	30	50	50	10
PF modification	Mod	~440 g/mol	150	150	30	50	50	10

$$\varepsilon_{el} = \frac{MOR}{MOE} [-] \quad (4)$$

and plastic (ε_{pl}) results from the difference between ε_{max} and ε_{el} as shown in Eq. (5):

$$\varepsilon_{pl} = \varepsilon_{max} - \varepsilon_{el} [-] \quad (5)$$

Ratio of plastic to total deformation might be regarded as a measure for brittleness of the material.

2.4.2 Impact bending test: An impact pendulum machine (CEAST Resil Impactor) was equipped with an instrumented 25 J hammer. The span between the support rollers was set to 115 mm, according to standard DIN 52189-1 (1981). IBS is given by the absorbed energy during fracture referred to the cross-sectional area of the specimen.

2.4.3 Cyclic bending tests: Cyclic bending tests were performed in a Wöhler-test series on fatigue testing machine DHM-Prüfsysteme (Clausthal-Zellerfeld, Germany, supported by SysCon easyTest software). In addition to the driving force generated with a pneumatic cylinder instead of a servomotor, the bending test set-up resembled those used for static testing: two lateral support rollers with a span of 150 mm and a central force application.

Tests were performed with pulsating loads until specimen failure, whereby the upper and lower stress limit were calculated according to Eq. (8) and the corresponding maximum and minimum strain values according to Eq. (7).

Upper stress limit (σ_{up}) was given by the intended load level and lower stress limit (σ_{low}) was set to a value close to zero. A sinusoidal waveform with a constant mean stress (σ_{mean}) was calculated by Eq. (6):

$$\sigma_{mean} = \frac{(\sigma_{up} + \sigma_{low})}{2} = const. \quad (6)$$

and constant stress amplitude (σ_{amp}) in Eq. (7):

$$\sigma_{amp} = \sigma_{max} - \sigma_{min} = \sigma_{mean} - \sigma_{min} = const. \quad (7)$$

was chosen to avoid high dynamic damaging effects caused by abrupt load reversion like in triangular or square waveforms (Gong and Smith 2003; Smith et al. 2003). The test frequency of 10 Hz was a trade-off between an opportune test duration and prevention of thermal degradation by rapid internal friction. Specimens designated for one Wöhler-test series were distributed into sub-samples of five specimens. The stress level (SL) of one single test is given by σ_{up} and individual strength of the tested specimen (MOR_{spec}) as in Eq. (8):

$$SL = \frac{\sigma_{max}}{MOR_{spec}}. \quad (8)$$

During one Wöhler series, the SL per sub-sample was decreased stepwise, beginning at ~95%, to a stress level where the specimens (theoretically) would never fail.

In the present study, the MOR_{spec} of each specimen was estimated from its individual MOE_{spec} and correlation between the average MOR_{mat} and average MOE_{mat} of the examined material that had been determined in the preceding static three-point bending tests, used under static bending test, as in Verkasalo and Leban (2002) and Baar et al. (2015), shown in Eq. (9):

$$MOR_{spec} = \frac{MOE_{spec} \times MOR_{mat}}{MOE_{mat}}. \quad (9)$$

The number of cycles to failure (N_f) was recorded for each specimen. A threshold of one million cycles without any visible crack was regarded as fatigue limit. The belonging load level gives cyclic fatigue strength (CFS) of the wood in its modification state.

A more detailed view into the fatigue behavior of a single specimen is gained by contemplating weakening of the material during the fatigue test and creep behavior within the phase of stationary (secondary) creep. Figure 1 represents increasing minimum and maximum strain throughout the testing phase. The initial phase (I – phase of primary creep) is characterized by a low amount of creep and decreasing creep rate (see also Figure 2), followed by the quasi-linear secondary stage (II – phase of secondary, stationary creep) where we observed slow proportional linear increase as a result of time-dependent constant loading. The final stage (III – phase of tertiary creep) resulted in accelerated and sudden increase in strain and fatigue failure. The blue line represents cyclic creep and the red line represents maximum deflection.

Figure 1 aims to show behavior of increasing travel of a specimen and, on the other hand, its reduction in modulus. These indicate our measure of fatigue.

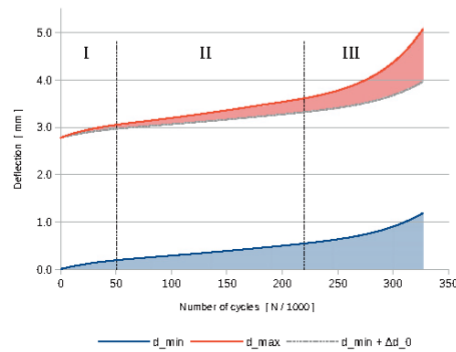


Figure 1: d_{min} and d_{max} represent increasing minimum and maximum strain. Lines present a measure of fatigue upper (red) and lower (blue) minimum strain through number of cycles and typical creep behavior.

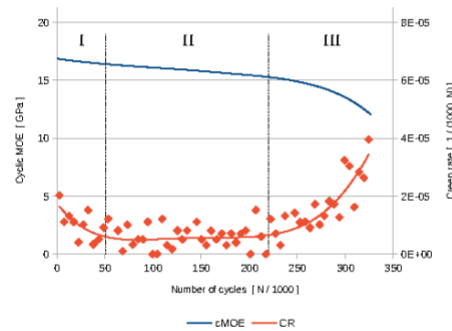


Figure 2: (I) Primary phase with decreasing CR and decelerated reduction of cMOE; (II) stationary creep with low CR and linear decrease of cMOE; (III) accelerated creep with increasing CR and rapidly decreasing cMOE.

Figure 2 presents decreasing cyclic modulus of elasticity in the upper blue line (cMOE) throughout the three phases as caused by weakening of the material. The lower red line indicates creep rate (CR). Initial high CR is a result of specimen positioning, followed by the linear secondary stage. After a certain number of cycles, fatigue effect was observed in a sudden CR increase that ended with failure of the specimen and, thus, end of the test.

Specimen weakening due to cyclic fatigue manifests in a decreasing cyclic modulus of elasticity (cMOE) throughout the fatigue test. The cMOE of a designated load cycle (N) is calculated according to Eq. (10):

$$cMOE_N = \frac{\Delta\sigma_N}{\Delta\varepsilon_N} = \frac{\sigma_{up,N} - \sigma_{low,N}}{\varepsilon_{max,N} - \varepsilon_{min,N}} \quad (10)$$

with stress values ($\sigma_{up,N}$ and $\sigma_{low,N}$) and corresponding strain values ($\varepsilon_{max,N}$ and $\varepsilon_{min,N}$) at the load reversion points of the contemplated load cycle. Cyclic creep caused by so-called mean stress (σ_{mean}) effect (constant σ_{mean} throughout testing time) manifests in a progression of minimum strain ($\varepsilon_{min,N}$) throughout the fatigue test. Within the phase of stationary creep, cyclic creep rate (CR) per load cycle might be determined by linear regression between minimum strain values and number of load cycles as in Eq. (11):

$$CR = \frac{\Delta\varepsilon_{min,N}}{\Delta N} \quad (11)$$

with $\Delta\varepsilon/\Delta N$ representing slope of the regression line.

3 Results

3.1 Results of the modification: WPG bulking and density

Results for WPG, bulking, density after modification and moisture content of modified and reference pine and beech wood specimens are shown in Table 2. WPG for pine and beech was found to be 31.7 and 24.2%, respectively. As expected, bulking in tangential direction was larger than in radial direction for both wood species. Bulking in longitudinal was found to be very low, with almost no increase. Increase in the density from initial state was found to be 20% for pine and 25% for beech. It must be pointed out that calculations were performed within the same sample and cannot be comparable with values from the reference sample. Determined WPG for pine and beech was similar to

values obtained by other studies. Franke et al. (2017) impregnated beech wood with different PF molecular sizes and different concentrations and obtained 25% WPG by using 20% PF concentration and 450 Mn molecular weight. Xie et al. (2016) modified Scots pine with different PF concentrations and molecular weight around 400 Mn and obtained various WPG, some with an increase similar to 35%. Increase in density and bulking can be one of the first indicators of successful impregnation. In this study, higher WPG was found for pine, which is related to wood density, and a solid content of PF resin. WPG can be calculated to any desired increase for every wood species as a ratio between cell wall density and wood density. Penetration of low molecular weight PF resin into the cell wall was already provided in a study done by Furuno et al. (2004). Incorporating the polymer into the wood structure causes a so-called bulking effect that results in the increase in volume of a specimen towards its original volume (Hill 2006). Wood species with higher density reach higher volumetric swelling (Kollman and Côté 1968). Kollman and Côté, in their book, explained how helical arrangement of fibrils affect radial and tangential shrinking for softwoods. A few other theories regarding swelling and shrinking were described by Skaar (1988), i. e., how arrangement of various tissues and cell types, fibril alignment, cell-wall layering and difference in early – and latewood can differentiate in shrinking and swelling. Any of these reasons can contribute to the differences observed in our case as penetration of molecules can affect the same spots.

Moisture content (MC) after three weeks of conditioning was equilibrated on average 10.2% for reference specimens and 4.5% for modified specimens. Furthermore, it is necessary to mention that lower MC for modified wood due to the effects of impregnation was expected. It has to be taken into account that modification slows down the effect of water vapor sorption. This means that MC of 4.5% might not be the equilibrium moisture content at standard climate conditions. Hosseinpourpia (2016) confirmed lower MC and different behavior for PF impregnated wood species. PF-occupied molecules in the wood structure

Table 2: Calculated average properties of pine and beech samples after treatment with standard error in parentheses, bulking in radial (Bul_{rad}), tangential (Bul_{tan}), and longitudinal (Bul_{lon}) direction and an average MC at 65% relative humidity.

Sample	TT	WPG (%)	Bul _{rad} (%)	Bul _{tan} (%)	Bul _{lon} (%)	ρ_1 (kg/m ³)	MC (%)
Pine	Ref	–	–	–	–	535 (3.8)	10.1
	Mod	31.7 (0.36)	1.65 (0.03)	3.44 (0.03)	0.06 (0.00)	682 (2.2)	4.5
Beech	Ref	–	–	–	–	654 (2.1)	10.2
	Mod	24.2 (0.27)	2.77 (0.06)	8.17 (0.13)	0.06 (0.01)	803 (1.8)	4.5

prevent water vapor from penetration into the wood as well as closing gaps and diffusion paths.

One of the main contributions of resin mono/oligomers is, subsequently, polymerization within the cell, creating a matrix formation between PF molecules and wood. In addition to reduction in MC of wood, polymerization causes side effects such as cross-linking molecules forming a rigid matrix and poor pliability of the cell wall (Mai 2016). In Figure 3, SEM images of the Ref (a) and Mod (b) cross-sections for pine are presented. Pine structure consists of tracheids building early – and latewood for Ref; in the case of modified wood, this is less evident.

Figure 4 shows SEM images from cross-section for reference (a) and modified (b) beech. The main difference between pine and beech is in the wood anatomical

structure. Diffuse porous beech consists of fibers and vessels. The penetration of PF resin into the fibers, resulting in bulking, indicates the difference between reference (a) and modified (b) samples. Another observation was found inside the lumina where, in the case of modification, resin covered some of the visible pits (not shown). Overall, both wood species have presence of bulking effect and surface roughness after cutting the specimen.

3.2 Mechanical test: static test

Summary of the static test is provided in Table 3. Modification with PF resin influenced both the MOE and MOR for pine and beech specimens. Mean MOE of modified specimens was 21.4% higher than values for unmodified pine and 29.0% higher than values for unmodified beech. MOR of modified wood also increased, counting 17.8% higher MOR for pine and 18.0% higher MOR for beech.

Rowell (1998) attributed strength properties of lignocellulose materials as very dependent on MC of the cell wall, i.e., fiber stress at proportional limit and maximum

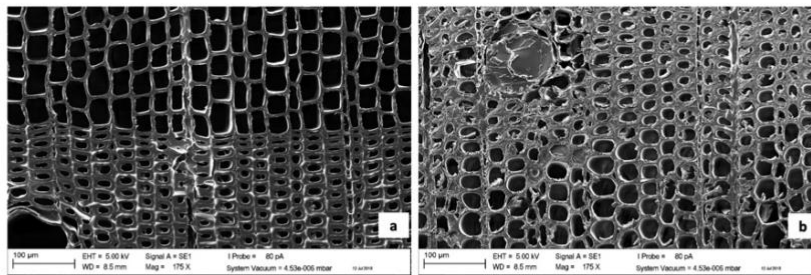


Figure 3: SEM cross-section image of pine Ref (a) and Mod (b).

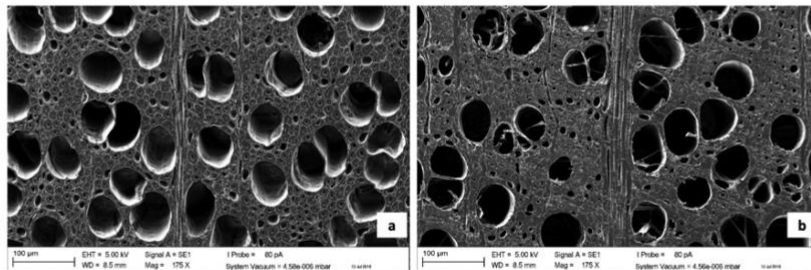


Figure 4: SEM cross-section image of beech Ref (a) and Mod (b).

Table 3: Calculated average values for MOE, MOR, total strain (ϵ_m), plastic strain (ϵ_{pl}), ratio between plastic deformation and total strain and LOP, with the standard error values in parenthesis.

	TT	MOE (GPa)	MOR (MPa)	ϵ_m (-)	ϵ_{pl} (-)	ϵ_{pl}/ϵ_m (%)	LOP (MPa)
Pine	Ref	11.9 (0.1)	102 (1.3)	0.013 (0.03)	0.009 (0.01)	66.7	63.3 (1.3)
	Mod	14.5 (0.7)	120 (2.5)	0.008 (0.01)	0.000 (0.00)	~0	112.7 (3.5)
Beech	Ref	11.8 (0.7)	125 (1.6)	0.017 (0.04)	0.006 (0.04)	36.4	70.6 (1.4)
	Mod	15.2 (0.9)	148 (2.5)	0.010 (0.01)	0.000 (0.01)	~0	126.0 (4.7)

strength. In this study, MC was highly affected by modification resulting in 55% lower MC compared to reference samples. A study from Deka and Saikia (2000) showed improved mechanical properties of PF modified hardwood *Anthocephalus cadamba*. Huang et al. (2013) also obtained improved MOE and MOR properties by modifying Chinese fir (*C. lanceolata*) with low molecular weight PF resin. However, Xie et al. (2013), in their review of the effect of chemical modification on mechanical properties of wood, pointed out that this is not always the case. Another example from a recent study, Wang et al. (2019), investigated properties of elastic modulus, hardness and storage modulus under quasi-static and dynamic mechanical testing by using nanoindentation technique on PF-impregnated Masson pine (*Pinus massoniana* Lamb.) using different resin concentrations. Results revealed that properties only improved with lower concentrations up to 20%. Properties above this level of concentration were found to remain the same or even start to decrease as an effect of increased bulking.

One major drawback was contributed to change in original elasto-plastic behavior. Elastic and plastic deformation were determined on measured specimens from the stress strain diagrams. A high ϵ_p deformation at break was visible for reference samples at 36.4 and 66.7% for pine and beech, respectively. Generally, ~0% plastic deformation was observed for Mod samples in both wood species. LOP for modified specimens was found to be only 7.3% lower than average MOR for pine and 14.7% lower than average MOR for beech. While in the case of unmodified wood, pine and beech met 38.0 and 43.6% lower LOP, respectively.

The unexpected low mechanical performance of modified beech wood could be attributed to insufficiencies of the modification process. Deka et al. (2002) demonstrated that resin treatment with PF increases MOE and MOR with no remarkable effect on the specific gravity. Furthermore, it was shown that by increasing WPG using PF, the mechanical performance improves. This might help to understand the better performance of pine reported in the present study as the density of reference beech was only around 120 kg/m³ higher than the one of pine. Total

bulking was also greater in the case of beech, which in turn, leads to lower strength because the breaking force is referred to a larger cross section area.

3.3 Dynamic test: impact bending strength (IBS) and cyclic fatigue test

Results from impact bending strength (IBS) are represented by peak energy in Table 4. The modification was found to have greater effect on pine. Decrease in IBS for modified pine compared to reference was 59.8% while for beech it was 35.9%. This can be attribute this to higher WPG, which resulted in rigid matrix creation between the wood and adhesive. According to Kollman and Cote (1968), differences between pine and beech could originate from the initial properties of the material. Beech and pine both gain on the impact work with increasing density. Coniferous wide annual rings are related to low toughness, due to broad rings resulting in lower density of wood. Diffuse-porous beech was found to have greater toughness. High energy absorbance can be explained by energy transmission through long splits and coarse splinters. Type of rupture in modified wood was significantly different from the reference, showing shorter splits than those found in reference wood.

The effect of modification with PF resin expresses an important reduction in dynamic impact bending strength (Mai 2016). According to Xie et al. (2007), this phenomenon is typical when it comes to chemical modification with curing resins for the cell wall as deposits cause reduction of movement in polysaccharides and cell wall matrix. For

Table 4: Impact bending strength with peak energy (w_{peak}), standard error (StErr), and number (N) of evaluated specimens.

TT	Pine			Beech		
	w_{peak}	StErr	N	w_{peak}	StErr	N
Ref	16.26	0.53	49	18.59	0.54	50
Mod	6.54	0.22	47	11.91	0.47	47

modified samples, high reduction was recorded in fragile brittle breaking of wood, showing no ability to absorb energy while in contact. This type of behavior was expected due to high increased brittleness of the material.

3.3.1 Cyclic fatigue strength

Cyclic fatigue strength decreased with increasing SL for all the samples as presented in Figure 5. Fatigue limit for reaching 10^6 loading cycles for reference pine and beech was 67%. For modified samples, 58 and 53% fatigue strength were found for pine and beech, respectively.

In this case, reaching 10^6 cycles was a measure of fatigue life. However, not all of the values undergo 10^6 repetitions as not all of the designated specimens in a particular SL were able to fulfill the desired number of cyclic repetitions.

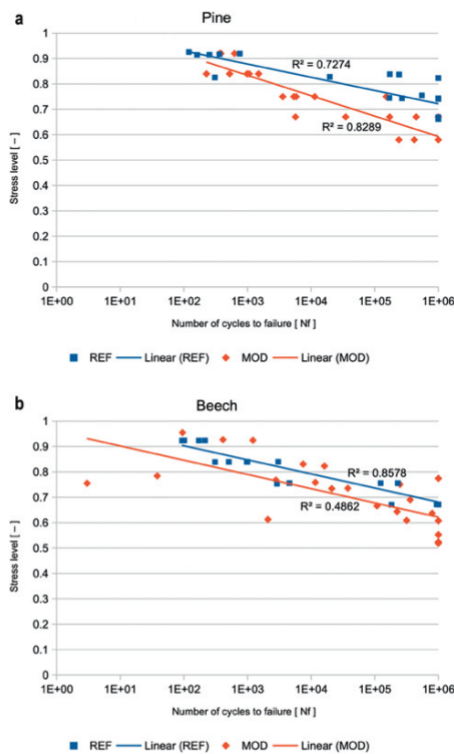


Figure 5: Cyclic SN fatigue diagram for pine (a) and beech (b).

The relationship between SL_{real} and number of cycles to failure (N_f) for pine and beech are presented in Figure 5. Measure of fatigue strength is the number of cycles for each individual specimen at a certain stress level, which is plotted with colored points. Color is typical for treatment type: blue indicates reference specimens and red indicates modified specimens. The linear regression line represents a trend in behavior of tested specimens under a different SL . It can be seen that shortened N_f is given by treated samples, meaning higher stress level resulted in lower number of cycles.

In both modified wood cases, additional SL lower than 60% has been introduced to gradually reach desired number of cyclic repetitions. All results for lowest SL in Mod are plotted within one single point, as all of the specimens reached the final number of cycles. It was observed that, on average, pine Ref specimens survived the highest number of loading cycles overall (4.71×10^5), followed by Mod beech (3.39×10^5), Mod pine (3.21×10^5), and Ref beech (2.81×10^5). In total, 32 and 17% decrease in average number of cycles was found between Ref and Mod for pine and beech, respectively. For pine specimens, high variability in the SL was observed. The slope in Figure 5 is a linear regression line, showing intensity of reduction in CFS. One can see that more intense reduction was observed in the number of cycles for modified wood. This evidence was more typical for pine, meaning that high SL had greater effect on modified pine. For beech, a lower regression line was found, showing similar behavior to Ref. In the case of beech, higher number of cycles was recorded throughout the test for modified wood compared to pine. Due to low number of evaluated specimens and high variability in wood, it is difficult to say which modification was more affected by the treatment. By linear regression line, one can observe that pine experienced higher reduction; however, low R^2 is not a strong indicator. Finally, this kind of observation was already supported with IBS tests.

3.3.2 Creep rate for identifying the range of stationary (secondary) creep

Results for pine and beech creep rate are summarized in Figure 6. Specimens loaded under higher SL experienced higher creep rate.

This correlates with the completely different material behavior. Modified samples showed linear elastic behavior up to the MOR, while reference material switched from elastic to plastic far below the MOR. The LOP of pine referred to MOR is 62% in case of beech this ratio is 57%. Even though the drop of the CR occurs at a SL of around

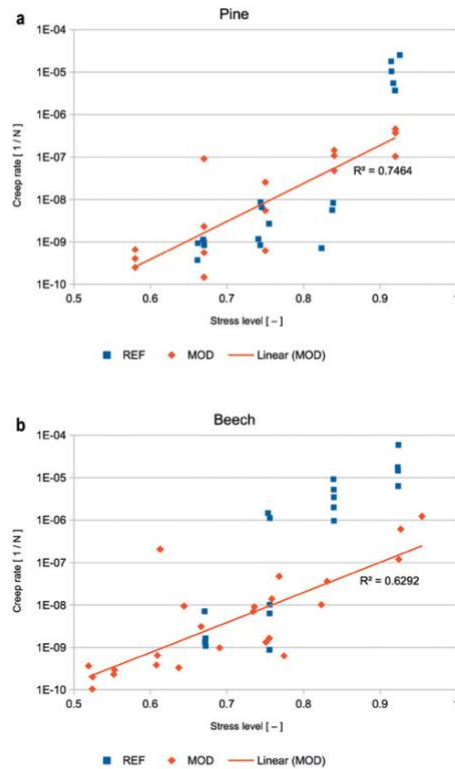


Figure 6: Creep rate (CR) for pine (a) and beech (b). A linear regression line was better fitting for CR in modified samples. Reference samples had higher CR at high SL until a sudden sharp drop occurred, usually below 75% SL.

75%, a change of the material behavior from elastic to plastic as a reason for this finding appears to be plausible.

3.3.3 Cyclic modulus of elasticity

Plotted samples in Figure 7, are showing average values of cMOE for pine and beech. Based on previous results, it was expected that increasing accumulative travel of a specimen, as the effect of cyclic creep, would result in reduction of elasticity as fatigue under constant force loading causes weakening of the material. The main variable here is changing dL_{max} (Figure 1) as load is constant. It was observed that, in the case of modified specimens, dL_{max} remains unchanged, resulting in constant linear cMOE. This

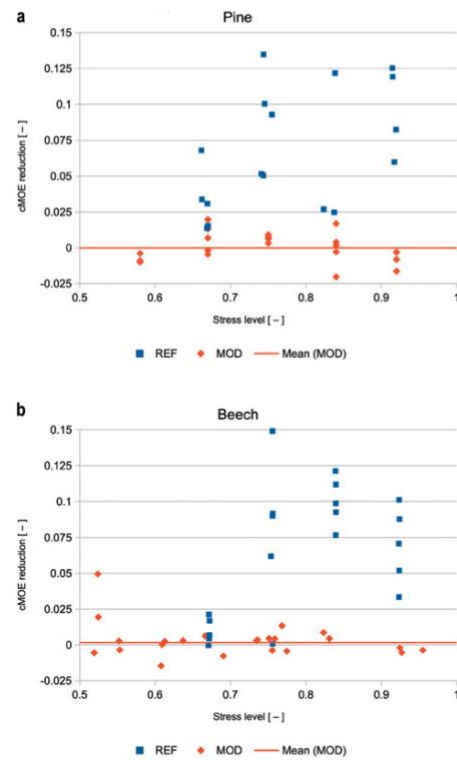


Figure 7: Reduction in cMOE as a function of stress level for pine (a) and beech (b).

is indicated by the red linear line in Figure 7. This can be related to high LOP for modified samples calculated under the static tests. It has been described before, that modified wood has limited ability for absorbing plastic deformation, which was accumulating in the reference samples.

Results obtained in the state of stationary creep level show that modulus of elasticity was decreasing for reference samples. Constant modulus was observed for Mod samples with more stable behavior. This may be explained as follows: in the case of modified wood, one can see no reduction in cMOE, showing no fatigue failure leading to unpredictable failure of specimen. The cMOE for Mod was constant throughout all SL. On the other hand, specimens from the Ref sample show weakening in the material while tests were causing softening, resulting in decreasing cMOE. Therefore, it could be concluded that cMOE can be used as an indicator of fatigue in material, which can ultimately

lead into failure. Modulus remained constant when approaching CFS. Good correlation between CR and SL was found, but no relation between cMOE and SL. For the Ref sample, when reduction in cMOE is present one can be able to predict failure of the specimens.

4 Conclusions

Cell wall modification with low molecular weight phenol formaldehyde (PF) resin impregnation successfully contributed to improved performance of three-point bending in MOE with 21.4% increase for pine and 29.0% increase for beech. MOR improved close to 18% for both wood species. High limit of proportionality for modified wood species, describes the brittle material behavior that was identified as a main drawback for dynamic test in impact bending strength (IBS) and cyclic fatigue strength (CFS). CFS experienced negative effect of modification. Fatigue limit for reaching 10^6 loading cycles was 67% for reference sample, 58% for modified pine and 53% for modified beech from overall average static strength. Cyclic loading repetitions were found to cause decrease in cyclic creep with decreasing stress. The cyclic modulus of elasticity did not change in the case of modification at any stress level and remained constant. It can be concluded that pine and beech wood, impregnated with low molecular weight PF resin, perform much differently from unmodified wood. Therefore, it is important to take into account that dynamic mechanical properties, no matter the improved static performance, suffer greater reduction in IBS and CFS and show different creep rate level. High rigidity of modified material resulting in reduced ability for plastic deformation, prevents prediction when material starts to fatigue. More research is needed to get clearer results with greater variety of specimens.

Author contribution: All the authors have accepted responsibility for the entire content of this submitted manuscript and approved submission.

Research funding: The authors gratefully acknowledge the European Commission for funding the InnoRenew project (grant agreement #739574) under the Horizon2020 Widespread-Teaming program and the Republic of Slovenia (investment funding from the Republic of Slovenia and the European Union's European Regional Development Fund) as well as the Slovenian Research Agency (ARRS) for funding infrastructural program IO-0035 and bilateral project BI-DE/17-19-15.

Conflict of interest statement: The authors declare no conflicts of interest regarding this article.

References

- Ahmed, S.A., and Adamopoulos, S. (2018). Acoustic properties of modified wood under different humid conditions and their relevance for musical instruments. *Appl. Acoust.* 140: 92–99.
- Ashby, M.F. (2010). *Materials selection in mechanical design*, 4th. ed. Butterworth-Heinemann, Oxford. p. 640.
- Baar, J., Tippner, J., and Rademacher, P. (2015). Prediction of mechanical properties - modulus of rupture and modulus of elasticity - of five tropical species by nondestructive methods. *Maderas. Cienc. Tecnol.* 17: 2.
- Bicke, S., Mai C., and Millitz H. (2012). Modification of beech veneers with low molecular weight phenol formaldehyde for the production of plywood: durability and mechanical properties. In: *Conference: ECWM6 - The Sixth European Conference on Wood Modification*. Ljubljana, Slovenia.
- Deka, M., and Saikia, C.N. (2000). Chemical modification of wood with thermosetting resin: effect on dimensional stability and strength property. *Bioresour. Technol.* 73: 179–181.
- Deka, M., Saikia, C.N., and Baruah, K.K. (2002). Studies on thermal degradation and termite resistant properties of chemically modified wood. *Bioresour. Technol.* 84: 151–157.
- DIN 52186. (1978). *Testing of wood; bending test*. DIN German Institute for Standardization, Berlin, German.
- DIN 52189-1. (1981). *Testing of wood; determination of impact bending strength*. German Institute for Standardisation, Berlin, German.
- Epmeier, H., Westin, M., and Rapp, A. (2004). Differently modified wood: comparison of some selected properties. *Scand. J. Forest. Res.* 19: 31–37.
- Franke, T., Axel, M., Lenz, C., Nadine, H., and Pfriem, A. (2017). Microscopic and macroscopic swelling and dimensional stability of beech wood impregnated with phenol-formaldehyde. *PRO LIGNO* 13: 373–378.
- Furuno, T., Imamura, Y., and Kajita, H. (2004). The modification of wood by treatment with low molecular weight phenol-formaldehyde resin: a properties enhancement with neutralized phenolic-resin and resin penetration into wood cell walls. *Wood Sci. Technol.* 37: 349–361.
- Gabrielli, C.P., and Kamke, F.A. (2010). Phenol-formaldehyde impregnation of densified wood for improved dimensional stability. *Wood Sci. Technol.* 44: 95–104.
- Gascon, G.P., Millitz, H., Mai, C., and Thévenon, M.F. (2015). Enhanced termite resistance of scots pine (*Pinus sylvestris* L.) solid wood by phenol - formaldehyde treatment. *Wood Res.* 60: 873–880.
- Gong, M., and Smith, I. (2003). Effect of waveform and loading sequence on low-cycle compressive fatigue life of spruce. *J. Mater. Civ. Eng.* 15: 93–99.
- Hill, C. (2006) *Wood modification*. Wiley, Chichester. p. 239.
- Hosseinpourpia, R., Adamopoulos, S., and Mai, C. (2016). Dynamic vapour sorption of wood and holocellulose modified with thermosetting resins. *Wood Sci. Technol.* 50: 165–178.
- Huang, Y., Fei, B., Yu, Y., and Zhao, R. (2013). Effect of modification with phenol formaldehyde resin on the mechanical properties of wood from Chinese fir. *Bio Resour.* 8: 272–282.
- Kielmann, B.C., Butter, K., and Mai, C. (2018). Modification of wood with formulations of phenolic resin and iron-tannin-complexes to improve material properties and expand colour variety. *Eur. J. Wood Wood Prod.* 76: 259–267.

- Kielmann, B.C., Militz, H., Mai, C., and Adamopoulos, S. (2013). Strength changes in ash, beech and maple wood modified with a N-methylol melamine compound and a metal-complex dye. *Wood Res.* 58: 343–350.
- Klein, B. (2009). *Leichtbau-Konstruktion – Berechnungsgrundlagen und Gestaltung*, 6th ed. Vieweg, Wiesbaden. p. 493.
- Klüppel, A. (2017). Hardness and indentation modulus of resin-treated wood. *Int. Wood Prod. J.* 8: 41–44.
- Klüppel, A., Cragg, S.M., Militz, H., and Mai, C. (2015). Resistance of modified wood to marine borers. *Int. Biodeterior. Biodegrad.* 104: 8–14.
- Kollmann, F.F.P., Côté, W.A.J. (1968). *Principles of wood science and technology - solid wood*, Vol. 1. Springer, München.
- Mai, C., Elder, T. (2016). Wood: chemically modified. In: *Reference module in materials science and materials Engineering*. Encyclopedia of Materials: Science and Technology, 2001: pp. 9603–9606.
- Ramage, M.H., Burrige, H., Busse Wicher, M., Fereday, G., Reynolds, T., Shah, D. U., Wu, G., Yu, L., Fleming, P., Densley-Tingley, D., et al. (2017). The wood from the trees: The use of timber in construction. *Renew. Sustain. Energy Rev.* 68: 333–359.
- Ratnasingam, J., and Mutthiah, N. (2017). Fatigue life of oil palm wood (OPW) for furniture applications. *Eur. J. Wood Wood Prod.* 75: 473–476.
- Rowell, R. M. (1998). Property enhanced natural fibre composite materials based on chemical modification. In: *Science and technology of polymers and advanced materials*. Pra-sad, P. N., Mark, J. E., Kandil, S. H., and Kafafi, Z. H. (Ed.) Plenum, New York, NY. pp. 717–732.
- Sandberg, D., Haller, P., and Navi, P. (2013). Thermo-hydro and thermo-hydro-mechanical wood processing: an opportunity for future environmentally friendly wood products. *Wood Mater. Sci. Eng.* 8: 64–88.
- Sasaki, Y., Oya, A., and Yamasaki, M. (2014). Energetic investigation of the fatigue of wood. *Holzforschung* 68: 843–848.
- Sharapov, E., Mahnert, K.C., and Militz, H. (2016). Residual strength of thermally modified *Scots pine* after fatigue testing in flexure. *Eur. J. Wood Wood Prod.* 74: 875–884.
- Skaar, C. (1988). *Wood-water relations*. Springer, Berlin. p. 283.
- Smith, I., Landis, E., and Gong, M. (2003). *Fracture and fatigue in wood*. Wiley, Chichester. p. 242.
- Stamm, A. J., and Tarkow H. (1947). Dimensional stabilization of wood. *J. Phys. Chem.* 51: 493–505.
- Sugimoto, T., and Sasaki, Y. (2007). Fatigue life of structural plywood under two-stage panel shear load: a new cumulative fatigue damage theory. *J. Wood Sci.* 53: 211–217.
- Sugimoto, T., Sasaki, Y., and Yamasaki, M. (2007). Fatigue of structural plywood under cyclic shear through thickness I: fatigue process and failure criterion based on strain energy. *J. Wood Sci.* 53: 296–302.
- Sugimoto, T., and Sasaki, Y. (2006). Effect of loading waveform on the fatigue of structural plywood in shear through thickness. In: *Proceedings of 9th World Conference on Timber Engineering (WCTE 2006)*. Portland, Oregon, pp 1818–1825.
- Tsai, K.T., Ansell, M.P. (1990). The fatigue properties of wood in flexure. *J. Mater. Sci.* 25: 865–878.
- Verkasalo, E., and Leban, J.M. (2002). MOE and MOR in static bending of small clear specimens of Scots pine, Norway spruce and European fir from Finland and France and their prediction for the comparison of wood quality. *Pap Puu Pap Tim.* 84: 332–340.
- Wan, H., and Kim, M.G. (2006). Impregnation of southern pine wood and strands with low molecular weight phenol-formaldehyde resins for stabilization of oriented strandboard. *Wood Fiber Sci.* 38: 314–324.
- Wang, X., Chen, X., Xie, X., Yuan, Z., Cai, S., Li, Y. (2019). Effect of phenol formaldehyde resin penetration on the quasi-static and dynamic mechanics of wood cell walls using nanoindentation. *Nanomaterials* 9(10): 1409.
- Xie, Y., Krause, A., Militz, H., Turkulin, H., Richter, K., and Mai, C. (2007). Effect of treatments with 1,3-dimethylol-4,5-dihydroxy-ethyleneurea (DMDHEU) on the tensile properties of wood. *Holzforschung* 61: 43–50.
- Xie, Y., Fu, Q., Wang, Q., Xiao, Z., and Militz, H. (2013). Effects of chemical modification on the mechanical properties of wood. *Eur. J. Wood Wood Prod.* 71: 401–416.
- Xie, Y., Xu, J., Militz, H., Wang, F., Wang, Q., Mai C., and Xiao Z. (2016). Thermo-oxidative decomposition and combustion behavior of Scots pine (*Pinus sylvestris* L.) sapwood modified with phenol- and melamine-formaldehyde resins. *Wood Sci. Technol.* 50: 1125–1143.

Chapter 3

Summary of Studies

3.1 Article 1

In Article 1, fracture properties under mode I were experimentally evaluated on two structural adhesives, one non-structural adhesive, and bonded beech wood. Main objectives of the paper were to: (i) evaluate the testing method utilising single edge notched-three-point bending tests for characterisation of bondline fracture properties, (ii) characterise fracture properties of selected adhesive systems, (iii) evaluate the impact of wood grain orientation on fracture properties, and finally (iv) assess impact of two elevated temperatures on bondline performance compared to the control group. Standardised lap-shear tests showed that all the tested adhesives meet the required bondline strength for tested environment and successfully confirmed the bonding parameters. In terms of fracture testing force-displacement (F/δ) diagrams clearly demonstrated higher initial stiffness of RT group ahead of TR group while TR resulted in less abrupt failures. As a result of composite softening, or change in moisture the difference between initial stiffness became less evident when groups were exposed to elevated temperatures. EPI resin resulted in the highest observed G_c and G_f values when tested at standard climate conditions but, on the other hand, experienced the most severe decrease in fracture properties with temperature treatments. The same adhesive showed the most significant changes regarding the wood plane orientation, which was less evident for polyurethane, and melamine urea formaldehyde. Under the standard climate conditions in TR plane, EPI resulted in an average G_c of 0.80 N/mm and G_f of 5.13 N/mm. Melamine urea formaldehyde with an average $G_c = 0.50$ N/mm and $G_f = 3.14$ N/mm outperformed polyurethane with an average $G_c = 0.25$ N/mm and $G_f = 1.39$ N/mm, respectively. Treatment of specimens at elevated temperatures resulted in reduced fracture performance regardless of wood grain orientation or the adhesive system. The most severe impact on fracture properties were obtained for groups tested at 140 °C, where the highest G_c and G_f were found in TR plane for EPI (0.27 N/mm and 1.78 N/mm) followed by melamine urea formaldehyde (0.19 N/mm and 1.47 N/mm) and polyurethane (0.18 N/mm and 1.14 N/mm). Analytical results obtained by linear models fitted the experimental results with R^2 of G_c model = 0.62 and R^2 of G_f model = 0.79. Hypotheses H1 and H1.1 were addressed and confirmed in this study by showing diversly obtained

G_c and G_f of different adhesive types as well as by differentiating along TR and RT plane orientation.

Overall the study showed that the SEN-TPB test employing the data reduction scheme used may be used for fracture analysis of adhesive bond with desired wood grain orientation selection and smaller bondline area which may reduce the imperfections in the interphase. With the increasing temperature treatment of the specimens, impact on fracture properties was gradually reduced. In general, higher the treating temperature, higher the impact on fracture properties.

3.2 Article 2

This study discusses the use of three-point end-notched flexure test under mode II for selected structural and non-structural adhesive types and bonded beech wood, to compute strain energy release rate by means of equivalent crack length and digital image correlation data. Further experimental data was turned into finite element models including cohesive zone models for selected adhesives to numerically analyse the influence of friction during the shear test and influence of material stiffness by wood grain orientation. Study on Mode II describes fracture phenomena in shear direction using the three-point end-notched flexure test and the compliance-based beam method on beech wood for EPI, melamine urea formaldehyde polyurethane, and phenol resorcinol formaldehyde resin. The following important outcomes of the study should be considered. The highest mean critical strain energy release rate (G_{IIc}) of 5.40 N/mm was obtained for polyurethane adhesive followed by 2.33 N/mm, 1.80 N/mm, and 1.59 N/mm for melamine urea formaldehyde, EPI and phenol resorcinol formaldehyde respectively. With that, all values were found to have higher G_{IIc} for solid beech wood (1.41 N/mm) than the reported values from literature. Such findings may be considered beneficial in favor of bonded elements. The behavior of melamine urea formaldehyde, EPI, and phenol resorcinol formaldehyde was found to be brittle with steady crack initiation and self-similar propagation behavior, which was demonstrated with stable strain energy release rate over the displacement slip at the crack tip after failure. However, this was not true for ductile-like polyurethane adhesive selected for this study, where failure was not as evident which suggests modification of the method for ductile-like adhesive, or alternative testing method. The finite element model utilised three different material properties expressed by: (i) orthotropic elastic model, (ii) orthotropic elasto-plastic model with the same compression and tension yield stresses, and (iii) orthotropic elasto-plastic model with different compression and tension yield values. All three material models were used to simulate all used adhesives. The models fitted well with experimental data with less than 5 % relative difference. The numerical model further confirmed negligible effect of friction on bending stiffness of the specimens, while suggesting that grain angle within longitudinal orientation of the specimen would impact flexural stiffness and ultimate load. With this, the study showed and confirmed H1 also under mode II testing

regime by concluding that fracture properties (G_c and G_f) are highly dependent on adhesive type.

3.3 Article 3

Article 3 focused on the experimental analyses of flexible thick adhesive connections using double-lap-shear geometry. Reverse cyclic shear tests following EN 12512 and ISO 16670 standards for joints with mechanical fasteners for timber structures were used to evaluate thick flexible adhesive as an alternative connection type. In the study, three different adhesives with different mechanical properties (stiffness and elongation at break) and two different bondline thicknesses (10 and 15 mm) were tested as an alternative energy dissipating connection to common mechanical timber connections. Based on static shear test, dedicated cyclic protocols were prepared for each adhesive type and bondline thickness. Strength capacities for 10 mm thick connection resulted in 1.74 MPa, 1.71 MPa, and 1.48 MPa for selected PUR adhesives PST, PTS, and PS respectively. Levels of the obtained values in experimental tests were found to be lower compared to the specified pure adhesive strength and strain values. This may be explained with non-optimal adhesion between adhesive and adherent for which optimisation of surface or primer selection should be considered. The difference in average strength capacity between 15 mm and 10 mm thick connections was found to be 32 %, 19 %, and 19 % lower for PS, PST, and PTS adhesive type, respectively. Static shear tests showed that with increasing bondline thickness elastic and plastic stiffness was reduced by an average 25 % regardless of adhesive type. Numerical simulation agreed well with experimental data and confirmed that increasing bondline thickness resulted in shear stress reduction. Hysteresis loops from the reverse cyclic diagrams exhibit a high proportion of elastic deformation but usually low deformation capacity. The cyclic tests results on adhesive connections were analytically compared with the common mechanical screw-type half-lap connections obtained from literature based on the similar test regimes. The following conclusions were agreed upon: (i) thicker adhesives resulted with higher elastic and plastic deformation capacity, (ii) adhesive connections performed with higher stiffness and strength capacity compared to mechanical dowel-type screwed connections (iii) strength degradation capacity after three fully reversed cycles with less than 20 % drop in resistance between the 1st and the 3rd loading cycle was fulfilled at all displacement levels before failure was reached, (iv) deformation capacity, ductility, and energy dissipation were in favor of mechanical screw-type connections. The adhesive with the lowest stiffness but highest elongation at break (PTS) was found to have the most beneficial performance with stiffness to strength capacity ratio. Hypotheses H2 was addressed within this study and the application of thick flexible adhesives for timber-to-timber connections with low capacity of energy dissipation was confirmed. The other observed beneficial mechanical performance may satisfy other applications i.e. glued-in-rod, half-lap, spline joint connections, or applications with other building elements (window frames, steel, glass connections) which have been confirmed in other studies.

3.4 Article 4

The fourth article studied the effects of wood modification using resin impregnation on dynamic properties. Low molecular weight phenol formaldehyde resin was used to impregnate the wood cell wall structure of Scots pine and European beech, two commercially important wood species. With the classical vacuum impregnation, followed by drying and curing of the resin, both wood species were first tested under static three-point bending test to confirm that static bending of treated modified samples exhibit improved mechanical performance, with 21.4 % and 29.0 % higher modulus of elasticity for pine and beech respectively. Modulus of rupture of the modified sample was found to be 18 % higher for both wood species. According to that the stress level of modified species was adjusted for cyclic fatigue testing. For the dynamic assessment of modified timber, cyclic three-point bending tests were conducted in the standardised environment. Stress levels were adjusted according to ultimate strength and gradually decreased until fatigue limit of 10^6 sinusoidal loading cycles, as a study threshold, was reached. Modification showed negative impact on dynamic fatigue strength where cyclic fatigue strength was found to be 67 % for control group, 58 % for modified pine, and 53 % for modified beech based on proposed stress level defined by static bending tests which confirmed H3 proposed in this thesis. Additionally, during the test, the cyclic modulus of elasticity did not show any change for the modified samples and no reduction in creep rate within the secondary creep phase was observed for modified timber. Moreover, impact bending strength was 59.8 % and 35.9 % lower for modified pine and beech compared to the untreated control group. The key point of this study suggests that dynamic mechanical properties of phenol-formaldehyde modified pine and beech wood are truly different from untreated materials by showing reduced capacity of plastic deformation causing no signs of fatigue or early failure in the materials. It is, therefore, important to be aware of these properties when considering such materials for use as a load bearing member.

Chapter 4

Conclusions

4.1 Summary

The main goal of this thesis was to address several innovative adhesive applications and experimental methods in the field of adhesive use in structural timber elements.

To address the three research questions and hypotheses posed in section 1.2, the following research was conducted: (i) fracture properties of beech wood adhesive bondline among different adhesives, (ii) mechanical properties of thick flexible adhesives joints, and (iii) dynamic strength properties of resin-modified beech and pine wood.

Across the four conducted studies we showed how important it is to apply different methods for testing adhesive applications for diverse use of timber in structural applications. Our aim is to improve and widen the understanding of wood-adhesive composite characteristics and thereby expand their applications.

From a wider perspective, the findings reported in this thesis highlight the complexity of material variability, from selection of the adhesive systems to the type of wood species, and show how these variabilities reflect in the performance of composites, joints, or modified wood.

Research Question 1

For the fracture mechanism of bonded beech wood (Article 1, 2), we showed how various adhesive systems behave with respect to fracture properties such as G_c and G_f and these findings addresses H1. The work confirms some previous findings which discuss different testing regimes and methods and how they provide a wide range of information for describing the characteristics of composites. In the articles different methods, appropriate for testing the selected adhesives on bonded beech wood, were utilised and evaluated; however, the need to make adjustments for further studies was noted: modification of the selected factor and adjustment of the testing method for PUR adhesives for Article 1 and 2 respectively. Treatment of bondline at an elevated temperature was found to have a negative impact on fracture properties, while bonding on different wood plane orientation (H1.1) (radial and tangential plane) showed how fracture properties differ as a result of

the anatomical structure of wood and how this results in different fracture properties. This emphasises that bondlines exposed to an elevated temperature suffer higher fracture reduction under opening mode I regime and also that crack propagation in bondline is different with regard to bonding wood plane direction for bonded beech wood. Exposure of bonded beech wood to shear stress under mode II regime showed improved fracture properties compared to fracture of solid wood, meaning that bonded beech wood under such circumstances did not suffer reduction in G_c and G_f values. The cohesive law models developed in Article 2 for selected adhesives agreed with the experimental results which also confirmed the selected testing approach. Furthermore, the finite element models used showed that (1) wood grain orientation in the bonded beams does have an impact on the flexural stiffness, and ultimate load and (2) friction between lamellas resulted in negligible effects.

Research Question 2

Rigid and creep resistance adhesive thin bondlines are desired in achieving good quality bondline; on the contrary, Article 3 showed the advantages of flexible adhesives as a replacement for typical mechanical screw-type connections in timber joints and consequently, satisfactorily meet the desired requirements for low seismic areas for timber buildings as hypothesised in H2. Mechanical properties of thick flexible adhesive joints reflected adhesive material properties but the full potential of adhesives was achieved which argues poor adhesion or surface treatment. With the increased adhesive joint thickness, strength capacity was reduced for all the tested adhesives, in addition to a reduction in elastic and plastic stiffness. Nevertheless analytical comparison of adhesive joints with mechanical dowel-type connection showed that the tested adhesives performed under higher stiffness and strength capacity. Though rarely used in timber engineering, thick adhesive bondlines can be successfully used in timber connections and satisfy low capacity needs of energy dissipation according to selected parts from Eurocode 8.

Research Question 3

Article 4 evaluates the impact of PF impregnation on dynamic properties of solid timber, such as fatigue and impact bending strength, which supports hypothesis H3 proposed in the thesis. Within the study we showed how PF modified beech and pine wood improve under static bending tests but when specimens were exposed to dynamic cyclic bending tests, the level of fatigue strength was lower compared to untreated wood. Influence of wood modification changed the capacity ratio between elastic to plastic deformation with increased brittleness of the materials. These changes were found to be more severe if the material was exposed to the cyclic loading mechanism. The observed changes in elastic-plastic deformations during the cyclic loading tests were negligible and specimens showed no visible stationary creep and resulted in more sudden material failure. The key finding of this study shows how modified material behaves under different loading mechanisms and that properties based on static loadings should not be generalised for

dynamic ones. Future studies should more comprehensively and holistically address these topics to resolve these problems on a wider selection of modified materials and under different testing conditions.

4.2 Contribution to Science and Considerations for Future Research

In this thesis, we addressed different applications of adhesives, from rigid structural adhesive bondlines intended for load bearing capacity tested under fracture properties, to thick highly flexible adhesives which were successfully used in combination with timber as an innovative joining connection. In addition, wood impregnation with low molecular weight phenolic resins, a historically known wood modification approach, was addressed from the perspective of dynamic mechanical loading. With such a diverse range of adhesive applications, this thesis shows relevancy and emphasises the importance of adhesive studies in the field of wood material science.

The three articles focused on European beech which is becoming an economically and environmentally important hardwood species with the potential for increased use in timber engineering across Central Europe. Beech wood has good bonding characteristics but lacks dimensional stability and durability. Bonding beech wood into advanced engineering products can be of benefit in a wide range of applications and products. Stronger evidence in favour are the ongoing climate changes that will impact the future structure of our forests. Therefore, research studies on beech are of high interest.

In Article 1 and 2 we examined fracture properties of adhesive bondline in bonded beech wood. For two different testing regimes (mode I and II), fracture of adhesives on bonded beech were tested with novel methods. These studies provided some clear answers on how fracture properties differ among adhesive systems, testing methods, and in particular cases, the impact on the environment. In Article 1 we confirmed the desired lap-shear strength properties for all the adhesives, but showed that when bondline is exposed to crack opening (mode I), the fracture behaviour is very specific to particular adhesive systems. A similar distinction was also confirmed for adhesive bondline loaded in shear (mode II). Another important finding was that G_c values for adhesives were higher for bonded beech than for clear beech. Differences among adhesives were respected in the design of cohesive laws, which delivered higher precision in material modelling.

Though both articles demonstrated the adaptability of the selected testing methods, some adjustment of the methods needs to be considered for future work. For example, in Article 1, factor k used for G_c calculations was adopted from literature and adjusted. After evaluating the proposed linear model, it was concluded that R^2 deviations along the studied fracture properties suggest an error introduced by the selection of factor k for calculating G_c . On the contrary, G_f calculated directly from the obtained experimental force-displacement diagrams, showed a better match in the proposed linear model, also

resulting in higher R^2 value. This clearly indicates an improvement in the selected calculation method or adjustment of the k factor. Furthermore, Article 2 successfully showed that all the adhesives improved composite properties of bonded beech wood against solid wood, which is a beneficial result in terms of bonding applications. The method based on the three-point end-notched flexure test was shown to be more suitable for rigid-like adhesive systems but less so for the flexible PUR adhesive. Due to the high plastic strains developed in wood on tested PUR specimens, we claim that geometry together with wood material are outperformed by the elastic capacity of the PUR adhesive. This study suggests that future work should better adjust the test method and/or specimen geometry. Such and similar studies report and validate the structural integrity of tested materials or composites which is important for understanding their behaviour under stress and failure mechanisms. Future studies should focus on a more comprehensive approach including a wider range of material inputs such as wood type, surface properties, anatomical plane direction, as well as environmental and manufacturing conditions. These studies showed how various adhesive systems exhibit different performance; in addition, research should also more clearly demonstrate the factors that contribute to these changes which can enable an optimal match of wood species and adhesive systems, and thereby, result in improved manufacturing processes.

Moving from thin rigid-like bondlines the past studies have already shown desirable behaviour of flexible polyurethane adhesives in various building applications. Though the studies that focus on adhesive-wood interactions are limited, they show great potential for future studies on connections in various joint types, loading mechanism, environments, etc. Article 3 demonstrated an innovative approach by using flexible thick adhesive bondlines to create wood-adhesive joints for structural elements, to replace mechanical type connections. Using flexible adhesives in timber joints can further evolve into novel types of joints in combination with other building materials and applications. This study further showed that there are opportunities for improved adhesion between materials which would result in higher mechanical properties of joints. For now, small-scale adhesive joints have been shown to satisfy requirements for low seismic areas but behaviour on large scale timber members in combination with other building materials still remains unclear.

This thesis has emphasised the complexity of multilevel wood-adhesive interactions but resin wood modification should not be overlooked. Modified wood was and will continue to be used for enhanced outdoor applications. Literature review in the introduction demonstrated how various methods of modification impact wood mechanical properties. Wood modification with phenolic resins has a long history in the research and applicational field but dynamic mechanical properties remain poorly known. For that reason, Article 4 looked at the dynamic mechanical properties of solid wood and the effects of wood resin modification on its dynamic properties. Both modified pine and beech exhibited stiffer and stronger behaviour under static bending loads compared to untreated wood. Accordingly, their ultimate stress levels for cyclic fatigue exposure were

set higher compared to untreated materials. The study clearly demonstrated that fatigue strength of modified wood was lower than for untreated wood. Because of the changes in elastic-plastic behaviour of modified material during the cyclic loading, specimens also did not show any signs of weakening which means that stiffness of the material did not change throughout the test. Eventually the material failed without any notable visible change in its performance. As it can be seen, Article 4 clearly demonstrates how resin modification impacts static and dynamic properties. The topics related to dynamic properties are very important, especially since wood modification is often conducted on wood species that are for outdoor use and can also be used as a load bearing elements. The rheological properties of resin modified wood in combination with dynamic loading mechanisms would offer a more comprehensive understanding of the change in mechanical properties. Nevertheless, embrittlement of wood after exposure to various modification processes is common, which brings us to many more new materials that should undergo dynamic testing and should be studied to determine the effect of modification on their behaviour and to what level this behaviour is impacted.

Bibliography

- [1] F. ASDRUBALI, B. FERRACUTI, L. LOMBARDI, C. GUATTARI, L. EVANGELISTI, G. GRAZIESCHI, A review of structural, thermo-physical, acoustical, and environmental properties of wooden materials for building applications, *Build. Environ.* 114 (2017) 307–332. <https://doi.org/10.1016/j.buildenv.2016.12.033>.
- [2] C.R. FRIHART, Wood adhesives: Past, present, and future, *For. Prod. J.* 65 (2015) 4–8. <https://doi.org/10.13073/65.1-2.4>.
- [3] M.H. RAMAGE, H. BURRIDGE, M. BUSSE WICHER, G. FEREDAY, T. REYNOLDS, D.U. SHAH, G. WU, L. YU, P. FLEMING, D. DENSLEY-TINGLEY, J. ALLWOOD, P. DUPREE, P.F. LINDEN, O. SCHERMAN, The wood from the trees: The use of timber in construction, *Renew. Sustain. Energy Rev.* 68 (2017) 333–359. <https://doi.org/10.1016/j.rser.2016.09.107>.
- [4] T. VALLÉE, T. TANNERT, S. FECHT, Adhesively bonded connections in the context of timber engineering—A Review, *J. Adhes.* 93 (2017) 257–287. <https://doi.org/10.1080/00218464.2015.1071255>.
- [5] C.G. HUNT, C.R. FRIHART, M. DUNKY, A. ROHUMAA, Understanding wood bonds-going beyond what meets the eye: A critical review, *Rev. Adhes. Adhes.* 6 (2018) 369–463. <https://doi.org/10.7569/RAA.2018.097312>.
- [6] M.D. BANEJA, L.F.M. DA SILVA, Adhesively bonded joints in composite materials: An overview, *Proc. Inst. Mech. Eng. Part L J. Mater. Des. Appl.* 223 (2009) 1–18. <https://doi.org/10.1243/14644207JMDA219>.
- [7] F.A. KAMKE, J.N. LEE, Adhesive penetration in wood: a review, *Wood Fiber Sci.* 39 (2007) 205–220.
- [8] A.A. MARRA, *Technology of Wood Bonding: Principles in Practice*, New York Van Nostrand Reinhold, New York, 1992.
- [9] I. GAVRILOVIĆ-GRMUŠA, M. DUNKY, J. MILJKOVIĆ, M. DJIPOROVIĆ-MOMČILOVIĆ, Influence of the degree of condensation of urea-formaldehyde adhesives on the tangential penetration into beech and fir and on the shear strength of the adhesive joints, *Eur. J. Wood Wood Prod.* 70 (2012) 655–665. <https://doi.org/10.1007/s00107-012-0599-6>.

- [10] M. STERLEY, Characterisation of green-glued wood adhesive bonds, Linnaeus University, 2012.
- [11] F. SIMON, G. LEGRAND, Overview of European standards for adhesives used in wood-based products, *J. Adhes. Sci. Technol.* 24 (2010) 1611–1627. <https://doi.org/10.1163/016942410X507722>.
- [12] S. VEIGEL, J. FOLLRICH, W. GINDL-ALTMUTTER, U. MÜLLER, Comparison of fracture energy testing by means of double cantilever beam-(DCB)-specimens and lap joint testing method for the characterization of adhesively bonded wood, *Eur. J. Wood Wood Prod.* 70 (2012) 3–10. <https://doi.org/10.1007/s00107-010-0499-6>.
- [13] I. SMITH, E. LANDIS, M. GONG, Fracture and Fatigue in Wood, (2003) 246.
- [14] B. RIVER, Fracture of Adhesive-Bonded Wood Joints, *Handb. Adhes. Technol. Revis. Expand.* (2003). <https://doi.org/10.1201/9780203912225.ch15>.
- [15] F. STOECKEL, J. KONNERTH, W. GINDL-ALTMUTTER, Mechanical properties of adhesives for bonding wood-A review, *Int. J. Adhes. Adhes.* 45 (2013) 32–41. <https://doi.org/10.1016/j.ijadhadh.2013.03.013>.
- [16] M. IZZI, D. CASAGRANDE, S. BEZZI, D. PASCA, M. FOLLESA, R. TOMASI, Seismic behaviour of Cross-Laminated Timber structures: A state-of-the-art review, *Eng. Struct.* 170 (2018) 42–52. <https://doi.org/10.1016/j.engstruct.2018.05.060>.
- [17] C. BARILE, C. CASAVOLA, G. PAPPALETTERA, P.K. VIMALATHITHAN, Damage propagation analysis in the single lap shear and single lap shear-riveted CFRP joints by acoustic emission and pattern recognition approach, *Materials (Basel)*. 13 (2020). <https://doi.org/10.3390/ma13183963>.
- [18] G. JEEVI, S.K. NAYAK, M. ABDUL KADER, Review on adhesive joints and their application in hybrid composite structures, *J. Adhes. Sci. Technol.* 33 (2019) 1497–1520. <https://doi.org/10.1080/01694243.2018.1543528>.
- [19] K. ARKADIUSZ, R. KONRAD, Z. BOGUSŁAW, T. KOZIK, Mechanical Behavior of Polyurethane Adhesives Applied to Timber Joints in Repair of Historical Timber Structures, in: *Struct. Anal. Hist. Constr., RILEM Book*, Springer, Cham, 2019: pp. 1603–1612. <https://doi.org/10.1007/978-3-319-99441-3>.
- [20] K. RODACKI, Z. BOGUSŁAW, A. KWIECIEŃ, M. TEKIELI, K. FURTAK, The Strength of Wooden (Timber)-Glass Beams Combined with the Polyurethane Adhesive - DIC and Finite Element Analysis, in: *Struct. Anal. Hist. Constr., RILEM Book*, 2019: pp. 323–331. <https://doi.org/10.1007/978-3-319-99441-3>.
- [21] M. PREMROV, B. BER, A. ŠTRUKELJ, Cyclic and shaking-table tests of timber-glass buildings, *Int. J. Comput. Methods Exp. Meas.* 5 (2017) 928–939. <https://doi.org/10.2495/CMEM-V5-N6-928-939>.

- [22] P. JELUŠIČ, S. KRAVANJA, Flexural analysis of laminated solid wood beams with different shear connections, *Constr. Build. Mater.* 174 (2018) 456–465. <https://doi.org/10.1016/j.conbuildmat.2018.04.102>.
- [23] M. ANGELIDI, A.P. VASSILOPOULOS, T. KELLER, Ductile adhesively-bonded timber joints – Part 1: Experimental investigation, *Constr. Build. Mater.* 179 (2018) 692–703. <https://doi.org/10.1016/j.conbuildmat.2018.05.214>.
- [24] M. BRUNNER, M. LEHMANN, S. KRAFT, U. FANKHAUSER, K. RICHTER, J. CONZETT, A flexible adhesive layer to strengthen glulam beams, *J. Adhes. Sci. Technol.* 24 (2010) 1665–1701. <https://doi.org/10.1163/016942410X507759>.
- [25] S. ZÖLLIG, A. FRANGI, S. FRANKE, M. MUSTER, Timber structures 3.0 - New technology for multi-axial, slim, high performance timber structures, in: *WCTE 2016 - World Conf. Timber Eng.*, Vienna, Austria, 2016.
- [26] C. HILL, *Wood modification: chemical, thermal and other Processes*, Wiley, England, 2006.
- [27] D. SANDBERG, A. KUTNAR, G. MANTANIS, Wood modification technologies - A review, *IForest.* 10 (2017) 895–908. <https://doi.org/10.3832/ifor2380-010>.
- [28] C.P. GABRIELLI, F.A. KAMKE, Phenol-formaldehyde impregnation of densified wood for improved dimensional stability, *Wood Sci. Technol.* 44 (2010) 95–104. <https://doi.org/10.1007/s00226-009-0253-6>.
- [29] T. FURUNO, Y. IMAMURA, H. KAJITA, The modification of wood by treatment with low molecular weight phenol-formaldehyde resin: A properties enhancement with neutralized phenolic-resin and resin penetration into wood cell walls, *Wood Sci. Technol.* 37 (2004) 349–361. <https://doi.org/10.1007/s00226-003-0176-6>.
- [30] B. PIZZO, P. LAVISCI, C. MISANI, P. TRIBOULOT, The compatibility of structural adhesives with wood, *Holz Als Roh - Und Werkst.* 61 (2003) 288–290. <https://doi.org/10.1007/s00107-003-0384-7>.
- [31] M. STERLEY, E. SERRANO, B. KÄLLANDER, Building and construction: Timber engineering and wood-based products, in: Robert D. Adams (Ed.), *Adhes. Bond. Sci. Technol. Appl.*, 2nd ed., 2021: pp. 571–603. <https://doi.org/10.1016/B978-0-12-819954-1.00021-6>.
- [32] K. TSERPES, A. BARROSO-CARO, P.A. CARRARO, V.C. BEBER, I. FLOROS, W. GAMON, M. KOZŁOWSKI, F. SANTANDREA, M. SHAHVERDI, D. SKEJIĆ, C. BEDON, V. RAJČIĆ, A review on failure theories and simulation models for adhesive joints, *J. Adhes.* 98 (2021) 1855–1915. <https://doi.org/10.1080/00218464.2021.1941903>.
- [33] J. XAVIER, J. MORAIS, N. DOURADO, M.F.S.F. DE MOURA, Measurement of mode I and mode II fracture properties of wood-bonded joints, *J. Adhes. Sci. Technol.* 25 (2011) 2881–2895. <https://doi.org/10.1163/016942411X576563>.
- [34] J. XAVIER, J.R.A. FERNANDES, J.J.L. MORAIS, O. FRAZÃO, Fracture

- behaviour of wood bonded joints under modes I and II by digital image correlation and fibre Bragg grating sensors, *Cienc. e Tecnol. Dos Mater.* 27 (2015) 27–35. <https://doi.org/10.1016/j.ctmat.2015.06.001>.
- [35] N. DOURADO, M.F.S.F. DE MOURA, S. MOREL, J. MORAIS, Wood fracture characterization under mode I loading using the three-point-bending test. Experimental investigation of *Picea abies* L., *Int. J. Fract.* 194 (2015) 1–9. <https://doi.org/10.1007/s10704-015-0029-y>.
- [36] J. XAVIER, M. OLIVEIRA, J.J.L. MORAIS, M.F.S.F. DE MOURA, Determining mode II cohesive law of *Pinus pinaster* by combining the end-notched flexure test with digital image correlation, *Constr. Build. Mater.* 71 (2014) 109–115. <https://doi.org/10.1016/j.conbuildmat.2014.08.021>.
- [37] J. XAVIER, J.R.A. FERNANDES, O. FRAZÃO, J.J.L. MORAIS, Measuring mode I cohesive law of wood bonded joints based on digital image correlation and fibre Bragg grating sensors, *Compos. Struct.* 121 (2015) 83–89. <https://doi.org/10.1016/j.compstruct.2014.11.017>.
- [38] F.G.A. SILVA, J. XAVIER, F.A.M. PEREIRA, J.J.L. MORAIS, N. DOURADO, M.F.S.F. MOURA, Determination of cohesive laws in wood bonded joints under mode I loading using the DCB test, *Holzforschung.* 67 (2013) 913–922. <https://doi.org/10.1515/hf-2013-0012>.
- [39] F.G.A. SILVA, J.J.L. MORAIS, N. DOURADO, J. XAVIER, F.A.M. PEREIRA, M.F.S.F. DE MOURA, Determination of cohesive laws in wood bonded joints under mode II loading using the ENF test, *Int. J. Adhes. Adhes.* 51 (2014) 54–61. <https://doi.org/10.1016/j.ijadhadh.2014.02.007>.
- [40] A. MAJANO-MAJANO, A.J. LARA-BOCANEGRA, J. XAVIER, F. PEREIRA, J. MORAIS, Direct evaluation of mode I cohesive law of eucalyptus bonded joints, *Procedia Struct. Integr.* 37 (2021) 492–499. <https://doi.org/10.1016/j.prostr.2022.01.114>.
- [41] T. EHRHART, European beech glued laminated timber, 2019. <https://doi.org/10.3929/ethz-b-000402805>.
- [42] I. GLAVNIĆ UZELAC, I. BOKO, N. TORIĆ, J. VRANKOVIĆ LOVRIĆ, Application of hardwood for glued laminated timber in Europe Subject, *Gradjevinar.* 72 (2020) 607–616. <https://doi.org/doi.org/10.14256/JCE.2741.2019>.
- [43] M. RHÊME, J. BOTSIS, J. CUGNONI, P. NAVI, Influence of the moisture content on the fracture characteristics of welded wood joint. Part 2: Mode II fracture, *Holzforschung.* 67 (2013) 755–761. <https://doi.org/10.1515/hf-2012-0145>.
- [44] M. RHÊME, J. BOTSIS, J. CUGNONI, P. NAVI, Influence of the moisture content on the fracture characteristics of welded wood joint. Part 1: Mode I fracture, *Holzforschung.* 67 (2013) 747–754. <https://doi.org/10.1515/hf-2012-0144>.

- [45] V. SEBERA, M. REDÓN-SANTAFÉ, M. BRABEC, D. DĚCKÝ, P. ČERMÁK, J. TIPPNER, J. MILCH, Thermally modified (TM) beech wood: Compression properties, fracture toughness and cohesive law in mode II obtained from the three-point end-notched flexure (3ENF) test, *Holzforschung*. 73 (2019) 663–672. <https://doi.org/10.1515/hf-2018-0188>.
- [46] J.L. GÓMEZ-ROYUELA, A. MAJANO-MAJANO, A.J. LARA-BOCANEGRA, J. XAVIER, M.F.S.F. DE MOURA, Evaluation of R-curves and cohesive law in mode I of European beech, *Theor. Appl. Fract. Mech.* 118 (2022). <https://doi.org/10.1016/j.tafmec.2021.103220>.
- [47] A. MAJANO-MAJANO, M. HUGHES, J.L. FERNANDEZ-CABO, The fracture toughness and properties of thermally modified beech and ash at different moisture contents, *Wood Sci. Technol.* 46 (2012) 5–21. <https://doi.org/10.1007/s00226-010-0389-4>.
- [48] W. HU, Y. LIU, S. LI, Characterizing mode I fracture behaviors of wood using compact tension in selected system crack propagation, *Forests*. 12 (2021) 1–13. <https://doi.org/10.3390/f12101369>.
- [49] P. WATSON, S. CLAUSS, S. AMMANN, P. NIEMZ, Fracture properties of adhesive joints under mechanical stresses, *Wood Res.* 58 (2013) 43–56.
- [50] S. AMMANN, P. NIEMZ, Mixed-mode fracture toughness of bond lines of PRF and PUR adhesives in European beech wood, *Holzforschung*. 69 (2015) 415–420. <https://doi.org/10.1515/hf-2014-0096>.
- [51] G. CLERC, A.J. BRUNNER, S. JOSSET, P. NIEMZ, F. PICHELIN, J.W.G. VAN DE KUILEN, Adhesive wood joints under quasi-static and cyclic fatigue fracture Mode II loads, *Int. J. Fatigue*. 123 (2019) 40–52. <https://doi.org/10.1016/j.ijfatigue.2019.02.008>.
- [52] H. YOSHIHARA, T. KAWAMURA, Mode I fracture toughness estimation of wood by DCB test, *Compos. Part A Appl. Sci. Manuf.* 37 (2006) 2105–2113. <https://doi.org/10.1016/j.compositesa.2005.12.001>.
- [53] H. YOSHIHARA, Examination of the mode I critical stress intensity factor of wood obtained by single-edge-notched bending test, *Holzforschung*. 64 (2010) 501–509. <https://doi.org/10.1515/HF.2010.083>.
- [54] I. GAVRIC, Seismic behaviour of cross-laminated timber buildings, University of Trieste, Italy, 2013.
- [55] A. CECCOTTI, C. SANDHAAS, M. OKABE, M. YASUMURA, C. MINOWA, N. KAWAI, SOFIE project – 3D shaking table test on a seven-storey full-scale cross-laminated timber building, *Earthq. Eng. Struct. Dyn. Earthq.* 42 (2013) 2003–2021. <https://doi.org/https://doi.org/10.1002/eqe.2309>.
- [56] R. SCOTTA, L. MARCHI, D. TRUTALLI, L. POZZA, A dissipative connector for CLT buildings: Concept, design and testing, *Materials (Basel)*. 9 (2016) 1–17.

- <https://doi.org/10.3390/ma9030139>.
- [57] M. LATOUR, G. RIZZANO, Cyclic behavior and modeling of a dissipative connector for cross-laminated timber panel buildings, *J. Earthq. Eng.* 19 (2015) 137–171. <https://doi.org/10.1080/13632469.2014.948645>.
- [58] A. IQBAL, S. PAMPANIN, A. PALERMO, A.H. BUCHANAN, Performance and design of LVL walls coupled with UFP dissipaters, *J. Earthq. Eng.* 19 (2015) 383–409. <https://doi.org/10.1080/13632469.2014.987406>.
- [59] A. BAIRD, T. SMITH, A. PALERMO, S. PAMPANIN, Experimental and numerical Study of U-shape Flexural Plate (UFP) dissipaters, in: *NZSEE Conf.*, Auckland, New Zealand, 2014: pp. 1–9. http://db.nzsee.org.nz/2014/poster/2_Baird.pdf.
- [60] A. HASHEMI, P. ZARNANI, R. MASOUDNIA, P. QUENNEVILLE, Seismic resistant rocking coupled walls with innovative Resilient Slip Friction (RSF) joints, *J. Constr. Steel Res.* 129 (2017) 215–226. <https://doi.org/10.1016/j.jcsr.2016.11.016>.
- [61] T. ROUSAKIS, A. ILKI, A. KWIECIEN, A. VISKOVIĆ, M. GAMS, P. TRILLER, B. GHIASSI, A. BENEDETTI, Z. RAKICEVIĆ, C. COLLA, O.F. HALICI, B. ZAJĄC, Ł. HOJDYS, P. KRAJEWSKI, F. RIZZO, V. VANIAN, A. SAPALIDIS, E. PAPADOULI, A. BOGDANOVIC, Deformable Polyurethane Joints and Fibre Grids for Resilient Seismic Performance of Reinforced Concrete Frames with Orthoblock Brick Infills, *Polymers (Basel)*. 12 (2020) 2869. <https://doi.org/10.3390/polym12122869>.
- [62] A. KWIECIEN, G. DE FELICE, D. V. OLIVEIRA, B. ZAJĄC, A. BELLINI, S. DE SANTIS, B. GHIASSI, G.P. LIGNOLA, P.B. LOURENÇO, C. MAZZOTTI, A. PROTA, Repair of composite-to-masonry bond using flexible matrix, *Mater. Struct. Constr.* 49 (2016) 2563–2580. <https://doi.org/10.1617/s11527-015-0668-5>.
- [63] Ł. ZDANOWICZ, S. SERĘGA, M. TEKIELI, A. KWIECIEN, Polymer flexible joint as a repair method of concrete elements: Flexural testing and numerical analysis, *Materials (Basel)*. 13 (2020) 1–14. <https://doi.org/10.3390/ma13245732>.
- [64] M. GAMS, A. KWIECIEN, J. KORELC, T. ROUSAKIS, A. VISKOVIĆ, Modelling of Deformable Polymer to be Used for Joints between Infill Masonry Walls and R.C. Frames, *Procedia Eng.* 193 (2017) 455–461. <https://doi.org/10.1016/j.proeng.2017.06.237>.
- [65] A. KWIECIEN, P. KRAJEWSKI, Ł. HOJDYS, M. TEKIELI, M. SŁOŃSKI, Flexible adhesive in composite-to-brick strengthening-experimental and numerical study, *Polymers (Basel)*. 10 (2018) 356. <https://doi.org/10.3390/polym10040356>.
- [66] A.T. AKYILDIZ, A. KOWALSKA-KOCZWARA, A. KWIECIEN, Stress distribution in masonry infills connected with stiff and flexible interface, *J. Meas. Eng.* 7 (2019) 40–46. <https://doi.org/10.21595/jme.2019.20449>.

- [67] P. SZEPTYŃSKI, Comparison and experimental verification of simplified one-dimensional linear elastic models of multilayer sandwich beams, *Compos. Struct.* 241 (2020) 112088. <https://doi.org/10.1016/j.compstruct.2020.112088>.
- [68] M.D. BANEJA, L.F.M. DA SILVA, Mechanical Characterization of Flexible Adhesives, *J. Adhes.* 85 (2009) 261–285. <https://doi.org/10.1080/00218460902881808>.
- [69] M.D. BANEJA, L.F.M. DA SILVA, R.D.S.G. CAMPILHO, The effect of adhesive thickness on the mechanical behavior of a structural polyurethane adhesive, *J. Adhes.* 91 (2015) 331–346. <https://doi.org/10.1080/00218464.2014.903802>.
- [70] K. HASEGAWA, A.D. CROCOMBE, F. COPPUCK, D. JEWEL, S. MAHER, Characterising bonded joints with a thick and flexible adhesive layer-Part 1: Fracture testing and behaviour, *Int. J. Adhes. Adhes.* 63 (2015) 124–131. <https://doi.org/10.1016/j.ijadhadh.2015.09.003>.
- [71] A.T. AKYILDIZ, A. KWIECIEŃ, B. ZAJĄC, P. TRILLER, U. BOHINC, T. ROUSAKIS, A. VISKOVIĆ, Preliminary in-plane shear test of infills protected by PUFJ interfaces. // Brick and block masonry - From historical to sustainable masonry, in: K. Jan, K. Arkadiusz, Ł. Bednarz (Eds.), *Proc. 17th Int. Brick/Block Mason. Conf. (17thIB2MaC 2020)*, Taylor & Francis Group, Kraków, Poland, 2020: pp. 968–975.
- [72] N. LASOWICZ, A. KWIECIEŃ, R. JANKOWSKI, Experimental study on the effectiveness of polyurethane flexible adhesive in reduction of structural vibrations, *Polymers (Basel)*. 12 (2020) 1–21. <https://doi.org/10.3390/polym12102364>.
- [73] M. POPOVSKI, E. KARACABEYLI, Seismic behaviour of cross-laminated timber structures, in: *15th World Conf. Timber Eng. WCTE*, Lisbona, 2012.
- [74] I. GAVRIC, M. FRAGIACOMO, M. POPOVSKI, A. CECCOTTI, Behaviour of Cross-Laminated Timber Panels under Cyclic Loads, in: S. Aicher, H.-W. Reinhardt, H. Garrecht (Eds.), *Mater. Joints Timber Struct.*, Springer Netherlands, Dordrecht, 2014: pp. 689–702.
- [75] B. STEFANOWSKI, M. SPEAR, P. ANDREW, REVIEW OF THE USE OF PF AND RELATED RESINS FOR MODIFICATION OF SOLID WOOD, in: *Conf. Timber 2018*, 2018.
- [76] A. AHMED, SHEIKH, S. ADAMOPOULOS, Acoustic properties of modified wood under different humid conditions and their relevance for musical instruments, *Appl. Acoust.* 140 (2018) 92–99. <https://doi.org/10.1016/j.apacoust.2018.05.017>.
- [77] T. FRANKE, M. AXEL, C. LENZ, H. NADINE, A. PFRIEM, Microscopic and macroscopic swelling and dimensional stability of beech wood impregnated with phenol-formaldehyde, *PRO LIGNO*. 13 (2017) 373–378.

- [78] P. GASCON-GARRIDO, H. MILITZ, C. MAI, M.-F. THÉVENON, Enhanced Termite Resistance of Scots Pine (*Pinus Sylyvestris* L.) Solid Wood by Phenol - Formaldehyde Treatment, *Wood Res. 60* (2015) 873–880.
- [79] B.C. KIELMANN, K. BUTTER, C. MAI, Modification of wood with formulations of phenolic resin and iron-tannin-complexes to improve material properties and expand colour variety, *Eur. J. Wood Wood Prod.* 76 (2018) 259–267. <https://doi.org/10.1007/s00107-017-1180-0>.
- [80] A. KLÜPPEL, S.M. CRAGG, H. MILITZ, C. MAI, Resistance of modified wood to marine borers, *Int. Biodeterior. Biodegrad.* 104 (2015) 8–14. <https://doi.org/10.1016/j.ibiod.2015.05.013>.
- [81] A. KLÜPPEL, Hardness and indentation modulus of resin-treated wood, *Int. Wood Prod. J.* 8 (2017) 41–44. <https://doi.org/10.1080/20426445.2016.1268358>.
- [82] Y. XIE, Q. FU, Q. WANG, Z. XIAO, H. MILITZ, Effects of chemical modification on the mechanical properties of wood, *Eur. J. Wood Wood Prod.* 71 (2013) 401–416. <https://doi.org/10.1007/s00107-013-0693-4>.
- [83] M. DEKA, C.N. SAIKIA, Chemical modification of wood with thermosetting resin : effect on dimensional stability and strength property, *Evaluation.* 73 (2000) 179–181.
- [84] Y. HUANG, B. FEI, Y. YU, R. ZHAO, Effect of modification with phenol formaldehyde resin on the mechanical properties of wood from Chinese fir, *BioResources.* 8 (2013) 272–282.
- [85] S. BICKE, C. MAI, H. MILITZ, Modification of beech veneers with low molecular weight phenol formaldehyde for the production of plywood: Durability and mechanical properties, in: *Proc. Eur. Conf. Wood Modif.*, Ljubljana, Slovenia, 2012: pp. 363–366.
- [86] M. FLECKENSTEIN, V. BIZIKS, C. MAI, H. MILITZ, Modification of beech veneers with lignin phenol formaldehyde resins in the production of laminated veneer lumber (LVL), *Eur. J. Wood Wood Prod.* 76 (2018) 843–851. <https://doi.org/10.1007/s00107-017-1275-7>.
- [87] P.D. EVANS, S. KRAUSHAAR GIBSON, I. CULLIS, C. LIU, G. SÈBE, Photostabilization of wood using low molecular weight phenol formaldehyde resin and hindered amine light stabilizer, *Polym. Degrad. Stab.* 98 (2013) 158–168. <https://doi.org/10.1016/j.polymdegradstab.2012.10.015>.
- [88] S. BOLLMUS, C. BEERETZ, H. MILITZ, Tensile and impact bending properties of chemically modified scots pine, *Forests.* 11 (2020). <https://doi.org/10.3390/f11010084>.
- [89] B.C. KIELMANN, H. MILITZ, C. MAI, S. ADAMOPOULOS, Strength Changes in Ash, Beech and Maple Wood Modified With a N-Methylol Melamine Compound and a Metal-Complex Dye, *Wood Res.* 58 (2013) 343–350.

- [90] H. EPMEIER, M. WESTIN, A. RAPP, Differently modified wood: Comparison of some selected properties, *Scand. J. For. Res.* 19 (2004) 31–37. <https://doi.org/10.1080/02827580410017825>.
- [91] R. HOSSEINPOURPIA, S. ADAMOPOULOS, C. MAI, Dynamic vapour sorption of wood and holocellulose modified with thermosetting resins, *Wood Sci. Technol.* 50 (2016) 165–178. <https://doi.org/10.1007/s00226-015-0765-1>.
- [92] C. MAI, T. ELDER, *Wood: Chemically Modified*, 2016. <https://doi.org/10.1016/B978-0-12-803581-8.03537-2>.
- [93] J. SCHIJVE, FATIGUE PROPERTIES BT - Fatigue of Structures and Materials, in: J. Schijve (Ed.), *Fatigue Struct. Mater.*, Springer Netherlands, Dordrecht, 2009: pp. 141–169. https://doi.org/10.1007/978-1-4020-6808-9_6.
- [94] K.T. TSAI, M.P. ANSELL, The fatigue properties of wood in flexure, *J. Mater. Sci.* 25 (1990) 865–878.
- [95] M. GONG, I. SMITH, Effect of waveform and loading sequence on low-cycle compressive fatigue life of spruce, *J. Mater. Civ. Eng.* 15 (2003) 93–99. <https://doi.org/10.1061/ASCE0899-1561200315:193>.
- [96] T. SUGIMOTO, Y. SASAKI, M. YAMASAKI, Fatigue of structural plywood under cyclic shear through thickness II: A new method for fatigue life prediction, *J. Wood Sci.* 53 (2007) 303–308. <https://doi.org/10.1007/s10086-006-0865-5>.
- [97] Y. SASAKI, A. OYA, M. YAMASAKI, Energetic investigation of the fatigue of wood, *Holzforschung.* 68 (2014) 843–848. <https://doi.org/10.1515/hf-2013-0147>.
- [98] T. SUGIMOTO, Y. SASAKI, Fatigue of structural plywood under cyclic shear through thickness III: Energy dissipation performance, *J. Wood Sci.* 54 (2008) 169–173. <https://doi.org/10.1007/s10086-007-0929-1>.
- [99] M.N. YILDIRIM, B. UYSAL, A. OZCIFCI, A.H. ERTAS, Determination of fatigue and static strength of scots pine and beech wood, *Wood Res.* 60 (2015) 679–685.
- [100] A.. SEKHAR, N.. SHUKLA, Some studies on the influence of specific gravity on fatigue strength of Indian timbers, *J. Indian Acad. Wood Sci.* 10 (1979) 1–5.
- [101] J. RATNASINGAM, N. MUTTHIAH, Fatigue life of oil palm wood (OPW) for furniture applications, *Eur. J. Wood Wood Prod.* 75 (2017) 473–476. <https://doi.org/10.1007/s00107-016-1109-z>.
- [102] E. SHARAPOV, K.C. MAHNERT, H. MILITZ, Residual strength of thermally modified Scots pine after fatigue testing in flexure, *Eur. J. Wood Wood Prod.* 74 (2016) 875–884. <https://doi.org/10.1007/s00107-016-1082-6>.
- [103] 302-1 BS EN, Adhesives for load-bearing timber structures - Test methods, (2013).
- [104] 422 NT BUILD, *Wood: Fracture energy in tension perpendicular to the grain.*

- Nordtest Method, 11 (1993).
- [105] N. DOURADO, M.F.S.F. DE MOURA, J. MORAIS, A numerical study on the SEN-TPB test applied to mode I wood fracture characterization, *Int. J. Solids Struct.* 48 (2011) 234–242. <https://doi.org/10.1016/j.ijsolstr.2010.09.020>.
- [106] H. YOSHIHARA, Influence of span/depth ratio on the measurement of mode II fracture toughness of wood by end-notched flexure test, *J. Wood Sci.* 47 (2001) 8–12. <https://doi.org/10.1007/BF00776638>.
- [107] R.M.R.P. FERNANDES, J.A.G. CHOUSAL, M.F.S.F. DE MOURA, J. XAVIER, Determination of cohesive laws of composite bonded joints under mode II loading, *Compos. Part B Eng.* 52 (2013) 269–274. <https://doi.org/10.1016/j.compositesb.2013.04.007>.
- [108] BS EN 12512 Timber structures - Test methods - Cyclic testing of joints made with mechanical fasteners, (2001) 1–18.
- [109] ISO 16670 Timber structures — Joints made with mechanical fasteners — Quasi-static reversed-cyclic test method, (2003) 1–9.
- [110] DIN 52186 - Testing of wood; bending test, Inst. Stand. Berlin, Ger. (1978).
- [111] DIN 52189-1 - Testing of wood; determination of impact bending strength., Inst. Stand. Berlin, Ger. (1981).

Povzetek v slovenskem jeziku

5.1 Uvod

Danes z uporabo lesa ustvarjamo sodobne gradbene trende pri gradnji večnadstropnih lesenih stavb. Les ima kot gradbeni material številne pozitivne lastnosti, med drugim dobro razmerje med trdnostjo in maso, dobre toplotne in izolativne lastnosti, hkrati pa njegova relativno nizka masa zagotavlja dobre protipotresne lastnosti. Les je trajnosten material z majhnim okoljskim odtisom, njegov ogljični odtis pa je celo negativen. Tehnologija njegove obdelave in gradbena tehnologija sta vse naprednejši, zato les postaja kot gradbeni material vse bolj zaželena alternativa betonu in jeklu [1].

Zaradi naravnih omejitev glede dimenzije žaganih lesenih elementov so se v začetku 19. stoletja pojavili prvi leseni lepljeni gradbeni elementi, za njihovo pripravo pa so uporabljali naravna lepila. Ta so po drugi svetovni vojni zamenjala sintetična lepila, ki so odpornejša na vodo in vlago, so enostavnejša za uporabo in ekonomsko dostopnejša [2]. Danes je že več kot 65 odstotkov lesenih izdelkov lepljenih [5]. Razvoj konstrukcijskega kompozitnega lesa (KKL), kot so na primer lameliran lepljen les (GLT), lameliran furnirni les (LVL), križno lameliran les (CLT) in drugi, skupaj z večjo ozaveščenostjo trajnostni gradnji z uporabo obnovljivih materialov sta, še posebej v gradnji visokih in večnadstropnih lesenih stavb, v zadnjih desetletjih pripeljala do povečanega zanimanja za njihovo rabo [3]. V primerjavi z masivnim lesom ima KKL boljše mehanske lastnosti, lahko ga izdelujemo v različnih dimenzijah in iz drevesnih debel manjših premerov, njegove lastnosti pa se odražajo tudi v večji dimenzijski stabilnosti [1,3,4].

Lepljenje je tehnika spajanja materialov s tvorjenjem lepilnega spoja med dvema površinama – lepljencema [6]. Lepilo, ki tvori lepilni spoj, mora prenašati obremenitve med zlepljenimi elementi in presegati stopnjo koncentracije napetosti, ki jo spoj lahko prenese [7], za njegovo porušitev pa je odgovoren najšibkejši člen v lepilnem spoju [8]. Razumevanje porušitve lepilnega spoja vodi do postopnih izboljšav pri razvoju bolj učinkovitih lepil predvsem pa tudi poznavanje kako nastajajo in kako se razlikujejo same porušitve [5]. Za celovito obravnavo tematike je potrebno poznavanje značilnosti tako lepil kot tudi lepilnih sistemov v povezavi z lesom ter njunih združenih lastnosti.

Šibek lepilni spoj vodi do razslojevanja in posledično krajše življenjske dobe lepljenih elementov. Eden od načinov proučevanja trdnosti lepilnega spoja je z določevanjem njegovih lomnih lastnosti. Širjenje loma ob preseženi napetosti, kateri sledi napredovanje

razpoke, vodi do njegove mehanske porušitve. Z določevanjem sproščanja kritične energije loma lahko izdelamo numerične modele kohezivnih con, ki temeljijo na napetostno-deformacijski spremembi kohezijskih površin [38]. Numerično izdelani modeli so uporabno orodje pri numeričnih simulacijah, s katerimi lahko analiziramo lepilne spoje. Tovrstne informacije so uporabne pri oblikovanju in optimizaciji kompozitnih elementov ter njihovih spojev. Hkrati literatura poudarja pomanjkljivosti informacij, pridobljenih s trenutnimi standardiziranimi testi z uporabo strižnih testov, saj je rezultat trdnosti takšnega testiranja vprid bodisi trdnosti lesa ali trdnosti lepilnega spoja. Ne omogoča pa boljše presoje oz. analize katerekoli drugih karakteristik takšnega spoja, kot na primer lomnih lastnosti [31]. Lomne lastnosti različnih lepilnih sistemov pri lepljenju evropske bukovine še niso podrobneje raziskane. Izsledki teh analiz so pomembni, še posebej zato, ker zaradi klimatskih sprememb v osrednji Evropi bukovina postaja vse pomembnejši surovinski vir, saj se bukev vedno bolj uveljavlja na rastiščih, kjer sedaj dominira smreka.

V sedanji praksi lepljenja lesa so lepilni spoji praviloma tanki in pogosto togi. Taki spoji ne omogočajo velikih deformacij, saj previsoke napetosti vodijo do hipnih porušitev. Pri oblikovanju lesenih zgradb imajo mehanski spoji ključno vlogo pri zagotavljanju trdnosti konstrukcijskih elementov, hkrati pa njihova duktilnost skrbi, da zagotovijo ustrezno količino disipacije energije v primeru potresa [16]. Podobne učinke lahko dosežemo z deformabilnimi, fleksibilnimi lepili, ki so bili v preteklosti že predmet proučevanja, predvsem pri obnovi lesenih spojev v kulturni dediščini, ojačitvah nosilcev les-steklo in stenski elementi iz lesa in stekla [19-21]. Zagotavljanje disipacije energije pri potresu z uporabo debeloslojnih fleksibilnih lepilnih spojev v lesenih konstrukcijah še ni bilo obširno proučevano, zato takšne študije prinašajo izvirne rezultate s tega področja.

Pri lepljenju lesa je lepilni spoj bistvenega pomena za prerazporejanje napetosti, vendar imajo lepilne smole poleg tega še številna druga področja uporabe. Intenzivno jih proučujemo kot kemikalije za modifikacijo lesa z impregnacijo, z namenom doseganja izboljšanih lastnosti lesa na več področjih. S postopki modifikacije lesu lahko izboljšamo življenjsko dobo, dimenzijsko stabilnost ter določene mehanske lastnosti [26,27]. Uveljavljen postopek modifikacije lesa je kemična modifikacija z uporabo duromernih smol monomerov in oligomerov z nizko molekulsko maso. Splošni mehanizem impregnacije lesa s tovrstnimi smolami je, da molekule vstopijo v strukturo lesa (celično steno) in v njej polimerizirajo. To povzroči povečanje prostornine celične stene in spremenjene higroskopske lastnosti celične stene [26]. Ena izmed dobro uveljavljenih smol za doseganje tovrstnih učinkov je fenol formaldehidna (FF) smola, ki je v lesni industriji uveljavljena že več kot 50 let in se uporablja kot lepilo za izdelavo inženirskih lesnih produktov. Impreg in Compreg sta bila med prvimi komercialno dostopnimi izdelki, pri katerih so bile lesene furnirske plošče impregnirane s FF smolami, in stisnjene z zamreženim polimerom v kompozitne plošče (Impreg) ali dodatno stisnjene pod visokim tlakom za doseganje povečane gostote (Compreg). Takšni materiali zagotavljajo boljše dimenzijske lastnosti npr. dimenzijsko stabilnost [75]. Številne študije poročajo o

pozitivnih učinkih tovrstne modifikacije na izbrane mehanske lastnosti [83-86]. Na drugi strani je znano, da impregnacija lesa z izbranimi impregnacijskimi sredstvi (vključno s FF smolami) lahko tudi negativno vpliva na mehanske lastnosti, saj se dinamične lastnosti pri analizi udarne žilavost drastično poslabšajo [85,87,88,89]. Alkalne komponente v fenolnih smolah lahko vodijo do sprememb v celičnih stenah lesa, kar pripomore k zmanjšanju njihovih elastičnih lastnosti [29]. To vodi do reoloških sprememb lesa, zato tega pojava ne smemo zanemariti. Raziskav o vplivu modifikacije lesa s FF smolami na dinamične mehanske lastnosti t.j. udarna žilavost, in utrujanje so redke, zato je ključno dobro poznavanje njenih učinkov predvsem z vidika uporabnosti tako modificiranih elementov v konstrukcijske namene.

V okviru doktorske disertacije smo proučili nekatere vrzeli v znanju o lepilnih spojih na področju lepljenja konstrukcijskih materialov. V ta namen smo izvedli dve študiji, kjer smo ocenili lomne lastnosti lepilne spojev pri lepljenju evropske bukovine z uporabo izbranih konstrukcijskih lepil. Debele lepilne spoje, izdelane s fleksibilnimi lepili, smo proučili z vidika uporabnosti takšnih spojev pri cikličnih obremenitvah, da bi ugotovili, ali kot konstrukcijski vezni člen omogočajo disipacije energij (npr. ob potresu). Za oceno učinka modifikacije lesa s fenol formaldehidnimi lepilnimi smolami na dinamične mehanske lastnosti lesa, smo za konec v študiji proučevali še učinke utrujanja takšnega lesa.

5.2 Raziskovalni nameni, cilji in hipoteze

Splošni raziskovalni cilj tega dela je opisati interakcije med lesom in lepilom, ki so pomembne za poznavanje njihove uporabe pri lesenih gradbenih elementih. Za raziskovalno delo smo opredelili naslednja raziskovalna vprašanja:

1. Kako se lomne lastnosti razlikujejo glede na vrsto uporabljenega lepila?
2. Ali se lahko fleksibilna lepila uporabljajo kot alternativa mehanskim veznim spojem v leseni gradnji?
3. Kako modifikacija lesa z lepilnimi smolami vpliva na lastnosti dinamične trdnosti?

Na podlagi podanih raziskovalnih vprašanj smo doktorsko nalogo razdelil na tri dele, ki smo jih obravnavali v štirih študijah.

V člankih 1 in 2 opisujemo lomne lastnosti izbranih lepil pri lepljenju evropske bukovine. Študiji proučujeta dva testna načina; Nateg (način I) in strig v ravnini (način II). Glavni raziskovalni cilji v članku 1 so bili: (i) preveriti verodostojnost preizkuševalne metode, in oceniti (ii) vpliv lepilnega sistema (iii), vpliv povišane temperature in (iv) usmerjenosti lesnih vlaken na lomne lastnosti lepilnih spojev. V članku 2 dalje opisujemo lomne lastnosti lepilnega spoja pri spajanju bukovega lesa v načinu II z namenom doseganjem

naslednji ciljev: (i) ocena ustreznosti izbrane metode glede na lepilni sistem in tip testiranja (ii) priprava kohezijskih modelov za izbrana lepila na podlagi vhodnih eksperimentalnih podatkov in njihovi analiz, (iii) opis lomnih lastnosti lepil in (iv) ocena vpliva trenja in vpliva usmerjenosti lesnih vlaken na točnost eksperimentalnih metod z uporabo numeričnih metod končnih elementov. V članku 3 smo se osredotočili na primernost uporabe debelega fleksibilnega lepilnega spoja za absorpcijo in disipacijo energije, kot alternativni način spajanja s klasičnimi kovinskimi spoji v lesni gradnji. Glavni cilji te študije so oceniti vpliv (i) lastnosti lepila in (ii) debeline lepilnega spoja ter (iii) primerjava lepilnih spojev z mehanskimi veznimi elementi. V zadnji eksperimentalni študiji (članek 4) obravnavamo dinamično trdnost modificiranega lesa z lepilno smolo s poudarkom na naslednjih ciljih: (i) modifikacija lesa s polimeri z nizko molekularno maso, (ii) ugotoviti vpliv modifikacije na statično upogibno trdnost, udarno upogibno trdnost in (iii) trdnost pri cikličnem utrujanju ter (iii) proučiti ciklično lezenje pri modificiranih in nemodificiranih vzorcih.

5.3 Materiali in metode

5.3.1 Članek 1

V članku 1 smo uporabili dve konstrukcijski lepili (poliuretansko – PUR in melamin-urea formaldehidno - MUF) ter ne-konstrukcijsko lepilo na osnovi emulzijskih polimerov in izocianatov (EPI), za lepljenje evropske bukovine z namenom proučevanja lomnih lastnosti lepilnih spojev v načinu I. V skladu s standardom EN 302-1 [103] smo pripravili vzorce za izvedbo strižnih testov s preklopom, da bi preverili ustreznost izbranih parametrov pri lepljenju glede na v standardu zahtevane mehanske strižne lastnosti lepilnih spojev. Za analize lomnih karakteristik spojev smo lamele evropske bukovine pred lepljenjem ustrezno razžagali, skobljali ter uravnovesili pri 20 °C in 65 % relativne zračne vlažnosti. Za namen proučevanja vpliva orientacije vlaken ter smeri spajanja lesa smo lamele in vzorce pripravili tako, da smo dobili vzorce z dvema ravninama lepilnega spoja z usmerjenostjo RT in TR, pri čemer prvi indeks označuje smer pravokotno na ravnino razpoke, drugi indeks pa smer širjenja razpoke. Indeksa R in T sta v angleškem jeziku indikatorja za radialno (R) in tangencialno (T) smer orientacije lesa. Pri lepljenju smo upoštevali izbrane parametre, kot smo jih uporabili pri pripravi vzorcev za strižne teste s preklopom. Iz zlepljenih lamel smo iz sredine razžagali manjše kocke, ki so bile oblikovane tako, da je bila polovica kocke zlepljena, druga polovica pa je predstavljala umetno ustvarjeno zarezo. Pri ter smo upoštevali geometrijo, kot je opredeljena v standardu NT BUILD 422 [104] za testiranje lomnih lastnosti lesa v načinu I. Preizkus je posnemal metodo enojne zareze s tritočkovnim upogibnim testom [35], ki smo ga izvedli na univerzalnem testirnem stroju. Da bi ocenili vpliv povišane temperature na lomne lastnosti, smo dve izbrani skupini vzorcev pred testiranjem uravnovesili pri temperaturah 70 °C in 140 °C. Podrobnejši opis priprave in uravnovešanja vzorcev je opisan v članku

1. Za izračun kritične vrednosti sproščanja lomne energije (G_I) in kritično energijo loma (G_c) je bil uporabljen postopek, ki so ga razvili Dourado in sod. [105]. Glede na majhno velikost vzorcev smo faktor k (uporabljen v analizi) iz predlagane študije prilagodili. Skupno lomno energijo (G_f) smo izračunali kot površino pod diagrami sile in pomika (F/δ). Za oceno vpliva temperature na modul elastičnosti bukovega lesa v vzdolžni in tlačni smeri smo opravili tudi tlačni preskus temperiranih vzorcev, katerega vrednosti smo uporabili pri izračunih (G_I). Na podlagi rezultatov smo izdelali linearni model, ki smo ga prilagodili logaritemsko transformirani funkciji z neodvisnimi spremenljivkami za G_f in G_c . Posamezen model je zajemal spremenljivke: lepila, orientacije in temperiranja. Analitični rezultati so predstavljeni kot srednje vrednosti s 95 % intervalom zaupanja, primerjave pa so izražene kot razmerja med srednjimi vrednostmi vsakega predstavljenega dejavnika. Tukeyjev test HSD smo uporabili za preverjanje razlik pri strižnih testih in tlačnih testih.

5.3.2 Članek 2

V drugem članku smo se osredotočili na eksperimentalno vrednotenje lomnih lastnosti treh konstrukcijskih lepil: PUR MUF in PRF (fenolno-resorcinol formaldehidno) ter nekonstrukcijskega lepila EPI v načinu II, obremenjenih s tritočkovnim upogibnim testom s končno čelno zarezo in z upoštevanjem Timoškove teorije nosilcev, ki velja do meje elastičnosti. Po meji elastičnosti smo z uporabo metode, ki temelji na modelu kompozitnih nosilcev z upoštevanjem povezanosti slojev (ang.: compliance-based beam method) in ekvivalentne dolžine razpoke, določili kohezijske zakone različnih lepljenih spojev na bukovini. Lamle evropske bukovine smo ploskovno zlepili ter geometrijo vzorcev pripravili v skladu z načinom, ki so ga opisali Yoshihara in sod, [106]. Končno čelno zarezo smo pripravili tako, da smo na površino lamel namestili teflonski trak, ki je preprečeval širjenja lepila skozi celotno površino lamel. Vse vzorce smo pred testiranjem uravnovesili pri 20 °C in 65 % relativne zračne vlažnosti. Za namen uporabe digitalne korelacije slike smo površine vzorcev prekrili s črno-belimi stohastičnim vzorcem. Tritočkovne upogibne preskuse smo izvedli na univerzalnem testirnem stroju, digitalno korelacijo slike pa smo uporabili za optično odčitavanje premikov opazovanih točk in izračun deformacij na površini vzorcev. Diagrame sile in pomika (F/δ) smo pridobili z univerzalnim testirnim strojem, ki je bil sinhroniziran z odčitavanjem optičnih meritev vzorcev. Premike (w) v neposredni bližini konice zareze smo uporabili za analizo napredovanja razpoke z njenim širjenjem tekom strižnega zdrsa. Hitrost sproščanja energije (G_{IIc}) smo izračunali v skladu z literaturo [36,107], ki podrobneje opisuje postopek sheme redukcije podatkov in krivulje G_{II-w} (širjenje razpoke). Eksperimentalne rezultate smo uporabili pri numerični analizi končnih elementov, pri katerih smo uporabili robne pogoje podobne eksperimentalnim testom. Kohezijski zakon smo izdelali kot bilinearno funkcijo. Pri numerični analizi smo kot karakteristike bukovine uporabili tri različne modele materiala. S predlaganim modelom končnih elementov smo opravili dve občutljivostni analizi, za oceno (i) vpliva koeficienta trenja

med lesenimi lamelami in (ii) vpliva usmeritev kota vlaken v vzdolžni smeri na obnašanje lepljenca. Parametri in eksperimentalni testi, skupaj z opisom izvedbe numeričnih simulacij, so predstavljenih v članku 2.

5.3.3 Članek 3

V okviru članka 3 smo uporabili protokole, predlagane v standardih EN 12512 in ISO 16670 [108,109], za preizkušanje mehanskih veznih elementov za lesene konstrukcije. Standarda predlagata uporabo cikličnih strižnih testov, s katerimi smo ocenjevali možnost uporabe fleksibilnih lepilnih spojev, kot veznih elementov. Uporabili smo tri PUR lepila z različnimi mehanskimi lastnostmi, ter dve debelini lepilnega spoja (10 in 15mm). Lepilne spoje smo naredili na smrekovini (*Picea abies* L.), vzorci pa so bili pripravljene za testiranje dvojnega strižnega spoja s preklopom. Pred testiranjem smo vzorce ustrezno uravnovesili v standardiziranih razmerah (20 °C in 65 % relativna zračna vlažnost). Eksperimentalne teste smo opravili na univerzalnem testirnem stroju. Sprva smo opravili statične strižne teste, na podlagi slednjih pa smo za posamezno skupino lepil ter določeno debelino spoja pripravili protokole povratnega cikličnega strižnega preizkusa. Na podlagi rezultatov monotoni testov in histereznih zank pri cikličnem obremenjevanju, smo le te analizirali skladno s predlaganimi standardiziranimi metodami za analizo; elastične in plastične togosti, strižnega modula, sile in pomika na meji tečenja, največje obremenitve ter pomika pri največji obremenitvi, največje strižne trdnosti, sile pri porušitvi, pomika pri porušitvi, maksimalne strižne deformacije ter duktilnosti. Za primerjavo rezultatov pridobljenih testov smo s pomočjo navedb iz literature [54] opravili analitično primerjavo med pogosto uporabljenimi mehanskimi spoji, ki so značilni za spajanje lesnih elementov. Upoštevali smo lepilne spoje, spoj z enim vijakom in spoj s serijo enako razporejenih vijakov. Poleg tega smo eksperimente modelirali z uporabo metode končnih elementov za numerične analize obnašanja vzorca ter z občutljivostno študijo preverili vpliv debeline lepilnega spoja s scenariji "kaj, če", ki eksperimentalno niso bili preizkušeni.

5.3.4 Članek 4

V zadnjem članku (članek 4) smo se osredotočili na vpliv modifikacije lesa z lepilnimi FF smolami na dinamične mehanske lastnosti lesa. Za testiranje smo izbrali les rdečega bora kot predstavnika iglavcev ter evropsko bukovino kot predstavnika listavcev. Za vsako lesno vrsto smo pripravili referenčno skupino nemodificiranega lesa, drugo skupino pa smo impregnirali z lepilno smolo FF z nizko molekulsko maso, da smo dosegli prepojenost celične stene lesa s tem sredstvom. Vse vzorce smo uravnovesili pri klimatskih razmerah 20 °C in 65 % relativne zračne vlažnosti. Vzorce, namenjene za modifikacijo, smo potopili v vodno raztopino FF in vzpostavili vakuum, da so se vzorci

navzeli raztopine. Po 30 min navzemanja smo vzorce pričeli sušiti pri sobni temperaturi in zračni vlažnosti, čemur je sledil počasen režim sušenja v sušilniku. V zadnji fazi smo temperaturo v sušilniku dvignili na 140 °C, s čimer smo opravili končno zamreženje monomerov v polimerno matriko v lesu. Do nadaljnjega testiranja smo vzorce hranili v pri omenjenih razmerah uravnovešanja. Za modificirane vzorce smo izračunali odstotek povečanja mase (*ang.* weight percentage gain), kot rezultat modifikacije. Učinkovitost modifikacije smo na prečnih prerezi izbranih vzorcev lesa preverili tudi z elektronskim vrstičnim mikroskopom. Sprva smo opravili statične tri-točkovne upogibne teste na univerzalnem testirnem stroju po standardni preskusni metodi DIN 52186 [110]. Za vse vzorce smo določili modul elastičnosti, določen delež vsake skupine vzorcev pa smo testirali do porušitve, da smo pridobili porušne trdnosti materiala. Na podlagi korelacije med modulom elastičnosti in porušne trdnosti materiala smo pripravili velikostne razrede obremenjevanja za posamezni material. Ciklične tritočkovne upogibne teste smo izvajali pri frekvenci obremenjevanja 10 Hz s sinusno obliko obremenitve. Velikostne razrede smo zmanjševali tako dolgo, da so vzorci dosegli mejo utrujanja s številom doseženih obremenitev 10^6 , kar smo za našo študijo določili kot mejo odpornosti na utrujanje. Rezultate smo prikazali na Wöhlerjevi krivulji oz. dinamični krivulji trdnosti, kot razmerje med obremenitvijo in številom doseženih ciklov obremenjevanja do porušitve oz. prekinitve testa. Na podlagi cikličnih diagramov smo ocenili tudi spremembo cikličnega elastičnega modula skozi interval utrujanja, ter učinek cikličnega utrujanja na lezenje materiala. Poleg tega smo opravili še Charpyjev udarni preizkus, kot je opredeljen v standardu DIN 52189 [111], za ugotavljanje vpliva modifikacije na udarno žilavost.

5.4 Rezultati in diskusija

5.4.1 Članek 1

V članku 1 smo obravnavali tri lepila pri lepljenju evropske bukovine, pri čemer smo eksperimentalno ocenili lomne lastnosti v načinu I, pri treh različnih temperaturah uravnovešanja vzorcev. Lepilni spoj lepila EPI je dosegel najvišje vrednosti G_c in G_f v standardnih kontrolnih razmerah, lomne lastnosti tega lepila pri povišanih temperaturnih pa so se, v primerjavi z ostalima dvema lepiloma, najbolj poslabšale. Prav pri tem lepilu so se pokazale najznačilnejše spremembe tudi pri analizi vpliva usmerjenosti lesnih vlaken, saj je bil ta vpliv manj očiten pri PUR in MUF lepilu. Izpostavitve vzorcev povišanim temperaturam je negativno vplivala na lomne lastnosti ne glede na usmerjenost lesnih vlaken ali lepilni sistem. V standardnih razmerah je EPI lepilo v smeri TR doseglo povprečni vrednosti G_c 0,80 N/mm in G_f 5.13 N/mm. Lomne lastnosti MUF lepilnih spojev s povprečno vrednostjo $G_c = 0,50$ N/mm in $G_f = 3.14$ N/mm pa so bile boljše od lepilnega spoja PUR s povprečnimi vrednostmi $G_c = 0,25$ N/mm oziroma $G_f = 1.39$ N/mm. Vrednosti so predstavljene za vzorce z usmeritvijo TR. Analitični rezultati, pridobljeni z linearnimi modeli, so se dobro ujemali z eksperimentalnimi rezultati, pri čemer je bil

koeficient korelacije (R^2) modela za $G_c = 0,62$ in R^2 modela za $G_f = 0,79$. Na podlagi modelov smo ugotovili, da odstopanja R^2 nakazujejo na napako, ki je nastala pri izbiri parametrov pri izračunu vrednosti G_c . Vrednosti za G_f se namreč bolje ujemajo z linearnim modelom, saj je pri tem modelu vrednost G_f izračunana neposredno iz eksperimentalnih meritev z uporabo diagramov sile in pomika. V splošnem smo s študijo pokazali, da je izbrana metoda preizkušanja z enojno zarezo s tritočkovnim upogibnim testom in z uporabo predlagane sheme za redukcijo podatkov iz obstoječe literature lahko uporabljena za tovrstne analize. Na tak način je možno ovrednotiti lomne lastnosti lepilnih spojev z možnostjo izbire želene usmerjenosti lesnih vlaken pri pripravi lepilnega spoja, s čimer lahko zmanjšamo vplive anomalij, ki se v lesu pojavljajo zaradi intrinzičnih lastnosti tega naravnega materiala. Pokazali smo tudi, kako pomemben je vpliv temperature na lomne značilnosti lepilnega spoja kot tudi usmerjenost lesnih vlaken pri lepljenju. Vzporedno s testiranjem lomnih lastnosti smo opravili tudi standardizirane strižne teste, pri čemer so trdnostne karakteristike različnih lepil zadostovale njihovim ocenam ustreznosti skladno z standardom EN 302-1. S tem smo želeli poudariti pomen zavedanja o zahtevah zaradi okoliščin, v katerih se nahajajo lepilni spoji, ter pomembnost dodane vrednosti testiranja na lomne lastnosti v primerjavi z obstoječimi standardizirani strižnimi preizkusi.

5.4.2 Članek 2

V članku 2 smo obravnavali uporabo tritočkovnega upogibnega testa s končno čelno zarezo v načinu II za namene določevanja lomnih lastnosti lepilnih spojev med izbranimi lepilnimi sistemi pri lepljenju bukovine. Eksperimentalne podatke meritev kritične vrednosti sproščanja lomne energije z metodo ekvivalentne dolžine zareze in podatke digitalne korelacije slike smo uporabili v numeričnih modelih končnih elementov. Izdelali smo kohezivne modele za testirana lepila in nadalje preverili vpliv trenja v strižni ravnini testiranja, ter vpliv usmeritve lesnih vlaken na togost materiala. Z rezultati te študije smo pokazali naslednje pomembne ugotovitve. Najvišjo srednjo vrednost kritične vrednosti sproščanja lomne energije (G_{lc}), 5,40 N/mm smo ugotovili pri testiranju PUR lepilnega spoja, čemur sledijo z 2,33 N/mm, 1,80 N/mm in 1,59 N/mm MUF, EPI in PRF lepilo. Vrednosti vseh rezultatov so bile višje od vrednosti G_{lc} za masiven bukov les (1,41 N/mm), kot ga navaja literatura. Razliko v strižni trdnosti in togost lepljenih elementov lahko pripišemo prav večji togosti in strižni trdnosti lepil v primerjavi z lesom, kar pa je lahko praktičen indikator, da lepilni spoj povečuje togost lepljenih elementov. Takšne ugotovitve nakazujejo, da je lepljenje bukovih elementov smiselno, saj pri tem ne poslabšujemo njihovih lomnih lastnosti. Pri MUF, EPI in PRF lepilnih spojih smo opazili krhke lome, ki so se v začetni fazi obremenjevanja obnašali enakomerno z začetnim napredovanjem razpoke in njenem nadaljnjem širjenju. To se je odražalo s stabilno stopnjo sproščanja vrednosti lomne energije po zdrsu premika konice razpoke v obliki njenega samovoljnega/prostega napredovanja. Te značilnosti nismo opazili pri bolj duktilnem poliuretanskem lepilu, ki smo ga tudi preizkušali v tej študiji. Pri slednjem

porušitev ni bila tako očitna, kar kaže na smiselnost izbire drugačne metode za preizkušanje ustreznosti bolj duktilnih lepila. V modelu končnih elementov smo uporabili tri različne lastnosti materialov, ki smo jih izrazili kot (i) ortotropen elastičen model, (ii) ortotropen elasto-plastični model z enako tlačno in natezno mejo plastičnosti in (iii) ortotropen elasto-plastičen model z različnima tlačno in natezno mejo plastičnosti. Ti numerični modeli so se dobro ujemali z eksperimentalnimi podatki, z manj kot 5 % relativne razlike med rezultati. S pomočjo numeričnih modelov smo pokazali, da je vpliv trenja med lamelami na upogibno togost vzorcev in najvišjo doseženo silo zanemarljivo majhen, ter da ima usmerjenost vlaken lesa večji vpliv na maksimalno doseženo silo, kot na samo togost testiranega vzorca. Na podlagi tega lahko zaključimo, da tudi za lomne značilnosti v načinu II velja, da ima največji pomen variabilnost posameznega lepilnega sistema ali način priprave vzorcev, kar izvira iz značilnosti lesa in lepila, ter od metode preskušanja.

5.4.3 Članek 3

V tretjem članku smo se osredotočili na eksperimentalno analizo debelih fleksibilnih lepilnih spojev z uporabo strižnega testa z dvojnim preklopom. Preizkusili smo tri različna lepila z različnimi mehanskimi lastnostmi (togost in raztezek do pretrga) z dvema različnima debelinama lepilnih spojev (10 in 15 mm), da bi ocenili možnost disipacije energije v primerjavi s klasičnimi mehanskimi spoji. Na podlagi statičnih strižnih testov smo posamezno skupino glede na lepilni sistem in debelino prilagodili cikličnim protokolom obremenjevanja. Za 10 mm debele lepilne spoje smo za izbrana PUR lepila z oznakami PST, PTS in PS, izmerili strižne trdnosti 1,74 Mpa, 1,71 Mpa in 1,48 Mpa. Izmrejene vrednosti pri testiranju spojev so bile nižje v primerjavi z podanimi karakteristikami posameznega tipa lepila. Slednje smo pripisali predvsem slabši oprijemljivosti med lepilom in površino lesa, za kar bi bilo potrebno površino bolj primerno pripraviti, bodi si mehansko ali z alternativnimi temeljnimi premazi (ang.: *primer*), da bi lahko celoma izkoristili potencial lepila. Razlika v povprečni trdnosti lepil v strigu med 15 mm in 10 mm debelimi spoji je bila pri lepilnem sistemu PS nižja za 32 % oz. 19 % za lepila PST in PTS. Statični strižni testi so pokazali, da se z večanjem debeline spojev elastična in plastična togost v povprečju zmanjšata za 25 %, ne glede na vrsto lepila. Numerične simulacije so se dobro ujemale z eksperimentalnimi podatki in potrdile, kako se z večanjem debeline lepilnega spoja zmanjšuje strižna napetost. Histerezne zanke iz cikličnih diagramov so pokazale na velik delež elastične deformacije, vendar nižjo sposobnost deformabilnosti. Ovrednotene rezultate cikličnih testov smo analitično primerjali s preklonimi spoji z uporabo vijakov, ki so bili testirani skladno z omenjenima standardoma. Na podlagi opravljenih testov in primerjav lahko zapišemo sledeče ugotovitve: (i) debelejša lepila so imela večjo elastično in plastično deformacijsko sposobnost, (ii) lepilni spoji so se v primerjavi z izbrano shemo vijačnih spojev izkazali z večjo togostjo in trdnostjo, (iii) zmogljivost ohranjanja trdnosti pri cikličnem obremenjevanju ob zaključenih treh ciklih (z upadom trdnosti manj kot 20 % med prvim

in tretjim ciklom obremenjevanja) je bila izpolnjena pri vseh pomikih do porušitve, (iv) visoka deformacijska zmogljivost, duktilnost in disipacija energije so bili v prid mehanskim vijačnim spojem. Ugotovili smo, da je lepilo s karakteristikami najmanjše togosti a največjim raztezkom do pretrga (PTS) ustvarilo najbolj učinkovit lepilni spoj z ugodnim razmerjem med togostjo in trdnostjo. S tem smo potrdili možnost uporabe debelih fleksibilnih lepil spojev za spajanje lesenih elementov za doseganje nizke zmogljivosti disipacije energije, medtem ko lahko preostale ugodne mehanske lastnosti zadovoljijo alternativnim uporabam, npr: spajanje jeklenih palic, preklopni spoji ali spoji z utorom, ali kombinacijo z drugimi gradbenimi elementi (okenski okvirji, jeklo, steklo), ki so bili kot taki ocenjeni v drugih študijah.

5.4.4 Članek 4

V zadnjem članku (Članek 4) smo obravnavali, kako modifikacija lesa z impregnacijo z lepilno smolo vpliva na dinamične mehanske lastnosti lesa. Da bi dosegli impregnacijo celične stene dveh komercialno pomembnih lesnih vrst, rdečega bora in evropske bukve, smo uporabili fenolformaldehidno smolo z nizko molekulsko maso. Klasičnemu postopku vakuumske impregnacije je sledilo sušenje in zamreževanje smole. Obe lesni vrsti, s tretirano in kontrolno skupino, smo testirali na upogibne lastnosti s statičnim tritočkovnim upogibnim testom, ki je za tretirano skupino vzorcev pokazal izboljšanje mehanskih lastnosti, saj smo izmerili 21 % (pri borovini) oziroma 29 % (pri bukovini) višji modul elastičnosti. Porušna trdnost je bila pri obeh vrstah, v primerjavi s kontrolnimi nemodificiranimi vzorci, višja za 18 %. Skladno s pridobljenimi vrednostmi smo za posamezno skupino prilagodili velikostne razrede obremenjevanja za ciklično tritočkovno upogibno utrujanje. Velikostne razrede smo prilagodili mejni pričakovani trdnosti materiala in jih postopoma zmanjševali, dokler nismo dosegli meje utrujanja pri 10^6 ciklih obremenitev. Modifikacija lesa s FF smolo je negativno vplivala na dinamično trdnost, pri čemer je bila meja odpornosti na utrujanje za kontrolni, netrenirani skupini 67 %, med tem ko se je ta vrednost za modificirani bor zmanjšala na 58 % in za modificirano bukev na 53 % glede na predvideno povprečno statično trdnost. Poleg tega smo ovrednotili tudi stopnjo spremembe cikličnega elastičnega modula pri modificiranih vzorcih, kot tudi učinek lezenja skozi celoten cikel obremenjevanja vzorcev. Ugotovili smo, da se pri modificiranem lesu ciklični elastični modul ni spreminjal, temveč ohranjal konstanto vrednost; sprememba med plastično in elastično deformacijo je ostajala nespremenjena. Pri modificiranih vzorcih smo tudi opazili, da se stopnja lezenja v sekundarni fazi prav tako ni spremenila. Študija je dodatno potrdila drastično zmanjšanje dinamične udarne žilavosti modificiranih vzorcev. Slednja se je v primerjavi s kontrolnimi skupinami za les bora zmanjšala za 60 %, 36 % zmanjšanje pa smo opazili pri bukovini. Glavni rezultati študije kažejo, da se dinamične mehanske lastnosti fenolformaldehidno modificiranega borovega in bukovega lesa razlikujejo od netretiranega materiala, saj kažejo zmanjšano zmožnost plastične deformacije. Zato tudi pri dinamičnem testiranju lesa nismo zaznali običajnih znakov utrujanja materiala.

Modificirani les se je po določenem številu ciklov obremenjevanja enostavno porušil. To je tudi ključno sporočilo te zadnje študije, s čimer želimo poudariti, kako pomembno je dobro, celovito poznavanje lastnosti materialov, še posebej kadar govorimo o rabi materialov za nosilne elemente.

5.5 Zaključek

V tej eksperimentalno usmerjeni doktorski disertaciji smo raziskovali in pokazali široko in pestro uporabo lepilnih sistemov v raznovrstnih scenarijih, kjer lepila uporabljamo v različnih razmerah in so izpostavljena raznolikim obremenitvam. Doktorska disertacija poudarja pomen uporabe različnih metod preskušanja lepil, ki jih uporabljamo v konstrukcijske namene. Na splošno ugotovitve študij, opisanih v tej disertaciji, poudarjajo vpliv variabilnosti materialov, kot so lepilni sistemi in izbrane vrste masivnega lesa, na obnašanje kompozitnih – lepljenih materialov, veznih elementov ali modificiranih lesenih elementov. Na treh področjih (članek 1,2,4) obravnavamo aplikacije lepljenja oz. uporabo lepilnih smol na lesu evropske bukve, ki postaja gospodarsko in okoljsko pomembna predstavnic listnatih vrst v srednji Evropi, in bi jo lahko v prihodnje vse pogosteje uporabljali v lesenih konstrukcijah. Z vidika lomne mehanike lepilnih spojev pri lepljenju evropske bukovine (članka 1 in 2) smo predstavili, da za izbrana lepila ki ustrezajo standardnim zahtevam za konstrukcijska lepila, dosegajo precej raznolike lomne lastnosti glede na določen lepilni sistem. Poleg tega smo poudarili, kako lahko različni pristopi k testiranju privedejo do širšega nabora informacij, ki podrobneje opisujejo razlike med lepilnimi sistemi ter preverili možnost izbranih testirnih pristopov za proučevanje lomnih lastnosti. Prav tako se je za pomembno izkazalo, da dejavnika povišane temperature tretiranja vzorcev ter vpliv usmerjenost lesnih vlaken pomembna vplivata na lomne lastnosti lepilnih spojev. V skladu z zahtevami Evrokoda 8 smo z mehanskimi testi ocenili in analizirali debele fleksibilne spoje, ki bi bili lahko neobičajna alternativa mehanskim spojem. Običajno je za doseganje kvalitetnega lepilnega spoja potrebno dosegati toge in proti lezenju odporne tanke lepilne spoje, vendar smo v članku 3 predstavili, kako je mogoče na inovativen način uporabiti prednosti debelejših plasti fleksibilnih lepil in z njihovo uporabo nadomestiti klasične mehanske vijajne spoje. Na tak način lahko pri konstrukcijskih elementih celo dosežemo zahteve potresne varnosti za nizko intenzivna seizmična območja. Kljub močni razširjenosti fenolnih smol v lepilih, ki jih uporabljajo v lesni industriji, te niso nujno namenjene le lepljenju, saj jih lahko uporabimo tudi za impregnacijo in kemično modifikacijo masivnega lesa. Taka modifikacija lahko povzroči neželene spremembe, zato smo v zadnji študiji kritično ocenili negativne vplive kemične modifikacije lesa na njegovo utrujanje. Na prvi pogled zanemarljive spremembe v razmerju elasto-plastičnih deformacij pomembno vplivajo na reološke lastnosti lesa saj na ta način močno spremenijo njegove značilnosti. Zato je ključno prepoznati in razumeti, kako je potrebno ravnati s takšnimi materiali, še posebej kadar govorimo o njihovi rabi v gradbene namene. Bodoče študije morajo podrobneje obravnavati opisana področja, saj

bomo na ta način dosegli širše in boljše poznavanje kompozitnih materialov, ne smemo pa zanemariti, da razmere, v katerih uporabljamo te kompozite, pomembno vplivajo na njihovo ustreznost. Nenazadnje smo s študijo pokazali, kako raznolika in pestra je raba lepil oz. lepilnih smol na področju znanosti o lesu ter kako lahko alternativni in inovativni pristopi dodatno širijo njihovo uporabno vrednost.

Appendix

The appendix contains the supplementary material published in the support of Article 1. The material is published in full, but the raw data is excluded from this appendix. The record is available online [112].

The G_f values represent the total work needed required for complete crack propagation (complete separation) and it is directly correlated with fracture energy by incorporating the area of the specimen residual cross-sections. The values reported for the G_f values are therefore higher by the magnitude of the cross-section area.

Reference:

[112] BURNARD, MICHAEL, PEČNIK, JAKA GAŠPER, Statistical analysis for: Mode I fracture of beech-adhesive bondline at three different temperatures, Data set. Zenodo (2022). <https://doi.org/10.5281/zenodo.7143370>.

Supplementary Table 1: Summary of the linear model of G_c . Base condition: Control, RT, EPI. Model call (R language): $\log(G_c) \sim \text{adhesive} + \text{treatment} + \text{orientation (plane)} + \text{adhesive:treatment} + \text{adhesive:orientation} + \text{treatment:orientation}$

Coefficient	estimate	standard error	t-statistic	p	Significance
(Intercept)	-0.1799	0.1351	-1.3312	0.1850	
adhesiveMUF	-0.5795	0.1769	-3.2753	0.0013	**
adhesivePUR	-1.3150	0.1779	-7.3912	0.0000	***
treatment70°C	-0.9297	0.1764	-5.2696	0.0000	***
treatment140°C	-1.2534	0.1798	-6.9729	0.0000	***
orientationRT	-0.7379	0.1627	-4.5352	0.0000	***
adhesiveMUF:treatment70°C	0.6903	0.2158	3.1983	0.0017	**
adhesivePUR:treatment70°C	0.8510	0.2173	3.9167	0.0001	***
adhesiveMUF:treatment140°C	0.2937	0.2211	1.3285	0.1859	
adhesivePUR:treatment140°C	0.9042	0.2275	3.9736	0.0001	***

adhesiveMUF:orientationRT	0.7167	0.1791	4.0021	0.0001	***
adhesivePUR:orientationRT	0.6021	0.1829	3.2920	0.0012	**
treatment70°C:orientationRT	-0.3300	0.1770	-1.8640	0.0642	
treatment140°C:orientationRT	-0.3096	0.1826	-1.6954	0.0920	

* Significant at $p < 0.05$, ** Significant at $p < 0.01$, *** Significant at $p < 0.001$

Residual standard error: 0.4826 on 158 degrees of freedom

Multiple R-squared: 0.6174, Adjusted R-squared: 0.5859

F-statistic: 19.61 on 13 and 158 DF, p-value: $< 2.2e-16$

Supplementary Table 2: Summary of the linear model of Gf. Base condition: Control, TR, EPI. Model call (R language): $\log(Gf) \sim \text{adhesive} + \text{treatment} + \text{orientation} + \text{adhesive:treatment} + \text{adhesive:orientation} + \text{treatment:orientation}$

Coefficient	estimate	standard error	t-statistic	p	Significance
(Intercept)	7.0608	0.0965	73.1593	0.0000	***
adhesiveMUF	-0.6781	0.1264	-5.3664	0.0000	***
adhesivePUR	-1.5437	0.1271	-12.1492	0.0000	***
treatment70°C	-1.1597	0.1260	-9.2046	0.0000	***
treatment140°C	-1.2104	0.1284	-9.4291	0.0000	***
orientationRT	-1.0357	0.1162	-8.9129	0.0000	***
adhesiveMUF:treatment70°C	1.0072	0.1541	6.5347	0.0000	***
adhesivePUR:treatment70°C	1.0271	0.1552	6.6190	0.0000	***
adhesiveMUF:treatment140°C	0.4227	0.1579	2.6777	0.0082	**
adhesivePUR:treatment140°C	1.1466	0.1625	7.0556	0.0000	***
adhesiveMUF:orientationRT	1.0532	0.1279	8.2356	0.0000	***
adhesivePUR:orientationRT	1.1113	0.1306	8.5079	0.0000	***
treatment70°C:orientationRT	-0.4114	0.1264	-3.2546	0.0014	**
treatment140°C:orientationRT	-0.3829	0.1304	-2.9365	0.0038	**

* Significant at $p < 0.05$, ** Significant at $p < 0.01$, *** Significant at $p < 0.001$

Residual standard error: 0.3447 on 158 degrees of freedom

Multiple R-squared: 0.7892, Adjusted R-squared: 0.7718

F-statistic: 45.5 on 13 and 158 DF, p-value: $< 2.2e-16$

Supplementary Table 3: Predicted median Gf and Gc for each factor combination with 95% CI.

Adhesive	Treatment temperature	Orientation	Gf (N/mm)			Gc (N/mm)		
			Median	95 % CI lower bound	95.% CI upper bound	Median	95 % CI lower bound	95.% CI upper bound
EPI	Control	TR	1165.04	963.03	1409.41	0.84	0.64	1.09
MUF	Control	TR	591.58	489.21	715.39	0.47	0.36	0.61
PUR	Control	TR	248.80	205.62	301.05	0.22	0.17	0.29
EPI	70°C	TR	365.50	302.10	442.21	0.33	0.25	0.43
MUF	70°C	TR	508.07	420.09	614.46	0.37	0.28	0.48
PUR	70°C	TR	218.00	178.77	265.84	0.21	0.16	0.27
EPI	140°C	TR	347.28	286.45	421.03	0.24	0.18	0.31
MUF	140°C	TR	269.16	222.36	325.81	0.18	0.14	0.23
PUR	140°C	TR	233.55	189.49	287.86	0.16	0.12	0.21
EPI	Control	RT	413.75	342.01	500.54	0.40	0.31	0.52
MUF	Control	RT	601.94	497.77	727.91	0.46	0.35	0.60
PUR	Control	RT	268.50	221.90	324.89	0.20	0.15	0.26
EPI	70°C	RT	85.99	71.08	104.04	0.11	0.09	0.15
MUF	70°C	RT	342.48	283.18	414.20	0.26	0.20	0.34
PUR	70°C	RT	155.86	128.76	188.67	0.13	0.10	0.17
EPI	140°C	RT	84.11	67.66	104.57	0.08	0.06	0.11
MUF	140°C	RT	186.79	154.31	226.10	0.13	0.10	0.17
PUR	140°C	RT	171.90	139.47	211.87	0.10	0.08	0.14

Supplementary Table 4:

Comparisons between median Gc and Gf plane orientation for control, 70 °C and 140 °C samples and each adhesive type; 95 % confidence intervals were adjusted using Tukey's method for a family of three comparisons.

			<i>Gc (95 % CI)</i>			<i>Gf (95 % CI)</i>		
Comparison	Temperature	Adhesive	Ratio	95 % CI lower bound	95.% CI upper bound	Ratio	95 % CI lower bound	95.% CI upper bound
TR/RT	Control	EPI	2.09	1.52	2.89	2.82	2.24	3.54
TR/RT	Control	MUF	1.02	0.74	1.41	0.98	0.78	1.23
TR/RT	Control	PUR	1.15	0.83	1.58	0.93	0.74	1.17
TR/RT	70 °C	EPI	2.91	2.11	4.01	4.25	3.38	5.35
TR/RT	70 °C	MUF	1.42	1.03	1.96	1.48	1.18	1.86
TR/RT	70 °C	PUR	1.59	1.15	2.21	1.4	1.11	1.77
TR/RT	140 °C	EPI	2.85	2.03	4.00	4.13	3.24	5.26
TR/RT	140 °C	MUF	1.39	1.01	1.92	1.44	1.14	1.82
TR/RT	140 °C	PUR	1.56	1.11	2.19	1.36	1.07	1.73

Comparisons between median G_c and G_f for each adhesive pair under control, , 70 °C and 140 °C conditions and both plane orientations; 95 % confidence intervals were adjusted using Tukey's method for a family of three comparisons.

Comparison	Temperature	Orientation	G_c (95 % CI)			G_f (95 % CI)		
			Ratio	95 % CI lower bound	95. % CI upper bound	Ratio	95 % CI lower bound	95. % CI upper bound
EPI / MUF	Control	TR	1.78	1.18	2.71	1.97	1.46	2.66
EPI / PUR	Control	TR	3.72	2.45	5.67	4.68	3.47	6.32
MUF / PUR	Control	TR	2.09	1.38	3.17	2.38	1.76	3.21
EPI / MUF	Control	RT	0.87	0.57	1.32	0.69	0.51	0.93
EPI / PUR	Control	RT	2.04	1.34	3.11	1.54	1.14	2.08
MUF / PUR	Control	RT	2.34	1.54	3.56	2.24	1.66	3.02
EPI / MUF	70 °C	TR	0.9	0.59	1.36	0.72	0.53	0.97
EPI / PUR	70 °C	TR	1.59	1.04	2.44	1.68	1.24	2.28
MU / PUR	70 °C	TR	1.78	1.16	2.72	2.33	1.72	3.16
EPI / MUF	70 °C	RT	0.44	0.29	0.66	0.25	0.19	0.34
EPI / PUR	70 °C	RT	0.87	0.57	1.33	0.55	0.41	0.75
MU / PUR	70 °C	RT	1.99	1.31	3.03	2.2	1.63	2.97
EPI / MUF	140 °C	TR	1.33	0.87	2.03	1.29	0.95	1.75
EPI / PUR	140 °C	TR	1.51	0.97	2.35	1.49	1.08	2.04
MU / PUR	140 °C	TR	1.13	0.73	1.76	1.15	0.84	1.58
EPI / MUF	140 °C	RT	0.65	0.42	1.01	0.45	0.33	0.62
EPI / PUR	140 °C	RT	0.83	0.52	1.31	0.49	0.35	0.68
MU / PUR	140 °C	RT	1.27	0.82	1.97	1.09	0.79	1.49

Statistical analysis for: Fracture characterization of beech-adhesive bondline in mode I at three different temperatures

Michael Burnard, InnoRenew CoE & University of Primorska [mike.burnard@innorenew.eu]
Jaka Gašper Pečnik, InnoRenew CoE & University of Primorska [jaka.pecnik@innorenew.eu]

2022-07-15

Contents

1	Introduction	1
2	Data import	1
3	Regression	3
3.1	Test distribution	3
3.2	Fit a regression model	5
4	Estimating performance	11
4.1	Predicted values	12
4.2	Effect sizes	14
4.3	Visualising effect sizes	16
5	Acknowledgements	17

1 Introduction

This document describes the data and analytical process of a study examining some aspects of mechanical performance of solid wood composites. We were interested in certain properties of solid wood composites made using different adhesives with different grain orientations at the bondline, then treated at different temperatures prior to testing.

Performance was tested by assessing fracture energy and critical fracture energy, lap shear strength, and compression strength of the composites. This document concerns only the fracture properties, which are the focus of the related paper.

Notes:

- the raw data is provided alongside this upload, but the processing is not addressed here.
- the authors of this document are a subset of the authors of the related paper.
- this document and the related data files were uploaded at the time of submission for review. An update providing the doi of the related paper will be provided when it is available.

2 Data import

We import a cleaned and processed dataset with the following variables:

1. treatment: the temperature the wood component was thermally treated at prior to layup. Categorical variable taking one of three values: control (no thermal treatment), 70C, 140C.
2. adhesive: the type of adhesive used in the composite component. Categorical variable taking one of three values: EPI (=Emulsion Polymer Isocyanate), MUF (=Melamine-urea-formaldehyde), PUR (=Polyurethane)
3. orientation: the grain orientation of the wood components in the composite. Categorical variable taking one of two values: T (=Tangential, RT), R (=Radial, TR)
4. id: a unique identifier. Numeric, sequential, applied entry into the dataset.
5. Gc: critical fracture energy. Continuous numeric value. One of the two modeled values.
6. Gf: fracture energy. Continuous numeric value. One of the two modeled values.

The treatment combinations result in 18 total combinations (3 x 3 x 2). 10 samples were prepared, but some failed prior to complete testing, resulting in 172 total observations for each Gc and Gf.

```
#import the data and add degree symbol to temps
#update factor order to follow the temperature increase
#Rename bondline orientation to provide clarity.
d.frac <- read_csv("Fracture_GcGf_v1.csv") |>
mutate(
  treatment =
    case_when(
      treatment == "control" ~ "Control",
      treatment == "70C" ~ "70°C",
      treatment == "140C" ~ "140°C"
    ),
  treatment = fct_relevel(factor(treatment), "Control", "70°C", "140°C"),
  orientation = if_else(orientation == "R", "TR", "RT")
)

## Rows: 172 Columns: 9
## -- Column specification -----
## Delimiter: ","
## chr (3): treatment, adhesive, orientation
## dbl (6): no., Gc, Et, CO, Fmax, Gf
##
## i Use `spec()` to retrieve the full column specification for this data.
## i Specify the column types or set `show_col_types = FALSE` to quiet this message.
# observations per treatment
d.frac |> group_by(treatment, adhesive, orientation) |>
  summarise(observations = n())

## `summarise()` has grouped output by 'treatment', 'adhesive'. You can override
## using the `.groups` argument.

## # A tibble: 18 x 4
## # Groups:   treatment, adhesive [9]
##   treatment adhesive orientation observations
##   <fct>      <chr>      <chr>          <int>
## 1 Control    EPI         RT              10
## 2 Control    EPI         TR              10
## 3 Control    MUF         RT              10
## 4 Control    MUF         TR              10
## 5 Control    PUR         RT              10
## 6 Control    PUR         TR              10
## 7 70°C      EPI         RT              10
## 8 70°C      EPI         TR              10
```

```
## 9 70°C MUF RT 10
## 10 70°C MUF TR 10
## 11 70°C PUR RT 10
## 12 70°C PUR TR 9
## 13 140°C EPI RT 7
## 14 140°C EPI TR 10
## 15 140°C MUF RT 10
## 16 140°C MUF TR 10
## 17 140°C PUR RT 8
## 18 140°C PUR TR 8
```

3 Regression

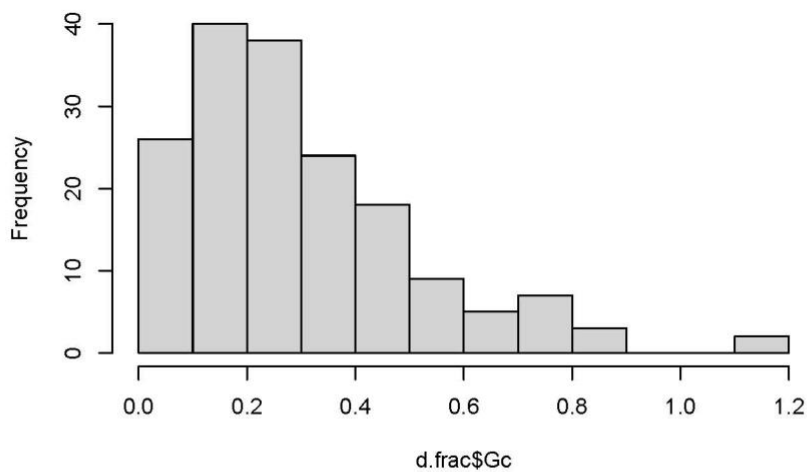
We will perform ordinary least square regression separately for G_c and G_f as independent variables. Due to skewed data, the independent variable in both models were log transformed.

3.1 Test distribution

A log transformation was necessary to meet the assumptions of a linear regression (model testing below.)

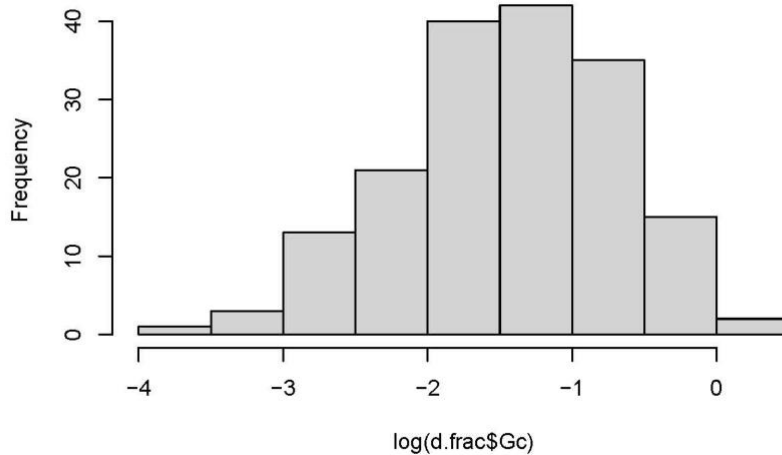
```
#Critical Fracture Energy
hist(d.frac$Gc)
```

Histogram of d.frac\$Gc



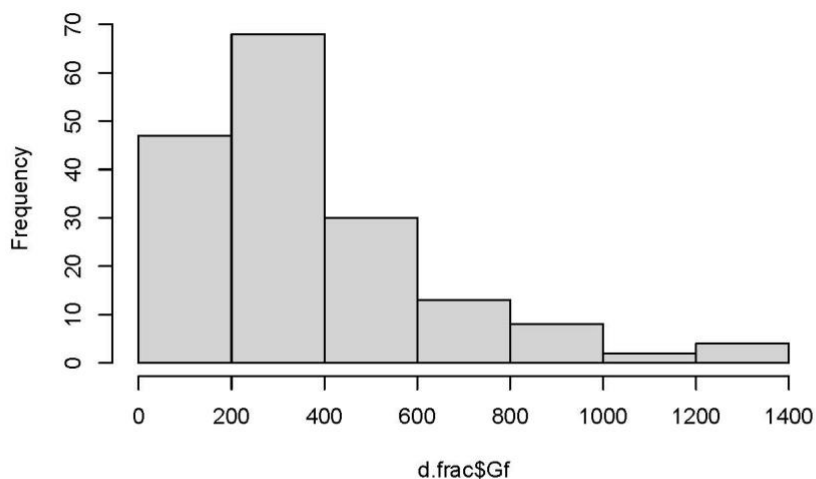
```
hist(log(d.frac$Gc))
```

Histogram of log(d.frac\$Gc)

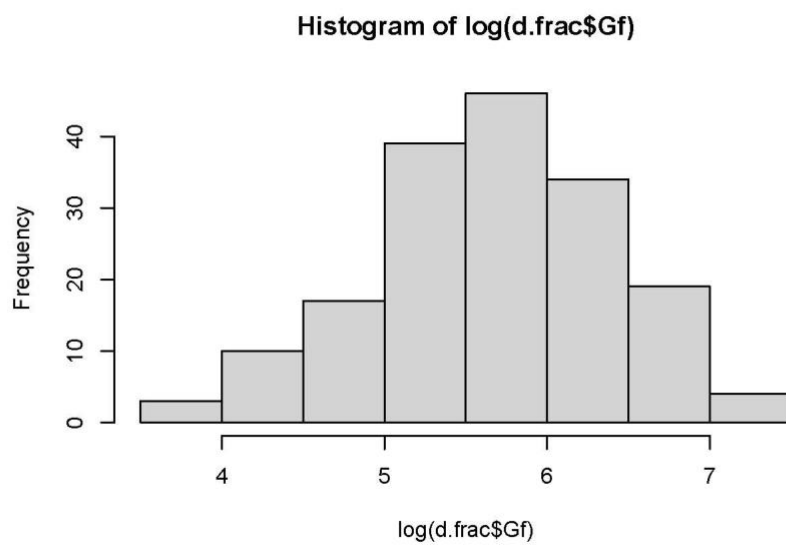


```
#Fracture energy
hist(d.frac$Gf)
```

Histogram of d.frac\$Gf



```
hist(log(d.frac$Gf))
```



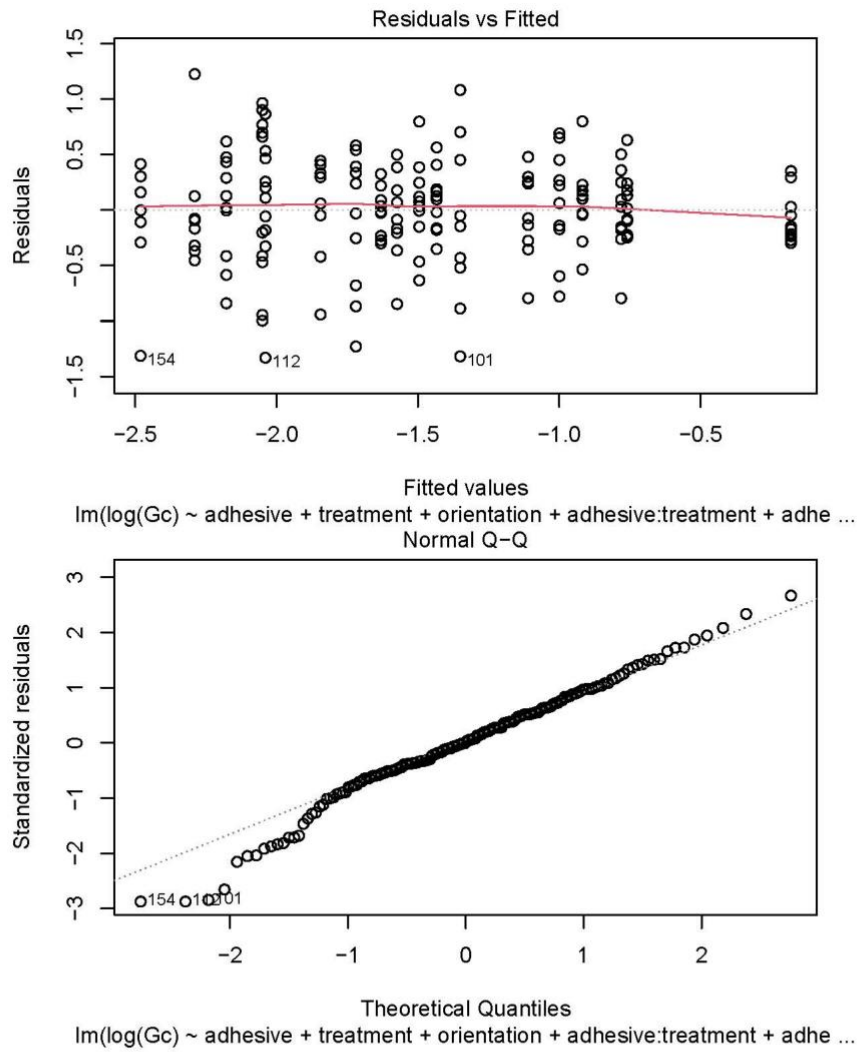
3.2 Fit a regression model

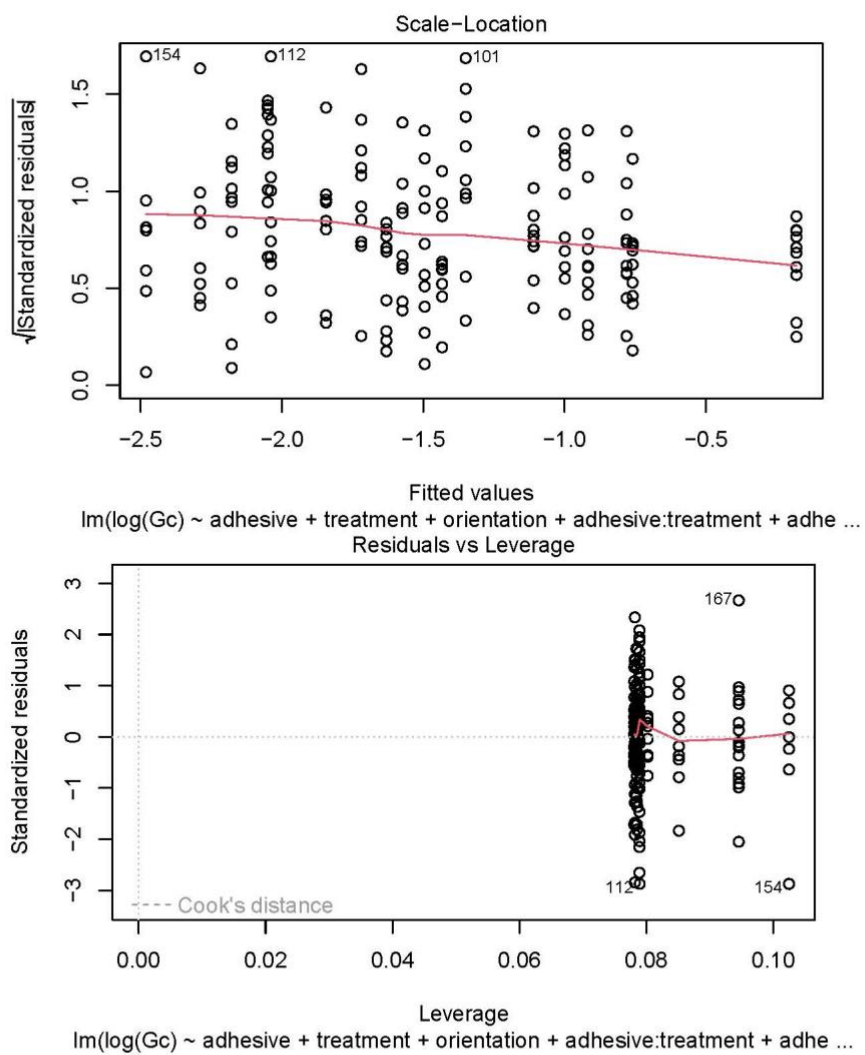
We fit two models for both independent variables: a non-interaction model and a model with all two-way interactions (no three-way interactions).

Model fit was assessed visually.

```
#fit a linear model
gc.lmr <- lm(log(Gc) ~ adhesive + treatment + orientation, data=d.frac)
gc.lm<- lm(log(Gc) ~ adhesive + treatment + orientation + adhesive:treatment +
            adhesive:orientation + treatment:orientation, data=d.frac)

#assess fit: sufficient.
plot(gc.lm)
```





```
#plot(gc.lmr)
# compare models
anova(gc.lmr, gc.lm) #choose the interaction model - gc.lm, as it explains more variation.
## Analysis of Variance Table
##
```

```

## Model 1: log(Gc) ~ adhesive + treatment + orientation
## Model 2: log(Gc) ~ adhesive + treatment + orientation + adhesive:treatment +
##   adhesive:orientation + treatment:orientation
##   Res.Df    RSS Df Sum of Sq    F Pr(>F)
## 1      166 47.994
## 2      158 36.800  8    11.194 6.0079 9.841e-07 ***
## ---
## Signif. codes:  0 '***' 0.001 '**' 0.01 '*' 0.05 '.' 0.1 ' ' 1

#view model output
summary(gc.lm)

##
## Call:
## lm(formula = log(Gc) ~ adhesive + treatment + orientation + adhesive:treatment +
##   adhesive:orientation + treatment:orientation, data = d.frac)
##
## Residuals:
##      Min       1Q   Median       3Q      Max
## -1.33037 -0.24023  0.00645  0.29467  1.22532
##
## Coefficients:
##              Estimate Std. Error t value Pr(>|t|)
## (Intercept)      -0.9178    0.1351  -6.791 2.13e-10 ***
## adhesiveMUF         0.1371    0.1769   0.775 0.439442
## adhesivePUR        -0.7129    0.1779  -4.007 9.45e-05 ***
## treatment70°C     -1.2596    0.1764  -7.140 3.21e-11 ***
## treatment140°C    -1.5630    0.1884  -8.294 4.50e-14 ***
## orientationTR       0.7379    0.1627   4.535 1.13e-05 ***
## adhesiveMUF:treatment70°C  0.6903    0.2158   3.198 0.001671 **
## adhesivePUR:treatment70°C  0.8510    0.2173   3.917 0.000133 ***
## adhesiveMUF:treatment140°C 0.2937    0.2211   1.329 0.185913
## adhesivePUR:treatment140°C 0.9042    0.2275   3.974 0.000107 ***
## adhesiveMUF:orientationTR -0.7167    0.1791  -4.002 9.63e-05 ***
## adhesivePUR:orientationTR -0.6021    0.1829  -3.292 0.001227 **
## treatment70°C:orientationTR 0.3300    0.1770   1.864 0.064174 .
## treatment140°C:orientationTR 0.3096    0.1826   1.695 0.091969 .
## ---
## Signif. codes:  0 '***' 0.001 '**' 0.01 '*' 0.05 '.' 0.1 ' ' 1
##
## Residual standard error: 0.4826 on 158 degrees of freedom
## Multiple R-squared:  0.6174, Adjusted R-squared:  0.5859
## F-statistic: 19.61 on 13 and 158 DF,  p-value: < 2.2e-16

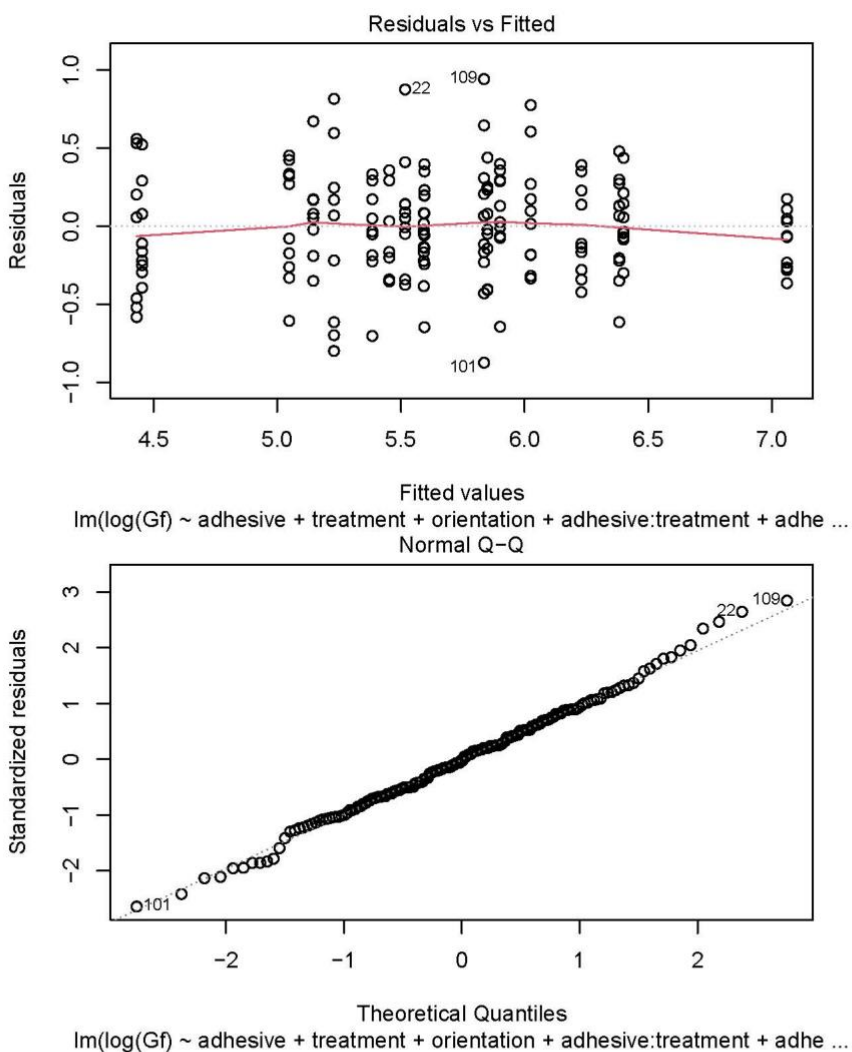
#save output for supplementary materials
gc.lm.out <- broom::tidy(summary(gc.lm))
write_csv(gc.lm.out, "gc_out.csv")

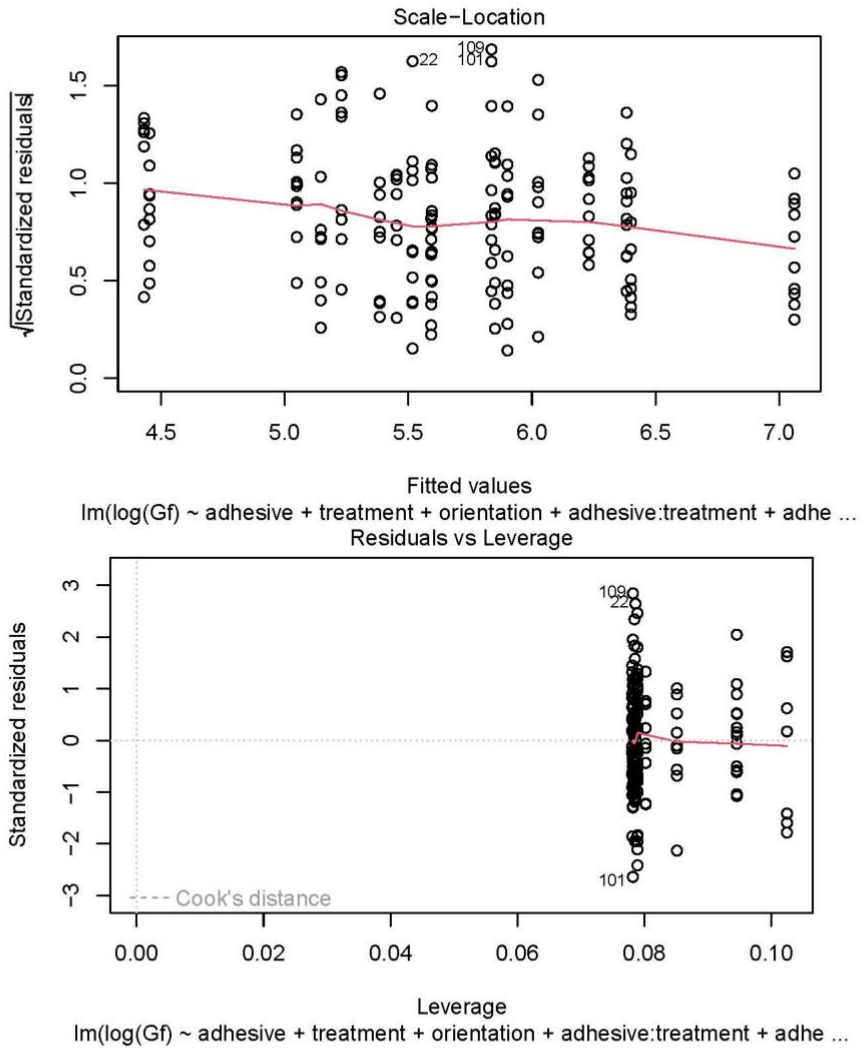
gf.lmr <- lm(log(Gf) ~ adhesive + treatment + orientation, data=d.frac)
gf.lm <- lm(log(Gf) ~ adhesive + treatment + orientation + adhesive:treatment +
  adhesive:orientation + treatment:orientation, data=d.frac)

#we can use the estimates to look at effect sizes

#assess fit
plot(gf.lm)

```





```
#plot(gf.lmr)

#compare models
anova(gf.lmr, gf.lm) #choose the interaction model - d.lm2

## Analysis of Variance Table
##
```

```

## Model 1: log(Gf) ~ adhesive + treatment + orientation
## Model 2: log(Gf) ~ adhesive + treatment + orientation + adhesive:treatment +
##   adhesive:orientation + treatment:orientation
##   Res.Df    RSS Df Sum of Sq    F    Pr(>F)
## 1      166 41.663
## 2      158 18.768  8    22.895 24.093 < 2.2e-16 ***
## ---
## Signif. codes:  0 '***' 0.001 '**' 0.01 '*' 0.05 '.' 0.1 ' ' 1

#view model output
summary(gf.lm)

##
## Call:
## lm(formula = log(Gf) ~ adhesive + treatment + orientation + adhesive:treatment +
##   adhesive:orientation + treatment:orientation, data = d.frac)
##
## Residuals:
##      Min       1Q   Median       3Q      Max
## -0.87355 -0.22033 -0.00726  0.21582  0.94126
##
## Coefficients:
##              Estimate Std. Error t value Pr(>|t|)
## (Intercept)      6.02519   0.09651  62.429 < 2e-16 ***
## adhesiveMUF       0.37513   0.12636   2.969 0.003457 **
## adhesivePUR      -0.43233   0.12706  -3.403 0.000846 ***
## treatment70°C    -1.57115   0.12599 -12.470 < 2e-16 ***
## treatment140°C  -1.59332   0.13457 -11.840 < 2e-16 ***
## orientationTR     1.03566   0.11620   8.913 1.15e-15 ***
## adhesiveMUF:treatment70°C  1.00723   0.15413   6.535 8.33e-10 ***
## adhesivePUR:treatment70°C  1.02710   0.15518   6.619 5.34e-10 ***
## adhesiveMUF:treatment140°C  0.42271   0.15787   2.678 0.008197 **
## adhesivePUR:treatment140°C  1.14655   0.16250   7.056 5.09e-11 ***
## adhesiveMUF:orientationTR -1.05325   0.12789  -8.236 6.35e-14 ***
## adhesivePUR:orientationTR -1.11134   0.13062  -8.508 1.28e-14 ***
## treatment70°C:orientationTR  0.41144   0.12642   3.255 0.001389 **
## treatment140°C:orientationTR  0.38290   0.13040   2.936 0.003816 **
## ---
## Signif. codes:  0 '***' 0.001 '**' 0.01 '*' 0.05 '.' 0.1 ' ' 1
##
## Residual standard error: 0.3447 on 158 degrees of freedom
## Multiple R-squared:  0.7892, Adjusted R-squared:  0.7718
## F-statistic: 45.5 on 13 and 158 DF, p-value: < 2.2e-16

#save output for supplementary materials
gf.lm.out <- broom::tidy(summary(gf.lm))
write_csv(gf.lm.out, "gf_out.csv")

```

4 Estimating performance

Our primary interest is not in the raw model output, but in predicting performance (in terms of G_c and G_f for different treatment combinations) then making comparisons between treatment conditions.

4.1 Predicted values

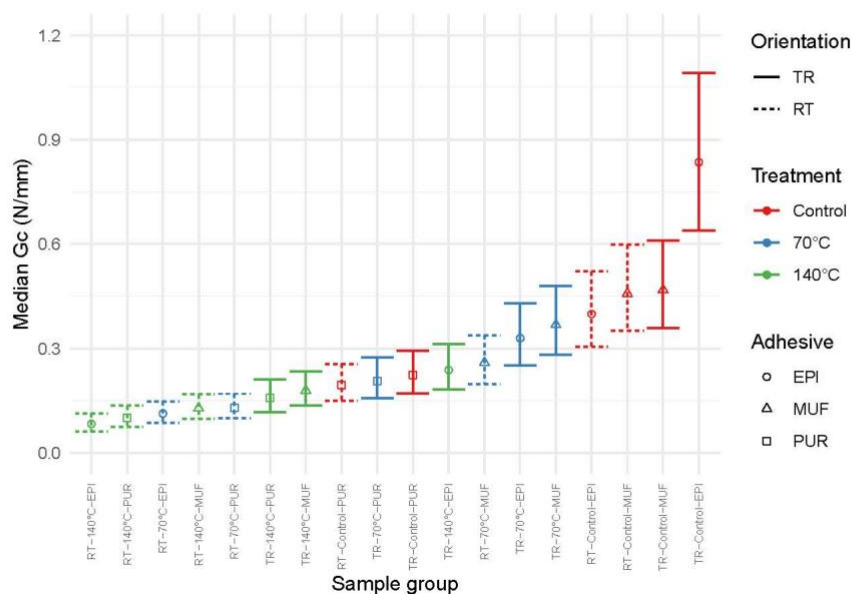
We first predict the median Gc or Gf for each treatment combination. We record the output as tables and figures.

```
#make a data frame with all treatment combinations
d.pre <- expand.grid("adhesive" = c("EPI", "MUF", "PUR"),
  "treatment" = c("Control", "70°C", "140°C"),
  "orientation" = c("TR", "RT"))

#we use the predict function to get estimates from the model
#then use exp to convert from the log transformed to the
#original scale. This means we are predicting *medians* not means.
#we also include 95% confidence intervals
gc.pre <- as_tibble(cbind(d.pre,
  exp(predict(gc.lm, newdata=d.pre,
    interval="confidence"))))

#we add nice labels and re order based on fit (the predicted median)
gc.pre <- gc.pre |> mutate(label = str_c(orientation, treatment, adhesive, sep="-"),
  label = fct_reorder(label, fit))

#Plot
ggplot(data=gc.pre, aes(y=fit, ymin=lwr, ymax=upr, x=label,
  colour=treatment, linetype=orientation,
  shape=adhesive)) + theme_minimal() +
  geom_point(size=1.5) +
  geom_errorbar() +
  labs(y="Median Gc (N/mm)",
  x="Sample group") +
  scale_shape_manual(values=c(1,2,0), name="Adhesive") +
  scale_colour_brewer(palette="Set1", name="Treatment") +
  scale_linetype_discrete(name="Orientation") +
  scale_y_continuous(limits=c(0,1.2), breaks=seq(0,1.2,0.3)) +
  theme(axis.text.x = element_text(angle=90, hjust=1, vjust=0.5, size=6))
```

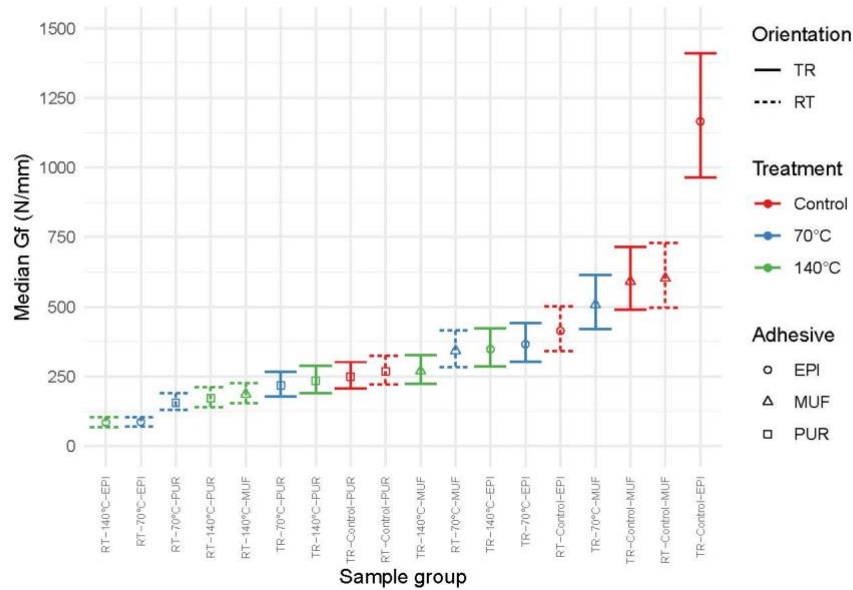


```

# repeat of above for gf
gf.pre <- as_tibble(cbind(d.pre,
  exp(predict(gf.lm, newdata=d.pre, interval="confidence"))))

gf.pre <- gf.pre |> mutate(label = str_c(orientation, treatment, adhesive, sep="-"),
  label = fct_reorder(label, fit))
ggplot(data=gf.pre, aes(y=fit, ymin=lwr, ymax=upr, x=label,
  colour=treatment, linetype=orientation,
  shape=adhesive)) + theme_minimal() +
  geom_point(size=1.5) +
  geom_errorbar() +
  labs(y="Median Gf (N/mm)",
  x="Sample group") +
  scale_shape_manual(values=c(1,2,0), name="Adhesive") +
  scale_colour_brewer(palette="Set1", name="Treatment") +
  scale_linetype_discrete(name="Orientation") +
  scale_y_continuous(limits=c(0,1500), breaks=seq(0,1500,250)) +
  theme(axis.text.x = element_text(angle=90, hjust=1, vjust=0.5, size=6))

```



4.2 Effect sizes

We are interested in the effect size of different treatment combinations. That is, we want to compare the difference in Gc or Gf between two levels of the same factor (like R / T or EPI / MUF). There are two caveats to consider:

1. We have an interaction effect in our model, so we are comparing performance between levels of one factor (e.g., adhesive) for each combination of the other two factors.
2. Because we are working from a model with a log transformed independent variable, we are comparing the ratio between medians rather than differences. This means we report a multiplicative difference between medians. If a ratio is reported to be 2 for x/y , we report that the x performed 2 times better than y .

We use marginal means from the emmeans package to calculate these values.

Examples for one case from each model are provided below. Confidence intervals are adjusted using Tukey's method. P-values are not reported, but can be extracted manually or using another package.

```
#first we save the output of emmeans to a variable
#using type="response" converts from log to the original scale.
gc.em <- emmeans(gc.lm, ~ adhesive | orientation * treatment, type="response")
gf.em <- emmeans(gf.lm, ~ adhesive | orientation * treatment, type="response")

#We extract pairwise comparisons (as ratios) using pairs()
#and we wrap that in confint() to get confidence intervals
gc.pairs <- as_tibble(confint(pairs(gc.em, adjust="tukey")))

#view the output arranged as preferred.
gc.pairs %>% arrange(desc(treatment), orientation)
```

```

## # A tibble: 18 x 8
##   contrast orientation treatment ratio   SE   df lower.CL upper.CL
##   <fct>      <fct>      <fct>   <dbl> <dbl> <dbl>   <dbl>   <dbl>
## 1 EPI / MUF RT      140°C 0.650 0.122 158 0.417 1.01
## 2 EPI / PUR RT      140°C 0.826 0.162 158 0.520 1.31
## 3 MUF / PUR RT      140°C 1.27 0.235 158 0.820 1.97
## 4 EPI / MUF TR      140°C 1.33 0.238 158 0.871 2.03
## 5 EPI / PUR TR      140°C 1.51 0.284 158 0.966 2.35
## 6 MUF / PUR TR      140°C 1.13 0.210 158 0.731 1.76
## 7 EPI / MUF RT      70°C 0.437 0.0774 158 0.288 0.664
## 8 EPI / PUR RT      70°C 0.871 0.155 158 0.571 1.33
## 9 MUF / PUR RT      70°C 1.99 0.354 158 1.31 3.03
## 10 EPI / MUF TR      70°C 0.895 0.158 158 0.589 1.36
## 11 EPI / PUR TR      70°C 1.59 0.288 158 1.04 2.44
## 12 MUF / PUR TR      70°C 1.78 0.320 158 1.16 2.72
## 13 EPI / MUF RT      Control 0.872 0.154 158 0.574 1.33
## 14 EPI / PUR RT      Control 2.04 0.363 158 1.34 3.11
## 15 MUF / PUR RT      Control 2.34 0.415 158 1.54 3.56
## 16 EPI / MUF TR      Control 1.79 0.316 158 1.17 2.71
## 17 EPI / PUR TR      Control 3.72 0.663 158 2.45 5.67
## 18 MUF / PUR TR      Control 2.09 0.370 158 1.37 3.17

#repeat for Gf
#depending on direction of the effect size (greater or less than one)
#it can be useful to use reverse=TRUE within pairs() as it is simply
#easier to discuss ratios when they are greater than 1.
gf.pairs <- as_tibble(confint(pairs(gf.em, adjust="tukey")))

gf.pairs %>% arrange(desc(treatment), orientation)

## # A tibble: 18 x 8
##   contrast orientation treatment ratio   SE   df lower.CL upper.CL
##   <fct>      <fct>      <fct>   <dbl> <dbl> <dbl>   <dbl>   <dbl>
## 1 EPI / MUF RT      140°C 0.450 0.0603 158 0.328 0.618
## 2 EPI / PUR RT      140°C 0.490 0.0684 158 0.352 0.681
## 3 MUF / PUR RT      140°C 1.09 0.144 158 0.795 1.49
## 4 EPI / MUF TR      140°C 1.29 0.165 158 0.954 1.75
## 5 EPI / PUR TR      140°C 1.49 0.200 158 1.08 2.04
## 6 MUF / PUR TR      140°C 1.15 0.152 158 0.843 1.58
## 7 EPI / MUF RT      70°C 0.251 0.0317 158 0.186 0.338
## 8 EPI / PUR RT      70°C 0.552 0.0703 158 0.408 0.746
## 9 MUF / PUR RT      70°C 2.20 0.279 158 1.63 2.97
## 10 EPI / MUF TR      70°C 0.720 0.0909 158 0.534 0.970
## 11 EPI / PUR TR      70°C 1.68 0.217 158 1.23 2.28
## 12 MUF / PUR TR      70°C 2.33 0.300 158 1.72 3.16
## 13 EPI / MUF RT      Control 0.687 0.0868 158 0.510 0.927
## 14 EPI / PUR RT      Control 1.54 0.196 158 1.14 2.08
## 15 MUF / PUR RT      Control 2.24 0.284 158 1.66 3.03
## 16 EPI / MUF TR      Control 1.97 0.249 158 1.46 2.66
## 17 EPI / PUR TR      Control 4.68 0.595 158 3.47 6.32
## 18 MUF / PUR TR      Control 2.38 0.301 158 1.76 3.21

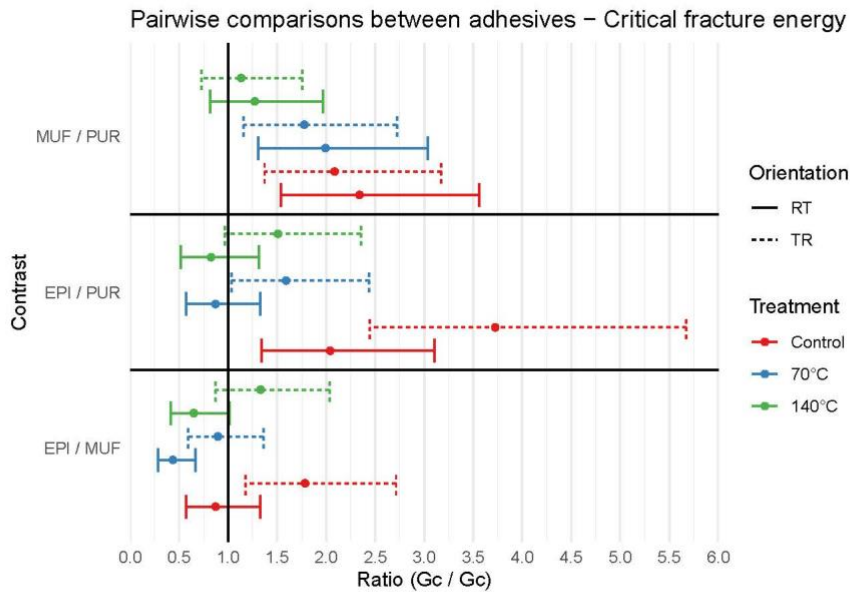
```

4.3 Visualising effect sizes

To visualise effect sizes, we plot the point estimates of the ratio between compared factor levels with their 95% confidence intervals. We use colour and linetype to differentiate between the other factor levels. We add a solid line at ratio = 1, to make it easier to distinguish significant effects (i.e., those that do not cross 1).

The examples below are for Gc and Gf based on the output of the effect size estimates above.

```
#we plot the output
#when error bars
ggplot(data=gc.pairs, aes(x=contrast, y=ratio, ymax=upper.CL, ymin=lower.CL,
                        colour=treatment, linetype=orientation)) + theme_minimal() +
  geom_point(position=position_dodge(width=0.9)) +
  geom_errorbar(position=position_dodge(width=0.9)) +
  geom_hline(yintercept=1) +
  geom_vline(xintercept=c(1.5,2.5)) +
  coord_flip() +
  scale_y_continuous(limits=c(0,6), breaks=seq(0,6,.5), expand=c(0,0)) +
  scale_linetype_discrete(name="Orientation") +
  scale_color_brewer(palette = "Set1", name="Treatment") +
  labs(title="Pairwise comparisons between adhesives - Critical fracture energy",
       y="Ratio (Gc / Gc)", x="Contrast") +
  theme(
    panel.grid.major.y = element_blank()
  )
)
```

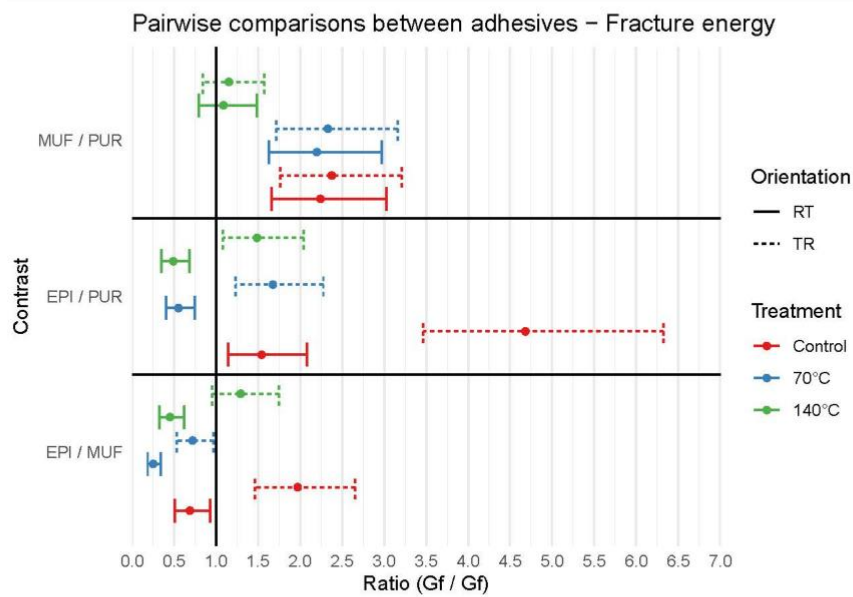


```
ggplot(data=gf.pairs, aes(x=contrast, y=ratio, ymax=upper.CL, ymin=lower.CL,
                        colour=treatment, linetype=orientation)) + theme_minimal() +
  geom_point(position=position_dodge(width=0.9)) +
```

```

geom_errorbar(position=position_dodge(width=0.9)) +
geom_hline(yintercept=1) +
geom_vline(xintercept=c(1.5,2.5)) +
coord_flip() +
scale_y_continuous(limits=c(0,7), breaks=seq(0,7,.5), expand=c(0,0)) +
scale_linetype_discrete(name="Orientation") +
scale_color_brewer(palette = "Set1", name="Treatment") +
labs(title="Pairwise comparisons between adhesives - Fracture energy",
      y="Ratio (Gf / Gf)", x="Contrast") +
theme(
  panel.grid.major.y = element_blank()
)

```



5 Acknowledgements

This work has been conducted with the financial support of the European Commission for the InnoRenew project (Grant Agreement #739574) under the Horizon2020 Widespread-2-Teaming program, Republic of Slovenia (Investment funding of the Republic of Slovenia and the European Union of the European Regional Development Fund), Slovenian Research Agency (infrastructure program IO-0035) and Slovenian Research Agency (basic research funding No. P4-0430). The authors also acknowledge the grant provided by Czech Science Foundation: "Experimental and numerical assessment of the bearing capacity of notches in timber beams at arbitrary locations using LEFM" (#21-29389S).

Declaration

I declare that this thesis does not contain any materials previously published or written by another person except where due reference is made in text.

Jaka Gašper Pečnik